Wissenschaftszentrum Weihenstephan

Lehrstuhl für Molekulare Ernährungsmedizin

Diet induced obesity differentially affects mitochondrial function in skeletal muscle and liver of C57BL/6J mice

Kerstin Elisabeth Haas

Vollständiger Abdruck der von der Fakultät Wissenschaftszentrum Weihenstephan für Ernährung, Landnutzung und Umwelt der Technischen Universität München zur Erlangung des akademischen Grades eines

Doktors der Naturwissenschaften

genehmigten Dissertation.

Vorsitzender: Univ.-Prof. Dr. B. Küster

Prüfer der Dissertation:

1. Univ.-Prof. Dr. M. Klingenspor
2. Univ.-Prof. Dr. H. Daniel

Die Dissertation wurde am 08.04.2014 bei der Technischen Universität München eingereicht und durch die Fakultät Wissenschaftszentrum Weihenstephan für Ernährung, Landnutzung und Umwelt am 22.09.2014 angenommen.

Index of Contents

Index of Figures

Index of Tables

Abbreviations

ADP/ATP	adenosine diphosphate/ triphosphate
Acad	acyl-CoA dehydrogenase
Acsl	long chain acyl-CoA synthase
ANOVA	analysis of variance
ApoB/E	apolipoprotein B/E
AUC	area under the curve
BCA	bicinchoninic acid
BMI	body mass index
BSA	bovine serum albumin
°C	Celsius degree
C	control
CACT	carnitine acylcarnitine transferase
cDNA	complementary deoxyribonucleic acid
CoA	Coenzyme A
Cpt1a/b	carnitine palmitoyltransferase 1 b
CS	Citrate Synthase
Ct	cytosol
Cyt c	cytochrome c
DAG	diacylglycerol
DMSO	dimethylsulfoxide
DNA	deoxyribonucleic acid
DTNB	5,5'dithiobis(2-nitrobenzoic acid)
ER	endoplasmic reticulum
EtOH	ethanol
ETF/ETFDH	electron transfer flavoprotein/-dehydrogenase
FCCP	Carbonyl cyanide 4-(trifluoromethoxy)phenylhydrazone
g	gram
G3P/G3P-DH	glycerol-3 phosphate/-dehydrogenase
Gcn	gastrocnemius muscle
GePS	Genomatix Pathway System
GPx	glutathione peroxidase
GR	glutathione reductase
GSH	glutathione
GSSG	glutathione disulfide
HCl	hydrogen chloride
HF	high fat
H_2O_2	hydrogen peroxide
iAUC	incremental area under the curve
IMM	inner mitochondrial membrane
IPA	Ingenuity Pathway Analysis
ipGTT	intraperitoneal glucose tolerance test
KCl	potassium chloride
KOH	potassium hydroxide
kJ	kilo joule
Mal	malate

MAM	mitochondria-associated membrane
mg	milligram
µg	microgram
min	minute
ml	milliliter
µl	microliter
mM	millimolar
µM	micromolar
mt	mitochondrial
MUFA	monounsaturated fatty acids
n3	omega -3
n6	omega -6
n.a.	not analyzed
Nafld	non-alcoholic fatty liver disease
NEFA	nonesterified fatty acids
Nfe2l2 or Nrf2	nuclear factor erythroid-derived 2-like 2
nm	nanometre
NMR	nuclear magnetic resonance
Nnt	nicotinamide nucleotide transhydrogenase
n.s.	not significant
OMM	outer mitochondrial membrane
PC	palmitoylcarnitine
PUFA	polyunsaturated fatty acids
Q	ubiquinone
R^2	coefficient of determination
RFU	relative fluorescence units
RNA	ribonucleic acid
ROS	reactive oxygen species
rRNA	ribosomal ribonucleic acid
RT	room temperature
s	second
SFA	saturated fatty acids
Sod (Cu/Zn or Mn)	superoxide dismutase (copper/zink = Sod1; mn = Sod2)
SPF	specific pathogen free
TCA	tricarboxylic acid cycle
TG	triglyceride
U	unit
UPR	unfolded protein response
VLDL	very low density lipoprotein
v/v	volume/volume
WHO	World Health Organisation
wt %	weight percent
x	times
x g	times gravity

Summary

Obesity and related health problems including systemic insulin resistance and non-alcoholic fatty liver disease represent the health burdens of affluent society. Mitochondria are the key players in the energy production of all cells. Reduction in mitochondrial function was associated with skeletal muscle insulin resistance and fat accumulation in the liver. Especially mitochondrial reactive oxygen species (ROS) production is discussed to eventually overcome detoxification mechanisms leading to damage in cells and signaling pathways, in particular insulin. Therefore this thesis seeks to clarify whether mitochondrial ROS production in skeletal muscle is driven to excess in the state of diet induced obesity and precedes insulin resistance. Furthermore the mechanism of hepatic fat accumulation was investigated with respect to mitochondrial function, ROS production and a proteome analysis of mitochondria- and organelle-enriched fractions.

Aging reduces many metabolic functions and has barely been considered in rodent studies so far. Thus, a particular focus of this research was the age of C57BL/6J mice at onset of high fat feeding. Adolescent (8 weeks of age), young adult (16 weeks of age) or middle-aged (52 weeks of age) male mice were fed a palm oil based high fat diet (45 energy % from fat) or a control diet (12 energy % from fat). The major phenotype influenced by aging was body mass gain. Middle-aged mice put on significantly more mass during 9 weeks of feeding than young adult and adolescent mice. The adolescent group also increased lean mass, because of their pubertal age.

For mitochondrial function in skeletal muscle a timeline of events was generated to monitor changes in the glucose homeostasis and mitochondrial ROS production. Whereas glucose homeostasis was rapidly changed after onset of high fat feeding and glucose tolerance progressively declined, mitochondrial ROS production in skeletal muscle was normal up to 26 weeks of high fat feeding. Oxygen consumption and acylcarnitine release, a marker for impaired mitochondrial β-oxidation, monitored in isolated skeletal muscle mitochondria, were unaffected by high fat diet feeding. The glutathione redox system served as marker for oxidative stress *in vivo*. Indeed, skeletal muscle of the middle-aged high fat-fed mice displayed a more oxidized redox environment. This might render this age group more susceptible to oxidative stress than younger mice.

High fat feeding for 9 weeks induced fat accumulation in the liver, but only in young adult and middle-aged mice, not in the adolescent group. Mitochondrial ROS production was increased

without high fat diet induced changes in proton leak. The proteome analysis of mitochondria-enriched fractions identified proteins mainly allocated to mitochondria, but also to endoplasmic reticulum, peroxisomes and lysosomes. A balanced antioxidative response was initiated in liver of high fat-fed mice by upregulated targets of nuclear factor erythroid-derived 2-like 2 (Nrf2). As particular merit of the present study an interaction site of Nrf2 and mitochondria was confirmed and may provide a mechanistic link between the induction of Nrf2-mediated gene expression and mitochondrial ROS production.

Regarding the fatty acid flux in hepatocytes, mitochondrial β-oxidation was not clearly enhanced or suppressed, although the bioenergetic analysis hinted towards limited mitochondrial β-oxidation at least for long chain fatty acids. Peroxisomal fatty acid oxidation was clearly suppressed by high fat diet. The procedure to mature VLDL, including translation, ER protein processing, and VLDL lipidation, was enhanced. The age-related difference in triglyceride accumulation connected to progressive reduction of lysosomal proteins. Lysosomes are involved in controlled degradation of lipid droplets in the liver, therefore the reduction in lysosomal proteins may account for an inefficient mobilization of triglycerides in liver of high fat-fed mice. This might be exacerbated by a tendency towards reduced mitochondrial mass in livers of middle-aged mice, which was independent of high fat feeding, but could trigger the imbalance that eventually lead to hepatic fat accumulation.

In conclusion hepatic mitochondria are more susceptible to high fat diet induced changes than skeletal muscle mitochondria, which perform robustly despite established insulin resistance. The complex hepatic network of organelle interactions has to be further elucidated. As obesity and related health problems mostly affect humans in their second half of life, the age has to be considered more thoroughly in future studies.

Zusammenfassung

Übergewicht und die damit verbundenen gesundheitlichen Folgen, wie systemische Insulin Resistenz und nicht-alkoholbedingte Fettleber, sind die Bürden der modernen Wohlstandsgesellschaft. Mitochondrien spielen die zentrale Rolle im Energie-Metabolismus aller Zellen. Eine verminderte Funktion der Mitochondrien, beziehungsweise eine erhöhte Produktion reaktiver Sauerstoffspezies (ROS), stehen in der Diskussion Zellen zu schädigen und Signalwege, z.B. von Insulin, zu inhibieren. Deshalb wurde in dieser Arbeit untersucht, ob durch die Entstehung ernährungsbedingten Übergewichts die mitochondriale ROS Produktion im Skelettmuskel exzessiv erhöht ist und dies eine Insulinresistenz bedingt. Außerdem wurde die Entstehung einer Fettleber hinsichtlich mitochondrialer Funktion, ROS Produktion und die Regulierung auf Protein-Ebene in Mitochondrien und anderen Organellen mittels einer Proteom-Analyse untersucht.

Das Altern eines Organismus ist verbunden mit einer Verminderung vieler Stoffwechselprozesse; dies wurde bisher nur unzureichend in tierexperimentellen Studien berücksichtigt. Ein besonderer Schwerpunkt der Arbeit lag auf dem Alter der ausschließlich männlichen C57BL/6J Mäuse zu Beginn der Hochfett-Fütterung. Adoleszenten Mäusen mit einem Alter von 8 Wochen, erwachsenen Mäusen mit einem Alter von 16 Wochen und Mäusen mittleren Alters mit 52 Wochen wurde ein Hochfett-Futter (45 Energie-% Fett) mit Palmöl als hauptsächlicher Fettquelle gefüttert, die Vergleichsgruppe im entsprechenden Alter erhielt ein Kontroll-Futter (10 Energie-% Fett). Die erzielte Gewichtszunahme wurde hauptsächlich vom unterschiedlichen Alter der Tiere beeinflusst. Mäuse mittleren Alters, die fettreich gefüttert wurden, nahmen signifikant mehr zu als die jüngeren hochfett-gefütterten Mäuse. Die adoleszenten Mäuse nahmen auch an fettfreier Masse zu, was auf das noch anhaltende Wachstum in dieser Altersgruppe hinweist.

Eine Zeitreihe wurde erstellt um die Entwicklung einer ernährungsbedingten Glukoseintoleranz der mitochondrialen ROS Produktion im Skelettmuskel gegenüberzustellen. Die Glukosehomöostase änderte sich sehr schnell, nachdem die Mäuse auf das fettreiche Futter umgestellt wurden, während die mitochondriale ROS Produktion der aus Skelettmuskelzellen isolierten Mitochondrien sich nicht veränderte bis zu einem Fütterungszeitraum von 26 Wochen. Sauerstoffverbrauch und Acylcarnitin-Abgabe, welche als Marker für eine beeinträchtigte β-Oxidation herangezogen wird, wurden nicht durch die Fütterung von fettreichem Futter beeinflusst. Als Marker für oxidativen Stress *in vivo* zeigte das Glutathion-Redox-System eine oxidative Verschiebung im Skelettmuskel von hochfett-

gefütterten Mäusen der ältesten Gruppe, was auf einen Zusammenhang zwischen dem Alter der Mäuse und der Entwicklung von ernährungsbedingtem oxidativen Stress im Skelettmuskel hindeutet.

Die fettreiche Fütterung über neun Wochen führte zur Anreicherung von Triglyceriden in der Leber in erwachsenen Mäusen und Mäusen mittleren Alters, nicht jedoch in der adoleszenten Gruppe. Die mitochondriale ROS Produktion war erhöht, ohne dass sich die Leckatmung der Lebermitochondrien fettreich-gefütterter Mäuse änderte. In einer Proteom-Analyse wurden die Proteine aus der Mitochondrien-angereicherten Fraktion bestimmt. Dabei konnten neben mitochondrialen Proteinen auch Proteine des endoplasmatischen Retikulums (ER), ribosomale, peroxisomale und lysosomale Proteine identifiziert wurden. Als antioxidative Antwort waren eine Reihe Proteine nach Hochfett-Fütterung erhöht, die unter der Kontrolle des Transkriptionsfaktors nuclear factor erythroid-derived 2-like 2 (Nrf2) exprimiert werden. Es ist gelungen eine Verknüpfung zwischen Nrf2 und der äußeren mitochondrialen Membran zu bestätigen. Damit kann eine Hypothese vorgestellt werden, wie mitochondriale ROS Produktion direkt eine Nrf2-vermittelte Genexpression auslösen kann.

Die Proteom-Analyse zeigte neben einer unwesentlichen Regulierung von Proteinen der mitochondrialen β-Oxidation eine deutliche Reduzierung des Fettsäureabbaus in Peroxisomen nach fettreicher Fütterung. Dem gegenüber war der Metabolismus zur Herstellung von very low density lipoprotein (VLDL) erhöht, einschließlich Translation, Prozessierung im ER und Anreicherung von Lipiden an VLDL. Die altersbedingte Anreicherung von Triglyceriden in der Leber nach Hochfett-Fütterung war mit einer stärkeren Reduktion von lysosomalen Proteinen in älteren Mäusen verbunden. Lysosomen vermitteln unter anderem den Abbau von Lipidtröpfchen in der Leber. Die Entstehung einer Fettleber kann demnach durch die angedeutete unzureichende Mobilisierung der Triglyceride in der Leber fettreich-gefütterter Mäuse und zusätzlich durch tendenziell weniger Mitochondrien in Mäusen mittleren Alters unabhängig von der Fütterung, begünstigt werden.

Es konnte nachgewiesen werden, dass Skelettmuskelmitochondrien im Laufe der Entstehung einer Insulinresistenz ihre Funktion nicht verändern und diese somit nicht auslösen. Lebermitochondrien hingegen zeigten eine erhöhte ROS Produktion im Laufe einer fettreichen Fütterung. Das Zusammenspiel der Zellorganellen während der Entstehung einer Fettleber bedarf weiterer Forschung. Die hier aufgezeigten metabolischen Veränderungen sind zudem auch altersabhängig. Demnach ist es notwendig, für das Alter kontrollierte tierexperimentelle Studien durchzuführen, besonders im Hinblick darauf, dass Übergewicht und die gesundheitlichen folgen überwiegend Menschen im fortgeschrittenen Alter betreffen.

1 <u>Introduction</u>

1.1 Obesity and related health complications

1.1.1 Epidemiologic data

Dietary energy supply is mandatory for survival in all metazoans, which includes mammals and finally humans (Samuel & Shulman 2012). Body weight maintenance is literally a balance between energy intake and expenditure. When energy demand is less than the ingested calories, the excess is stored as fat such increasing body mass (Seale & Lazar 2009). Actually, the system to store energy for future requirements is live-saving, but our modern society struggles with the excessive availability of food (Samuel & Shulman 2012). Especially unhealthy eating and physical inactivity promote a positive energy balance in a so called obesogenic environment (Hills *et al.* 2013). Noteworthy, causes for obesity are multifactorial in humans, including environmental impacts e.g. socio-economic status (Giskes *et al.* 2011) or maternal obesity during pregnancy (Rauh *et al.* 2013), and genetic variants (Kopelman 2007).

The morbid accumulation of fat which severely impacts health can be summarized as obesity. And the prevalence of obesity is rising worldwide. For adult humans, body weight is categorized by the body mass index (BMI), dividing the body mass in kilogram by the squared height in centimeter. Overweight is classified when the BMI reaches 25 or more, obesity starts at a BMI of 30 (Kopelman 2000). Consulting the Factbook, published by the Organization for Economic Co-operation and Development (OECD) in 2013, surveys state more than 50 % of people older than 15 above the normal weight range in many industrialized countries (Figure 1). Latest data from Germany were obtained from the Microzensus in 2009 and classify 51.4 % of adult Germans with a BMI of 25 or higher. In countries including Germany and even in Korea and Japan, the portion of obesity among the population increased since the year 2000 (OECD 2013). Bioinformatic models predict the prevalence of obesity in the year 2025 up to 50 % in nations like the USA, the UK or Australia (Kopelman 2000).

An aspect which must not be neglected is that also worldwide prevalence of overweight and obese children is increasing and strongly associated with complications in health and social state in later life (Kopelman 2007). A comprehensive survey in adolescents aged 11 to 15 shows a considerable percentage of adolescents carrying too much weight; in Germany this is about 13 %, in the USA almost 30 % of interviewed pupils (Haug *et al.* 2009). On the other

side, obesity increases with increasing age. In the elderly (aged 65 and above), prevalence of obesity increases over the last years, too. But also age per se changes numerous metabolic routes, e.g. thyroid or steroid hormonal status, altered satiety signaling and decreased muscle mass, which favor to put on weight. During lifespan, the maximal weight is typically reached in middle aged men between 50 and 60 (Michalakis *et al.* 2013), which can be applied to data obtained for the German population (Mikrozensus 2009).
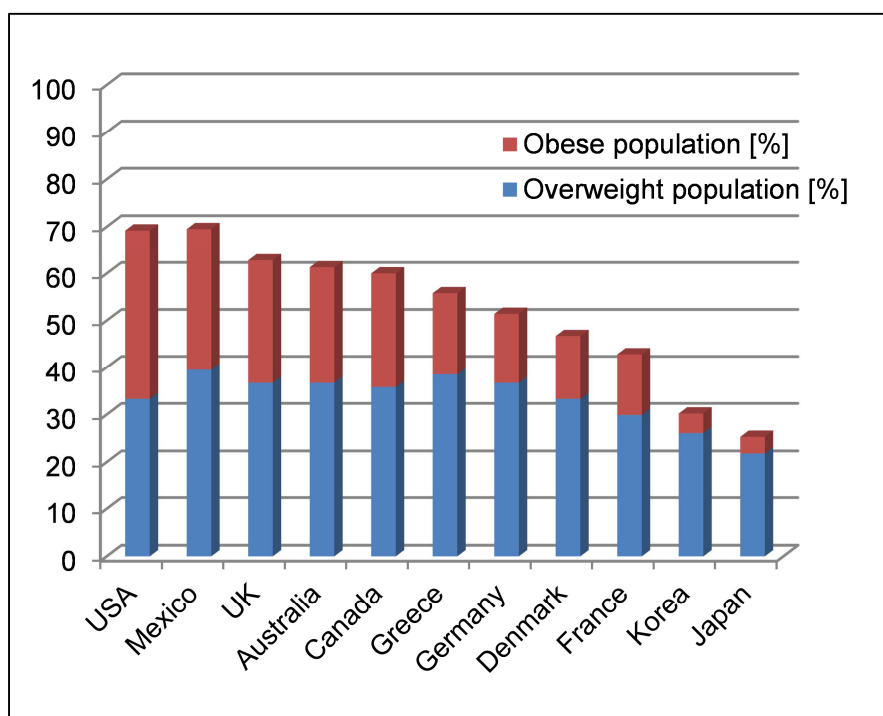
Figure 1: Prevalence of overweight and obesity among the adult population (OECD 2013)

1.1.2 Associated health problems

Obesity is strongly associated with a bunch of health complications among them the metabolic syndrome, insulin resistance of peripheral tissues, cardio-vascular and respiratory complications, arthritis, accumulation of uric acid, complications due to gall stones, and some cancers (Michalakis *et al.* 2013). Obesity, especially when the BMI passes 35 is associated with higher all-cause mortality (Flegal *et al.* 2013). The World Health Organization (WHO) states "cardio-vascular disease and diabetes" as the top cause of death globally accounting for about one third of age-standardized mortality (WHO 2013).

The metabolic syndrome serves as collective term for metabolic derangements which increase the risk for the development of type 2 diabetes and/or cardiovascular disease. It comprises cut points for blood pressure and the concentration of triglycerides and high density lipoprotein in the blood and impaired glucose tolerance (Kahn *et al.* 2005).

Furthermore the estimation of central obesity by waist circumference is considered as valuable predictor for the metabolic syndrome and its unfavorable health outcomes (Alberti *et al.* 2009). Type 2 diabetes is characterized as metabolic disorder by the loss of insulin sensitivity in peripheral tissues and eventually failure of the insulin producing cells. Late complications of this disease are microvascular occlusions due to chronic hyperglycemia, which lead to blindness, nephropathy and lesions of the lower extremities (American Diabetes 2013).

In the context of the metabolic syndrome non-alcoholic fatty liver disease (Nafld) is regarded as the hepatic manifestation taking essentially part in lipid homeostasis (Kawano & Cohen 2013). In human studies, Nafld has emerged to increase the risk for diabetes (Masuoka & Chalasani 2013). Steatosis, which means fat accumulation in the liver, is one of the main features of Nafld (Masuoka & Chalasani 2013), (Gambino *et al.* 2011). Following the so called two-hit hypothesis, a second event, e.g. inflammation or imbalanced redox environment, induces progressive liver damage, ending in liver cirrhosis, steatohepatitis or hepatoma (Gambino *et al.* 2011).

1.1.3   Fat in peripheral tissues

A distinct feature of obesity is the distribution of fat in non-adipose tissue (Boren *et al.* 2013). Under physiological conditions adipose tissue is the designated storage for fat. Insulin promotes fat uptake into adipose tissue (Czech *et al.* 2013). When insulin signaling is disturbed in consequence of chronic dietary oversupply, however, lipolysis and thus release of fatty acids from the adipose tissue is increased (Amir & Czaja 2011), (Greenberg *et al.* 2011). Eventually the fat is stored in non-adipose tissue, such as liver, skeletal muscle and heart. The effects of fat accumulation in the non-adipose periphery impact insulin sensitivity, tissue metabolism and functionality (Boren *et al.* 2013). Undesired effects of fat and fat-derivatives are summarized as lipotoxicity (Chow *et al.* 2010). Usually fatty acids are converted to triglycerides and stored as lipid droplets to prevent lipotoxic effects. Excessive lipid droplet accumulation in liver may interfere with insulin resistance (Greenberg *et al.* 2011). The breakdown of lipid droplets has been found critical in the regulation of lipid homeostasis. In this context a specialized form of autophagy, called lipophagy, has come into focus of research. In an obese state, the correct assembly of lipid droplets determined for degradation and/or the degradation process itself, promoted by lysosomes have been found deranged (Liu & Czaja 2013). In addition to morbid accumulation of fat, aging is associated with less control of cellular events by autophagy (Amir & Czaja 2011).

A mouse model of diet induced obesity reflects the phenotypic adaptations in this work to investigate molecular adaptations. Obesity related fat accumulation in the liver and mitochondrial function in skeletal muscle and liver are on the main focus for this thesis.

1.2   Fat handling in the liver

In the physiological situation dietary fat, incorporated into chylomicrons in the intestine, is delivered to either adipose tissue for storage or to energy-demanding organs, like skeletal muscle and heart. Depleted remnants of these chylomicrons reach the liver. These remnants are poor in triglycerides and mostly contain cholesterylesters (Williams 2008). The liver also takes up nonesterified fatty acids (NEFA) from the blood, mostly bound to albumin. Once entered the hepatocyte, fatty acids are activated by coupling to Coenzyme A and then processed through various routes (Figure 2). Mitochondria and the endoplasmic reticulum (ER) play the major roles in these processes. In the ER, fatty acids are fused to mono-, di- and triglycerides, to sterylesters and phospholipids. Mitochondria essentially break down fatty acids by β-oxidation. Resulting acetyl-CoA is introduced into the tricarboxylic acid (TCA) cycle which finally drives energy production and therefore finances all metabolic processes (Jiang *et al.* 2013). Moreover mitochondria provide the building blocks for de novo-lipogenesis (Jiang *et al.* 2013) and cholesterol biosynthesis (Faust & Kovacs 2013). There is a close cooperation between mitochondria and the ER in the synthesis of specific lipid-intermediates, such as phospholipids and ceramides, and steroid biosynthesis (Rieusset 2011), (Issop *et al.* 2013). A specific interaction site in the ER has been introduced to promote this cooperation, the so-called mitochondria-associated membrane (MAM) (Raturi & Simmen 2013). At this specific site, the two organelles are attached to each other by tethering proteins. Couples of these proteins have been identified and described (de Brito & Scorrano 2010).

There is an alternative route for fatty acid breakdown in peroxisomes, especially for very long chain-, branched chain- and dicarboxylic- fatty acids. In these organelles, which originate from the ER, the process of breaking down fatty acids partly resembles the mitochondrial β-oxidation, with respect to acetyl-CoA production. Furthermore peroxisomes essentially take part in cholesterol and bile acid synthesis (Faust & Kovacs 2013). Noteworthy, reduction of energy equivalents does not take place in peroxisomes, but reducing energy generates H_2O_2 and heat (Schrader & Fahimi 2006).
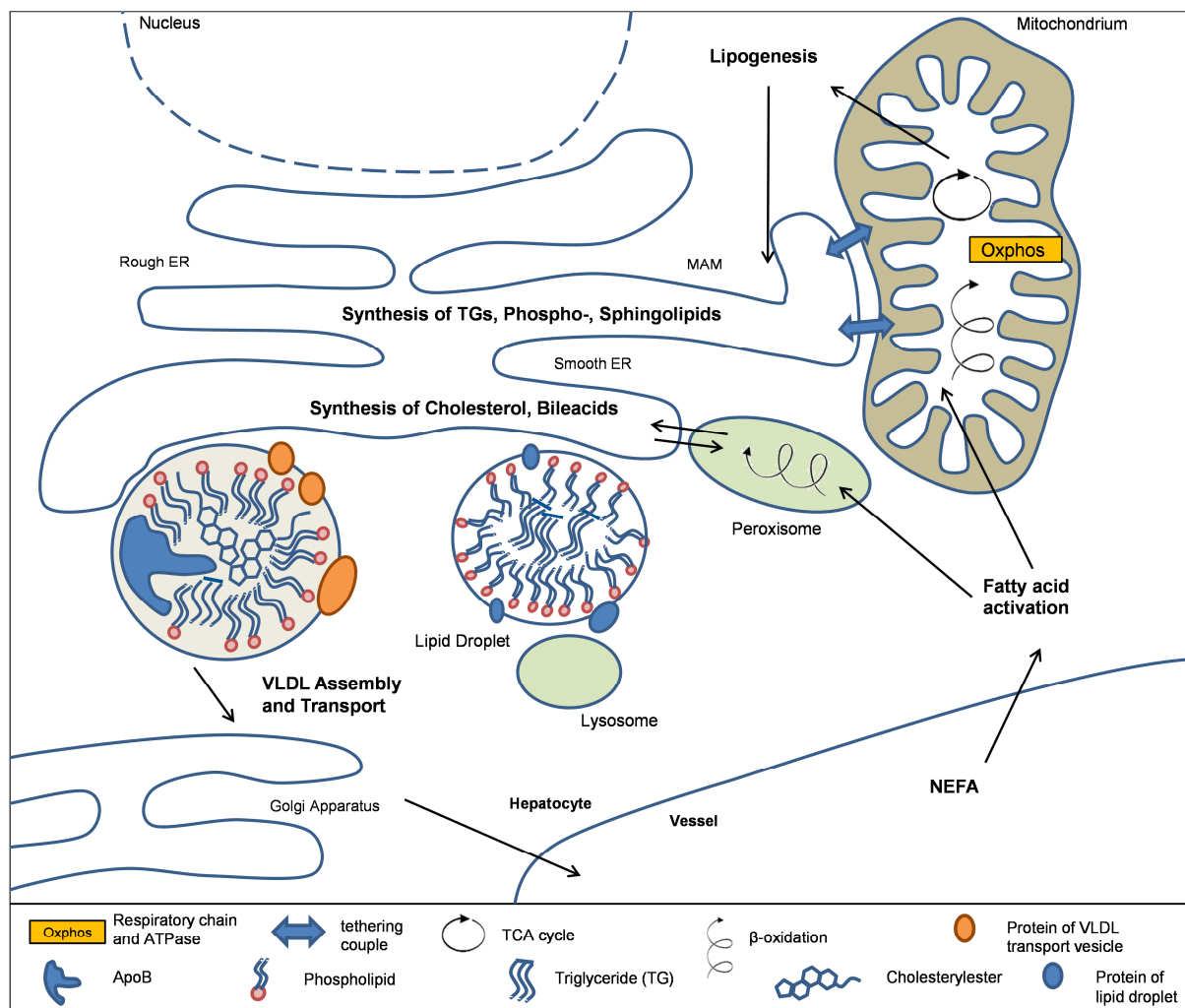
Figure 2: Flux of fatty acids through a hepatocyte
Description in the text

In general the liver is not a fat-storing organ. Products of de-novo lipogenesis are excreted in very low density lipoproteins (VLDL) to modulate the energy homeostasis (Kawano & Cohen 2013). The process to mature VLDL comprises multiple steps and originates in the ER. Apolipoprotein B (ApoB) is the core protein of VLDL particles and while proceeding in the ER it is continuously lipidated and enriched with mainly triglycerides (TG) and cholesterylesters (Sundaram & Yao 2010). Besides ApoB, other proteins, e.g. ApoE are added to the particle during the maturation, too. Intriguingly, VLDL secretion is the only way how triglycerides can be cleared from hepatocytes (Jiang *et al.* 2013). Before entering the circulation premature VLDL is budding from the ER to be finally modified in the Golgi apparatus (Jiang *et al.* 2013) (Kawano & Cohen 2013). The assembly of VLDL is strongly controlled, mainly by folding control of ApoB. Misfolded or poor lipidated ApoB is degraded by proteasomal and autophagic processes (Christian *et al.* 2013).

For transient storage of fat in non-adipose tissue, triglycerides and other lipid-derivatives can be enveloped by a simple phospholipid layer to be stored as lipid droplet, also being assembled in the ER. The droplets are equipped with lipases, able to release fatty acids, when needed. Furthermore lipophagy has been introduced to play an important role in regulated breakdown of lipid droplets (Boren *et al.* 2013). In this process lysosomal mediated hydrolysis of the autophagosome cargo is initiated by the fusion of lysosomes with the autophagosome (Liu & Czaja 2013). Lysosomes are organelles that contain a large variety of hydrolases to break down macromolecules (Chapel *et al.* 2013) in an acidic environment (Saftig & Eskelinen 2008). Lysosomal proteins have been shown to impact longevity, as the age-related decrease of lysosomal activity leads to accumulation of unfavorable cell debris (Saftig & Eskelinen 2008).

1.3   Regulation of energy metabolism by insulin

1.3.1   Insulin action in muscle

When talking about obesity and related health problems, the role of insulin must not be neglected. Changes in insulin-mediated glucose disposal from the blood can be observed long before overt type 2 diabetes is diagnosed (Jelenik & Roden 2012). Skeletal muscle is estimated to take up the largest part (up to 80 %) of blood glucose upon a meal mediated by insulin. Upon binding of insulin to its receptor, a multistep signaling cascade is started, including receptor autophosphorylation, activation of insulin receptor substrate 1 and 2 and consequently protein kinase B (Chow *et al.* 2010). Insulin action provides glucose uptake in skeletal muscle for immediate use or for building up glycogen as storage (Samuel & Shulman 2012). Storage of glucose as fat is possible in skeletal muscle via de novo-lipogenesis, but this route is not extensively used under physiological conditions (Savage *et al.* 2007).

Insulin resistance describes a term, when the responsiveness to the hormone insulin is attenuated and abrogated. The routes within the cells are not further maintained by insulin (Boden 2011). In skeletal muscle reduced sensitivity to insulin is accompanied by low glycogen stores and glucose oxidation (Samuel & Shulman 2012). It was established that the high availability of fat reduces the oxidation of glucose by a mechanism introduced as glucose-fatty acid cycle by Sir Philip Randle (Randle *et al.* 1963). Although lipid infusion was shown to blunt insulin sensitivity in skeletal muscle (Samuel & Shulman 2012) by promoting systemic insulin resistance (Czech *et al.* 2013) and the accumulation of lipids, so called intramyocellular lipids (IMCL) are strongly associated with insulin resistance (Muoio & Neufer 2012), there are some controversies. Especially the athlete's paradox questions the role of

IMCL to promote insulin resistance, as endurance sports increases IMCL in the skeletal muscle (Tarnopolsky *et al.* 2007), but athletes remain highly insulin sensitive (Goodpaster *et al.* 2001). In this context several hypotheses have been formulated, that e.g. only specific lipid-intermediates promote insulin resistance, e.g. diacylglycerol (DAG) and ceramides (Samuel & Shulman 2012). The imbalance in the cellular redox environment, caused by increased mitochondrial production of reactive oxygen species (ROS) interferes with the insulin signaling pathway, too. It was recently proposed that a chronic shift in the cellular systems that buffer radical production at some point changes the whole-cell redox environment. Consequent activation of "stress-sensitive" kinases blocks the insulin cascade in skeletal muscle (Muoio & Neufer 2012), (Fisher-Wellman & Neufer 2012). Both, lipid mediated and redox-related pathways are closely linked to mitochondrial function (see 1.5). Therefore the resolution of mitochondrial function in the etiology of skeletal muscle insulin resistance provides one major aim in the present thesis. The studies on mitochondrial function in skeletal muscle focus on age of the mice, because fat accumulation in skeletal muscle is a feature of aging (Michalakis *et al.* 2013) as is gradually reduction in insulin sensitivity, rendering the elderly more susceptible for developing associated metabolic disease (Jelenik & Roden 2012).

1.3.2   Insulin action in liver

The liver maintains blood glucose levels during fasting. This is achieved by a two-sided mechanism, each side contributing about half to the hepatic glucose output. Storages of glycogen can be degraded and glucose derives from gluconeogenesis (Savage *et al.* 2007). Insulin stops de-novo synthesis of glucose, and simultaneously glycogen synthesis and de-novo lipogenesis is promoted (Samuel & Shulman 2012). Interestingly VLDL secretion is reduced by insulin via controlling ApoB degradation (Boren *et al.* 2013). When liver cell do not respond to insulin any more, gluconeogenesis in the liver is not reduced resulting in permanent glucose output from liver (Czech *et al.* 2013). With respect to lipid handling reduced insulin sensitivity inconsistently affects pathways, an observation recently defined as "pathway-selective insulin resistance and responsiveness" (Boren *et al.* 2013), (Wu & Williams 2012). In detail this term describes that VLDL secretion is not depressed anymore in the insulin resistant state, while lipogenesis, which is positively regulated by insulin, is still high (Wu & Williams 2012).

The lipid intermediates, described in the context of insulin resistance in skeletal muscle, are also discussed in hepatic insulin resistance. It remains still unsolved if fat accumulation in the liver precedes insulin resistance (Boren *et al.* 2013). Furthermore the unfolded protein

response (UPR) is discussed to promote especially hepatic insulin resistance, although it has not been clarified yet, if UPR as per se protective mechanism directly disrupts the insulin signaling cascade. The UPR is started, when the capacity of the ER to process proteins exceeds the demands. As consequence of UPR lipogenesis is induced to account for an increased need of biomembranes and thus enlarge ER space to promote correct protein folding and processing (Samuel & Shulman 2012), (Ron & Walter 2007).

1.4 Mitochondrial functions

1.4.1 Organelle organization and molecule transport

Mitochondria are double-membrane organelles. They are organized in tubular networks and constantly undergo fusion and fission events. Fusion serves e.g. as adaptation to metabolic needs, whereas fission e.g. cuts defective parts and designates them for degradation (Rambold & Lippincott-Schwartz 2011). The outer mitochondrial membrane is permeable for small molecules, whereas the inner mitochondrial membrane is only permeable for protons (Navarro & Boveris 2007), short and medium chain fatty acids (Rinaldo *et al.* 2002) and hydrogen peroxide (Bashan *et al.* 2009). Other molecules, e.g. ADP, ATP, inorganic phosphate (P_i), intermediates of the TCA (Vial *et al.* 2010) or long chain fatty acids (Rinaldo *et al.* 2002) need specific transporters. The IMM expands its surface by forming cristae and separates the intermembrane space from the matrix (Navarro & Boveris 2007) (Figure 3).

1.4.2 Oxidative Phosphorylation – how mitochondria produce energy

The principle of oxidative phosphorylation was introduced by Peter Mitchell in the early sixties of the 20th century (Fisher-Wellman & Neufer 2012). The basal mechanism to use reductive force for electron transport down a gradient is evolutionary conserved and persistent since early development of life (Brand 2000). Electrons are fed into a transport chain within the IMM (Figure 3), which consists of large proteins within the membrane and soluble transporters (Brand 2000). Sites of electron entry are complex I, also known as Nadh-ubiquinone oxidoreductase (Nduf) and complex II (succinate dehydrogenase) of the respiratory chain using intermediates of the TCA (Navarro & Boveris 2007). They transfer electrons to ubiquinone (Q). Furthermore electron transport flavoprotein (ETF) receives electrons from the first step of the breakdown of fatty acids and by action of ETF dehydrogenase (ETFDH) the electrons pass to Q (Houten & Wanders 2010). Glycero-3 phosphate dehydrogenase (G3P-DH) resides in the intermembrane space and reduces glycero-3 phosphate (G3P) to dihydroxyacetone phosphate (DHAP) contributing electrons to

Q (Schonfeld & Wojtczak 2008). Sulfide-ubiquinone reductase (Hildebrandt & Grieshaber 2008) detoxifies hydrogen sulfide (H_2S), which significantly contributes electrons to the respiratory chain in rodents (Modis *et al.* 2013). The spatial arrangement of the complexes in cells is considered to be very tight with minimal transport distance. Therefore the single complexes assemble to supercomplexes (Navarro & Boveris 2007), which was experimentally evidenced in a wide range of tissues and species (Frenzel *et al.* 2010).
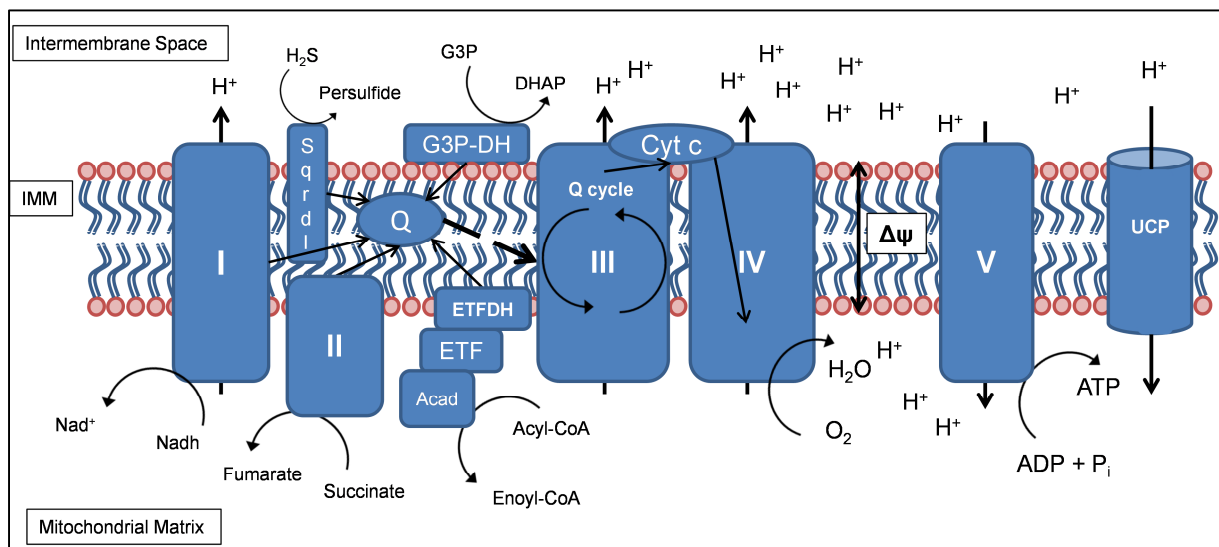
Figure 3: Principle of oxidative phosphorylation
Description in the text

Electrons are handed from Q to complex III, the alias of which is ubiquinone-cytochrome c oxidoreductase, going through the Q cycle to be accepted by cytochrome c. In complex IV, the cytochrome c reductase, the electrons reduce molecular oxygen (O_2) to water (H_2O). During this process along the reducing gradient, protons are actively pumped across the IMM by complex I, III and IV acting as proton pumps. The resulting gradient builds the protonmotive force, which consists of the difference in electrical loading (membrane potential or $\Delta\psi$) and to a small extent of the pH difference (Brand 2000). By controlled slipping back protons into the mitochondrial matrix, complex V, which is the ATP synthase, uses the protonmotive force to generate ATP (Navarro & Boveris 2007). The process of electron transport using redox couples and building up a proton gradient across the IMM is not perfectly efficient. Protons cross the IMM back into the matrix bypassing the ATP synthase but consuming oxygen at complex IV. This is called the proton leak. Besides the basal proton conductance, which is always present, an inducible leak respiration exists, e.g. promoted by uncoupling proteins (UCPs) (Brand 2000). In addition to heat production in brown adipose

tissue (Seale & Lazar 2009), uncoupling serves as controlled reduction of membrane potential to attenuate ROS production (Brand 2000).

1.4.3 ROS production and its metabolic consequences

The leakage of electrons from the respiratory transport chain is an unavoidable side-effect of oxidative metabolism. The reduction power of electron accepting sites in the complexes drives the probability of ROS production (Brand 2000). Sites of ROS production (Figure 4) are respiratory chain complexes (Perevoshchikova *et al.* 2013), glycero-3 phosphate dehydrogenase (Orr *et al.* 2012), α-ketoglutarate dehydrogenase, pyruvate dehydrogenase and ETF (Brand 2010). At complex I the electron transfer from flavin to an iron-sulfur cluster (Fe-S) as well as the further transition to the quinone reducing site are prone for electron slipping to form superoxide (Stowe & Camara 2009). At complex II the flavin site, serving as reduction equivalent during the dehydrogenation of succinate to fumarate and feeding electrons to the ubiquinone pool, was described to produce superoxide especially during fatty acid oxidation (Perevoshchikova *et al.* 2013). A connection between G3P-DH and the rate of superoxide production at complex II was established, proposing reverse electron flow from ubiquinone to complex II (Orr *et al.* 2012) (red arrow in Figure 4). At complex III electrons go through the Q cycle, which is a stepwise transfer process including two critical semiquinone conversions, one at the Q_o site towards the intermembrane space, one at the Q_i site towards the matrix (Turrens 2003). The Q_o site potentially releases the bigger part of ROS generated by complex III, whereas the release to the matrix might be insignificant. Reverse electron flow marks the situation when electrons flow "back" to the site where they were introduced to the electron transport chain (Brand 2010). Experimental setting that initiate reverse electron flow are not considered physiological (Schonfeld & Wojtczak 2012), (Schonfeld & Wojtczak 2008).

Superoxide is rapidly converted to hydrogen peroxide (H_2O_2) in both the mitochondrial matrix and the intermembrane space. In the matrix manganese-superoxide dismutase (Mn Sod or Sod2) converts superoxide (Forkink *et al.* 2010). In the intermembrane space this is catalyzed by copper/zinc-Sod (Cu/Zn Sod or Sod1) (Okado-Matsumoto & Fridovich 2001). Further conversion of H_2O_2 to H_2O is either mediated by catalase, glutathione peroxidase (GPx) or periredoxin. Catalase is only found in low abundance in mitochondria (Forkink *et al.* 2010) or not at all (Murphy 2009). The redox systems used by GPx and periredoxin (Prx) are glutathione (GSH) and thioredoxin (Trx) respectively. Glutathione disulfide (GSSG) is regenerated by glutathione reductase (GR) by oxidizing Nadph. Oxidized Trx is recovered by thioredoxin reductase, again using Nadph (Murphy 2009), (Forkink *et al.* 2010). The

mitochondrial pool of this reducing equivalent is maintained by the $Nadp^+$ dependent isocitrate-dehydrogenase, malic enzyme and nicotinamide nucleotide transhydrogenase (Nnt) (Murphy 2009), (Ronchi *et al.* 2013).
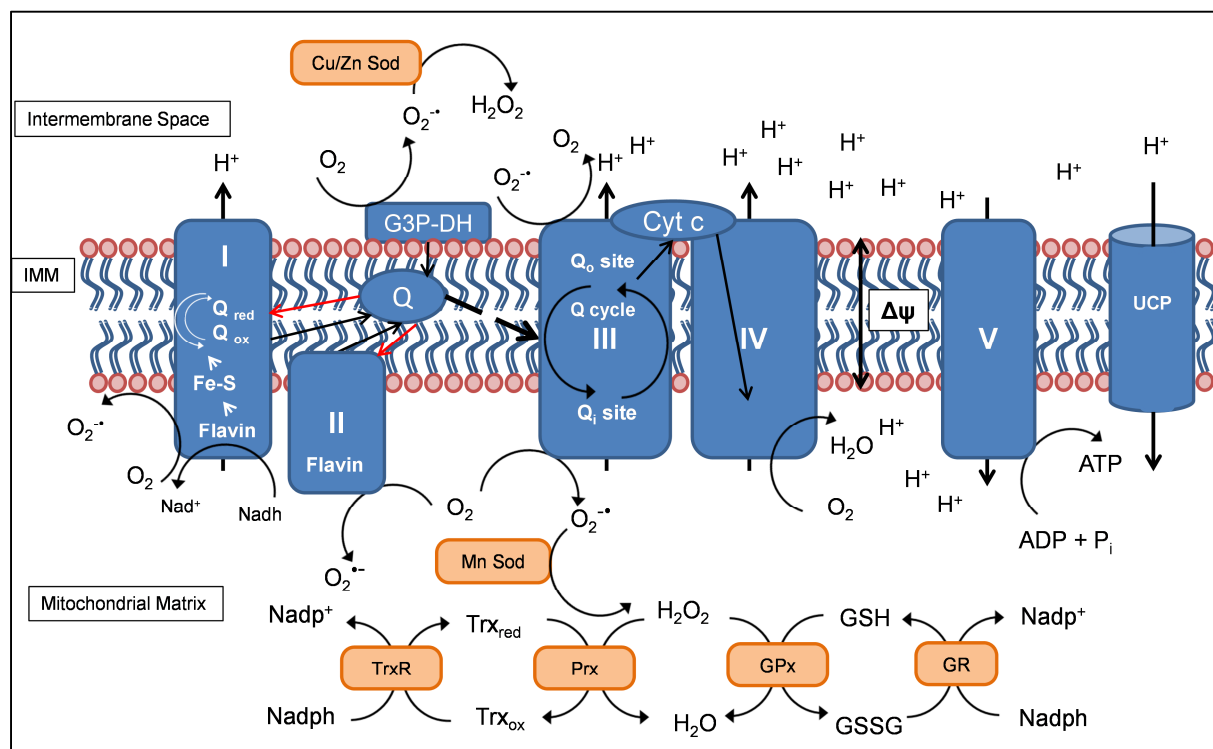
Figure 4: Sites of mitochondrial ROS production and detoxification processes
Description in the text

Within the physiological balance of the redox systems, ROS are nowadays accepted as signaling molecule maintaining essential cellular mechanisms, not only referring to superoxide and hydrogen peroxide, but also to nitric oxide and others (Bashan *et al.* 2009). When the availability of redox equivalents is outpaced by the generation of ROS, unfavorable oxidation occurs to macromolecules, especially proteins, fatty acids and deoxyribonucleic acid (DNA), the situation referred to as oxidative stress (Bashan *et al.* 2009). The balance of redox circuits (GSH, Trx) is critical and an oxidative shift may trigger pathologies (Jones 2008), (Fisher-Wellman & Neufer 2012). A redox-sensitive induction of antioxidative enzymes under the transcriptional control of nuclear factor erythroid-derived 2-like 2 (Nfe2l2 or Nrf2) provides a protective mechanism. This transcription factor is maintained inactive in the cytosol by its inhibitor Keap1. Conformational change due to oxidation of cysteine residues releases Nrf2 to translocate into the nucleus (Hansen *et al.* 2006). Antioxidative

enzymes include repair enzymes for oxidized lipids and proteins, chaperones and superoxide degrading enzymes (Kobayashi & Yamamoto 2006).

1.4.4 Fatty acid catabolism

Before initiation of breaking down fatty acids, activated fatty acids need to be imported into mitochondria using the carnitine shuttle. Activation of fatty acids is putatively carried out during import into the cell by fatty acid transport proteins. Additionally intracellular and intramitochondrial acyl-CoA synthases exist (Houten & Wanders 2010). At the outer mitochondrial membrane (OMM) carnitine palmitoyltransferase (Cpt1), an integral protein with two transmembrane domains (Rao *et al.* 2011), attaches carnitine to long chain fatty acids in exchange of Coenzyme A (CoA) (Figure 5). The activity of Cpt1 is coupled to the transport of activated fatty acids across the OMM by voltage-dependent anion channel (VDAC). In close contact an acyl-CoA synthase (Acsl) specifically activates long chain fatty acids (Lee *et al.* 2011a). The shuttling across the impermeable IMM is mediated by the carnitine acylcarnitine translocase (CACT) by importing the acylcarnitine and exporting free carnitine. Noteworthy this transport can be conducted in either direction. Inside the mitochondrial matrix, Cpt2 exchanges the carnitine residue back to CoA, thus the imported acyl-CoA is ready for breakdown (Houten & Wanders 2010). Short and medium chain fatty acids are able to penetrate through the membrane without active transport and are activated inside the mitochondria (Rinaldo *et al.* 2002). Fatty acids are first dehydrogenated by the specific acyl-CoA dehydrogenases for very long, long, medium, short chain acyl-CoA (Acad vl, l, m, s) feeding electrons to ETF. Resulting long chain enoyl-CoA undergoes the following three steps in a multi-enzyme complex the so-called mitochondrial trifunctional protein (mTFP). This membrane-bound complex catalyzes the hydration to 3-hydroxy-acyl-CoA, followed by dehydrogenation to 3-keto-acyl-CoA and finally cleavage of acetyl-CoA due to thiolase activity. The remaining acyl-CoA, shortened by two carbon-residues, is recycled through the four steps of β-oxidation. Depending on the chain length alternative enzymes take over the conversions catalyzed by mTFP (Rinaldo *et al.* 2002), (Houten & Wanders 2010). These specific enzymes for shorter acyl-CoAs (C ≤ 12) are crotonase, 3-hydroxy-acyl-CoA dehydrogenase (Hcdh), 3-ketoacyl-CoA thiolase (Acaa) for the release of acetyl-CoA (Wanders *et al.* 1999). Acetyl-CoA may alternatively arrive from glucose or amino acid breakdown (Owen *et al.* 2002). Reduction equivalents (Nadh) derived from either β-oxidation (Perevoshchikova *et al.* 2013) or TCA cycle (Satapati *et al.* 2012) are oxidized at complex I.
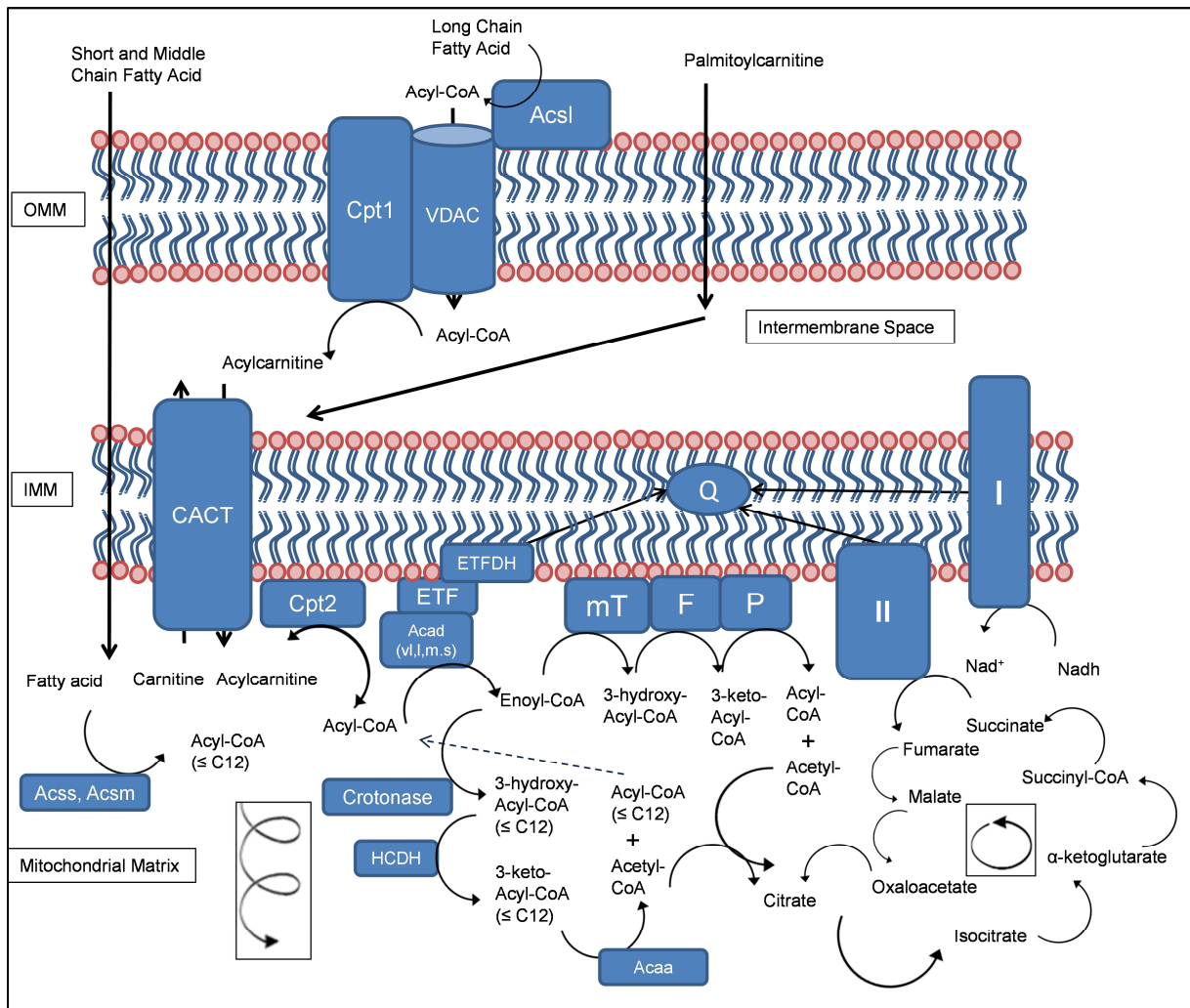
Figure 5: Principle of fatty acid import and break down in mitochondria

Description in the text

Acylcarnitines can be formed within the mitochondria (Houten & Wanders 2010). They can cross the IMM via CACT and are able to diffuse through membranes (Ramsay *et al.* 2001), especially acetyl-carnitine, the shortest representative (Schooneman *et al.* 2013). Acylcarnitines are present in the plasma and profiles of these lipid-species are routinely used as diagnostic markers for inherited disorders of enzymes involved in the β-oxidation (Wanders *et al.* 1999), (Schooneman *et al.* 2013). Rate limiting for the mitochondrial β-oxidation is the activity of Cpt1. This enzyme is reversibly blocked by malonyl-CoA, the basic block for de-novo lipogenesis (Houten & Wanders 2010), (Schooneman *et al.* 2013). Noteworthy, palmitoylcarnitine, as used to fuel isolated mitochondria, enters the mitochondria independently of Cpt1.

1.4.5   Mitochondrial functions beyond oxidative phosphorylation

Besides carbohydrates and fatty acids, amino acids can be used for substrate oxidation (Houten & Wanders 2010). Steps of amino acid catabolism take place in mitochondria, e.g. the breakdown of branched chain amino acids. Break down of amino acids, but also of odd numbered fatty acids (Chandler *et al.* 2011), provides intermediates of the TCA to refill intermediates that leave the mitochondria to serve as building block for gluconeogenesis and lipogenesis (Owen *et al.* 2002).

Moreover mitochondria detoxify hydrogen sulfide, which derives from the breakdown of sulfur containing amino acids by the transsulfuration pathway (Bouillaud & Blachier 2011). Nitrogen detoxification in terms of the urea cycle takes also place in mitochondria (Mitchell *et al.* 2009). Porphyrin, the iron-containing ring that heme consists of, is indispensable for many processes, e.g. oxygen transport or detoxification processes. The starting point, the last conversion of protoporphyrin and finally the attachment of iron are catalyzed by mitochondrial enzymes (Hamza & Dailey 2012).

Synthesis of complex lipids is achieved in mitochondria, in cooperation with the ER. The synthesis of phospholipids is crucial for maintenance and enlargement of biological membranes. Parts taken care of by mitochondria are the synthesis of phosphatidyl-ethanolamine from phosphatidylserine, which is shuttled into mitochondria from the ER (de Brito & Scorrano 2010). Proceeding from that, phosphatidylcholine is synthesized back in the ER via the PEMT pathway which transfers methyl-groups derived from adenosyl-methionine to phosphatidylethanolamine (Cole *et al.* 2012). Phosphatidylcholine is the main phospholipid present in lipoproteins involved in regulation of VLDL secretion (Cole *et al.* 2012). In addition mitochondria take part in the regulation of intracellular Ca^{2+} homeostasis (Raturi & Simmen 2013), (Rieusset 2011). Furthermore mitochondria act as sensors of exogenous or endogenous stressors and mediate the intrinsic apoptotic signaling (Guicciardi *et al.* 2013).

1.4.6   Mitochondrial function during aging

Mitochondrial function changes during aging. Oxidative damage to macromolecules is incompletely recovered and accumulates with increasing age hampering function. This is the main message of the "free radical hypothesis of aging" (Brewer 2010). Especially mitochondrial DNA is prone for oxidation (Gredilla *et al.* 2010). Damaged mtDNA produces less functional proteins, e.g. subunits of the respiratory chain complexes, thus increasing ROS production. This hypothesis was introduced as "mitochondrial theory of aging". Despite some critical aspects this hypothesis is regarded as potential, yet not mandatory mechanism

underlying the aging process (Alexeyev 2009). Bioenergetics functionally decline during aging. Electron transport slows, the ATP synthesis rate is reduced and the proton leak across the IMM is increased. For less efficient electron transfer reduced enzyme activity of complex I and IV is held responsible (Navarro & Boveris 2007). The arrangement of supercomplexes is deteriorated with increasing age (Frenzel *et al.* 2010). The observation of increased proton conductance of the IMM is captured in the hypothesis that higher rates of uncoupling reduce the membrane potential to attenuate the reducing pressure and therefore ROS production rates (Brand 2000). As extension of the free radical hypothesis of aging, the "redox hypothesis" describes a more oxidized balance within redox circuits and a consequently changed regulation pattern within the cellular metabolism (Jones 2008).

1.5   Mitochondria and insulin resistance in skeletal muscle

Reduced mitochondrial function was held causative for skeletal muscle insulin resistance, when a reduced mitochondrial mass and less active respiratory chain complexes were observed in skeletal muscle of diabetic and obese persons with impaired glucose homeostasis (Kelley *et al.* 2002), (Ritov *et al.* 2005). Furthermore reduced ATP synthesis rates were present in insulin-resistant first degree relatives of diabetic persons (Petersen *et al.* 2004). The accumulation of IMCL and the progression of insulin resistance could be caused by an inherited reduction in mitochondrial oxidative phosphorylation mediated by less substrate flux through mitochondria eventually impairing insulin signaling (Jelenik & Roden 2012). These major findings triggered a huge effort to understand the role of mitochondrial function in the pathogenesis of skeletal muscle insulin resistance.

The accumulation of fat in the muscle is an accepted consequence of chronic nutritional oversupply of fat. Acute hyperlipidemia, induced by lipid-infusion strongly reduces mitochondrial ATP synthesis (Jelenik & Roden 2012). There is a controversy regarding the regulation of fatty acid β-oxidation in the context of intramuscular fat accumulation. Insufficient capacity for oxidation of fatty acids was associated with higher levels of IMCL and lipid-derivatives like DAG or ceramides that promote insulin resistance. This connection has been challenged because a pile of studies in humans and rodents strongly indicate that mitochondrial capacity is far beyond the requirements and unlikely to exhaust (Muoio & Neufer 2012). Incomplete fatty acid oxidation, despite higher oxidation rates, potentially causes an excessive efflux of acylcarnitines from muscle (Koves *et al.* 2008). Conclusively it was suggested that in the state of high fat feeding cycles of β-oxidation mismatches the capacity of the TCA cycle leading to a depletion of TCA cycle intermediates. To date, of note,

the mechanistic link between acylcarnitine release and insulin resistance is missing (Schooneman *et al.* 2013).

A competitive view places elevation of H_2O_2 production due to chronically high dietary fat intake in presence of normal mitochondrial function, as trigger for insulin resistance. Experimentally evidenced in rats and C57BL/6J mice (Anderson *et al.* 2009), mitochondrial derived H_2O_2 provokes eventually a shift in redox environment, which activates stress-sensitive kinases when the buffer capacity of inhibitory phosphatases is exceeded and consequently blocks insulin signaling (Fisher-Wellman & Neufer 2012). Especially fatty acid oxidation harbours the potential to generate high rates of ROS production (Perevoshchikova *et al.* 2013). Converse results rather suggest oxidative stress to arise as consequence of skeletal muscle insulin resistance and progressively damaging mitochondria (Bonnard *et al.* 2008).

In recent years the controversy continued, insisting that there are conditions, when mitochondria contribute to skeletal muscle insulin resistance, especially when referring to the situation in humans (Goodpaster 2013). Yet there is no definite evidence that changes in mitochondria, neither functionally nor simply by abundance, cause insulin resistance in skeletal muscle (Dumas *et al.* 2009), (Muoio & Neufer 2012), (Holloszy 2013), (Schrauwen *et al.* 2010), (Jelenik & Roden 2012).

1.6   Mitochondria in fatty liver

Mitochondrial function tissue-specifically differs in general. Liver mitochondria produce more efficiently ATP by consuming less oxygen compared to skeletal muscle (Jelenik & Roden 2012). In this context lower rates of proton leak can be measured in the liver (Brand 2000). Functional assays failed to reveal a clear condition of mitochondrial bioenergetics to an insulin resistant state, as oxidative phosphorylation was either found increased, decreased or unchanged. Generally spoken, the same assumption of imbalanced fatty acid oxidation with respect to energy requirements can be applied for the liver as for muscle. Reduced β-oxidation may provoke lipid storage, whereas increased β-oxidation induces ROS production by creating high reduction pressure (Vial *et al.* 2010). As some studies connect the development of fatty liver with increased rates of β-oxidation, this may be regarded as compensative mechanism which is abrogated when ROS production rates exceed limits of compensation (Serra *et al.* 2012). The exact causalities of fat accumulation in the liver, especially the chronology of events is still under debate including the exact contribution of mitochondria (Vial *et al.* 2010).

1.7   Choice of mouse model and questions that will be addressed in this work

The inbred mouse strain C57BL/6J is widely used and accepted in the research of metabolic disease. It was characterized as mediate, but robust responder to high fat diet induced obesity in comparison to other frequently used inbred strains (Montgomery *et al.* 2013). Furthermore this mouse strain serves as valid model to monitor the development of skeletal muscle insulin resistance (Hoeks *et al.* 2011) and Nafld and was appreciated to provide basic understanding in the molecular pathways underlying metabolic adaptation (Nakamura & Terauchi 2013).

The controversial picture of mitochondria in the development of insulin resistance, the hallmark of type 2 diabetes, requires further research. For skeletal muscle the dependency of mitochondrial oxidative capacity and ROS production is aimed to be elucidated in the timeline of diet induced glucose intolerance. The hypothesis that mitochondria release uncontrolled amounts of acylcarnitines was tested by monitoring acylcarnitine concentrations directly at isolated mitochondria. The glutathione system was investigated to depict the state of the redox environment and the relation to actual rates of H_2O_2 production by mitochondria using a fatty acid-derived substrate.

The inconclusive data regarding the contribution of mitochondria to fatty liver in the complex fat processing in hepatocytes requires the illustration of the interplay of lipid metabolizing organelles in liver cells. Therefore a proteome analysis sought to clarify how mitochondrial pathways correlate with other organelles, especially the ER, when it comes to fat accumulation in response to a high fat diet. This was investigated in parallel with functional characterization of liver mitochondria paying particular attention to membrane potential and the related oxygen consumption and ROS production rates.

Mitochondrial function changes during aging and therefore it is essential to take into account that the challenge of high fat feeding may impact mitochondria in young mice to another extent than in older mice. Therefore adolescent, young adult and middle-aged mice were investigated to delineate diet- and age-specific effects in the development of diet induced obesity on metabolism in liver and skeletal muscle.

2   Material and Methods

Suppliers of all chemicals, kits, enzymes, antibodies and instruments are listed in the appendix (Table 14). When data were collected by cooperation partners, material and methods are described as provided by the contact person.

2.1   Mouse feeding studies

2.1.1   Housing, mice and experimental design

For all feeding experiments mice were single housed under standard housing conditions (12h/12h light/dark cycle and room temperature) with food and water ad libitum in a specific pathogen free (SPF) facility. Hygienic standards were approved every three months according to international (FELASA) guidelines.

Before feeding experiments were started, all mice received control diet for one week to acclimatize to the purified research diet. Mice were body mass matched before dividing them into control and high fat-fed group. Experimental diets consisted of defined nutrient sources with 12 energy-% fat in the control diet and 48 energy-% fat in the high fat diet. These research diets only differ in their fat amount by adding palm oil and reducing corn starch (Figure 6) to exclude that dietary influences others than fat content cause metabolic changes in the mice. The detailed fatty acid composition is presented in the appendix (Table 15).
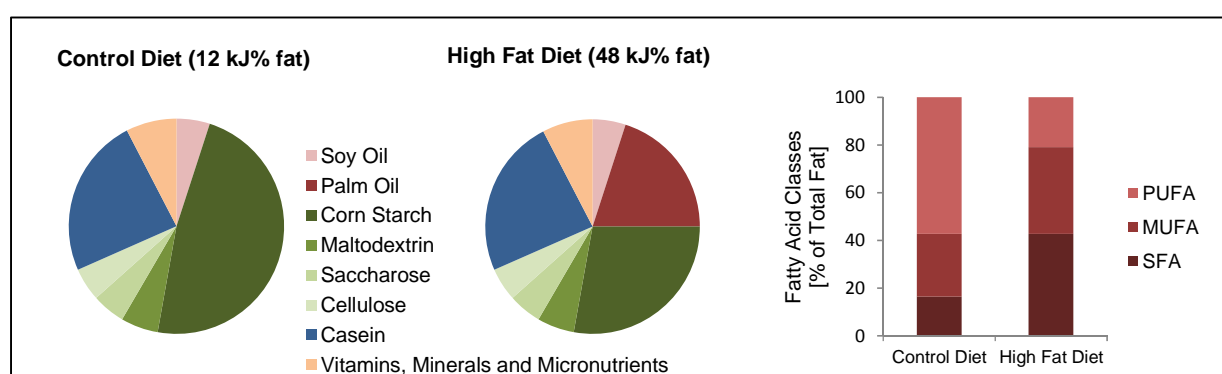
Figure 6: Composition of experimental diets and fatty acid composition

Parts of the pie chart represent weight percent; SFA – saturated fatty acids, MUFA – monounsaturated fatty acids, PUFA – polyunsaturated fatty acids

At onset of feeding mice of the adolescent group were 8 weeks old, young adult mice were 16 weeks of age and middle-aged mice were 52 weeks of age (Figure 7). Feeding experiments were performed for 1.5 weeks, 9 weeks and 26 weeks. Body composition was assessed using nuclear magnetic resonance (NMR) at the start and the end of the feeding experiment and before intraperitoneal glucose tolerance tests. At the end of the feeding period mice were fasted for 6 hours. Mice were killed by exposure to CO_2 until respiratory arrest and subsequent blood withdrawal from the vena cava. All protocols for animal experiments were conducted in accordance with the German guidelines for animal care and approved by the Department of Veterinary Affairs of the government of Oberbayern/Germany (Gz.: 55.2-1-54-2532-87-13). Adolescent and young adult male C57BL/6J mice were bred in house. One year old male C57BL/6J mice were purchased from Charles River.
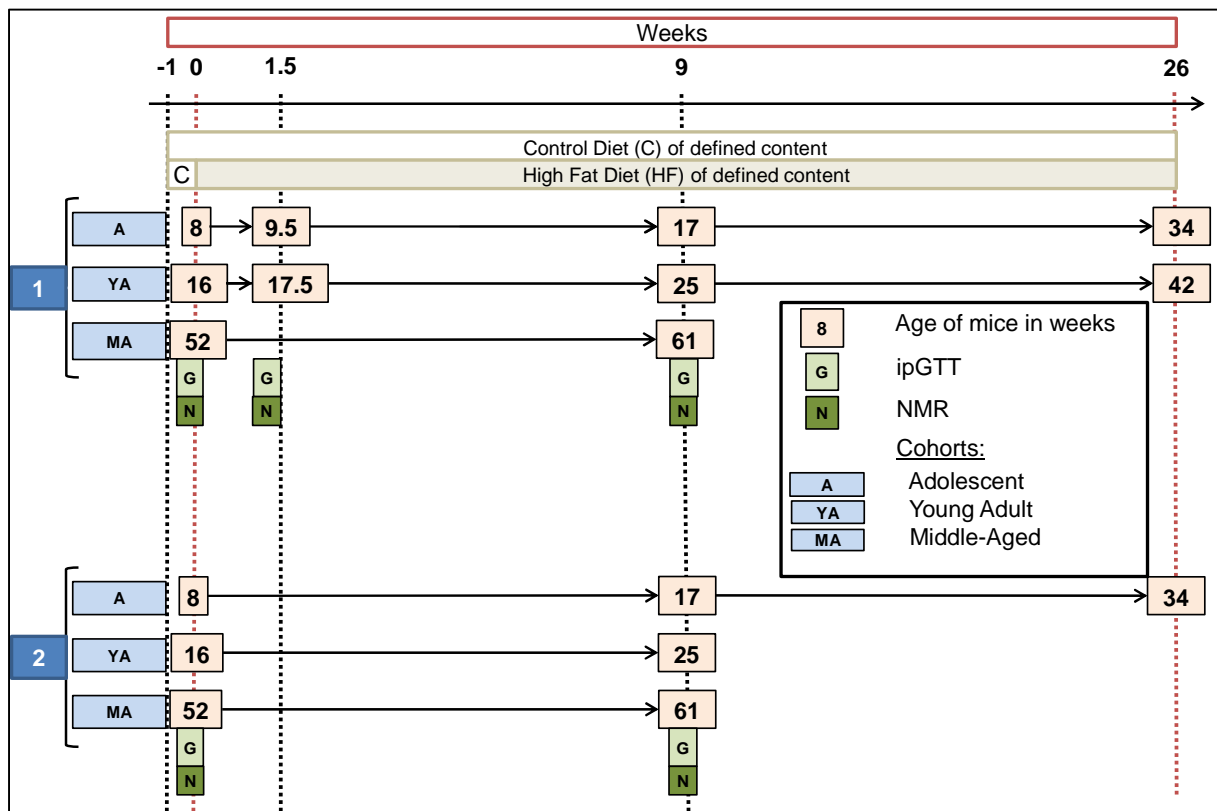
Figure 7: Workflow of the feeding experiments

Experimental setting 1 characterizes skeletal muscle mitochondria and setting 2 investigated the function of liver mitochondria.

2.1.2   *Intraperitoneal glucose tolerance test and fasting insulin*

An intraperitoneal glucose tolerance test (ipGTT) illustrates the process of glucose removal from the blood after a defined glucose injection and therefore provides information about the metabolic response to glucose consisting of insulin secretion and insulin action.

After a 6-hourly fast, which is recommended for ipGTT tests (Ayala *et al.* 2010), mice received 2.6 mg glucose per g lean mass, which approximates the amount of glucose calculated as 2 mg glucose per g body mass in a lean 25 g mouse. Blood glucose was monitored before the glucose injection and 15, 30, 60 and 120 minutes afterwards using a commercial hand-held glucometer. Blood droplets were received by a small incision at the tip of the mouse tail. As measure for glucose tolerance the total area-under-the-curve (AUC) was calculated by the trapezoidal rule (Andrikopoulos *et al.* 2008). As second measure the incremental AUC (iAUC) was calculated. For this only the increase above the fasting glucose concentration is calculated up to the time point when the initial blood glucose level is reached again. Therefore the incremental AUC accounts for differences in the basal blood glucose concentration to distinct between fasting hyperglycemia and the rate of glucose clearance.

Blood obtained after killing was centrifuged in heparin-coated tubes for plasma preparation for 5 min at 2000 x g. Plasma was frozen at -20°C. Insulin concentrations were determined using a commercial ELISA kit, which uses the method of an enzyme immunoassay in the sandwich order. In general the kit provides a 96 well plate coated with an anti-insulin antibody. Samples were prepared and incubated according to the manufacturer's instructions. The peroxidase coupled to the second antibody, was provided with its substrate 3,3',5,5'-tetramethylbenzidine. The reaction product is proportional to the amount of bound second antibody and therefore insulin was read photometrically at 450 nm in an absorbance plate reader.

2.2   **Tissue preparation and enrichment of liver mitochondria**

Liver was excised and the gall bladder was carefully removed. One defined lobe was removed and immediately frozen in liquid nitrogen. The remaining liver tissue was placed in ice-cold IP buffer with BSA. The liver was finely minced and rinsed in buffer IP with BSA to remove blood and connective tissue. The minced liver tissue was transferred to a glass homogenizer with Teflon pestle, homogenized with five strokes and centrifuged (Sorvall Evolution RC) at 800 x g for 10 min at 4°C to remove cellular debris. This step was repeated with the supernatant. Again, the supernatant was transferred in a new tube and pelletized at 9000 x g (10 min, 4°C). This crude mitochondrial fraction was resuspended in 1 ml of buffer

IP with BSA and dispersed on a density-gradient using Percoll®. The basis of this reagent is colloidal silica coated with polyvinylpyrrolidone with well-defined properties suitable for density centrifugation (Pertoft *et al.* 1978). For the three layers of the gradient Phase A, B and C were prepared and then mixed with Percoll® to the final concentration of 18 % (v/v) in Phase A, 30 % in Phase B and 60 % in Phase C, which results in a final sucrose concentration of 300 mM. Gradients consisting of 4 ml per Phase were casted in a 15 ml screw cap tube. After adding the mitochondrial crude fraction, the gradient tubes were centrifuged at 4500 x g for 30 min in a precooled (4°C) swinging buck rotor centrifuge (Eppendorf 5804 R). Mitochondrial protein, which was enriched at the layer between phase B and C (Figure 8) was carefully removed using a Pasteur pipette and diluted in IP buffer without BSA. Mitochondrial-enriched protein was pelletized at 9000 x g (10 min, 4°C) using the Sorvall Evolution RC centrifuge again. The pellet was resuspended in sucrose buffer IP without BSA and the last centrifugation step was repeated. The final pellet was dissolved in a minimum volume of IP buffer without BSA and protein concentration was determined using the Bradford reaction described in paragraph 2.8.1.
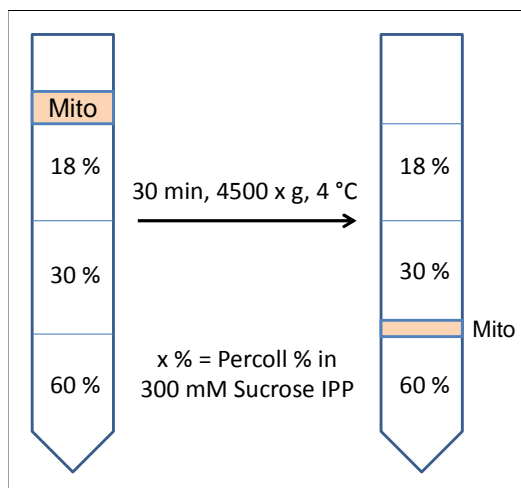
Figure 8: Percoll gradient centrifugation step

IP Buffer:
300 mM Sucrose, 5 mM TES, 0.2 mM EGTA; pH 7.2 at 4 °C with KOH,
with or without 0.1 % BSA (Albumin from bovine serum), freshly added

IPP Buffer:
300 mM Sucrose, 10 mM TES, 0.2 mM EGTA; pH 6.9 at 4 °C with KOH
with 0.1 % BSA (Albumin from bovine serum) freshly added

Phase A:

IPP Buffer + 23.9 g/l Sucrose

Phase B:

IPP Buffer + 44.2 g/l Sucrose

Phase C:

IPP Buffer + 154 g/l Sucrose

2.3   Tissue preparation and isolation of skeletal muscle mitochondria

For the preparation of isolated mitochondria, skeletal muscle tissue was collected from the hind limbs. The isolation method has been described elsewhere (Talbot & Brand 2005) with minor modifications. Summed up, skeletal muscle tissue, quickly freed from visible fat and connective tissue, was finely cut with scissors and rinsed in ice cold CP1 buffer. The minced tissue was stirred in CP2 buffer for 3 min on ice and further homogenized using a Polytron PT 3100 with a POLYTRON PT-DA 3020/2 dispersing aggregate three times for 4 s at 1800 U/min, followed by another 3 min stirring on ice. Mitochondrial fractions were now pelleted by differential centrifugation. All steps were conducted at 4°C for 10 min in the Sorvall Evolution RC centrifuge. Low centrifugation speed of 890 x g separates cellular debris from mitochondria, which remain in the supernatant. Consecutively the supernatant was transferred; mitochondrial protein was pelletized at 10400 x g and washed once by repeating the centrifugation step. The final pellet was spun down at 3800 x g and resuspended in a minimum volume of CP1 buffer. The protein concentration was determined using the Bradford method described in paragraph 2.8.1. For analysis in skeletal muscle tissue, gastrocnemius muscle (gcn), quadriceps muscle (QD) and tibialis anterior muscle (TA) of separate mouse cohorts were snap frozen and ground in liquid nitrogen. Mixed skeletal muscle refers to a mixture of QD and TA muscle.

CP1 Buffer:

100 mM KCl, 50 mM Tris-HCl, 2 mM EGTA, pH 7.4 at 4°C with KOH

CP2 Buffer (15 ml/mg tissue):

CP1 with additionally 1 mM ATP, 5 mM $MgCl_2$, 1 U/ml Protease from Bacillus licheniformis Type VIII (subtilisin A)

2.4   Triglycerides in tissues

Triglycerides in liver were analyzed using a commercial kit for detection of serum triglycerides, which was adjusted to the use in a 96 well plate. Tissue homogenates were prepared in a detergent-containing HB buffer. Liver and gcn tissue were finely ground in liquid nitrogen and 25 – 35 mg of the sample was added to 750 µl HB buffer. The samples were homogenized for 90 sec at maximum frequency (30/s) in a speed mill (Tissue Lyser II) and centrifuged at 23100 x g for 15 min at 4°C (Eppendorf 5417 R). The supernatant was transferred and heated up to 70°C while shaking for 5 min (Eppendorf Thermomixer Comfort). After cooling on ice for another 5 min, the homogenate was centrifuged as before. Protein concentrations were determined in the supernatant using the bicinchoninic acid (BCA) method described in paragraph 2.8.2.

In tissue homogenates triglycerides are cleaved by lipoprotein lipase and free glycerol is then converted to glycerol-1-P by glycerol kinase. In the next step glycerol-phosphate oxidase produces dihydroxyacetone-phosphate together with hydrogenperoxide which catalyzes the enzymatic generation of a quinoneimine dye with an absorbance maximum at 540 nm. The procedure is split into two measurements. Reagent A and B are provided by the kit. On the 96 well plate (Nunc transparent plate F96), 5 µl of each sample was incubated for 15 min at room temperature while shaking with 100 µl of Reagent A, which detects free glycerol by the procedure described above. After absorbance detection (Tecan Infinite M200) 25 µl of Reagent B was added, which contains lipase, and consequently glycerol from triglycerides is released. The incubation step was done as before and again absorbance was detected at 540 nm. Samples were measured in technical triplicates. For calculating the amount of triglycerides, the first abundance was subtracted from the second and the concentration was determined on basis of the glycerol standard curve measured in parallel.

HB Buffer:
10 mM NaH_2PO_4, 1 mM EDTA, adjusted to pH 7.4, 1 % v/v Polyoxyetylen-10-tridecylether, storage at 4°C

2.5   Phospholipid composition of isolated mitochondria

The phospholipid composition of isolated skeletal muscle and liver mitochondria was analyzed in a cooperation project with the University of Veterinary Medicine in Vienna according to a published protocol (Valencak *et al.* 2003). In short the phospholipid fraction of isolated mitochondria was extracted and separated on a silica gel thin layer chromatography plate (Kieselgel 60, F254, 0.5 mm, Merck). After visual detection under UV light the isolated fraction was transesterified, extracted by hexane and analyzed by gas liquid chromatography (Perkin Elmer Autosystem XL with Autosampler and FID; Norwalk, USA). Comparison of retention times with fatty acid methyl standards allowed identification of fatty acid moieties, which were expressed as weight percentage (wt %) (Valencak & Ruf 2011). The analysis comprised C 14-0, C 15-0, C 16-0, C 17-0, C 18-0 (summarized as saturated fatty acids, SFA), C 16-1(n-7) and C18-1(n-9) summed up as monounsaturated fatty acids (MUFA), C 18-2(n-6) and C 20-4(n-6) representing n6-fatty acids, C 18-3(n-3), C 20-5(n-3), C 22-5(n-3) and C 22-6(n-3), all n3-fatty acids, which are taken together with the n6-fatty acids as polyunsaturated fatty acids (PUFA).Unsaturation Index (UI) was calculated as described before (Couture & Hulbert 1995). Dr. Teresa Valencak performed the experiments.

2.6   Transmission Electron Microscopy of isolated mitochondria

Gastrocnemius muscle of each three adolescent control and high fat-fed mice was dissected and rapidly cut into cubes about 1 x1 x 1 mm length using a scalpel. Tissues were fixed in 2.5% electron microscopy grade glutaraldehyde in 0.1 M sodium cacodylate buffer pH 7.4 (Science Services, Munic, Germany), postfixed in 2% aqueous osmium tetraoxide dehydrated in gradual ethanol (30–100%) and propylene oxide, embedded in Epon (Merck, Darmstadt, Germany) and cured for 24 hours at 60°C. Semithin sections were cut and stained with toluidine blue. Ultrathin sections of 50 nm were collected onto 200 mesh copper grids, stained with uranyl acetate and lead citrate before examination by transmission electron microscopy (Zeiss Libra 120 Plus, Carl Zeiss NTS GmbH, Oberkochen, Germany). Pictures were acquired using a Slow Scan CCD-camera and iTEM software (Olympus Soft Imaging Solutions, Münster, Germany). This was done in cooperation with Research Unit Analytical Pathology at the Helmholtz Center Munich and measurements were conducted by Dr. Michaela Aichler.

2.7 Mitochondrial content

2.7.1 Citrate Synthase Activity

Citrate Synthase (CS) connects oxaloacetate and acetyl-CoA to citrate by releasing coenzyme A (CoA). The thiol-group of free CoA can be detected spectrometrically at 412 nm by its coupling to 5,5' dithiobis(2-nitrobenzoic) (DTNB) acid with NTB^{2-} as byproduct.

For tissue homogenates, 25-35 mg of ground muscle tissue and 15 – 20 mg of ground liver tissue were weight and added to 0.75 ml of ice-cold homogenization buffer. The tissue was homogenized in the speed mill (Tissue Lyser II) for 2 min at maximal frequency (30/s) using two stainless steel beads. Protein extraction was finished by 13000 x g centrifugation at 4°C for 10 min (Eppendorf 5417 R). Protein concentration was determined in the supernatant using the Bradford method (described in 2.8.1). For CS activity assay in tissue homogenates 10 µg and in mitochondrial preparations 5 µg protein were diluted 1 to 10 in assay buffer. Triton X 100 was added to 0.1 % (v/v) to the dilutions. On the 96 well plate (Nunc transparent F96) 10 µl per sample were added to the plate. The stock solution of DTNB was diluted 1 to 10 in assay buffer. End concentrations in 300 µl volume were 0.3 mM Acetyl-CoA and 50 mM oxaloacetate. Importantly, the measurement was started without oxaloacetate to define background absorbance at 412 nm. CS activity was initiated by injection of oxaloacetate after 5 minutes and absorbance was further followed for 10 minutes (Tecan Infinite M200). Measurements were carried out at 30°C. Three technical replicates were analyzed.

The CS activity is represented by the slope of increasing optical density at 412 nm over time. The slope of the forerun, which represents the background correction, is subtracted. The calculation of CS activity uses the depicted formula:

$$\text{Enzyme activity [µmol x min}^{-1} \text{ x mg}^{-1})] = [U/mg]: \quad \frac{\frac{OD}{min}*DF}{\varepsilon*dc}$$

OD/min – slope; DF – Dilution Factor; ε – extinction coefficient; d – coat thickness; c – protein concentration

The dilution factor is given by the volume of protein solution and the total volume. The extinction coefficient is defined for DTNB as 13.6 ml x µmol^{-1} x cm^{-1} (Alexson & Nedergaard 1988). Coat thickness is 0.75 cm in this type of plate filled with 300 µl. The protein concentration refers to the protein solution added first on the plate.

Homogenization Buffer:

50 mM Tris, 1 mM EDTA, pH 7.4 at RT with HCl

Assay Buffer:

100 mM Tris, 1 mM EDTA, 1 mM $MgCl_2$, pH 8.2 at RT with HCl

Stocks freshly prepared in Assay Buffer:

1 mM DTNB, 3.6 mM Acetyl-CoA, 3 mM Oxaloacetate

2.7.2   Mitochondrial deoxyribonucleic acid abundance

Mitochondrial deoxyribonucleic acid (mtDNA) abundance was measured using quantitative PCR in genomic DNA extracted from tissue homogenates using a commercial kit (Wizard® SV Genomic DNA Purification System). In short, about 20 mg of ground liver or 30 – 40 mg of ground muscle tissue was digested at 55°C over night and DNA was purified according to the manufacturer's instructions. Yield was quantified using the NanoQuant Plate (device of the Tecan Infinite M200). The nuclear primer pair targets an uncoding region in the murine chromosome 8 and the mitochondrial primer is directed around the chromosomal position 4300 assuring that amplification products of the primer pairs exclusively target mitochondrial and nuclear sequences respectively. For this procedure the LightCycler® 480 system was used with according consumables. Quantitative interpretation of PCR amplification was achieved by light emitting probes (Universal Probe Library, Roche). Ct-values, which define the cycle number, when amplification-related light emission exceeds the background, were used to calculate the initial amount of DNA assuming product doubling per cycle. Mitochondrial DNA abundance was related to nuclear DNA abundance.

Primer Sequences:

Mt left:	Mt right:
CAAATTTACCCGCTACTCAACTC	GCTATAATTTTTCGTATTTGTGTTTGG
Probe No. 101 (cat. no. 04692195001)	

Nuclear left:	Nuclear right:
TTTACAGGATCTCCAAGATTCAGA	GATCACCCCATGTGAACAAA
Probe No. 26 (cat. no. 04687574001)	

Volume/reaction:		*PCR Program:*
gDNA (25 ng/µl)	4 µl	95°C 5min
Primer left (20 µM)	0.2 µl	95°C 10 sec ⎤
Primer right (20 µM)	0.2 µl	60°C 20 sec ⎬ x45
Probe	0.2 µl	72°C 2 sec ⎦
ProbesMaster (2x)	5 µl	72°C 3min
Nuclease-free water	0.4 µl	
Total Volume	10 µl	

2.8   Protein Determination

2.8.1   Bradford Method

A ready-to-use reagent (RotiQuant) following the Bradford method for protein detection in aqueous solutions was applied according to manufacturer's instructions. The reaction of Coomassie Brilliant Blue G250 with proteins is proportionally to an absorbance shift and is detected at 595 nm (Bradford 1976). For recalculating protein concentrations, a standard curve of BSA (Albumin Fraction V) was diluted in the buffer, which was contained in the respective samples. Standard concentrations started at 0.2 mg/ml and went up to 2 mg/ml. Sample dilutions and standards were prepared in 50 µl volumes. RotiQuant reagent was diluted 2 parts in 5.5 parts distilled water, 200 µl was added per well (Nunc transparent F96). After 5 min incubation at room temperature absorbance change was detected photometrically (Tecan Infinite M200). Technical duplicates were carried out.

2.8.2   Bicinchoninic Acid Method

The bicinchoninic acid (BCA) Protein Assay Kit is a two component kit that applies the ability of peptide bonds to reduce Cu^{2+} to Cu^{1+}, which reacts with BCA and consequently changes the reagent's color (Smith *et al.* 1985). Absorbance was detected at 565 nm. The standard curve was prepared with BSA (Albumin Fraction V) spanning concentrations from 0.0625 mg/ml to 2 mg/ml. The assay preparation followed the manufacturer's manual. Plates and absorbance reader were used as described (2.8.1).

2.9 Oxygen consumption and respiratory capacity

2.9.1 Seahorse 96 Extracellular Flux Analyzer

Mitochondrial respiratory profiles were generated in the Seahorse 96 well Extracellular Flux Analyzer (96 XF). This allows eightfold technical replicates of biological samples with minimal amounts of mitochondrial protein. The principle of measurement was described for the 24-well format (Ferrick *et al.* 2008). Cartridges were preincubated with XF Calibrant (XF96 FluxPak) for at least 8 hours.

Mitochondria were diluted in 20 µl of respiration buffer. For analyses of skeletal muscle mitochondria 2 µg protein and for liver mitochondria 3 µg protein per well was used. Plates with added mitochondria were spun down at 2000 x g for 20 min in a precooled (4°C) swinging buck centrifuge (Eppendorf 5804 R) as described before (Rogers *et al.* 2011). While the initiation program (Protocol Step 1: Calibrate Probes) adjusts the cartridge in the machine, the wells containing mitochondria were filled up to 160 µl with respiration buffer including succinate and rotenone and warmed at 37°C until the machine was ready for measurement (15 – 20 min). Mitochondrial oxygen consumption was followed initially and after each of the two injections (Table 16 for protocol in the appendix).

Substrate oxidation was induced by succinate present in the respiration buffer and followed in the initial phase of the measurement. Maximal ATP – production was promoted by injection of ADP. Oligomycin was injected to block the ATP synthase. When palmitoylcarnitine/malate (PC/Mal) was used as oxidation substrate, mitochondria were incubated in respiration buffer and PC/Mal was injected with ADP for maximal physiological respiration. In parallel wells were injected with PC/Mal without ADP to induce leak respiration. Calculation of the oxygen consumption rate was automatically done by the seahorse 96 XF software version 1.3.

Buffer composition, final and stock concentrations relate to all functional measurements except indicated differently.

Respiration Buffer:
120 mM KCl, 5 mM KH_2PO_4, 3 mM Hepes, 1 mM EGTA, pH 7.2 with KOH and 0.3 % freshly added BSA (Albumin from bovine serum)

Final concentrations assaying liver mitochondria:
10 mM Succinate; 8 µM Rotenone; 6 mM ADP; 2.5 µg/ml Oligomycin; 4 µM FCCP; 4 µM Antimycin A

Final concentrations assaying skeletal muscle mitochondria either in Seahorse or clark electrode:

10 mM Succinate; 40 µM PC/5 mM Mal; 6 mM ADP; 2.5 µg/ml Oligomycin; 1 µM FCCP; 4 µM Antimycin A; 8 µM Rotenone

Storage Stocks of substrates and chemicals either in Seahorse or clark electrode:

1 M Succinate in H_2O, pH 7,4; 2.5 M Malate in H_2O, pH 7.4; 50 mM PC in H_2O

1 M ADP in H_2O, pH 7.4

2.5 mM Rotenone, 2 mg/ml Oligomycin, 2.5 mM FCCP, 2.5 mM Antimycin A, all in DMSO

Storage of aliquots at -20°C

2.9.2 Clark Electrode

Oxygen concentration is defined by a current from an energized (0.6 V) platinum cathode to an silver anode. The current is conducted by a potassium chloride solution and is proportional to the reduction of oxygen in the solution. The potassium chloride solution is separated to the experimental chamber via a polytetrafluoroethylene (Teflon) membrane, which is permeable to oxygen. Therefore, reduction of oxygen due to the current can be extrapolated to the oxygen concentration in the experimental solution (Clark *et al.* 1953), (Severinghaus 2002).

For monitoring oxygen consumption of isolated mitochondria a clark-type electrode (Digital Model 10) was used. The temperature was adjusted to 37°C and maintained by a water bath and with thermostat and pump (Julabo F12 and ED). The signal was transferred to a converter (Powerlab 26T) and displayed using the ChartLab6 software. One ml of warmed respiration buffer (see 2.9.1) was added to the stirred chamber together with 500 µg mitochondrial protein. The chamber was closed to avoid oxygen reflux. Substrates for oxidation, ADP and inhibitors were added with a Hamilton syringe via a small port in the chamber plug. Storage stocks and final concentrations were used as described (2.9.1).

Maximal oxygen concentration was defined as 406 nmol O per ml (Reynafarje *et al.* 1985). The slop of falling oxygen concentrations in the buffer over time was defined as oxygen consumption rate and calculated as nmol O_2 per min and mg protein. Due to limited sample material, technical replicates were done in duplicates.

2.9.3 Respiratory chain complexes' activity

Using a commercial platform for metabolic characterization, Mitoxis[®], the activity of respiratory chain complexes I to V was analyzed in gcn of adolescent and middle-aged mice. Enzyme assays were modified from established protocols: (Kramer *et al.* 2005), (Krahenbuhl *et al.* 1994) for Complex I to IV and (Bourgeron *et al.* 1992) for Complex V.

2.10   Membrane potential

2.10.1 Proton leak measurements

For liver mitochondria the proton leak was investigated. The monitoring of oxygen consumption measurements was applied in a Clark-type electrode coupled with a TPMP[+] filled electrode and a reference electrode containing potassium chloride. Thus simultaneously oxygen consumption and the distribution of TPMP[+] were recorded. This lipophilic cation accumulates in mitochondria depending on the proton gradient that is built over the inner mitochondrial membrane. The distribution follows the Nernst equation. A detailed description of the apparatus and the calculations is provided in Verena Hirschberg's thesis (Hirschberg 2012). A regression curve was fitted according to the modified exponential equation introduced before (Jastroch *et al.* 2012).

Liver mitochondria were diluted to 0.4 mg/ml in 2.5 ml respiration buffer. Complex I inhibitor rotenone, ATP-synthase blocker oligomycin and ionophore nigericin, which neutralizes the pH difference between mitochondrial matrix and the intermembrane space, were added, before respiration was initiated with succinate. In this condition mitochondria build up a proton gradient and oxygen consumption is only dependent on the basal leak. Succinate-dependent proton leak is competitively blocked by titrating malonate to define proton leak kinetics. For background correction, the chemical uncoupler FCCP was added which destroys the proton gradient. For calculating the absolute membrane potential in mV, a standard curve by titrating TPMP[+] concentration was carried out before each measurement. Oxygen consumption is plotted against membrane potential, which results in proton leak curves. Limitations in biological samples allowed two technical replicates.

Storage Stocks:

10 mM TPMP$^+$ in H$_2$O, stored at RT

1 M Succinate in H$_2$O, pH 7.4; 0.5 M Malonate in H$_2$O

2.5 mM Rotenone in DMSO; 2 mg/ml Oligomycin in DMSO; 100 µM Nigericin in pure EtOH;

2.5 mM FCCP in DMSO

Storage of aliquots at -20°C

Final concentrations:

Standard curve TPMP$^+$: 0.5 – 2.5 µM by titrating 5 x 2.5 µl of 0.5 mM working stock

10 mM Succinate, 7 µM Rotenone, 1 µg/ml Oligomycin, 0.15 µM Nigericin

Gradual inhibition of succinate dehydrogenase: 0.2 – 4.2 mM Malonate by successive

titrating 1, 2, 2, 4, 4 and 8 µl storage stock

1 µM FCCP

Nonlinear regression curve fit:

$y = a*x + b*e^{(c*x)}$

2.10.2 Safranin O assay

Relative membrane potential was analyzed by Safranin O, a fluorescent dye which distributes dependent on the membrane potential in the mitochondria or the buffer. Mitochondria were diluted to 0.1 mg/ml in 200 µl respiration buffer containing Safranin O. Rotenone was added, when succinate was used as substrate. The membrane potential was investigated in the in the presence or absence of ADP. Samples were assayed in triplicates on a black chimney shaped 96 well plate with transparent bottom and fluorescence was detected at excitation 495 nm and emission 586 nm (Tecan Infinite M200). After an initial phase of 5 minutes, PC/Mal or succinate were injected to allow mitochondria building up a membrane potential and steady state was monitored for another 10 minutes. Finally FCCP was manually added before measurements were continued. As membrane potential collapses all Safranin O accumulates in the buffer. Changes in membrane potential were calculated as difference of relative fluorescence units (RFU) in the uncoupled state after FCCP addition and RFU in response to substrate injection. This difference was expressed relative to the RFU when FCCP was injected (% Δ FCCP).

Storage Stocks:

8 mM Safranin O in respiration buffer without BSA, stored in black tubes at -20°C

other chemicals are described in 2.9.1

Final Concentrations:

8 µM Safranin O; 1 mM ADP; 8 µM Rotenone; 10 mM Succinate; 40 µM PC/5 mM Mal; 1 µM FCCP (50 µM working stock)

2.11   Reactive oxygen species production and cellular redox state

2.11.1 Hydrogen peroxide release by mitochondria

Superoxide, the predominant reactive oxygen species derived by mitochondria (Tahara *et al.* 2009), can be assessed indirectly by the release of hydrogen peroxide. Membrane permeable hydrogen peroxide (H_2O_2) reaches the mitochondrial surrounding and is converted by horseradish peroxidase (HRP) to form the fluorescent resorufin from Amplex Red, a well-documented molecule for assessing ROS production, in 1:1 stochiometry (Tahara *et al.* 2009), (Fisher-Wellman & Neufer 2012). Superoxide dismutase (SOD) was added to assure complete conversion of all superoxide directly released to the assay medium.

The procedure was described previously with minor modification (Grunz *et al.* 2012). Mitochondrial protein was diluted to 0.1 mg/ml in 200 µl respiration buffer. If not indicated differently, 0.3 % essential fatty acid-free BSA was added to the respiration buffer. Change in fluorescence was followed 10 min before adding succinate/rotenone or PC/Mal, which initiates mitochondrial oxygen consumption. Rotenone was added with succinate to prevent electron backflow to complex I. After injection of substrates fluorescence was detected for 30 min at excitation 560 nm and emission 590 nm (Tecan Infinite M200). Samples were analyzed in triplicates using black chimney shaped 96 well plates with clear bottom.

Substrate-specific hydrogen peroxide production was investigated in absence and presence of ADP. The increase of RFU over time was used to calculate hydrogen peroxide production rates. Therefore the slope after injection was corrected for background fluorescence assessed in the forerun. Absolute rates were calculated from H_2O_2 standard curves, for which a defined amount of hydrogen peroxide was added to the wells, which contained the assay medium as described before. Mitochondrial preparations which underwent several freeze-thaw cycles were added to the standard curves to mimic protein background fluorescence.

Storage Stocks:

10 mM Amplex Red in DMSO stored in aliquots (dark tubes) at -20°C; 0.4 mM Rotenone in pure EtOH; 2000 U/ml SOD in H_2O stored in aliquots at -20; 1000 U/ml HRP in H_2O stored in aliquots at 4°C

Final concentrations:

50 µM Amplex Red; 30 U/ml SOD; 6 U/ml HRP

2 µM Rotenone; 1 mM ADP; 10 mM succinate; 40 µM PC/5 mM Mal

Hydrogen Peroxide Standard Curve:

100 µM H_2O_2 working solution freshly prepared; RFU plotted against 0.2 – 1 nmol H_2O_2 for standard curve

2.11.2 Oxidative stress markers and antioxidative enzyme activities

In a cooperation project using the commercial platform Mitoxis® concentrations of malondialdehyde (MDA) (Conti *et al.* 1991) and the enzyme activity of glucose-6-phosphate dehydrogenase (G6PDH) (Beutler 1975), both markers of oxidative stress, were analyzed in gcn of adolescent and middle-aged animals. Furthermore enzyme activities of Catalase (Johansson & Borg 1988), Cu/Zn- and Mn-Superoxide Dismutase (SOD) (McCord & Fridovich 1969) and the components of the glutathione redox system were assessed. In detail glutathione synthase (GS), glutamate-cysteine ligase (GCS), glutathione peroxidase (GPx) and glutathione reductase (GR), were analyzed according to modified protocols (Paglia & Valentine 1967), (Beutler 1984), (Huang *et al.* 1993), (Muscari *et al.* 1998).

2.12   Acylcarnitine release by isolated mitochondria

Mitochondrial preparations were diluted in respiration buffer (2.9.1) to 0.1 mg/ml in 200 µl containing PC/Mal and ADP to induce substrate oxidation. Stocks and final concentrations are described in 2.9.1. Mitochondria were incubated in open cups at 37°C while shaking (Thermomixer) to assure oxygen saturation in the buffer. Afterwards mitochondria were spun down at maximal speed for 1 min in a table centrifuge (Eppendorf 5417 C). The supernatant was collected and spotted on a whatman paper (6 mm diameter) which was dried at RT in a speedvac centrifuge (Thermo Savant SPD 111V). Then samples were extracted for 20 min while shaking with 5 mM ammoniumacetate in ethanol containing an internal standard mixture of acylcarnitines (Chromsystems Instruments & Chemicals GmbH, Germany). Samples were separated on a HPLC column (Agilent Technologies, Germany) and acylcarnitines were detected by mass spectrometry (QTrap 5500, AB Scienx, USA). Sample analysis was conducted by Alexander Haag.

2.13   Protein Expression

2.13.1 Proteome Analysis of isolated liver mitochondria

Comprehensive changes due to nutritional impacts require comprehensive insights into cellular events as made available by proteomic analyses (Oh *et al.* 2011). Here, the combination of high resolution of the LC-MS/MS instrument, which allows to depict a great variety of proteins, and the high accuracy in mass detection for unambiguous assignment of masses to peptides by the elaborate bioinformatic algorithms, provided a capable tool for analyses of complex proteomes of e.g. whole cell systems (Pachl *et al.* 2013).

For the proteome analysis pools of liver mitochondrial preparations were created for each age and diet group. A total of 100 µg protein per group was used for further processing. Samples were reduced and alkylated by 50 mM dithiothreitol and 55 mM iodoacetamide prior to subjection to the Filter Aided Sample Preparation (FASP) protocol (Wisniewski *et al.* 2009a) using Microcon YM-30 filter units (Sartorius stedim biotech, Goettingen, Germany). After overnight digestion, peptides were eluted from the filters with 50 mM triethylammonium bicarbonate. From each sample 20 µg of peptides were separated into six fractions by strong anion exchange (SAX) as described previously (Wisniewski *et al.* 2009b). Thus, from each digested protein pool 3 technical replicates were performed. Peptides were separated on a pipet-based anion exchanger, which was prepared by stacking 6 layers of a 3M Empore Anion Exchange disk (Sigma-Aldrich, Germany) in a 200 µl pipet tip.

Columns were equilibrated with 100 µl MeOH, followed by 100 µl 1M NaOH and 100 µl Britton & Robinson (BR) buffer (pH 11). Peptides were loaded in BR buffer (pH 11). Flow-through equals first fraction. Fractions were subsequently eluted with BR buffer solutions of pH 8, 6, 5, 4 and 3, respectively. Each flow-through was captured on a stage tip containing three layers of C18 One Empore disk (Sigma-Aldrich, Germany) and purified as described (Rappsilber *et al.* 2007).

LC-MS/MS was performed on an Orbitrap Elite mass spectrometer coupled to an Eksigent nanoLC 1 D+ ultra system as described previously with minor modifications (Pachl *et al.* 2013). Quantitative analysis was performed by Progenesis (version 3.1; Nonlinear Dynamics, Newcastle, UK) and the Mascot search engine (version 2.3.0, Matrix Science, London, UK). Proteins selected for further analysis have to be identified in mass spectra of at least two of three technical replicates in each experimental group.

Sequences were searched against UniProt Knowledgebase (UniProtKB) mouse (26.10.2010; 73,688 sequences; 32,749,371 residues). Statistical analysis was achieved using 'R' (version 2.12.1) (Team 2011). Proteins exhibiting more than 50% missing values across three

replicates were excluded. Raw protein abundance values were first normalized using Variance Stabilization Normalization (VSN) (Huber *et al.* 2002). VSN is able to stabilize the variance across the entire intensity range and addresses the error structure in the data. To investigate the data distribution and ensure the appropriate application of statistical tools, normal quantile-quantile plots were created for all protein intensities in each sample. Variance stabilization normalization was applied to the data and variance-mean dependences were visually verified. Differential expression of samples was assessed with a moderated linear model using the limma package (Smyth 2004) in Bioconductor (Gentleman *et al.* 2004). Differences in protein expression between groups were estimated with the least squares linear model fitting procedure and tested for differential expression with moderated Student's t-statistic via the empirical Bayesian statistics described in the limma package (Smyth 2004). We accepted or rejected the null hypothesis on the basis of p values computed for the omnibus B-statistic via limma at a specified significance level. p values were adjusted for multiple testing to control the false discover rate at 5%. For multiple testing adjustments, we calculated the false discover rate using the algorithm of Benjamini and Hochberg (Benjamini 1995). p values, with appropriate multiple testing adjustment to control the false discovery rate at 5% allowed to identify differentially expressed proteins. K-means clustering was used to cluster 'control' vs. 'high fat' time points. The number of clusters was selected based on raw patterns within the data based on z-score ranking. Genomatix Pathway Analysis (GePS) and Ingenuity Pathway Analysis (IPA; version 1642223) were used for pathway analysis. This project was conducted in cooperation with the Chair of Proteomics and Bioanalytics. Protein digest, SAX, LC-MS/MS and data processing were conducted by Fiona Pachl. Data were statistically analyzed by Amin Gholami.

Proteins described by "putative uncharacterized" were exemplarily double checked regarding mass spectrometry data and protein matching. Identified proteins always comprise a list of Uniprot entries including validated and putative uncharacterized peptide sequences. Putative uncharacterized hits described here were aligned to Uniprot IDs of respective characterized enzymes using Clustal Omega (Sievers *et al.* 2011). Sequence identity is summarized in the appendix (Table 28).

BR buffer:
20 mM acetic acid, 20 mM phosphoric acid 85 %, 20 mM boric acid;
titrated with NaOH to desired pH

2.13.2 Western Blot

Quantitative detection of proteins was performed by the Western Blot methodology. Sodium dodecyl sulfate – polyacrylamide gel electrophoresis (SDS-PAGE) was conducted according to the Laemmli method. Protein pools were prepared as for the proteome analysis, added up to 25 µl with distilled water and mixed with the same volume of the double concentrated denaturation buffer. Samples were heated up to 95°C for 5 min while shaking and 10 µl, which equals 20 µg pooled protein was loaded on a vertical polyacrylamid gel. After separation protein was transferred to a nitrocellulose membrane in a semi-dry blotting chamber. Constant current was applied according to the area of the membrane (1 mA per cm^2). Blotting buffer was soaked in three layers of blotting paper both beneath membrane and gel and above. Current was applied for 1 hour. The membrane was cut according to protein size and blocked for 1.5 hours at RT. Primary antibodies Nrf2 and Pgam5 were incubated over night at 4°C. After washing the membrane secondary antibodies were incubated at RT for 1.5 hours. Fluorescence intensities of dyes attached to the second antibodies were scanned in the Odyssey scanner. The membrane was further incubated with primary antibody directed against CS and Sod2 for 1.5 hours at RT. After applying the correspondent secondary antibodies, the membrane was scanned again. Quantitative analysis was carried out using ImageJ software (Schneider *et al.* 2012).

Denaturing buffer (2 x):
0.125 M Tris-HCl, 4 % SDS, 0.2 M Dithiothreitol (DTT), 20 % Glycerol, 0.2% Bromphenol blue, 5% β-mercaptoethanol

Collection gel 5 %:
0.8 ml Acrylamide (30 %), 1.25 ml collection gel buffer 4 x, 2.86 ml MilliQ water, 50 µl SDS (10 %), 30 µl AMPS (10 %), 10 µl TEMED

Collection gel buffer 4 x (pH 6.8):
0.5 M Tris

Separation gel 12.5 %:
4.17 ml Acrylamide (30 %), 1.25 ml separation gel buffer 8 x, 4.43 ml MilliQ water, 100 µl SDS (10 %), 50 µl AMPS (10 %), 5 µl TEMED

Separation gel buffer 8 x (pH 8.8):
3 M Tris

Stock (10 x) Running buffer:
0.25 M Tris, 2.5 M glycine, 1 % SDS; freshly diluted 1:10 in distilled water

Stock (10 x)Transfer buffer (pH 9.2):
480 mM Tris, 13 mM SDS, pH adjusted with glycine; freshly diluted 1:10 in water and a final concentration of 20 % (v/v) methanol

TBS (pH 7.6):
200 mM Tris, 740 mM NaCl; optionally 0.1 % Tween 20 was added for TBST

Blocking Buffer:
3 % BSA (Albumin Fraction V) in TBS

Primary Antibodies Dilutions:
Nrf2 1:2500 in TBS, Pgam5 1:3000 in TBST, CS 1:5000 in TBST, Sod2 1:10000 in TBST + 3% BSA (Albumin Fraction V)

Secondary Antibodies Dilutions:
Infrared dye-coupled antibodies against rabbit or mouse, 1:20000 in TBST, each singly incubated

2.14   Gene expression

2.14.1 RNA isolation

Messenger ribonucleic acid (mRNA) was isolated from ground tissue by a phenolic extraction (TRIsure) and purification on a minicolumn system (SV Total RNA Isolation System). Ground tissue was kept in liquid nitrogen until adding about 20 mg to 1 ml of TRIsure. The mixture was immediately homogenized (Miccra D9) for 20 sec and incubated for 5 min at RT. Addition of 200 µl chloroform was followed by vigorous shaking and centrifuguation at 4°C for 15 min at 12000 x g (Eppendorf 5417 R) for phase separation. The clear upper phase was transferred into a new cup and mixed with 500 µl 75 % EtOH in DEPC treated water. Diethylpyrocarbonate (DEPC) prevents RNA degradation by inhibition of RNase enzymes. According to the protocol of the RNA isolation kit, columns were assembled, RNA was attached to the columns, genomic DNA was degraded and columns were washed with EtOH containing buffer according to the manufacturer's protocol. Finally RNA was eluted with nuclease-free water. Concentrations were determined using the NanoQuantPlate, a device of the Tecan Infinite M200.

Integrity of RNA is evaluated by visualizing ribosomal RNA (rRNA) on an agarose-gel. In a final volume of 10 µl, 2 µg of the RNA-sample was filled up nuclease-free water and 2 µl 6 x loading dye was added. The mixture was incubated at 65°C for 10 min to linearize the

nucleotide strand, cooled on ice afterwards and separated on an agarose-gel containing a dye (RotiSafe) which stains ribonucleic acid. Two clear bands representing 18s rRNA and 28s rRNA indicate good RNA quality, which was investigated under UV-light. The electrophoresis chamber (Biozym) was filled with TAE running buffer.

Agarose Gel:
1 % agarose dissolved in TAE buffer, 5 µl/100 ml RotiSafe

TAE buffer (50 x stock):
2 M TrisBase, 0.3 M acetic acid, 50 µM EDTA
1 x TAE for gel preparation and electrophoresis

6 x loading dye:
10 mM Tris-HCl (pH 7.6), 0.2 % Orange G, 60 % glycerol, 60 mM EDTA

2.14.2 cDNA synthesis

Complementary deoxyribonucleic acid (cDNA) was transcribed from messenger mRNA template using the viral enzyme reverse transcriptase. The application was provided in a ready-to use kit (QuantiTect Reverse Transcription Kit) and manufacturer's instructions were performed. In short, 1 µg RNA was applied to an incubation step, which removes genomic DNA and afterwards a provided mixture of oligonucleotides and reverse transcriptase were added for cDNA transcription.

2.14.3 Quantitative Polymerase Chain Reaction (qPCR)

Amount of mature mRNA depends on gene transcription. The PCR technique uses primer pairs that specifically bind the transcript of interest and overstretch an intron to discriminate between amplification products derived from cDNA or genomic DNA contaminations. The quantitative approach uses SybrGreen, which intercalates into DNA. This dye is quantified photometrically and the Ct-value (cycle threshold) is defined, when the fluorometric signal exceeds the background fluorescence. Using a standard curve of cDNA dilutions, the Ct-value can be recalculated to the relative amount originate template in the cDNA. The abundance of the gene of interest was normalized to a housekeeping gene to correct for interindividual variance. The assay was performed in a 384 well format. Samples were analyzed in technical triplicates in the LightCycler 480. Primer sequences are provided in the

appendix (Table 17). After the amplification cycles a melting curve assured correct primer binding.

Volume/reaction:		*PCR program:*	
cDNA (1:20 dilution)	1 µl	Denaturation:	95°C, 7:00 min
Primer left (5 nM)	1.25 µl	Cycle:	97°C, 0:10 min
Primer right (5 nM)	1.25 µl		53°C, 0:15 min } x 45
SensiMix No-ROX (2x)	6.75 µl		72°C, 0:20 min
Nuclease-free water	2.25 µl	Melting Curve:	60 – 95°C continuous,
			5 acquisition points per °C

2.15   Statistics

Data were statistically analyzed using Two-Way ANOVA (SigmaPlot 12.5, Systat Software Inc.,USA). Data that are not normally distributed were transformed to the corresponding log(x+1) value and subsequently analyzed. Significance was accepted when p-values of the respective test were less than 0.05. Table calculations and linear regression were analyzed by the Excel2010 software (Microsoft, USA). In graphs and tables data are always presented as mean ± standard deviation. Graphs were created using the GraphPad Prism4 Software (GraphPad Software, USA).

3 Results

The mice were either 8 weeks of age (adolescent), 16 weeks of age (young adult) or 52 weeks of age (middle-aged), when the high fat feeding experiment was started. Of note, the order in all graphs and tables starts with adolescent and ends with middle-aged, meaning the orders goes from youngest to oldest age. The high fat diet differs from the respective control diet only in the energy percent provided by palm oil by reducing the portion of starch. The feeding of this high fat diet is the intervention that causes metabolic adaptations. The characteristics of these adaptations are described in the context of the body mass and composition, mitochondrial function in the skeletal muscle and in the liver.

3.1 Phenotypes after 9 weeks of feeding

3.1.1 Body mass and body composition

The mouse strain C57BL/6J is susceptible to diet induced obesity. Therefore the high fat feeding was supposed to induce body mass gain. Adolescent, young adult and middle-aged mice robustly gained mass, when fed a high fat diet (Figure 9 A). Two-Way ANOVA statistics with repeated measured tested the difference of body mass between control-fed and high fat-fed group for each time point, when the body mass was recorded. Each age group was tested separately. After 1 week, body mass of high fat-fed mice was significantly higher than body mass of the age-matched control-fed mice. The body mass gain after 9 weeks of high fat feeding was similar in adolescent and young adult mice, whereas middle-aged mice fed a high fat diet put on significantly more body mass (Figure 9 B). This describes an age-dependent response to the high fat diet regarding body mass gain. Interestingly, adolescent control-fed mice increased the body mass, whereas the body mass of young adult and middle-aged mice fed the control diet was stable Figure 9 B).

The body mass change in the high fat-fed groups was due to increased fat mass. This increase in fat mass in response to high fat feeding was dependent on the age of the mice: the older the mice, the higher the fat mass gain was due to the high fat diet (Figure 9 C). The fat mass of control-fed mice was not different between the age groups (Figure 9 C). There was a significant interaction between the diet and the age regarding fat mass gain. High fat diet feeding did not change the lean mass of mice compared the age-matched control-fed mice. Two-Way ANOVA statistics revealed significant interactions between the two independent parameters age and diet for the body mass and fat mass gain.

In a subgroup of mice representing each age, the development of body composition from start to the endpoint after 9 weeks was investigated more in detail by calculating the fat mass and lean mass gain respectively (Table 18). Adolescent mice on either diet put on lean mass during the feeding period. Young adult mice slightly increased lean mass independently of the diet, whereas middle-aged mice even decreased to a small extent the lean mass during the 9 week period. Fat mass was virtually unchanged in control-fed mice of either age group, but fat mass gain was the higher, the older the high fat-fed mice were. This effect reflects the total fat mass (Figure 9 C).
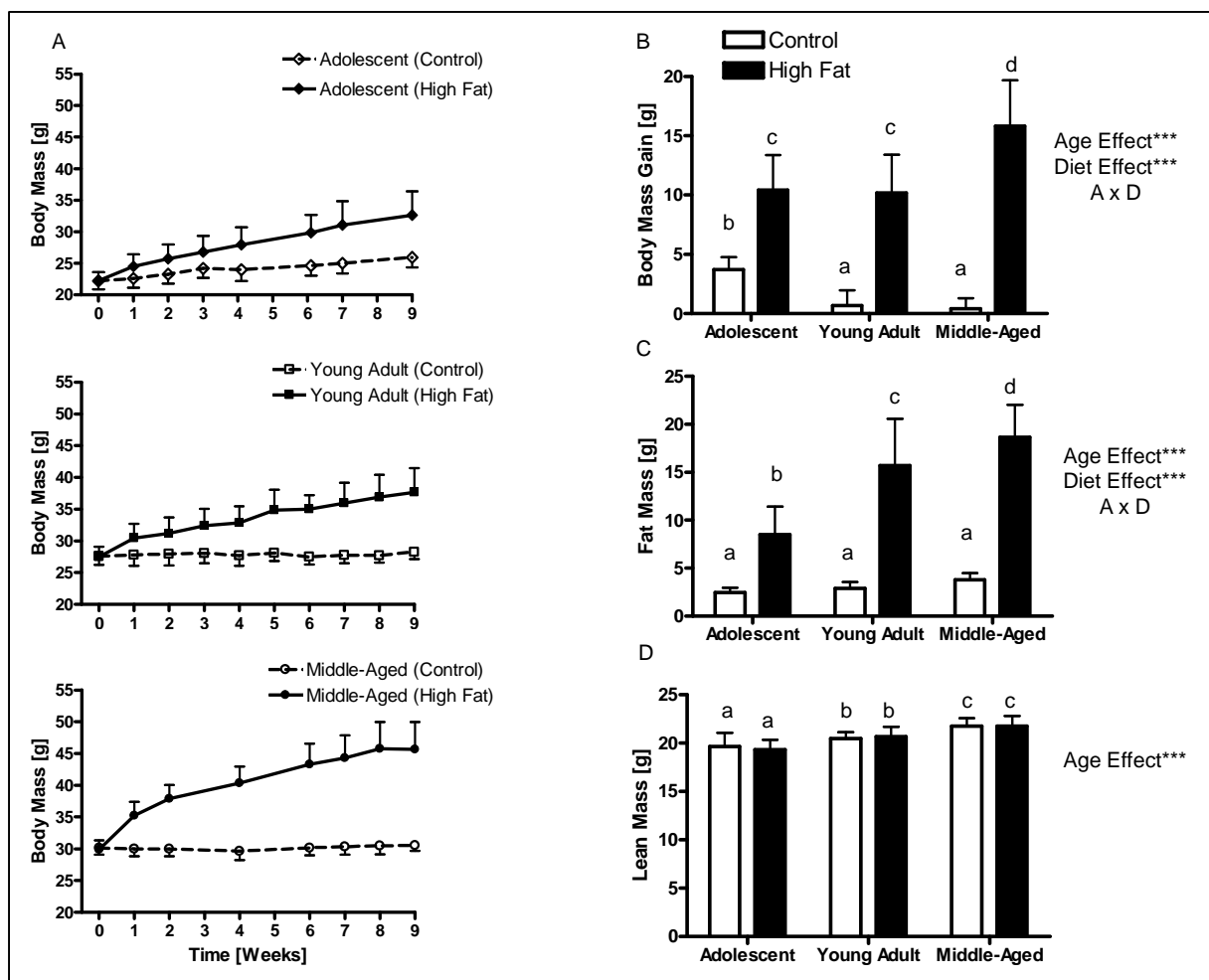
Figure 9: Body mass development and body composition after 9 weeks of high fat feeding.

A) Body mass development over 9 weeks of feeding in adolescent (n = 31), young adult (n = 32) and middle-aged mice (n = 24). Two-Way ANOVA with repeated measurements indicate significant differences in bodyweight between high fat-fed and control group of respective age after one week. B) Body mass gain after 9 weeks of feeding. Number of mice as in A); Two-Way ANOVA appoints general age effect, diet effect and interactions (A x D) with *** p < 0.001. Different letters indicate statistical difference after posthoc testing (Holm-Sidak). Fat mass (C) and lean mass (D) after 9 weeks of high fat feeding; statistic as in B); n = 14 for adolescent, n = 29 for young adult and n = 24 for middle-aged

Summed up, high fat feeding induced obesity in C57BL/6J mice. The older the mice at onset of high fat feeding, the more fat mass they accumulated. The adolescent mice representing the youngest group increased the lean mass independently of the diet, in other words, they still grew.

3.1.2   Glucose clearance and impaired glucose tolerance

Glucose tolerance is marked by the ability of the metabolism to balance the blood glucose concentration after a defined glucose load by the adequate release and effect of the hormone insulin. The influence of high fat feeding on the glucose homeostasis was investigated by intraperitoneal glucose tolerance tests (ipGTT). The first ipGTT was carried out directly before diet switch to avoid baseline differences between the diet groups. Due to technical difficulties the baseline measurement in the adolescent mice lacked the value at 60 min (Figure 10). The time points at 15, 30 and 120 did not reveal different blood glucose in adolescent mice before the high fat feeding was started. Therefore adolescent, young adult and middle-aged mice were considered well-matched regarding glucose tolerance for the diet groups (Figure 10 left column). After one week, young adult and middle-aged mice fed the high fat diet, already had increased blood glucose levels compared to the age-matched control-fed mice during the two-hourly monitoring following the intraperitoneal glucose injection. There was also a non-significant trend for increased blood glucose in adolescent high fat-fed mice (Figure 10 middle column). After 9 weeks of high fat feeding, blood glucose was elevated at least 30 and 60 minutes after the glucose application in adolescent, young adult and middle-aged high fat-fed mice compared to the age-matched control-fed mice (Figure 10 right column).

Glucose tolerance was more precisely analyzed by calculating the total area under the curve (AUC) and incremental AUC (iAUC) from the glucose curves. The iAUC describes the area above the fasting glucose concentration of the individual mouse and therefore corrects for hyperglycemia and concentrates on the dynamic of glucose clearance after the glucose injection. For the baseline measurement in the adolescent mice only the AUC was calculated due lacking value at 60 min the baseline measurement. The AUC in and iAUC were similar between the diet groups of the respective age at baseline (Figure 10 left column). Although glucose values did not significantly differ after 1 week of feeding between adolescent high fat-fed and control-fed mice, an increased AUC in the high fat-fed adolescent group indicated changed glucose tolerance. The iAUC was not different, so glucose clearance was not altered in adolescent high fat-fed mice after 1 week compared to the adolescent controls. In young adult and middle-aged mice fed a high fat diet, the iAUC was significantly increased

after 1 week of feeding compared to the age-matched control-fed mice (Figure 10 middle column). Therefore high fat-fed mice had already developed an impaired response to the glucose injection. Incremental AUCs did further increase in the high fat groups of all three ages after 9 weeks of high fat feeding (Figure 10 right column).
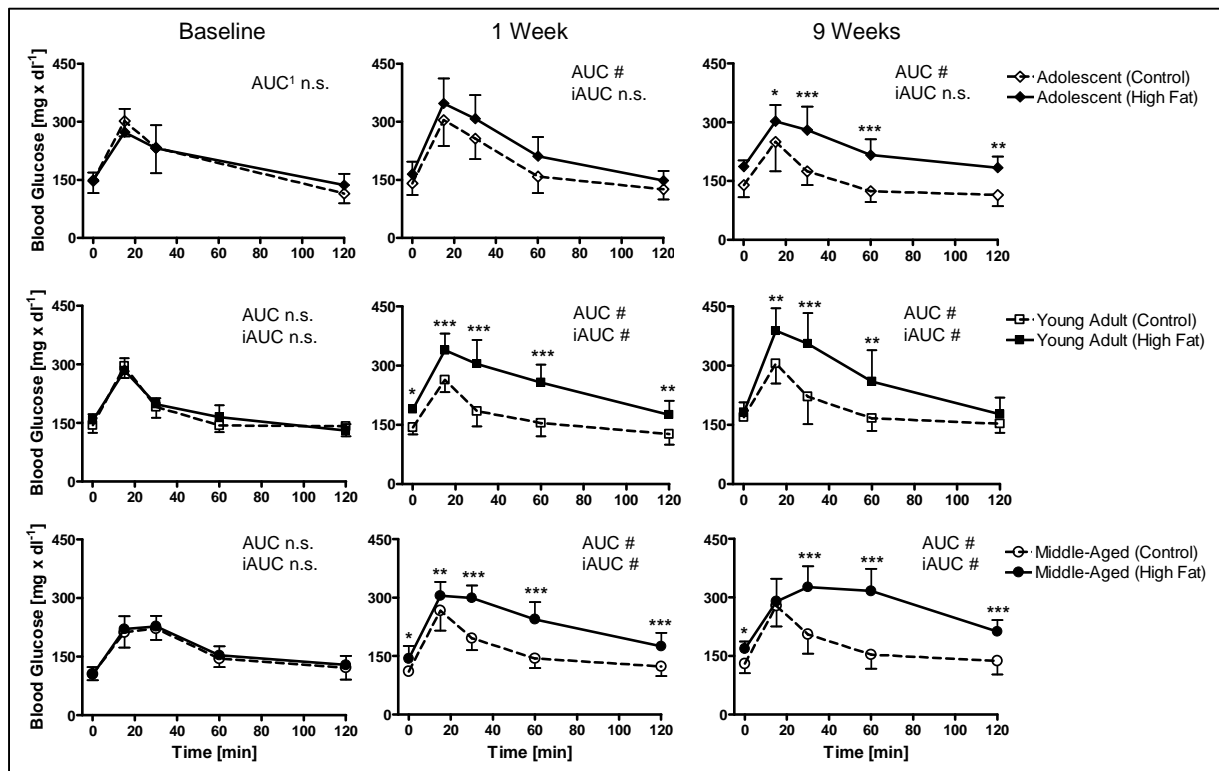
Figure 10: Intraperitoneal glucose tolerance tests during 9 weeks of high fat feeding in all three age groups

Baseline defines the time point just before diet switch. Differences of curves were tested by Two-Way ANOVA with repeated measurements. n = 6 per diet in the adolescent and young adult group; n = 12 per diet in the middle-aged group; * $p < 0.05$, ** $p < 0.01$, *** $p < 0.001$ by posthoc testing (Holm-Sidak). Area under the curve (AUC) and incremental AUC (iAUC) were tested by Two-Way ANOVA with repeated measurement for timeline. Hashtags refer to significant posthoc testing (Holm-Sidak)

Within the age groups the time line from baseline to the endpoint after 9 weeks was statistically analyzed to determine if the glucose homeostasis changes over time within one experimental group. In the young adult and middle-aged control-fed mice neither AUC nor iAUC changed over time. The adolescent control-fed mice showed a reduced AUC after 9 weeks when compared to the AUC after 1 week. In the adolescent high fat-fed mice did not change between the 9 week time point compared to the 1 week time point. In the young adult and middle-aged high fat-fed group the AUC and iAUC significantly increased after 1 week compared to the respective baseline. Both, total AUC and iAUC were not further increased after 9 weeks compared to the time point after 1 week in young adult high fat-fed mice. In middle-aged high fat-fed mice AUC significantly increased after 9 weeks compared to the

time point after 1 week, but the iAUC was unchanged when tested in these conditions (Appendix: Table 19). The comprehensive analysis of the glucose curves showed, that high fat feeding changed the glucose homeostasis in C57BL/6J mice. The older the mice are the more pronounced the effect of high fat feeding on glucose clearance was.

Hyperglycemia after fasting is another characteristic of alterations in the glucose homeostasis. Fasting blood glucose was determined before in the intraperitoneal glucose injections (Figure 10). Two-Way ANOVA was conducted with age and diet as independent variables. After 1 week of feeding, high fat diet significantly elevated fasting blood glucose. This holds true after 9 weeks. Within each age group Two-Way ANOVA was performed for the timeline. In adolescent and young adult high fat-fed mice hyperglycemia was not increased over time, whereas the hyperglycemia was increased during the time period in middle-aged high fat-fed mice (Figure 10). In comparable mouse cohorts fasting insulin was measured with respective fasting glucose after 9 weeks of high fat feeding. In all three age groups high fat diet induced hyperinsulinemia. In middle-aged mice fed a high fat diet for 9 weeks fasting insulin was dramatically increased compared to middle-aged control-fed mice and compared to the adolescent and young adult high fat-fed mice (Table 1). Taken together high fat feeding induced hyperglycemia and hyperinsulinemia. Aging exacerbated the development of hyperinsulinemia due high fat feeding.

Table 1: Fasting glucose and insulin after 9 weeks of high fat feeding in three different age groups

	Adolescent		Young Adult		Middle-Aged		Two-Way ANOVA
	Control	High Fat	Control	High Fat	Control	High Fat	
Fasting Glucose [mM]	8.9 ± 1.8^a	9.5 ± 1.3^a	8.9 ± 1.8^a	11.9 ± 1.2^b	7.2 ± 1.4^c	9.7 ± 1.0^a	*A, D*
Fasting Insulin [ng/ml]	0.6 ± 0.3^a	1.3 ± 0.6^b	0.6 ± 0.3^a	1.5 ± 0.5^b	$1.0 \pm 0.4^{a,b}$	4.2 ± 1.1^c	*A, D, A x D*

A – age effect, D – diet effect, n = 8 – 10 per diet and age group, different letters indicate significant differences upon posthoc testing (Holm-Sidak)

3.1.3   Phenotypic data after 26 weeks of feeding

The effects of a prolonged feeding period were monitored in adolescent and young adult mice. The high fat feeding induced constitutive body mass gain over the 26 week period. Adolescent mice started at a lower body mass than the young adult mice due to their pubertal age. Control-fed adolescent mice caught up with the young adult control-fed group after 26 weeks, whereas high fat-fed adolescent mice still weighed significantly less than

young adult high fat-fed mice. The body mass gain was identical in the high fat-fed groups (Table 2). Fasting insulin concentration was increased by high fat feeding. The fasting insulin in the adolescent and young adult high fat-fed mice after 26 weeks of feeding was similar to the middle-aged group after 9 weeks of high fat feeding. This result illustrates that hyperinsulinemia proceeded in the adolescent and young adult group when the high fat feeding was sustained.

Table 2: Phenotypic characteristics after 26 weeks of high fat feeding

		Adolescent		Young Adult		Two-Way ANOVA
		Control	High Fat	Control	High Fat	
Body Mass [g]	Baseline	22.9 ± 1.4^a	22.4 ± 1.8^a	27.2 ± 1.5^b	27.0 ± 1.2^b	*A*
	26 weeks	28.9 ± 1.3^a	44.5 ± 5.3^b	30.1 ± 1.0^a	49.3 ± 3.8^c	*A, D*
	Gain	6.0 ± 1.2^a	22.1 ± 4.9^b	2.9 ± 1.5^c	22.2 ± 4.1^b	*D*
Fasting Insulin [ng/ml]		0.5 ± 0.2^a	3.9 ± 2.7^b	0.9 ± 0.5^a	4.7 ± 3.1^b	*D*

A – age effect, D – diet effect, n = 10 – 13 per group for body mass,
n = 4 – 6 per group for fasting insulin, significant posthoc testing (Holm-Sidak)
is indicated by different letter

3.2   Mitochondrial characteristics and function in skeletal muscle

3.2.1   *Mitochondrial reactive oxygen species (ROS) production in skeletal muscle during the development of impaired glucose tolerance*

The hypothesis that reactive oxygen species (ROS) production in skeletal muscle mitochondria triggers impaired glucose tolerance and finally leads to skeletal muscle insulin resistance was tested. The development of impaired glucose homeostasis was assessed by ipGTT and described in detail in paragraph 3.1.2.

ROS production rates in isolated skeletal muscle mitochondria were tested after 1.5 weeks of feeding, when ipGTT indicates first changes in glucose homeostasis. The adolescent and young adult group of high fat-fed mice showed normal ROS production rates with complex-II linked substrate succinate. Rotenone was given to avoid reverse electron flow into complex I. After 9 weeks of high fat feeding in adolescent and young adult mice ROS production was still normal (Table 3). In absence of ADP ROS production of skeletal muscle mitochondria of young adult mice was lower than in adolescent mice. The presence of ADP abolishes this age effect between adolescent and young adult group after 9 weeks (Table 3). Pyruvate given with malate in absence and presence of ADP was exemplarily tested. There were no changes in the ROS production rate after 1.5 or 9 weeks of high fat feeding compared to the age-matched control-fed groups (data not shown). Palmitoylcarnitine with malate as fatty

acid derived substrate neither affected mitochondrial ROS production in skeletal muscle after 1.5 weeks (data not shown) nor after 9 weeks of high fat feeding (3.2.2).

Oxygen consumption was monitored with succinate/rotenone as substrate using the Clark electrode after 1.5 and 9 weeks of high fat feeding. Skeletal muscle mitochondria of high fat-fed mice consumed as much oxygen as mitochondria of control-fed mice of the respective age (Table 20 in the Appendix).

Table 3: Reactive oxygen species released by isolated skeletal muscle mitochondria fueled with succinate/rotenone after 1.5 weeks and 9 weeks of feeding

ROS Production Rate [nmol H_2O_2 x mg^{-1} x min^{-1}]		Adolescent		Young Adult		Two-Way ANOVA
		Control	High Fat	Control	High Fat	
1.5 weeks	- ADP	0.22 ± 0.13	0.21 ± 0.08	0.18 ± 0.04	0.17 ± 0.04	*n.s.*
	+ ADP	0.11 ± 0.06	0.09 ± 0.06	0.07 ± 0.04	0.05 ± 0.02	*n.s.*
9 weeks	- ADP	0.18 ± 0.06[a]	0.15 ± 0.04[a]	0.15 ± 0.02[a]	0.14 ± 0.01[a]	*A*
	+ ADP	0.04 ± 0.02	0.03 ± 0.01	0.05 ± 0.02	0.04 ± 0.01	*n.s.*

A – age effect, n.s. – not significant, n = 4 – 6 per group, significant posthoc testing (Holm-Sidak) by different letters

These data clearly demonstrate that mice fed a high fat-diet showed impaired glucose homeostasis together with hyperglycemia and hyperinsulinemia, but normal ROS production in skeletal muscle mitochondria. This does not support the hypothesis that elevated ROS production rates precede the impairment of the glucose homeostasis.

3.2.2   Skeletal muscle metabolism with excessive fatty acids supply in three different age groups

Increased fat storage in skeletal muscle is discussed as key feature combining lipotoxic effects of lipid excess and the accumulation of reactive fatty acid metabolites. Muscle mass was increased by high fat diet as indicated by Two-Way ANOVA (Figure 11 A). Posthoc testing corroborated this increase in gastrocnemius (gcn) muscle mass of young adult high fat-fed mice compared to the young adult control-fed group. Triglycerides accumulated after 9 weeks of high fat feeding in the gcn of all high fat-fed age groups (Figure 11 B). Thus, high fat feeding induced ectopic lipid accumulation.
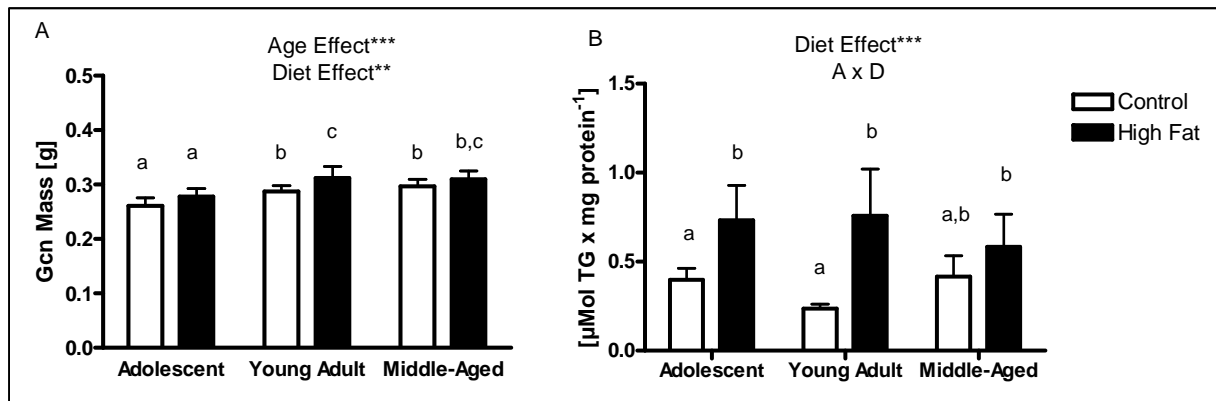
Figure 11: Mass and triglyceride content in gastrocnemius muscle after 9 weeks of high fat feeding.

A) Tissue mass represents the sum of both gastrocnemius (Gcn) muscle strands. B) Triglyceride (TG) in the gastrocnemius muscle of the respective mice. Two-Way ANOVA statistics are indicated with asterisks;** $p < 0.01$, *** $p < 0.001$, A x D – signficant interactions. Different letters origin in significant differences according to posthoc testing (Holm-Sidak). n = 5 – 6 per diet and age group.

3.2.2.1 Mitochondrial content and morphology in three age groups fed 9 weeks a high fat diet

The question whether high fat feeding influences mitochondrial biogenesis in skeletal muscle was addressed using the markers mtDNA abundance and citrate synthase (CS) activity. After 9 weeks of high fat feeding genomic DNA was isolated from mixed skeletal muscle of adolescent, young adult and middle-aged mice and the age-matched control-fed mice. The mtDNA abundance was not significantly different between the diet groups (Table 4). As alternative surrogate for mitochondrial protein CS activity is widely used (Hojlund *et al.* 2008). In mitochondrial preparations isolated from skeletal muscle the specific CS activity was measured. Irrespective of diet and age, CS activity was constant in mitochondrial preparations (Table 4). In tissue homogenates of mixed skeletal muscle, CS activity was higher in muscle of high fat-fed mice and increased with increasing age in general. Statistics using Two-Way ANOVA confirmed this diet effect. Interestingly, in adolescent mice CS activity was unchanged by high fat diet compared to the adolescent control-fed mice. To calculate mitochondrial protein mass in skeletal muscle, consequently, tissue CS was divided by specific mitochondrial CS (Raffaella *et al.* 2008). In skeletal muscle mitochondrial content was increased with high fat feeding. Indeed, posthoc testing showed a significant increase in the young adult high fat-fed mice compared to the young adult control-fed mice. In addition aging increased mitochondrial mass, because it was significantly lower in adolescent high fat-fed mice than in the other high fat-fed age groups, whereas in young adult and middle-aged high fat-fed mice mitochondrial content was similar. In the control-fed groups, mitochondrial mass increased significantly between the adolescent and young adult group as well as between the young adult and the middle-aged group. Taken together mitochondrial

mass estimated by CS activity increased with age in skeletal muscle, which is more pronounced by feeding high fat diet. The abundance of mtDNA did not identify an influence of high fat feeding on mitochondrial abundance in skeletal muscle.

Table 4: Mitochondrial mass in skeletal muscle and skeletal muscle mitochondria

	Adolescent		Young Adult		Middle-Aged		Two-Way ANOVA
	Control	High Fat	Control	High Fat	Control	High Fat	
Mixed Skm mtDNA[1]	1.0 ± 0.6	0.9 ± 0.6	1.0 ± 0.7	0.7 ± 0.6	1.0 ± 0.4	1.1 ± 0.5	*n. s.*
Mt CS act	0.87 ± 0.06	0.88 ± 0.05	0.91 ± 0.08	0.93 ± 0.04	0.90 ± 0.05	0.87 ± 0.05	*n. s.*
Mixed Skm CS act	0.27 ± 0.02^a	0.28 ± 0.03^a	0.34 ± 0.10^b	0.47 ± 0.04^c	0.44 ± 0.04^c	0.49 ± 0.05^c	*A, D, A x D*
Mt Mass	0.30 ± 0.02^a	0.31 ± 0.03^a	0.38 ± 0.11^b	0.53 ± 0.04^c	0.49 ± 0.04^c	0.55 ± 0.05^c	*A, D, A x D*

[1] *Data were standardized to age-matched control, n = 4 -8 per diet and age*
mt – mitochondrial, CS act– Citrate Synthase Activity in $[U \times (mg\ protein)^{-1}]$
mt Mass in $[(mg\ mt\ protein) \times (mg\ tissue\ protein)^{-1}]$
significant posthoc testing (Holm-Sidak) indicated by different letters

Morphology of skeletal muscle mitochondria was investigated in an extra cohort of adolescent mice to study the influence of high fat feeding on the ultrastructural characteristics of mitochondria. Electron microscopy was carried out on sections of the gastrocnemius muscle of each three mice fed a high fat or control diet for 9 weeks. Mitochondrial morphology was normal in samples of high fat-fed mice (Figure 12 A and B). Mitochondrial number and size distribution were comparable between the diet groups (Figure 12 C). This observation is in line with the result of CS activity in skeletal muscle homogenates of adolescent mice, because CS activity was not changed in adolescent high fat-fed mice compared to adolescent control-fed mice (Table 4). Therefore high fat diet increased mitochondrial mass in skeletal muscle in young adult and middle-age mice but not in adolescent mice.
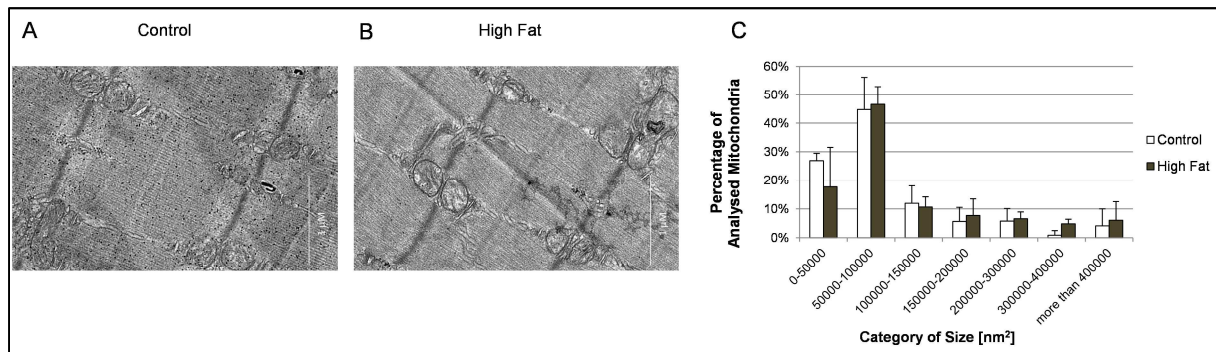
Figure 12: Electron microscopy of representative skeletal muscle mitochondria of adolescent mice after 9 weeks of feeding a high fat or control diet

A) Skeletal muscle section of adolescent control mouse and B) of adolescent high fat-fed mouse. C) Distribution of mitochondrial area of three mice per diet group and 4 sections per mouse

3.2.2.2   High fat diet feeding altered the fatty acid composition in mitochondrial membranes

The experimental diets did not only differ in their fat content but also in the fatty acid composition (Figure 6 and Table 15). The characteristics of fatty acid residues in phospholipids of membranes are essential for the membrane-related functions (de Wilde *et al.* 2008). To define the influence of high fat diet feeding, the consistence of phospholipids in mitochondrial membranes was investigated. All classes of fatty acids were changed by high fat diet feeding, except polyunsaturated fatty acids (PUFAs) (Table 5). Noteworthy, omega 6 (n6) and omega 3 (n3) fatty acids, which are summed up to the PUFA class, were contrariwise changed by high fat diet. While n6 fatty acid content increased in high fat-fed mice, n3 fatty acids content declined. The percentage of SFA increased with high fat diet in contrast to MUFA content which was reduced in membrane phospholipids after high fat feeding (Table 5). Aging influenced biomembrane composition in all fatty acid classes. Independently of diet, SFA and n6 content increased with increased age, but total PUFAs decreased with increased age. In MUFA and n3-fatty acids effects of age and diet interacted significantly (Table 5).

Taken together high fat diet changed the fatty acid composition of phospholipids in mitochondrial membranes towards more saturated fatty acids. Also aging increased the content of saturated fatty acids in biomembranes.

Table 5: Classes of fatty acids weight percent (wt %) present in membrane phospholipids of skeletal muscle mitochondria after 9 weeks of high fat feeding

	Adolescent		Young Adult		Middle-Aged		Two-Way ANOVA
	Control	High Fat	Control	High Fat	Control	High Fat	
Σ SFA	36.6 ± 0.7^a	38.4 ± 0.9^a	37.6 ± 0.9^a	38.9 ± 1.4^a	38.8 ± 2.4^a	41.9 ± 3.4^b	A, D
Σ MUFA	7.1 ± 0.2^a	4.7 ± 0.2^b	6.0 ± 1.0^c	5.0 ± 0.7^b	7.2 ± 0.5^a	6.2 ± 0.6^c	A, D, A x D
Σ PUFA	56.3 ± 0.9^a	56.9 ± 0.9^a	56.3 ± 0.6^a	56.1 ± 1.1^a	$54 \pm 2.8^{a,b}$	51.9 ± 3.9^b	A
Σ n6	22.9 ± 0.8^a	23.4 ± 0.6^a	19.7 ± 0.6^b	20.7 ± 0.7^b	20.8 ± 1.3^b	22.8 ± 1.9^a	A, D
Σ n3	33.4 ± 1.1^a	33.5 ± 1.3^a	36.6 ± 0.5^b	$35.4 \pm 0.6^{a,b}$	33.2 ± 3.7^a	29.1 ± 2.7^c	A, D, A x D
n3/n6	1.5 ± 0.1^a	1.4 ± 0.1^a	1.9 ± 0.1^b	1.7 ± 0.1^b	1.6 ± 0.3^a	1.3 ± 0.1^c	A, D, A x D
Σ UI	$277 \pm 5^{a,b}$	$274 \pm 6^{a,b}$	282 ± 3^a	$277 \pm 5^{a,b}$	263 ± 21^b	244 ± 18^c	A, D

SFA – saturated fatty acids, MUFA – monounsaturated fatty acids, PUFA – polyunsaturated fatty acids, n3 – omega 3 fatty acids, n6 – omega 6 fatty acids, UI – unsaturation index, n = 5 – 8 per group, A – age effect, D – diet effect, A x D – significant interaction significant posthoc testing (Holm-Sidak) indicated by different letters

3.2.2.3 Differential effects of high fat diet feeding on respiratory capacity in isolated skeletal muscle mitochondria

Oxygen consumption equalizes the rate of electrons transported through the respiratory chain. This electron flow is initiated by substrate oxidation and influenced by proton leak of the inner mitochondrial membrane (IMM) and ATP synthesis (Brand & Nicholls 2011). Therefore mitochondrial respiration was investigated in the absence of ADP to define the respiration rate due to proton leak and in presence of excessive ADP to define the respiration rate during maximal phosphorylation. To test the ability of mitochondria to metabolize fatty acids, palmitoylcarnitine and malate (PC/Mal) were used in combination for substrate oxidation.

Leak respiration was significantly increased by age and diet, indicating higher oxygen consumption in young adult and middle-aged high fat-fed mice. Here, posthoc testing revealed significantly increased oxygen consumption in skeletal muscle mitochondria of middle-aged high fat-fed mice compared to the age-matched control-fed mice (Figure 13 A). Membrane potential during leak respiration was unchanged by high fat diet but increased with increasing age of the mice (Figure 13 C). Plotting oxygen consumption against membrane potential illustrates how the two variables correlate. Residual oxygen consumption was calculated, which represents the portion of oxygen consumption that was not explained by the membrane potential (Figure 29 A and B in the appendix). The effect of high fat feeding is still significant and corroborated by the significant posthoc testing in the middle-aged high fat-fed mice compared to the control-fed middle-aged mice. In other words, skeletal muscle mitochondria of middle-aged high fat-fed mice consumed significantly more oxygen normalized for the membrane potential as skeletal muscle mitochondria of middle-

aged control-fed mice. In this age group high fat feeding therefore increased oxygen consumption without adequate increasing membrane potential during leak respiration. In adolescent and young adult mice, the residual oxygen consumption during leak respiration was not influenced by high fat feeding.
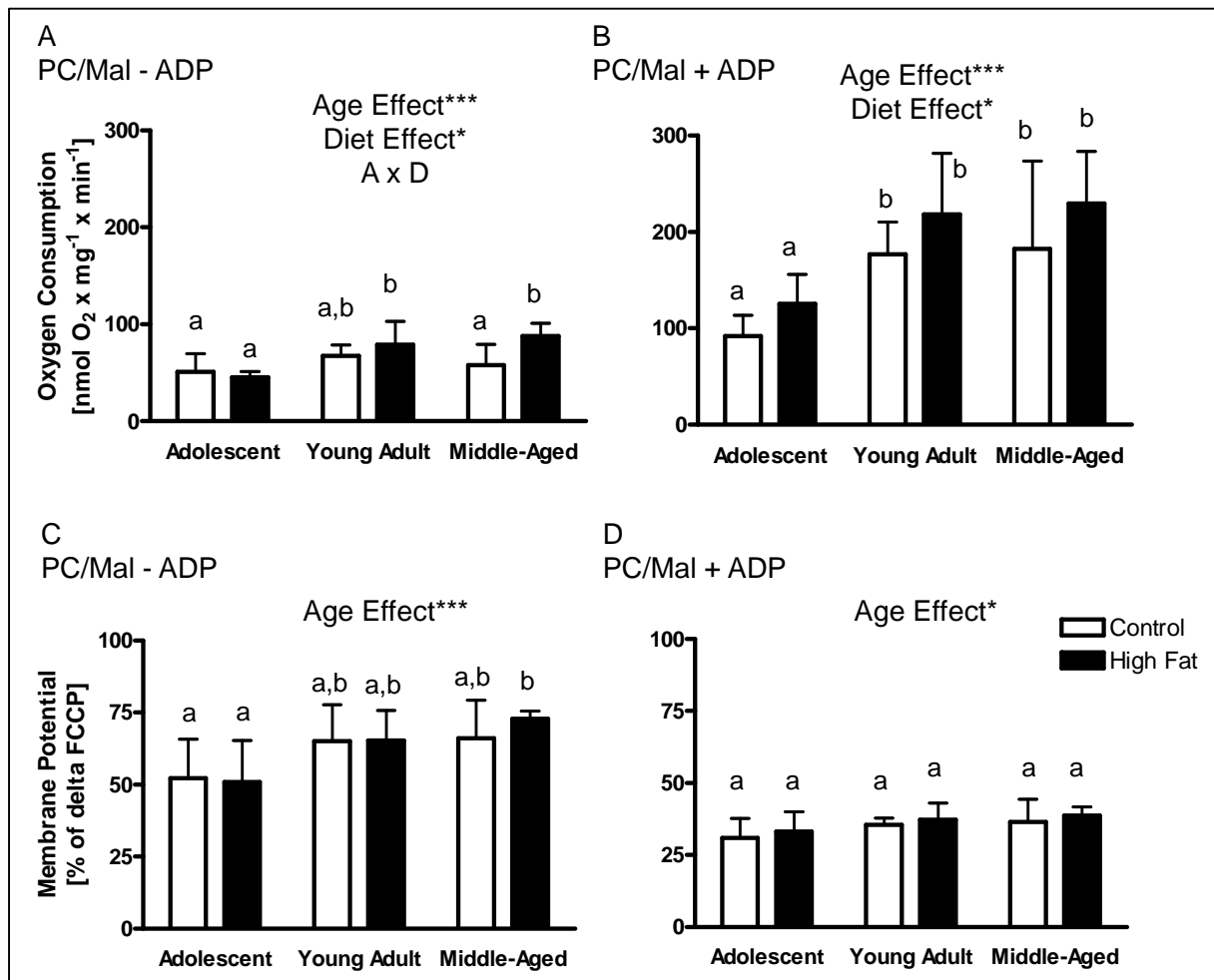
Figure 13: Respiratory characterization of skeletal muscle mitochondria after 9 weeks of feeding

A) Oxygen consumption rates with palmitoylcarnitine/malate (PC/Mal) in absence and B) presence of ADP. C) Corresponding membrane potential without ADP and D) with ADP; n = 5 – 8 per experimental group. Two-Way ANOVA statistics are given for age and diet effects with * p < 0.05, ** p < 0.01, *** p < 0.001. A x D – significant interaction, different letters indicate significant group differences after posthoc testing (Holm-Sidak)

ADP driven oxygen consumption increased with increasing age, but was not changed by high fat diet (Figure 13 B). Skeletal muscle mitochondria of adolescent mice consumed significantly less oxygen irrespective of the diet than skeletal muscle mitochondria of young adult and middle-aged mice. The significant effect of high fat diet was not substantiated by posthoc testing. Membrane potential was affected by the age of the mice during ADP stimulated respiration (Figure 13 D), but without significant posthoc testing for group

differences between age groups. In the phosphorylating state, the residual oxygen consumption was significantly influenced by the age of the mice (Figure 29 C and D). Here, skeletal muscle mitochondria of adolescent mice, irrespective of the diet, consumed significantly less oxygen normalized for the membrane potential, than young adult and middle-aged mice. Regression analysis sought to elucidate correlations between high fat diet induced differences in phospholipid composition (3.2.2.2) and oxidative capacity in isolated skeletal muscle mitochondria. Of note, mitochondrial oxygen consumption was not correlated to the composition of fatty acids in membrane phospholipids (data not shown).

Electron transport through the respiratory chain is restricted to the maximal enzymatic activity of the complexes of the respiratory chain (Navarro & Boveris 2007). The influence of high fat feeding on the maximal activity of Complexes I to V was analyzed using the commercial platform Mitoxis®. Therefore gcn muscle of discrete groups of adolescent and middle-aged high fat-fed and control-fed mice were sampled. Activity of Complex I, II and V was decreased by 10 to 20 % in middle-aged mice compared to adolescent mice but activity was unchanged by high fat diet (Table 21 in the appendix). Data were normalized to CS activity in muscle homogenates, which was increased with borderline significance per gram tissue in middle-aged high fat-fed mice ($p < 0.057$; data not shown), compared to the middle-aged control-fed mice. This confirmed CS measurements in mixed skeletal muscle tissue described before (3.2.2.1). In summary, leak respiration of skeletal muscle mitochondria of middle-aged mice was increased due to high fat feeding.

3.2.2.4   High fat diet did not provoke acylcarnitine-output per se

Acylcarnitines are recognized as byproducts of β-oxidation, when acyl-CoAs are incompletely oxidized and reesterified to carnitine. In the context of high fat feeding acylcarnitines accumulate in skeletal muscle (Koves *et al.* 2008). Acylcarnitine release of isolated mitochondria actively oxidizing fatty acids has not been reported yet. Therefore the output of acylcarnitine by isolated skeletal muscle mitochondria respiring on PC/Mal into the respiration buffer was quantified by mass spectrometry. Acylcarnitine release was not increased by mitochondria of high fat-fed mice compared to mitochondria of control-fed mice. In contrast, C6- and C8-acylcarnitine output was decreased with high fat diet (Figure 14). The highest concentration detected in the supernatant of the respiration medium was free carnitine (C0) and ascending C2 to C8. Interestingly, release of acylcarnitines of any length declined with increasing age. Intermediates of β-oxidation as hydroxyl-acylcarnitines or unsaturated acylcarnitine-residues were below the limit for quantification. The release of odd chain residues was unaffected by diet (data not shown).
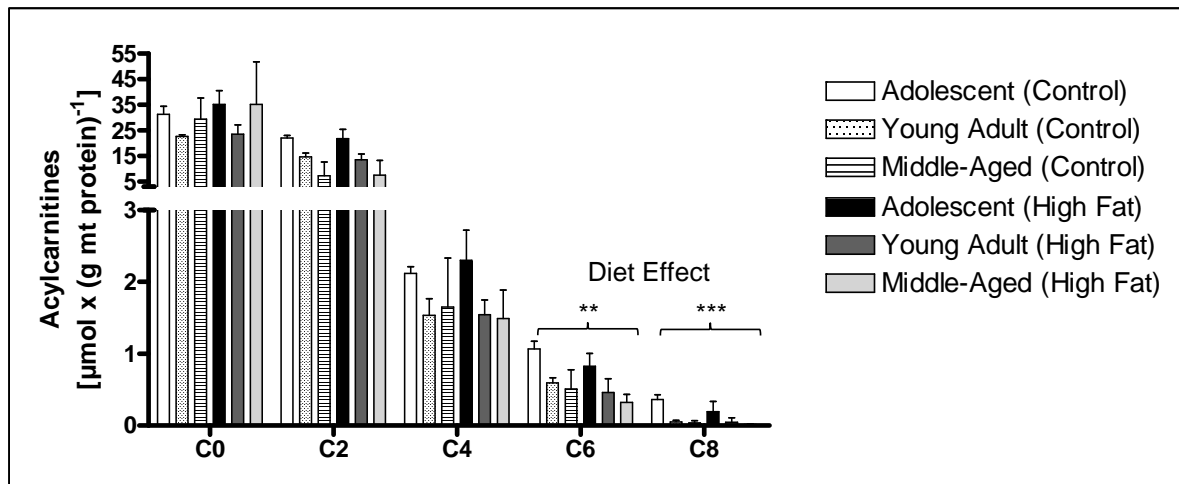
Figure 14: Acylcarnitine output of skeletal muscle mitochondria after 9 weeks of high fat feeding

The number after "C" terms the length of the carbon chain added to carnitine with C0 as free carnitine, Asterisks indicate significant diet effect according to Two-Way ANOVA for respective acylcarnitine species. n = 5 – 8 per group. Age effects detected for each single species are not indicated.

Substrate oxidation is the prerequisite for the electron flow measured as oxygen consumption (Brand & Nicholls 2011). Regressions between acylcarnitine release and the oxygen consumption rate during phosphorylation was analyzed to delineate correlations between the electron flow and the fatty acid oxidation. Free carnitine (C0) concentration in the supernatant was not correlated to the oxygen consumption rate (Figure 15 A). C2-, C4- and C6- carnitine output correlated negatively with respiration rates. As C2-, C4- and C6- carnitine release positively correlated with each other (data not shown), these carnitine residues were summed up and plotted against oxygen consumption (Figure 15 B). This analysis revealed that acylcarnitine release was dependent on oxygen consumption. To eliminate the influence of oxygen consumption a linear regression was calculated including all data points (Figure 15 B). The residuals define the portion of acylcarnitine release, which cannot be explained by the oxygen consumption rate and were analyzed for age and diet effects (Figure 15 C). Acylcarnitine release was not different between the age-matched diet groups when the influence of oxygen consumption was removed. Aging decreased the acylcarnitines release by mitochondria during fatty acid respiration. Interestingly, the diet effect seen for C6 (Figure 14 A) disappeared in this regression analysis, because the concentration of released C6 was the smallest of the three residues C2, C4 and C6 (Figure 15 B). Therefore the discrete effect of high fat diet on the C6 release did not influence the general correlation between substrate oxidation and oxygen consumption rate in skeletal muscle mitochondria.
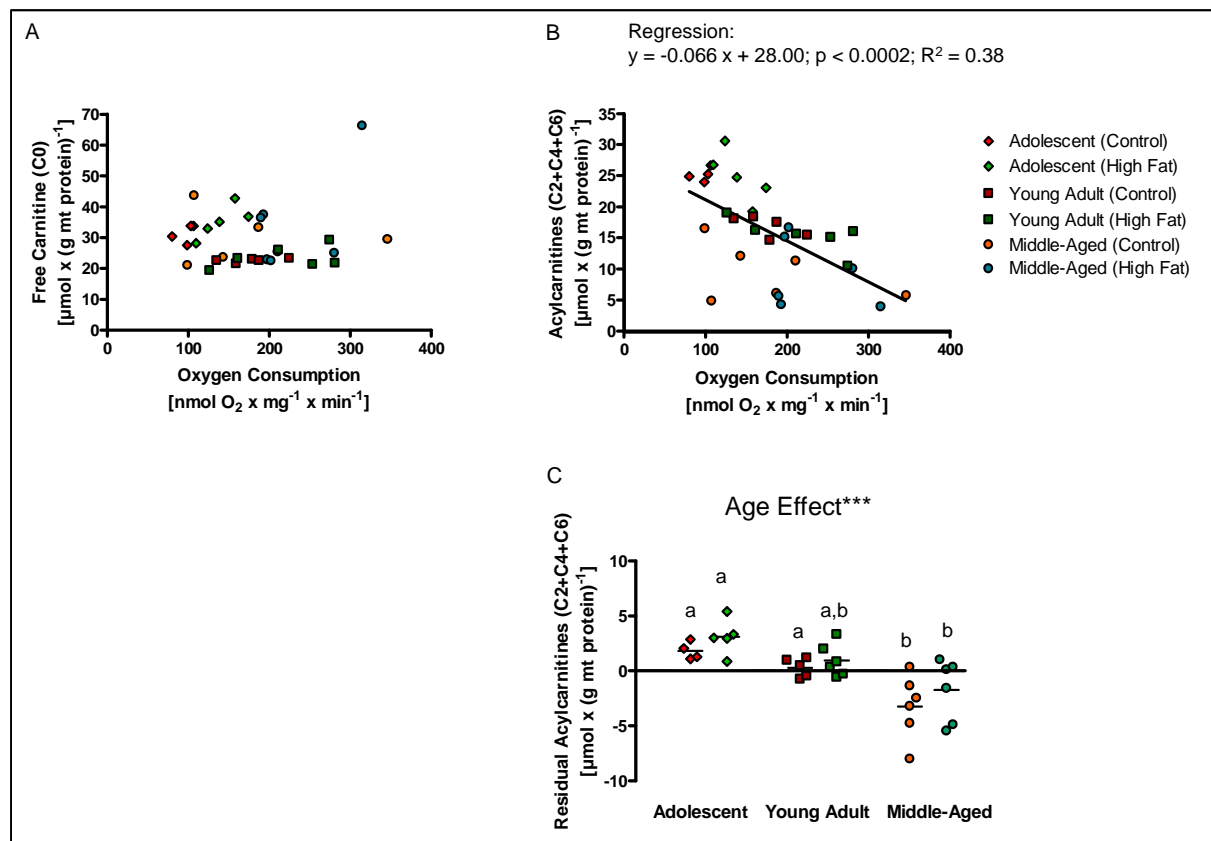
Figure 15: Acylcarnitine release and oxygen consumption in skeletal muscle mitochondria of mice fed a high fat and control diet for 9 weeks

A) Plot of free carnitine output to oxygen consumption. B) Plot of the sum of C2-, C4-, C6-acylcarnitine to oxygen consumption including linear regression equation C) Residual acylcarnitine release calculated by the regression equation of (B). Significant regression is accepted when $p < 0.05$. R^2 – coefficient of determination, different letters indicate significant posthoc testing (Holm-Sidak), n = 5 – 8 per group

As acylcarnitines are products from the β-oxidation the relative gene expression of genes related to β oxidation and key processes in fatty acid metabolism were investigated. Gene expression of carnitine palmitoyltransferase (CPT) 1b the step limiting enzyme of β-oxidation was unaltered in all age or diet groups (Table 22 in the appendix). Expression levels of the mitochondrial trifunctional protein, accounting for degradation of long chain fatty acids, were significantly but slightly increased in skeletal muscle of high fat- fed mice. Other enzymes of fatty acid oxidation were unregulated by high fat diet. Relative mRNA abundance of the short chain specific 3-hydroxyacyl-CoA dehydrogenase and 3-keto-acyl-CoA thiolase was reduced in middle-aged mice compared to the younger mice (Table 22 in the appendix). This is of particular interest, because mitochondria of middle-aged mice release less short-chain acylcarnitines (C2, C4, and C6) irrespective of the oxygen consumption rate, which might reflect a reduced enzyme expression of short chain specific β oxidative enzymes.

Summed up lipid intermediates arising from the β oxidation were produced to a normal extent in skeletal muscle mitochondria of high fat-fed mice. High amounts of acylcarnitine release further indicated low oxygen consumption and vice versa. Trifunctional protein was upregulated at transcript level indicating higher usage of long chain fatty acid derived energy equivalents in high fat-fed mice. Noteworthy, the high fat diet did not increase the rate of acylcarnitine output which is not explained by the correlation to the oxygen consumption.

3.2.2.5 Mitochondrial ROS production was increased and the glutathione redox system was more oxidized in middle-aged mice

Fatty acids are described with the potential to induce high rates of mitochondrial ROS production comprising different sites of origin (Seifert *et al.* 2010). Isolated skeletal muscle mitochondria of adolescent, young adult and middle-aged mice fed the high fat or control diet for 9 weeks were incubated with excessive fatty acids (PC/Mal). These data correspond to the respiration and membrane potential measurements described before (Figure 13). The ROS production rate was measured as H_2O_2 release which is proportional to the conversion of Amplex Red to the fluorescent resorufin.
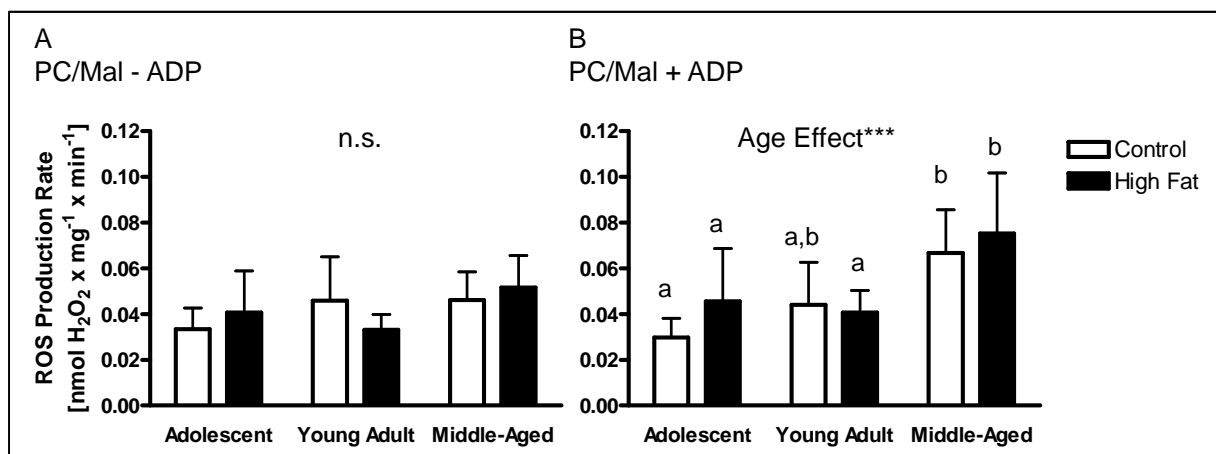
Figure 16: Reactive oxygen species production in skeletal muscle mitochondria after 9 weeks of high fat feeding

ROS production was induced with palmitoylcarnitine and malate in absence (A) and presence (B) of ADP. Two-Way ANOVA effects are given with *** $p < 0.001$, n.s. – not significant. Different letters indicate significant differences in posthoc testing (Holm-Sidak).

In adolescent and young adult mice H_2O_2 release was normal in mitochondria of high fat-fed mice compared to mitochondria of control-fed mice irrespective of ADP (Figure 16 A and B). In general middle-aged mice exhibited higher ROS production rates compared to the younger mice cohorts, when ADP was present in the respiration buffer (Figure 16 B). In the physiological most relevant condition, which is ADP-driven respiration, there is a small, non-

significant, tendency towards an increased ROS production by high fat diet in the adolescent and middle-aged groups (Figure 16 B). Regression analysis of ROS production rates with oxygen consumption, membrane potential, phospholipid composition and acylcarnitine release could not reveal any relevant correlations (data not shown).

Antioxidative strategies could attenuate ROS production before it is detected in the medium, so consequently the glutathione redox system was investigated. Within the Mitoxis® analysis (2.11.2) the redox state of gcn muscle in adolescent and middle-aged mice was examined. Superoxide dismutases (SOD Mn and Cu/Zn), Catalase and markers for oxidative stress, glucose-6 phosphate dehydrogenase (G6PDH) and malonedialdehyde (MDA), were neither changed by age nor by diet (Table 23 in the appendix). Besides catalase, Glutathione peroxidase (GPx) reduces H_2O_2 to water by oxidizing glutathione (GSH) to glutathione disulfide (GSSG). The GSH pool can be recycled from GSSG by glutathione reductase (GR) and alternatively GSH can de novo synthesized by glutathione synthase (GS) and glutamate-cysteine ligase (GCS). GSH content in muscle was unchanged by age or high fat diet (Figure 17 A), but enzymes of GSH synthesis were less active in the middle-aged group (Table 23). Notably, GSSG accumulated in gcn muscle of high fat-fed middle-aged mice, but in the respective controls GSSG content tends to be lower than in the adolescent group (Figure 17 B). This finding was accompanied with a significant increase in both GPx activity and GR activity in the middle-aged group (Figure 17 C, D). The latter was further elevated by high fat diet. Taken together a higher H_2O_2 release by mitochondria in middle-aged mice is quenched by Gpx and recovered by GR. In middle-aged mice under a high fat diet the elevated GSSG content still indicated a more oxidized redox state than in adolescent mice.
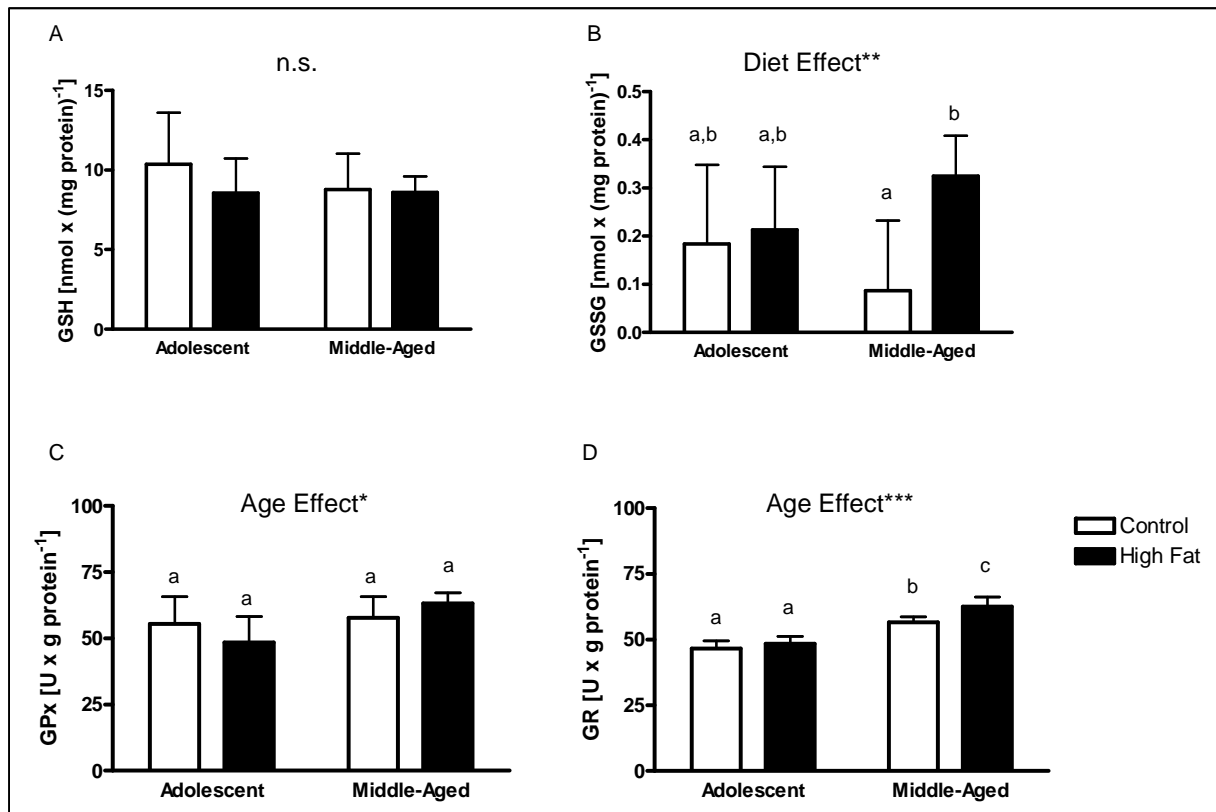
Figure 17: Glutathione redox system in gastrocnemius muscle of adolescent and middle-aged mice fed high fat or control diet for 9 weeks

A) Concentration of glutathione (GSH), B) Concentration of glutathione disulfide (GSSG). C) enzyme activity of glutathione peroxidase (GPx) and D) of glutathione reductase (GR). n = 6 per group. General age effect was analyzed by Two-Way ANOVA with * $p < 0.05$, ** $p < 0.01$, *** $p < 0.001$. Different letters indicate significant differences after posthoc testing (Holm-Sidak)

3.2.3   Mitochondrial function after 26 weeks of high fat diet

Characteristics of skeletal muscle mitochondria were exemplified in adolescent and young adult cohorts that were fed the high-fat diet for 26 weeks. Triglyceride levels were examined in a small cohort of 3 adolescent mice per diet group and showed significant accumulation of fat in the gastrocnemius muscle of high fat-fed mice (0.37 ± 0.03 vs 1.07 ± 0.48) for control-fed mice compared (vs) to high fat-fed mice in µmol triglycerides per mg muscle protein. Muscle mass of tibialis anterior muscle was not significantly increased in high fat-fed mice of adolescent and young adult cohorts, although there was a tendency ($p < 0.12$ for the independent variable "diet" using Two-Way ANOVA) towards higher muscle mass by high fat diet (Table 24 in the appendix). Mitochondrial DNA copy number was neither affected by high fat feeding nor by age in tibialis anterior muscle of adolescent and young adult mice. Enzyme activity of CS in isolated skeletal muscle mitochondria was normal (Table 24 in the appendix). Noteworthy, statistics were carried out for CS activity relative to mean of the age-

matched control group to avoid false positive age effects due to large differences in the storage period of mitochondrial preparations. Mitochondrial mass was not assessed.

Oxygen consumption was tested with palmitoylcarnitine to mimic excessive availability of fatty acids. Data of oxygen consumption rates of isolated skeletal muscle mitochondria were normalized to the age-matched controls of respective cohorts to eliminate technical effects due to different instruments used to assess oxygen consumption (Table 25 in the appendix). Skeletal muscle mitochondria of adolescent and young adult high fat-fed mice consumed more oxygen than the age-matched control-fed mice. Membrane potential was either monitored with the cation TPMP$^+$ or with Safranin O (2.10 for details), and therefore data are presented relative to the mean of age-matched control-fed mice. The ability to use fatty acid-derived substrate palmitoylcarnitine for building up a proton gradient was unaffected by high fat diet in adolescent and young adult mice. The release of H_2O_2 was normal in mitochondria of adolescent and young adult high fat-fed mice both in absence or presence of ADP compared to the age-matched control fed-mice. Summed up, skeletal muscle mitochondria of long term high fat-fed mice were not impaired regarding the respiratory function. Neither did they produce enormous amounts of ROS. Skeletal muscle mitochondria are robustly performing after chronic exposure to fat in excess, which is not in line with the hypothesis that early impairment of mitochondrial function due to high fat feeding induces skeletal muscle insulin resistance.

3.3   Mitochondrial characteristics and function in liver

3.3.1   Fatty liver and mitochondrial content

The liver serves as hub for glucose- and fat-metabolism combining breakdown and de novo synthesis of these macronutrients. Adolescent, young adult and middle-aged mice, which were fed high fat or control diet for 9 weeks, were analyzed to understand mechanisms regarding hepatic triglyceride accumulation in response to high fat diet feeding.

Liver mass was not affected by high fat feeding (Figure 18 A), but livers of high fat-fed mice accumulated triglycerides. The latter was seen in an age-dependent way: post-hoc testing revealed significant lipid accumulation in young adult and middle-aged mice fed a high fat diet, but not in adolescent mice (Figure 18 B). The absence of significant fat accumulation in adolescent mice will be further addressed by looking for potential protective mechanisms in the proteome analysis (paragraph 3.4). Statistical interaction between age and diet was observed.
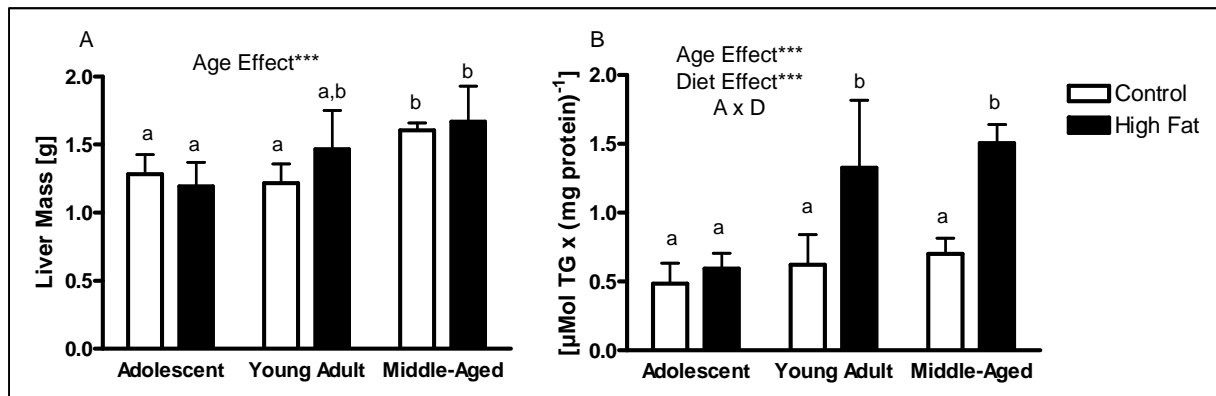
Figure 18: Liver mass and hepatic triglyceride content after 9 weeks of high fat feeding.

Two-Way ANOVA statistics are presented by asterisks *** $p < 0.001$ with A x D as significant interaction. Letters indicate differences according to posthoc testing (Holm-Sidak), n = 4 – 6 per group

The impact of fat accumulation on mitochondrial protein abundance and function was characterized by hepatic mitochondrial mass. Consumption of a high fat diet did neither affect mitochondrial DNA (mtDNA) abundance nor CS activity, which was analyzed in liver tissue homogenates and in mitochondria-enriched protein fractions (Table 6). Aging decreased CS activity in mitochondrial protein and in liver homogenates. Mitochondrial protein mass per liver protein mass was calculated (Raffaella *et al.* 2008), and a subsequent decline with increasing age was present, even though without significant posthoc testing between age groups (Table 6). In summary, a high fat diet and subsequent fat accumulation in the liver did not influence mitochondrial mass. This finding was confirmed in the proteome profile of CS analyzed in mitochondria-enriched protein pools (data not shown).

Table 6: Mitochondrial mass in liver after 9 weeks of high fat feeding

	Adolescent		Young Adult		Middle-Aged		Two-Way ANOVA
	Control	High Fat	Control	High Fat	Control	High Fat	
Liver Tissue mtDNA[1]	1.0 ± 0.5	0.6 ± 0.1	1.0 ± 0.4	1.2 ± 0.7	1.0 ± 0.1	1.1 ± 0.2	*n.s.*
Mt CS act	0.38 ± 0.12[a]	0.39 ± 0.03[a]	0.45 ± 0.12[a],b	0.54 ± 0.11[b]	0.40 ± 0.05[a]	0.39 ± 0.02[a]	*A*
Liver Tissue CS act	0.14 ± 0.02[a,b]	0.15 ± 0.02[a]	0.12 ± 0.01[b,c]	0.12 ± 0.02[b]	0.10 ± 0.01[c]	0.10 ± 0.01[c]	*A*
Mt Mass	0.42 ± 0.27[a]	0.39 ± 0.05[a]	0.35 ± 0.05[a]	0.23 ± 0.04[a]	0.26 ± 0.02[a]	0.26 ± 0.03[a]	*A*

[1] *Data for relative mtDNA abundance were normalized to age-matched controls*
Mt – mitochondrial, CS act - Citrate Synthase Activity [U x (mg protein)$^{-1}$]
Mt Mass - [(mg mt protein) x (mg tissue protein)$^{-1}$], A – age effect, n.s. – not significant
n = 4 – 10 per group, significant posthoc testing (Holm-Sidak) by different letters

3.3.2   Mitochondrial proton leak and ROS production in three age groups fed 9 weeks a high fat diet

Mitochondria-enriched protein suspensions were obtained by differential centrifugation from livers of adolescent, young adult and middle-aged mice fed the high fat or control diet for 9 weeks. Data presented in this paragraph are referred to as dataset 1 to distinguish these data from data obtained from other mouse cohorts that will be introduced later. Mitochondrial proton leak kinetics define the rate of oxygen consumption needed to build up the proton gradient when ATP synthesis is blocked. The impact of high fat feeding on the mitochondrial proton leak was tested. Mitochondria were subjected to succinate for substrate oxidation and proton leak was titrated with the competitive complex II inhibitor malonate. The oxygen consumption was plotted against the membrane potential and the regression fit was calculated (Jastroch *et al.* 2012). Proton leak kinetics were unchanged in mitochondria of high fat-fed mice compared to the age-matched control-fed mice (Figure 19 A). For each mouse the individual oxygen consumption at 170 mV membrane potential was calculated using the regression fit (Figure 19 B). Performing Two-Way ANOVA statistics for diet and age effects at the oxygen consumption at 170 mV, resulted in a significant age effect: The older the mice the more oxygen mitochondria consumed to build up 170 mV membrane potential. This evidence demonstrated that liver mitochondria of middle-aged mice are less coupled than mitochondria of adolescent mice, but the coupling state is not affected by high fat diet.
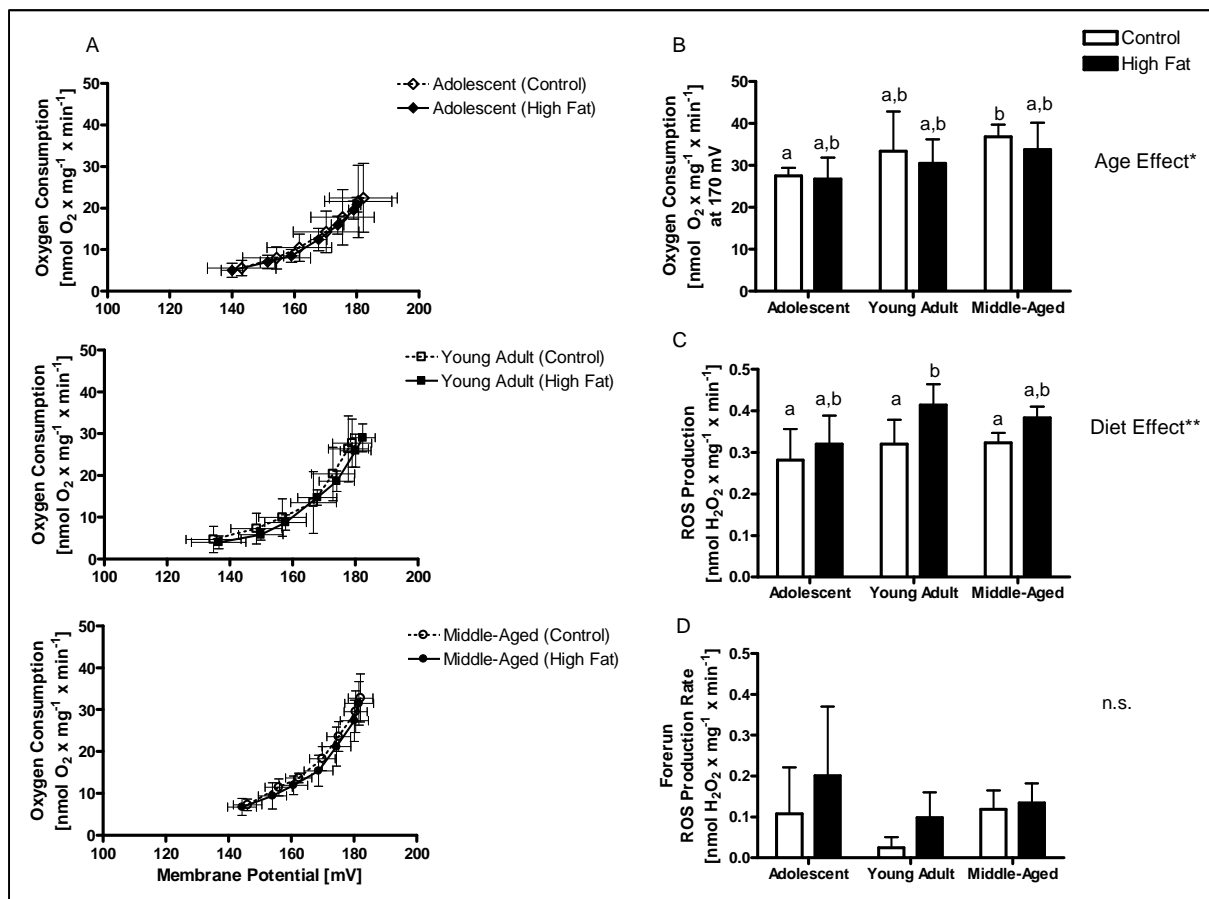
Figure 19: Proton leak kinetics and ROS production rates in hepatic mitochondria-enriched fractions induced with succinate/rotenone

A) Titration curves of oxygen consumption plotted against membrane potential when succinate is given as substrate in all three age groups. B) Oxygen consumption required to build up 170 mV membrane potential. C) ROS production rates in the respective mitochondrial fractions were measured in absence of BSA. D) ROS production rate in absence of substrate for mitochondrial respiration reflecting non-mitochondrial ROS sources. Two-Way ANOVA statistics are given with ** p < 0.01, different letter indicate significant posthoc testing (Holm-Sidak), n.s. – non significant, n = 4 – 6 per group

In the mitochondria-enriched protein fractions used for both functional measurements and proteome analyses, sources other than mitochondria potentially contributed to superoxide production. The forerun of the Amplex Red-based assay provided information about H_2O_2 produced independently of mitochondria, as this was measured in absence of a substrate that initiates mitochondrial respiration (Figure 19 D). Analyzed by Two-Way ANOVA for diet and age effects, there was no significant difference in non-mitochondrial H_2O_2 production. Therefore exclusively mitochondrial ROS production rates are sensitive to the high fat diet in this assay. During leak respiration with succinate/rotenone as substrate ROS production rates were assayed using the fluorescent oxidation product of Amplex Red. High fat diet increased ROS production rates by Two-Way ANOVA statistics (Figure 19 C). Posthoc testing revealed significantly increased ROS production in young adult high fat-fed mice and

a borderline significant trend towards increased ROS production in the middle-aged high fat-fed mice compared to the age-matched control-fed mice. Taken together, although mitochondrial leak respiration was normal in high fat-fed mice compared to the age-matched controls, there is an increased H_2O_2 emission from the respiratory chain.
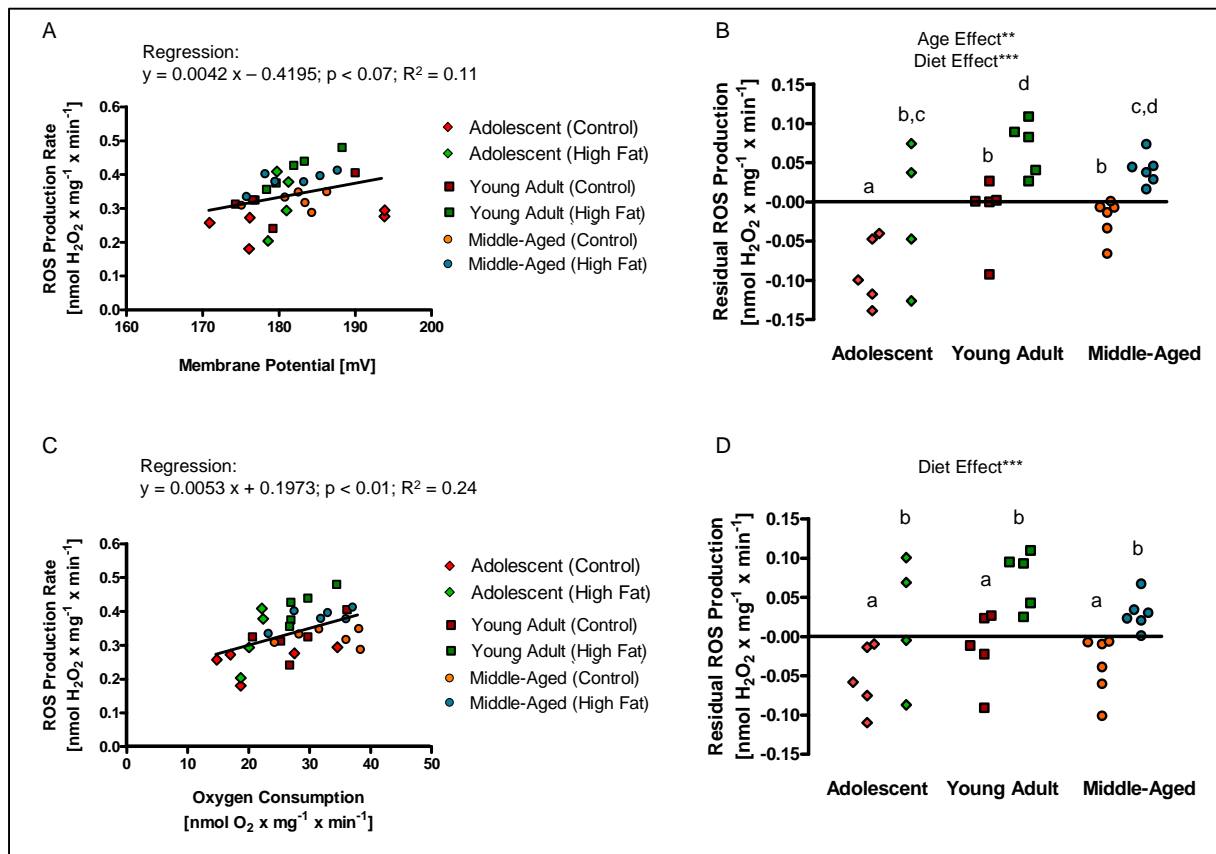
Figure 20: Regression analysis of membrane potential and oxygen consumption to ROS production rate

A) ROS production rate plotted against membrane potential (A) and oxygen consumption (C) with original data presented in Figure 19. B) + D) Residual ROS production when calculated according to regression equation

The rate of electrons leaking from the respiratory chain to form superoxide and subsequently H_2O_2 is dependent on membrane potential and oxygen consumption. With higher membrane potential, ROS production rates increase, too. Therefore effect of high fat feeding on ROS production was further investigated by eliminating the influence of membrane potential and oxygen consumption rates on mitochondrial superoxide generation. The ROS production rate was plotted against the respective membrane potential and oxygen consumption rates. The regression line was calculated for all data points irrespective of age and diet group. Then the residual ROS production rates were calculated. These values represent the ROS production that is not caused by membrane potential or oxygen consumption.

There was a borderline significant correlation between ROS production and membrane potential (Figure 20 A). It should be considered that two adolescent control-fed mice displayed an enormously low ROS production rate while having a high membrane potential. If these data points would be excluded, the correlation reaches significance. For comprehensive data presentation these data points were included in the regression line. Residual ROS production (Figure 20 B) was calculated on the base of the regression equation (Figure 20 A) and describes the difference between the regression and each individual data point at its given membrane potential. The residual ROS production was increased in liver mitochondria of high fat-fed mice compared to the age-matched control-fed mice irrespective of membrane potential (Figure 20 B), which was confirmed in all age groups by significant posthoc testing. Furthermore with increasing age mitochondrial residual ROS production were increased as well. The correlation and residual ROS production between ROS production rate and oxygen consumption rate was analyzed accordingly (Figure 20 C, D). The regression is highly significant (Figure 20 C). ROS production is increased by high fat diet independently of the oxygen consumption rate as seen by the residual ROS production (Figure 20 D). Summed up liver mitochondria of high fat-fed mice indeed released higher rates of ROS independently of membrane potential or oxygen consumption. Consequences of increased mitochondrial ROS production rates e.g. regarding the mitochondrial and cellular redox state were in detail examined by the proteome analysis in mitochondria-enriched liver protein fractions (see 3.4).

Liver mitochondria of another subset of mice were characterized regarding mitochondrial performance by giving succinate as substrate as well as by oxidizing palmitoylcarnitine to test the capacity for fatty acid oxidation (3.3.3). For these cohorts of adolescent, young adult and middle-aged mice, called dataset 2, succinate driven respiration, membrane potential and ROS production was measured. Hydrogen peroxide release from mitochondria fueled with succinate and rotenone was increased by high fat diet (Table 26 in the appendix) and therefore reproduced data set 1 (Figure 19 D). In dataset 2, oxygen consumption during leak respiration was increased with increasing age, which confirms again data received from the proton leak kinetics (Figure 19 A, B). This effect was consistent in ADP driven respiration (Table 26 in the appendix). Surprisingly, the membrane potential, here measured with the fluorescent Safranin O was reduced by high fat diet during leak respiration even though posthoc testing did not reach significance for the difference between high fat-fed mice and the age-matched control-fed mice. Aging significantly increased membrane potential during leak respiration in dataset 2 (Table 26 in the appendix). The effect of high fat diet disappeared in presence of ADP. Noteworthy, membrane potential was recorded in the fluorescent plate reader, and in parallel oxygen consumption was recorded in the Seahorse machine for mice of dataset 2. For dataset 1, membrane potential and oxygen consumption

were monitored in parallel in the clark electrode chamber by inserting a second sensor for the measurement of the membrane potential (2.10.1). In dataset 2, ROS production rates and membrane potential or oxygen consumption did not correlate. Despite some differences, the mitochondrial performance in dataset 2 partly corroborated the results for dataset 1 using succinate as substrate.

3.3.3 Mitochondrial fatty acid oxidation in three age groups of mice fed a high fat diet for 9 weeks

An excess of fatty acids was given to mitochondria-enriched fractions and oxygen consumption, membrane potential and ROS production were recorded, as well as acylcarnitine output. These measurements were conducted in adolescent, young adult and middle-aged mice of dataset 2 fed high fat or control diet for 9 weeks.

Table 7: Oxygen consumption (VO$_2$), membrane potential (Δψ) and ROS production rate (H$_2$O$_2$) with fatty-acid based substrate in liver mitochondrial preparations (dataset 2), n = 5 − 6 per group

PC/Mal		Adolescent		Young Adult		Middle-Aged		Two-Way ANOVA
		Control	High Fat	Control	High Fat	Control	High Fat	
VO$_2$	- ADP	11.6 ± 2.4[a]	9.0 ± 1.5[a]	16.0 ± 4.4[b]	14.5 ± 4.0[a,b]	22.1 ± 4.6[c]	20.3 ± 3.7[c]	A
	+ ADP	64.5 ± 17.2[a]	48.4 ± 8.0[b]	82.5 ± 10.8[a]	82.1 ± 25.3[a]	94.9 ± 23.2[c]	74.6 ± 9.0[a]	A, D
Δψ	- ADP	30.7 ± 6.1[a]	23.7 ± 8.1[a]	55 ± 8.1[b]	49.1 ± 15.4[b]	69.3 ± 16.8[b]	62.9 ± 15.8[b]	A
	+ ADP	39.9 ± 6.4[a,b]	33.7 ± 5.3[a]	47.2 ± 3.8[b]	45.9 ± 4.8[a,b]	52.7 ± 14.6[b]	49.2 ± 12.1[b]	A
H$_2$O$_2$	- ADP	0.17 ± 0.05[a]	0.15 ± 0.02[a,b]	0.12 ± 0.05[b]	0.11 ± 0.02[b]	0.13 ± 0.02[a,b]	0.13 ± 0.05[a,b]	A
	+ ADP	0.15 ± 0.04[a]	0.13 ± 0.05[a]	0.13 ± 0.03[a]	0.13 ± 0.05[a]	0.10 ± 0.03[a]	0.10 ± 0.03[a]	A

O$_2$ in [nmol O$_2$ x mg^{-1} x min^{-1}], Δψ in [% of Δ FCCP], H$_2$O$_2$ in [nmol H$_2$O$_2$ x mg^{-1} x min^{-1}]
PC/Mal – palmitoylcarnitine/malate, A – age effect, D – diet effect
Significant posthoc testing (Holm-Sidak) indicated by different letters

Liver mitochondria were provided with fatty-acid derived substrate palmitoylcarnitine in presence of malate. Oxygen consumption in absence of ADP, representing leak respiration, was significantly increased in young adult mice irrespective of the diet compared to the adolescent mice, and further significantly increased in middle-aged mice compared to young adult mice. High fat diet did not significantly influence leak respiration (Table 7). By the addition of ADP, when maximal physiological respiration was induced, hepatic mitochondria from high fat-fed mice consumed significantly less oxygen than mitochondria of age-matched control-fed mice. In mitochondria of middle-aged control-fed mice oxygen consumption was the highest. Significant effects were tested by the Holm-Sidak method. Differences driven by

high fat diet were significant in adolescent and middle-aged mice. In adolescent mice irrespective of diet oxygen consumption was significantly lower than in other age groups by pairwise comparison. The respiratory control ratio calculated as quotient of ADP-driven oxygen consumption and leak respiration was unchanged by diet (data not shown). Membrane potential was indicated by Safranin O fluorescence in the respiration buffer. The diet effect seen in oxygen consumption was not evident in the membrane potential. Mitochondria of middle-aged mice build up a bigger proton gradient than do younger mice which is consistent with the respiratory data. In contrast to the succinate-driven radical production, H_2O_2 release induced by PC/Mal is normal in liver mitochondria of high fat-fed mice (Table 7). Regression analysis between membrane potential or oxygen consumption and ROS production rates as for proton leak kinetics with succinate as substrate (Table 7) revealed no statistically significant correlations. In summary, liver mitochondria of high fat-fed mice metabolizing fatty acids reduced oxygen consumption together with a non-significant tendency towards reduced membrane potential, but with normal rates of H_2O_2 compared to control-fed mice.

Acylcarnitine release to the respiration buffer was examined in mitochondria respiring on palmitoylcarnitine and malate in presence of ADP to stimulate oxidative phosphorylation. Palmitoylcarnitine enters the mitochondria via the shuttle across the inner mitochondrial membrane (IMM) and is reconverted to palmitoyl-CoA in the mitochondrial matrix. The cycles of β-oxidation reduce the acyl chain by acetyl-CoA, resulting in 8 molecules acetyl-CoA from one molecule palmitoyl-CoA. The released acylcarnitines arise from reverse exchange of CoA to carnitine. Mitochondria of high fat-fed mice released significantly less acetylcarnitine (C2) and butyrylcarnitine (C4) than controls (Figure 21). Of note, the concentration of palmitoylcarnitine, which was initially subjected at 40 µM to the respiration buffer, was higher in the supernatant of mitochondria of high fat-fed mice compared to control-fed mice, although with borderline significance. Therefore the lower release of acylcarnitines in liver mitochondria of high fat-fed mice was accompanied by less uptake of palmitoylcarnitine through the shuttle across the IMM. In the β-oxidative cycle 8 molecules acetyl-CoA are cleaved from one molecule palmitoylcarnitine, which explains why the effect of a small decrease in palmitoylcarnitine uptake is clearly expressed in the short chain acylcarnitines. The regression of C2 + C4 + C6 + C8 as sum was plotted against oxygen consumption rate in the phosphorylating state was calculated (Figure 30 A). The distance of each data point to the regression line can be expressed as residual and defines the acylcarnitine output which is not explained by the oxygen consumption rate. Independently of the respiration rate, liver mitochondria of high fat-fed mice emitted less acylcarnitines (Figure 30 B).
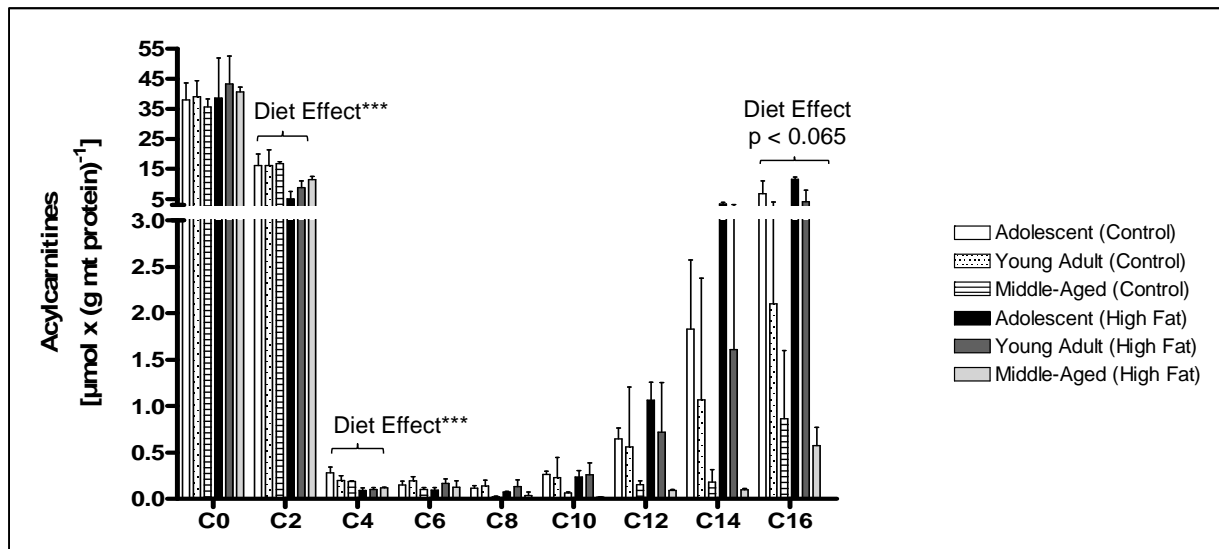
Figure 21: Acylcarnitine release by liver mitochondria of mice fed a high fat or control diet for 9 weeks

Acylcarnitine output during palmitoylcarnitine-driven respiration. The letter C is carnitine, the number accounts for the length of the added carbon chain with C0 as free carnitine. Two-Way ANOVA effects for high fat diet are indicated with *** $p < 0.001$, n = 3 – 5 per group

3.3.4   Mitochondrial function after 26 weeks of high fat diet

Long term feeding duration increased liver mass in adolescent mice (Figure 22 A). Triglycerides accumulated in livers of adolescent mice fed the high fat diet for 26 weeks comparable to young adult and middle-aged mice after 9 weeks of high fat feeding (Figure 18, Figure 22 B).
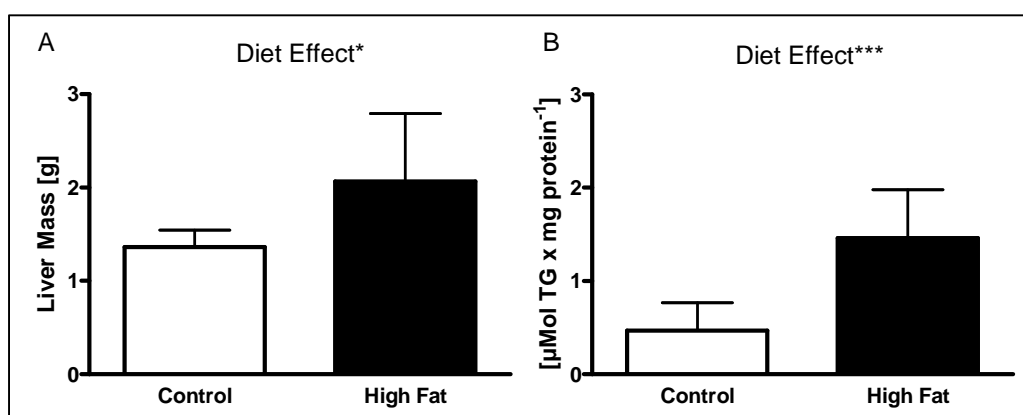
Figure 22: Liver mass and triglyceride content in adolescent mice fed for 26 weeks

A) Liver mass upon dissection, n = 9 per group. B) Hepatic triglyceride (TG) accumulation, n = 7 per group. Statistics refer to Student's t-test with * $p < 0.05$, *** $p < 0.001$

Mitochondrial content in liver of high fat-fed mice was normal after 26 weeks of high fat feeding as investigated by CS activity in mitochondrial fractions and liver tissue. Calculated mitochondrial mass did neither change due to a very long term high fat feeding (Table 8).

Table 8: Mitochondrial mass after 26 weeks of high fat feeding

	Adolescent		
	Control	High Fat	
Mt CS	0.55 ± 0.04	0.65 ± 0.14	*n.s.*
Liver Tissue CS	0.13 ± 0.01	0.14 ± 0.01	*n.s.*
Mt Mass	0.25 ± 0.04	0.21 ± 0.03	*n.s.*

Mt – mitochondrial, CS in [U x (mg protein)$^{-1}$]
Mt Mass - [(mg mt protein) x (mg tissue protein)$^{-1}$],

Proton leak kinetics were evaluated in liver mitochondria after 26 weeks of high fat feeding according to the procedure in mice fed for 9 weeks the high fat diet (3.3.2). Mitochondria of high fat-fed mice were as coupled as mitochondria of control-fed mice (Figure 23 A). The release of ROS was assessed with succinate in absence of ADP representing leak respiration and showed a tendency towards a higher H_2O_2 emission in liver mitochondria of high fat-fed mice compared to the control-fed mice. This trend was tested by Student's ttest but did not reach significance (Figure 23 B).
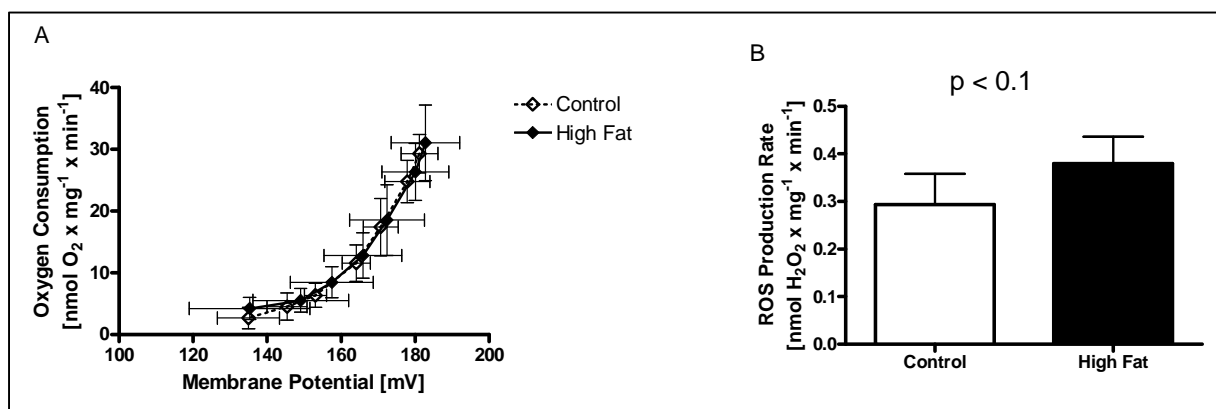
Figure 23: Proton leak kinetics and ROS production rate after 26 weeks of high fat feeding.
A) Succinate driven non-phosphorylating oxygen consumption with simultaneous recording of membrane potential. B) ROS production rate in the respective respiration state. n = 4 per group

The correlation between ROS production and membrane potential was investigated. For the 26 week period only 4 mice per diet group were measured and therefore data for maximal oxygen consumption, maximal membrane potential and ROS production (Figure 23 A + B)

were graphed together with the data of mice fed 9 weeks of high fat diet (Figure 24 A + B). Data for mice fed 26 weeks a high fat diet are depicted within the data points of mice fed 9 weeks a high fat diet disregarding age. Therefore residual ROS was calculated using the regression equations described before (Figure 20). After 26 weeks of high fat diet, ROS production rates that were not determined by membrane potential were significantly higher in hepatic mitochondria of high fat-fed mice than in mitochondria of control-fed mice (Figure 24 C). Hydrogen peroxide release independently of oxygen consumption was not statistically significant but tended to increase in mitochondria of high fat-fed mice. Summing up liver mitochondria of mice fed 26 weeks a high fat diet showed an increased ROS production rate independently of the well coupled membrane potential. This result reflects the H_2O_2 release observed in liver mitochondria after 9 weeks of high fat feeding. Thus, feeding a high fat diet for 26 weeks mitochondrial bioenergetics and ROS production rates don't suggest progressively impaired mitochondrial function.
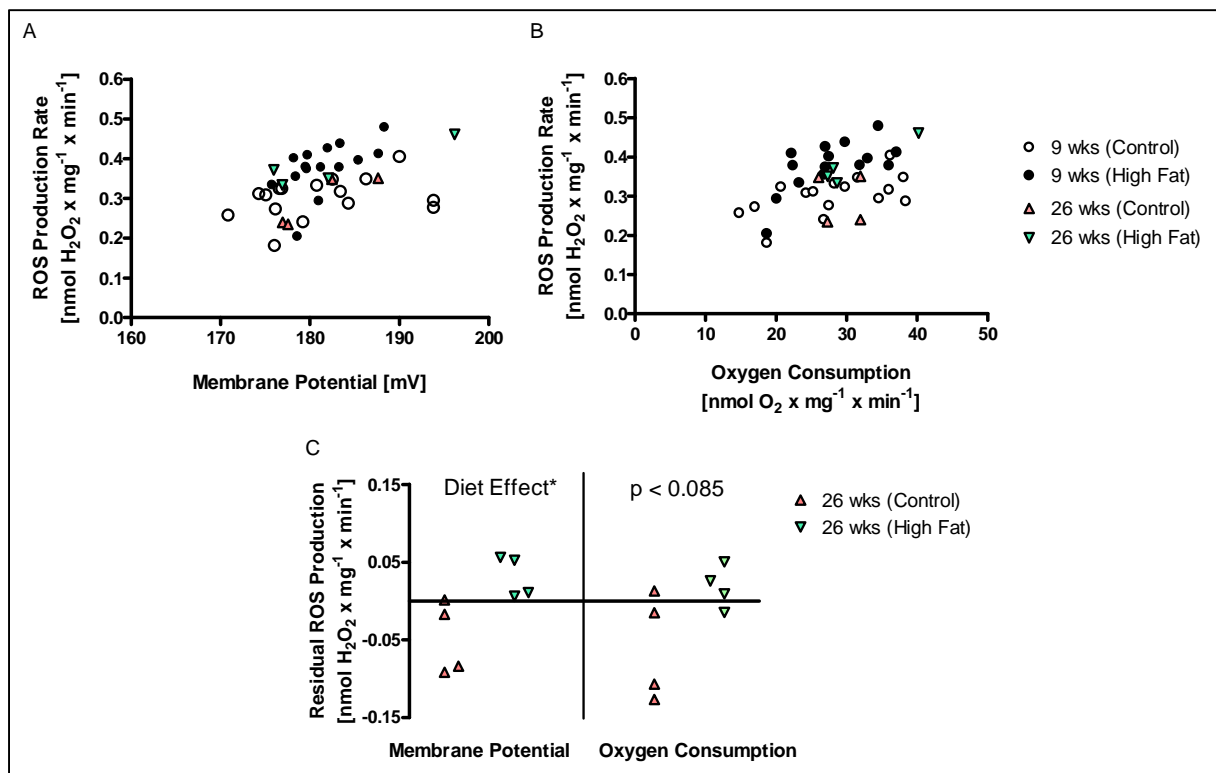
Figure 24: Regression analysis between ROS production rates, membrane potential and oxygen consumption respectively in liver mitochondria after 26 weeks of high fat feeding

A) ROS production rates were plotted against membrane potential and B) against oxygen consumption. Data of mice fed for 9 weeks are adopted from Figure 20. C) Residual ROS production was calculated to eliminate the influence of membrane potential and oxygen consumption respectively. * $p < 0.05$ according to Student's ttest, n = 4 per group

3.4   Proteome study in mitochondria-enriched protein fractions from liver

The proteomic approach was chosen to gain a more comprehensive insight in high fat diet induced changes in mitochondrial metabolic pathways and associations to other organelles. Therefore the hepatic protein suspension of mice fed a high fat or control diet for 9 weeks was enriched by density gradient centrifugation for mitochondria and organelles of comparable density and was subjected to state-of-the-art proteomic analysis (2.13.1).

3.4.1   Subcellular distribution and differentially expressed proteins

For each the adolescent, young adult and middle-aged mice of the high fat and control-fed group one pool of mitochondria-enriched protein was profiled for the proteome. Each pool was analyzed in technical triplicates. In total 1527 proteins were identified and 206 proteins were differentially expressed by high fat diet ($p < 0.05$). About one third of regulated proteins were downregulated in high fat-fed mice and about two thirds were upregulated as illustrated in a heat map (Figure 25 A). The abundance of proteins that were regulated by high fat diet was further analyzed regarding the age groups (Figure 25 B). Abundances of proteins were z-score transformed and proteins with similar age-related patterns were summarized as cluster using the k means algorithm (2.13.1). Two clusters (4, 6) described proteins that were downregulated by high fat diet; ten clusters were defined for proteins that were upregulated by high fat diet. Fold changes (FC) were calculated as quotient of the mean abundance of the high fat groups divided by mean of the control groups. Most proteins were regulated within the range of $0.5 < FC < 2$ (Figure 25 C). For pathway analysis, all 206 proteins, which were significantly regulated by high fat diet, were considered.

As expected not all of the identified proteins from mitochondria-enriched fractions could be designated as mitochondrial proteins. Combining gene ontology based Genomatix prediction and the Mito Carta, a compendium of more than one thousand mitochondrial proteins (Pagliarini *et al.* 2008), 826 (54%) of total 1527 identified proteins could be assigned to mitochondria. Proteins that were attributed to more than one compartment by Genomatix were hierarchically sorted to mitochondria, endoplasmic reticulum (ER), peroxisomes, lysosomes, ribosomes, vesicles and cytosol. The distribution results in 54 % mitochondrial proteins, 13 % ER proteins, 2 % peroxisomal, 3 % lysosomal and 5 % ribosomal proteins (Figure 25 D). Within differentially expressed proteins the distribution pattern to subcellular compartments was similar (Figure 25 D). All significantly regulated proteins including subcellular distribution and the age-related cluster are listed in the appendix (Table 27). Multiple subcellular allocations are given, where assigned by Genomatix.
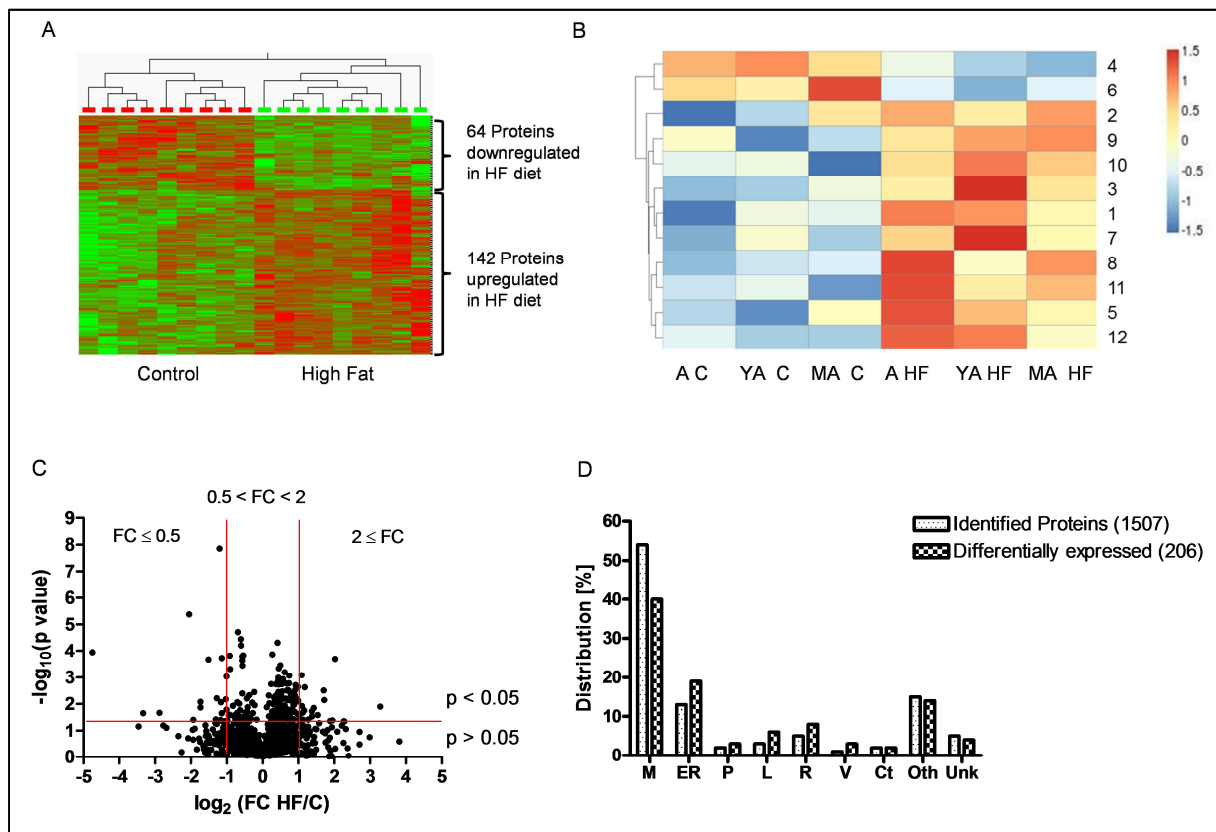
Figure 25: Characteristics of the proteome analysis in mitochondria-enriched protein fractions

A) Heat map of regulated proteins by high fat diet B) Age dependent pattern of protein abundances of the proteins regulated by high fat diet. Proteins were summarized to clusters according to k-means algorithms. Clusters are numbered right to the map. C) Volcano plot of all identified proteins. D) Subcellular distribution of proteins according to Genomatix pathway analysis. A – adolescent, YA – young adult, MA – middle-aged, C – control, HF – high fat, M – mitochondria, ER – endoplasmic reticulum, P – peroxisome, L – lysosome, R – ribosome, V – vesicle, Ct – cytosol, Oth – other, Unk - unknown

Regulation patterns of proteins by high fat diet took partly place dependent on the cellular compartment. Lysosomal proteins were downregulated and mostly attached to cluster 4 (Figure 25 B). Peroxisomal proteins were downregulated, too, and distributed half to cluster 4, half to cluster 6. One third of mitochondrial proteins regulated by diet were downregulated, two thirds (58 proteins) were upregulated. About half of the upregulated proteins are sorted in cluster 8 and 11. Protein function relates to multiple pathways in which mitochondria take part.

3.4.2   Metabolic pathways related to mitochondria

Pathway analysis was based on Genomatix Pathway System (GePS) and Ingenuity Pathway Analysis (IPA). Lists of pathway-related proteins were extended by database research, e.g. gene ontology (GO) terms or manual literature research. Differentially expressed proteins categorized as mitochondrial displayed no clear pathway dependent regulation. Proteins involved in the electron transport chain (GePS) or ATP synthesis (IPA) were partially induced or repressed in their abundance by high fat diet, among them subunits of complex I, V and cytochromes (Table 9). Breaking down fatty acids is the basis to for fat-derived energy equivalents (Jiang *et al.* 2013). Proteins of the mitochondrial β-oxidation were neither clearly induced nor suppressed by high fat diet (Table 9). Long acylchain specific (Wanders *et al.* 1999) trifunctional protein (Hadha) was slightly but significantly reduced in mitochondria of high fat-fed mice compared to control-fed mice, whereas short chain specific (Wanders *et al.* 1999) acyl-CoA dehydrogenase (Acads) and 3-ketoacyl-CoA thiolase (Acaa2) were induced by high fat diet. Of note, peroxisomal proteins of β-oxidation were reduced by high fat diet.

In addition to bioenergetics and fatty acid oxidation, urea cycle enzymes, catabolism of branched chain amino acids and heme biosynthesis were influenced by high fat diet. The urea cycle pathway and branched chain amino acid catabolism were neither clearly induced nor suppressed (Table 29 in the appendix). Two enzymes of the heme biosynthesis were downregulated in mitochondria of high fat-fed mice. Noteworthy, the pathway of superoxide detoxification was downregulated, too, due to downregulated catalase (Cat) and superoxide dismutase 1 (Sod1). Summed up mitochondrial bioenergetic proteins and substrate oxidation with regard to fatty acid breakdown was hardly changed by high fat diet on protein level. An interesting link was provided by the downregulated enzymes of direct superoxide conversion, which connects to the redox metabolism (3.4.6 and 3.4.7).

Table 9: Proteins named in the GePS biological process "*electron transport chain*" **and/or the IPA BioFunction** "*synthesis of ATP*" **and/or for** *"fatty acid β-oxidation"* **by either GePS or IPA**

Uniprot ID	Gene Symbol	Localization	FC	Annotated by
Electron transport chain and ATP synthesis				
A2AQ17	Ndufaf1	M	1.9	IPA
P52503	Ndufs6	M	0.8	IPA, GePS
A2AJX2	Ndufs4	M	0.7	GO[1]
Q544Z9	Cyb5	M	1.4	GePS
Q56A15	Cycs	M	0.9	GePS
Q4FK74	Atp5d	M	0.5	IPA
Q8C140	Slc25a13	M	1.1	IPA, GePS
Q9Z2I0	Letm1	M	1.3	IPA
Q80TX7	Opa1	M	1.3	IPA
Fatty acid β-oxidation				
Q3UKH3	Acaa2	M	2.3	IPA, GePS
Q8K370	Acad10	M	1.3	GO[2]
Q91W85	Acads	M	1.2	IPA, GePS
Q8BMS1	Hadha	M	0.9	IPA, GePS
Q3UNR3	Slc27a2	M, ER, P, V	1.7	IPA, GePS
Q8VCB0	Acox2	P	0.7	IPA, GePS
Q9DC50	Crot	M, P	0.5	GePS
Q9DBM2	Ehhadh	M, P	0.4	IPA, GePS

[1]Gene Ontology: mitochondrial respiratory chain complex I assembly
[2]*Gene Ontology: acyl-CoA dehydrogenase activity*
M – mitochondria, ER – endoplasmic reticulum, P – peroxisome, V - vesicle

3.4.3   High fat diet initiated translation and protein processing

Top scorer on the "canonical pathway" list provided by IPA was eukaryotic initiation factor 2 (EIF2) signaling. In the proteome analysis, the pathway covered 11 upregulated proteins from the small and large ribosomal subunits and regulatory proteins connected to translation by the pathway analyses (Table 10 upper part). Some proteins were up to 5 fold higher expressed in high fat-fed mice compared to control-fed mice, which indicated a comprehensive upregulation of the pathway.

Table 10: Proteins involved in GePS pathway *"translation"* **or** *"protein processing/glycosylation"* **and/or IPA canonical pathway** *"EIF2 Signaling"* **or** *"glycosylation of protein"* **and/or KEGG** *"protein processing in the ER"*

Uniprot ID	Gene Symbol	FC	Annotated by
Translation/ EIF2 Signaling			
Q3TK73	Rpl7	4.9	IPA, GePS
D3YTQ9	Rps15	3.3	IPA, GePS
D3Z5R8	Rps19	2.2	IPA, GePS
Q3UBI6	Rpl7	2.2	IPA, GePS
A2A9W4	Mrps7	1.6	IPA, GePS
Q5BLJ7	Rps13	1.6	IPA
Q497N1	Rps26	1.5	IPA
Q58EW0	Rpl18	1.5	IPA, GePS
B2CY77	Rpsa	1.4	IPA, GePS
Q9JJI8	Rpl38	1.4	IPA, GePS
Q9CWI9	Rps23	1.3	IPA, GePS
P14115	Rpl27a	1.2	IPA, GePS
Q8BN32	Pabpc1	1.7	IPA
D3YVH7	Pa2g4	1.6	GePS
Protein Processing in the ER/ Glycosylation of protein			
Q9CYN2	Spcs2	1.4	GePS
Q3TVJ8	Ssr4	1.3	KEGG
Q3TG02	Stt3a	1.3	KEGG, IPA, GePS
Q3TMR2	Ces6	2.4	IPA, GePS
Q3UC51	Ddost	1.4	KEGG, IPA, GePS
A2ACG7	Rpn2	1.4	KEGG, IPA, GePS
Q5RKP4	Rpn1	1.6	KEGG, IPA, GePS
Q3U026	Mogs	1.9	KEGG, IPA
B1AY76	Erp44	1.5	KEGG
A2AUF6	Hspa5 (Grp78)	1.3	KEGG
P27773	Pdia3	1.4	KEGG
Q3TF72	P4hb	1.3	KEGG
Q3TT79	Pdia4	1.3	KEGG
Q3TXE5	Canx	1.9	KEGG
B2MWM9	Calr	1.6	KEGG

Furthermore, consultation of the Kyoto Encyclopedia of Genes and Genomes (KEGG) pathway (Kanehisa & Goto 2000) identified a set of proteins involved in "protein processing in the ER" (Table 10 lower part). These proteins either serve in "glycosylation of proteins", "cell redox homeostasis" or "response to unfolded protein". Their unanimous upregulation

suggests that protein folding and maturation in ER was aggravated. For example calnexin (Canx), calreticulin (Calr) and protein disulfide isomerase a3 (Pdia3), also known as Erp57, are three members of the CRT/CNX-cycle controlling glycoprotein folding (Wang *et al.* 2012b). For ER resident protein 44 (Erp44), Pdia3, Pdia4 and prolyl-4 hydroxylase β (P4hb) the pathway "cell redox homeostasis" was provided by GePS. Furthermore GePS introduced the pathway "response to unfolded protein" for Erp44, heat shock protein 5a (Hsp5a), also known as glucose-regulated protein 78 (Grp78), and vesicle-associated membrane protein-associated protein B and C (Vapb). Taken together, multiple chaperones involved in quality control of protein folding were moderately upregulated in livers of high fat-fed mice. This eventually prevents the appearance of unfolded proteins, as the translational machinery is distinctly enhanced.

3.4.4   High fat diet induced phospholipid synthesis and VLDL maturation

The liver actively secretes triglycerides enveloped as very low density lipoproteins (VLDL). Two clearly induced proteins were apolipoprotein B and E, both essential molecules of VLDL particles (Jiang *et al.* 2013). In the proteome data "plasma lipoprotein particle organization" is given by GePS, and IPA provides "efflux of cholesterol" and "secretion of triacylglyceride" (Table 11). Noteworthy, regulation pattern of the proteins mentioned do not necessarily support increased VLDL secretion *in vivo*. The regulation of Scd1, Npc2 and Hsd17b2 were stated by IPA to decrease the VLDL secretion (Table 11).

In addition to results obtained by pathway analysis tools, literature provides evidence for proteins upregulated by high fat diet which are involved in the complex processes connected to VLDL maturation (Table 11 lower part). VLDL maturation involves a set of enzymes modifying lipids, e.g. esterification, as well as triglyceride lipases, providing fatty acids and proteins mediating correct lipidation of ApoB (Sturley & Hussain 2012), (Sundaram & Yao 2010). For microsomal triglyceride transfer protein (Mtp) a trend towards increased abundance was observed in high fat diet groups, which did not attain statistical significance ($p < 0.07$)

Table 11: GePS/IPA networks: Proteins for *"cholesterol efflux"* **(E),** *"cholesterol transport"* **(T),** *"cholesterol esterification"* **(Est), and proteins involved in** *"lipoprotein assembly"* **(Lipo) and** *"secretion of triglycerides"* **(S). The second paragraph of the table extends the network beyond GePS and IPA by proteins involved in VLDL maturation, phospholipid metabolism and ER to mitochondria tethering with literature references**

Uniprot ID	Gene Symbol	FC	Function (Annotation/Reference)
Cholesterol, triglyceride and lipoprotein metabolism			
Q3TX45	Apoe	3.7	E, S (IPA); T, Est, Lipo (GePS)
Q8CGG8	Apob	1.9	E, S (IPA);T (GePS)
Q8R0Y9	Soat2	1.8	E (IPA); T, Est, Lipo (GePS)
Q3TJI8	Hsd11b1	2.0	S (IPA)
Q547C4	Scd1	0.4	E (IPA); Est (GePS)
Q3TXQ4	Npc2	0.4	E (IPA); T (GePS)
P51658	Hsd17b2	1.5	S (IPA)
VLDL maturation and transport, phospholipid metabolism, ER to mitochondria tethering			
Q3UWB1	Ces1f (Tgh-2)	1.3	Microsomal hepatic triglyceride lipase (Okazaki *et al.* 2006)
O08601-2	Mtp[1]	1.2	protein lipidation, lipoprotein transport (GO term), (Wang *et al.* 2012a)
Q3TF72	P4hb (PDI)	1.3	Interference with Mtp for VLDL maturation (Wang *et al.* 2012a)
O35490	Bhmt	1.9	Concentration of phosphatidylcholine (IPA), one carbon metabolism (Dahlhoff *et al.* 2013), VLDL assembly (Sparks *et al.* 2006)
Q91X83	Mat1a	1.5	one-carbon metabolic process (GO term), VLDL assembly (Cano *et al.* 2011)
Q3UZ06	Sec22b	2.1	Intracellular transport (GePS), VLDL vesicle transport (Rahim *et al.* 2012)
Q0PD65	Rab2a	1.5	Intracellular transport (GePS)
Q0PD50	Rab8a	1.4	Intracellular transport (GePS)
Q3U621	Rab10	9.8	Intracellular transport (GePS), ER dynamics for phospholipid synthesis (English & Voeltz 2013)
Q3UDJ2	Sgpl1	4.9	Production of ethanolamine for phospholipids (Hla & Dannenberg 2012)
Q3TEX7	Mfn2[2]	2.1	Outer mitochondrial membrane to ER tethering (de Brito & Scorrano 2010)
Q3UJU9	Fam82a2 (Ptpip51)	1.4	Outer mitochondrial membrane to ER tethering (De Vos *et al.* 2012)
Q8BH80	Vapb	1.3	Outer mitochondrial membrane to ER tethering (De Vos *et al.* 2012)

[1] $p < 0.07$, [2] $p < 0.09$

The IPA annotation "concentration of phosphatidylcholine" (Table 11 lower part) connects to the synthesis of phospholipids. The availability of phospholipids and especially phosphatidylcholine is crucial for lipoprotein and lipid droplet production (Cole *et al.* 2012). Proteins of the one carbon metabolism have been connected to the phospholipid synthesis as well as one member of the ras related protein family; noteworthy, Rab10 was the strongest induced protein in the proteome analysis. As phospholipid synthesis takes part in

cooperation between ER and mitochondria (Rieusset 2011), the proteome was searched for tethering proteins. Indeed, mitochondria to ER contact sites were influenced by high fat diet (Table 11 lower part). Of note, mitofusin 2 (Mfn2), which can either reside on the ER membrane as well as on the outer mitochondrial membrane (de Brito & Scorrano 2010), was borderline significantly induced by high fat diet ($p < 0.09$). Taken together, IPA and GePS analysis revealed proteins upregulated by high fat diet, which were involved in lipoprotein maturation and cholesterol transport. Additionally this annotation can be enlarged towards a network, which provides the building blocks to mature VLDL combining mitochondrial and ER functions by tethering these two organelles.

3.4.5 Lysosomal degradation and diet-induced triglyceride accumulation

Intriguingly, adolescent high fat-fed mice did not accumulate triglycerides in the liver in contrast to young adult and middle-aged mice (Figure 18 B). In order to identify protective regulations in adolescent mice, a correlation was investigated between age-related regulation patterns of proteins, that were differentially expressed by high fat diet (Figure 25 B) and the hepatic phenotype.

The cluster that was best correlated to the phenotype ($R^2 = 0.7$) was cluster 4 (Figure 25 B), which comprises proteins, that were downregulated by high fat diet. The older the mice, the more reduced is the protein abundance. This cluster 4 comprised 14 regulated lysosomal proteins. The abundance of these individual proteins was correlated to the hepatic phenotype and regression analysis was conducted. Correlation coefficients showed for these proteins a strong negative association to the accumulation of liver triglycerides. Coefficient of determination (R^2) was calculated for these lysosomal proteins (Table 12). Lysosomal associated protein 2 (Lamp2), Phospholipase B-like 1 (Plbd1), cathepsin H (Ctsh), cathepsin S (Ctss) and cathepsin A (Ctsa) represented lysosomal proteins with $R^2 > 0.75$ and the calculated regression reached significance for these proteins (Table 12). Conclusively, the degree of downregulation of lysosomal proteins with increasing age is strongly associated with detrimental accumulation of triglycerides in liver of high fat-fed mice.

Table 12: Regression analysis of lsysosomal proteins downregulated by high fat diet and hepatic triglyceride accumualtion

Uniprot Accession	Gene Symbol	Correlation Coefficient (r)	Significance of regression (p)	Coefficient of Determination (R^2)
A2A430	Lamp2	-0.96	0.002	0.93
Q8VCI0	Plbd1	-0.92	0.009	0.85
Q3UCD6	Ctsh	-0.92	0.01	0.84
Q3UBR4	Ctss	-0.88	0.02	0.77
Q9D2D1	Ctsa	-0.87	0.02	0.76
B2RUD7	Psap	-0.78	0.07	0.60
Q3TXQ4	Npc2	-0.77	0.07	0.59
Q8CC47	Galns	-0.76	0.08	0.58
D3Z220	Ctsc	-0.69	0.13	0.47
Q3TC17	Ctsb	-0.68	0.14	0.46
Q3U6T2	Naga	-0.64	0.17	0.42
Q8R082	Dpp7	-0.57	0.24	0.33
Q3T9E5	Ncst	-0.56	0.25	0.31
Q8K2I4	Manba	-0.40	0.43	0.16

3.4.6   Regulation of antioxidative proteins and ER chaperones in the context of age-dependent triglyceride accumulation

Age-related clustering (Figure 25 B) were searched for upregulated mechanisms that potentially protected adolescent high fat-fed mice against hepatic fat accumulation. Therefore clusters were focused on that show the highest abundance in adolescent high fat-fed mice. This comprises clusters 1, 8, 11, 5, and 12 (Figure 25 B). ER chaperones Grp78, Pdia3, P4hb, Erp44, Canx and Calr were sorted to these clusters (Table 27 in the appendix). Furthermore proteins followed this patte, that were summarized in the Nrf2-dependent response to oxidative stress by IPA and GePS, namely Aldh3a2, Akr7a5, Hsp40 and Msra (Table 13, Table 27). Carbonic anhydrase 3, a radical scavenger (Raisanen *et al.* 1999), fitted this pattern, too. The antioxidative response being more pronounced in adolescent high fat-fed mice cannot be statistically tested in appropriate terms due to limited number of biological samples. The hypothesis that the antioxidative response was induced by the transcription factor Nrf2 was further analyzed.

3.4.7 Nuclear factor erythroid-derived 2-like 2 (Nfe2l2 or Nrf2) mediated stress response was connected to mitochondria

Liver mitochondria of high fat-fed mice released high rates of ROS (Figure 19 C). The main regulator of antioxidative gene expression is nuclear factor erythroid-derived 2-like 2 (Nrf2) (Kobayashi & Yamamoto 2006), which was described by IPA and GePS as upstream regulator of a group of proteins associated with cellular stress (Table 13). In addition to proteins that were indicated by the pathway analysis tools, crosschecking a list of Nrf2-regulated targets, screened by chemically induction of Nrf2 dependent gene expression (Kwak *et al.* 2003), revealed further associations to regulated proteins in the proteome study, not exclusively connected to oxidative stress. Intriguingly, regulation of some proteins, e.g. Sod 1 and catalase, do not support the activation of an Nrf2-mediated response (Table 13). Hydroxysteroid (11-beta) dehydrogenase 1 (Hsd11b1) and phosphoglycerate mutase 5 (Pgam5) were both co-cited with Nrf2 (GePS) and are described in literature to modulate Nrf2 activation. While Hsd11b1 takes part in the inactivation of Nrf2-dependent gene expression (Kratschmar *et al.* 2012), reduction of Pgam 5 was shown to increase Nrf2 translocation to the nucleus. Furthermore Pgam5 tethers Keap1 and Nrf2 to the outer mitochondrial membrane (Lo & Hannink 2008) and therefore juxtaposes Keap1 and Nrf2 to the site of mitochondrial ROS production.

Nrf2 itself was not identified in the proteome analysis but was suggested as upstream transcription factor by GePS and IPA, whereas Pgam5 was identified downregulated by high fat diet. Therefore the hypothesis was tested that Nrf2 is less abundant in mitochondria-enriched fractions of high fat-fed mice together with Pgam5. Accordingly, protein pools were subjected to a western blot analysis for Nrf2, Pgam5, CS and Sod2. Specific bands of the respective antibodies (Figure 26 A) were quantified by densitometry. The dataset 1 represents the protein pools that were analyzed in the proteome study, too.

Table 13: Proteins regulated by Nrf2 or regulating Nrf2

Uniprot ID	Gene Symbol	FC	Pathway/Function (Annotation/Reference)	Predicted regulation fits observed regulation (Y/N)
B1ATI0	Aldh3a2	2.1	Target of Nrf2 regulon[1], repair of lipiperoxides (Demozay *et al.* 2008)	Y
A2AMV3	Akr7a5	1.4	Nrf2-mediated oxidative stress response (IPA), repair of lipidperoxides (Li *et al.* 2006)	Y
Q5EBQ7	Msra	1.4	Co-cited transcription factor Nrf2 (GePS), repair of oxidized cysteine residues (Styskal *et al.* 2013)	Y
A2A8C9	Hsp40 (Dnajc11)	1.4	Nrf2-mediated oxidative stress response (IPA)	Y
Q3TXQ6	Cat	0.7	Nrf2-mediated oxidative stress response (IPA, GePS)	N
P08228	Sod1	0.6	Nrf2-mediated oxidative stress response (IPA, GePS)	N
Q91VS7	Mgst1	1.3	Nrf2-mediated oxidative stress response (IPA, GePS), repair of lipidperoxides (Kelner *et al.* 2000)	Y
Q64435	Ugt1a6	2.6	Co-cited transcription factor Nrf2 (GePS)	Y
O35728	Cyp4a14	0.4	Co-cited transcription factor Nrf2 (GePS), microsomal FAO (Gambino *et al.* 2011)	N
Q8VCW9	CYP2A12	1.8	Target of the Nrf2 regulon[1]	Y
B6VGH4	CYP1A2	1.6	Target of the Nrf2 regulon[1]	Y
O35490	BHMT	1.9	Target of the Nrf2 regulon[1]	Y
Q543J0	Uox	0.7	Target of the Nrf2 regulon[1]	Y
O88833	CYP4A10	0.5	Target of the Nrf2 regulon[1], microsomal FAO (Gambino *et al.* 2011)	N
Q8BJL4	LMAN2	1.6	Target of the Nrf2 regulon[1]	Y
Q9D8V0-3	HM13	1.7	Target of the Nrf2 regulon[1]	Y
O88668	Creg1	0.5	Target of the Nrf2 regulon[1]	N
Q3TJI8	Hsd11b1	2.0	Co-cited transcription factor Nrf2 (GePS), inactivates Nrf2 (Kratschmar *et al.* 2012)	--
A1A4A7	Pgam5	0.5	Co-cited transcription factor Nrf2 (GePS), tethers Nrf2 to mitochondria (Lo & Hannink 2008)	--

[1](Kwak *et al.* 2003)

The densitometric analysis followed by paired Student's t-test statistic confirmed significant downregulation of Pgam5 in dataset 1. Furthermore CS and Sod2 abundance was unregulated, which again confirmed proteome results. Nrf2 was represented in two bands at 57 kDa, which is specified by the manufacturer's instructions and at around 70 kDa, which is specified by UniprotKB. Both bands show a strong tendency towards reduction in mitochondria-enriched protein pools of high fat-fed mice in dataset 1, although this was not significant by statistics (Figure 26 B). In protein pools of data set 2, CS and Sod2 were unregulated by diet, Pgam, and Nrf2 tended to be reduced by high fat diet (Figure 26 C).

Combining these two datasets and performing paired t-tests corroborate reduced Pgam5 protein abundance accompanied with significantly reduced Nrf2 in high fat-fed mice (Figure 26 D).
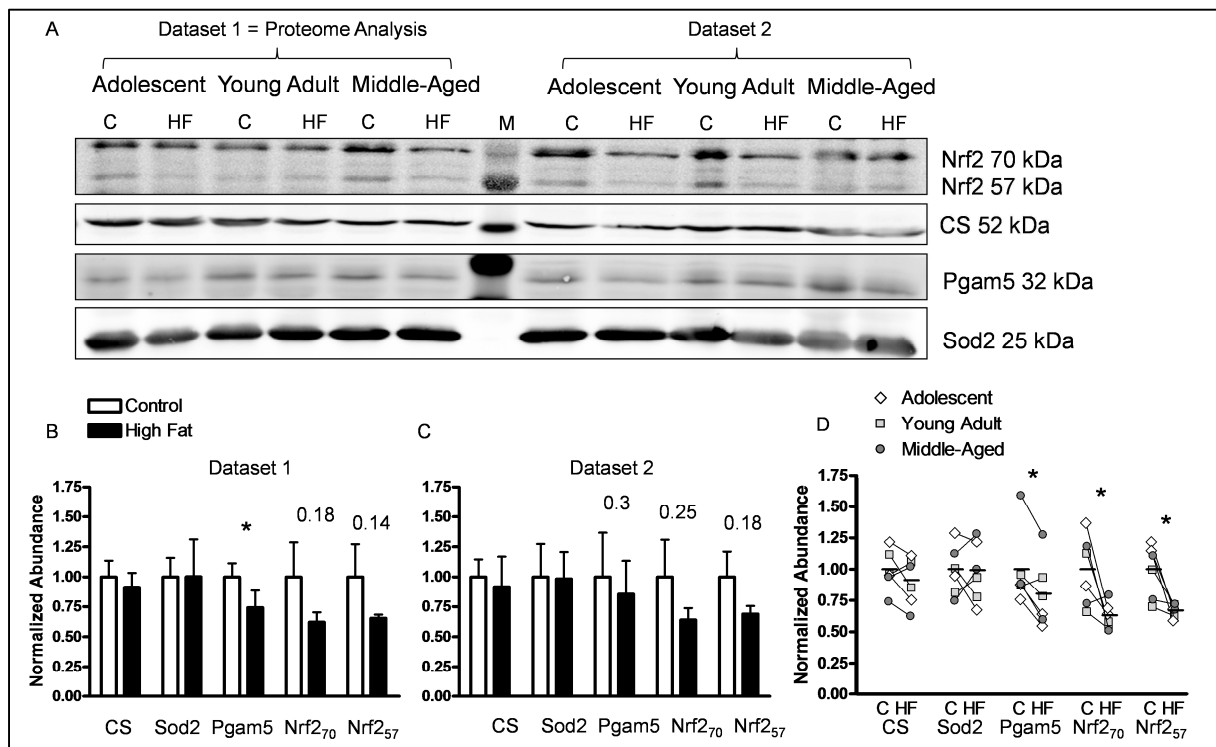
Figure 26: Validation of proteome data by western blot analysis

A) Blot of protein pools for specific bands indicated. B) Densitometric analysis of dataset 1 with paired, two-tailed Student's t-statistic; p-values are given, * p < 0.05, n = 3 per diet group. C) Densitometric analysis of dataset 2; statistics as explained for B. n = 3 D) combined data set and paired, two-tailed ttests, n = 6, lines connect control and high fat group of the respective age and data set.

Taken together, the proteome finding was confirmed by western blot analysis. Additionally the data strongly support a mechanistic connection between increased mitochondrial ROS production, Pgam5 downregulation and the initiation of an antioxidative response by Nrf2-dependent gene expression in livers of high fat-fed mice. The complex interaction in liver of high fat-fed mice will be further discussed and summarized as model of regulation (Figure 28).

4   Discussion

Diet induced obesity induces major metabolic adaptations, which involves the development of insulin resistance and triglyceride accumulation in skeletal muscle and liver. These organs play major roles in the regulation of blood glucose and fat metabolism (Savage *et al.* 2007). Mitochondria as the powerhouse of the cells may be involved in the adaptations of the metabolism to excessive dietary fat intake (Muoio & Neufer 2012). With aging many metabolic pathways change: The susceptibility to diet induced obesity increases, the sensitivity of peripheral tissue to insulin decreases and mitochondria-related redox functions may be less efficient (Michalakis *et al.* 2013). The present thesis aimed to monitor the impact of high fat diet and age. Therefore the high fat feeding experiments were performed in three different age groups: adolescent mice were 8 weeks of age at onset of feeding, young adult mice were 16 weeks of age and middle-aged mice were 52 weeks of age, when the high fat feeding was started (Figure 7).

4.1   C57BL/6J as model in obesity research

C57BL/6J mice have been chosen, because they are most commonly used as model for diet induced obesity and related complications such as impaired glucose tolerance (Clee & Attie 2007), (Montgomery *et al.* 2013). This mouse strain has been either classified as diabetes-prone or diabetes-resistant, most probably due to general differences in the definition of the diabetic state. In the C57BL/6J mouse strain a mutation in the nicotinamide nucleotide transhydrogenase (Nnt) gene has been characterized and implicated in a reduced insulin secretion from the β-cells (Toye *et al.* 2005). Despite this impairment C57BL/6J mice have not been observed to undergo β-cell failure, which is the final determinant of diabetes mellitus (Clee & Attie 2007). The implication of the Nnt mutation in the redox balance has been investigated in isolated liver mitochondria, which were fully functional. The glutathione redox system was more oxidized than in Nnt expressing mice. Some of the disease-like phenotypes reported in literature, may be related to the mutation. Under physiological conditions, NADPH pool might be sufficiently maintained by compensation of other NADPH generating systems (Ronchi *et al.* 2013).

In the present thesis, mitochondrial-derived ROS and the redox system were investigated to clarify its role in the development of obesity-induced skeletal muscle insulin resistance and fatty liver. Recent hypotheses argue for chronically enhanced release of ROS but in rates below the threshold of oxidative stress (Fisher-Wellman & Neufer 2012). The susceptibility of this mouse model towards enhanced ROS production rates and to develop a more oxidized

redox environment, may be regarded as adequate tool to illustrate even small diet induced changes in mitochondrial ROS production and consequences in the redox circuits, controlled by using littermates in the respective experiments.

4.2   Phenotypic response to high fat diet

4.2.1   Bodyweight development

In a very recent mouse strain comparison C57BL/6J mice were termed intermediate responders regarding weight gain and glucose homeostasis (Montgomery *et al.* 2013). The experiments reported in this thesis clearly delineate the age-specific body mass gain and body composition. Adolescent mice put on weight on both diets by means of lean mass. This indicates that mice in the adolescent group are not grown up yet. The partitioning of energy from feeding a high fat diet into growth was reported in mice fed a high fat diet shortly after weaning (Cordoba-Chacon *et al.* 2012). Between 6 and 12 months of age male C57BL/6J mice increase their body mass by displaying stable lean mass and increasing fat mass (Ackert-Bicknell *et al.* 2008). The observation of increased adiposity during life span in this mouse strain (Nishikawa *et al.* 2007) relates well to the human situation (Michalakis *et al.* 2013) and underlines the importance of aging effects in metabolic studies.

In the prolonged feeding experiment for 26 weeks mice gained continuously body mass in the range described before (Surwit *et al.* 1988), (Hoeks *et al.* 2011), (Hoffler *et al.* 2009). Interestingly, young adult mice fed a high fat diet for 26 weeks, weigh about as much as middle-aged mice fed for 9 weeks a high fat diet. This underlines the higher susceptibility of middle-aged mice for body mass gain. As limitation of the presented data, middle-aged mice were not subjected to the prolonged feeding protocol.

4.2.2   Glucose homeostasis

Glucose homeostasis was assessed by intraperitoneal glucose tolerance tests (ipGTT). In response to high fat feeding glucose handling was rapidly changed in the present study. Mice received a comparable amount of glucose, because the bolus was calculated regarding the lean mass, which is recommended for mouse models of obesity (Ayala *et al.* 2010). This excludes effects on glucose homeostasis that are simply caused by the fact that high fat-fed mice received more glucose and therefore strengthens the significance of the presented experiments.

In literature high fat diet induced glucose intolerance and hyperglycemia as soon as after three days (de Wilde *et al.* 2008), (Lee *et al.* 2011b), although another study showed that glucose clearance was normal after 2 weeks of feeding (Boudina *et al.* 2012). The total AUC in the here described adolescent group was increased after 1 week of feeding (Figure 10), but the iAUC was normal, indicating that the glucose clearance was still normal in adolescent mice. Rather fasting hyperglycemia, identified before as marker for increased basal hepatic gluconeogenesis when feeding a high fat diet (Lee *et al.* 2011b), accounted for the increased AUC in the adolescent group. In comparison to the adolescent group, the older mice displayed a more severe reduction in the metabolic responsiveness after 1 week high fat feeding (Figure 10). The glucose intolerance consistently proceeded in all age groups during the feeding period of 9 weeks, which is well in line with reports by others (Lee *et al.* 2011b), (Boudina *et al.* 2012). Fasting insulin concentration tended already to be elevated in middle-aged control mice compared to adolescent control mice (Table 1), which has been reported (Jacobson 2002), (Capel *et al.* 2011). Interactions between increasing adiposity and decreasing insulin sensitivity during aging were established in rodent models (Barzilai & Gupta 1999). Therefore the mouse model reflects the situation in humans.

In the context of aging it is compelling that middle-aged mice fed a high fat diet showed dramatically increased fasting insulin, which perfectly fits investigations in diet-induced obese C57BL/6J mice of this age reported before (Koonen *et al.* 2010). It is not far-fetched to conclude that this increase in insulin counterbalances to some extent decreased peripheral insulin sensitivity during the glucose challenge. In the long term feeding sustained hyperinsulinemia and hyperglycemia (Table 2) fit previous metabolic characterizations in C57BL/6J mice (Hoffler *et al.* 2009), (Hoeks *et al.* 2011). The prolonged model is relevant to display progressive metabolic changes and adaptations. Conclusively, investigations in three different age groups comprehensively illustrated interactions between the high fat-diet related and age-related changes in glucose metabolism. Thus the experimental design was suitable to study metabolic consequences of impaired glucose handling in skeletal muscle and liver.

4.2.3 Skeletal muscle insulin resistance

Monitoring glucose handling by GTT is unable to distinguish if reduced glucose clearance is due to less pancreatic insulin release or reduced insulin sensitivity (Ayala *et al.* 2010). Therefore the presented metabolic characterization did not experimentally prove that C57BL/6J mice developed skeletal muscle insulin resistance. Literature provides a considerable body of evidence that C57BL/6J mice indeed exhibit skeletal muscle insulin resistance during high fat feeding. This was substantiated by glucose uptake studies in

isolated soleus muscle of male C57BL/6J (Turner *et al.* 2007), (Boudina *et al.* 2012) and hyperinsulinemic euglycemic clamp studies (van den Berg *et al.* 2010), (Hoeks *et al.* 2011). In the abovementioned studies different sources of fat were used, among others a palm oil based diet (Hoeks *et al.* 2011), (van den Berg *et al.* 2010) representing mostly the diet used in the experiments presented in this thesis. In these studies, after 5 weeks of feeding skeletal muscle insulin resistance was detected. Regarding a timeline, mice were already glucose intolerant due to the results from glucose tolerance tests presented here, when the insulin resistance is established in skeletal muscle after approximately 5 weeks (Figure 27). End points of 9 and 26 weeks of feeding therefore should reflect the insulin resistant situation in skeletal muscle of high fat-fed mice.

4.2.4   Triglyceride accumulation in the liver and hepatic insulin resistance

Fat accumulates in hepatocytes when fat uptake and/or fat synthesis override fat utilization and/or export. After feeding a palm oil based high fat diet or control diet for 9 weeks, adolescent high fat-fed mice were resistant to hepatic fat accumulation. In contrast, young adult mice and middle-aged mice accumulated triglycerides in the liver (Figure 18 B). Increased triglyceride content in the liver, also referred to as fatty liver, has been reported in C57BL6J mice in response to a high fat diet before (Turner *et al.* 2009), (Yuzefovych *et al.* 2013), (Satapati *et al.* 2012), (Rubio-Aliaga *et al.* 2011), (Kirpich *et al.* 2011), (Kim *et al.* 2004). Interestingly, also adolescent mice were reported to accumulate hepatic triglycerides within several weeks, especially when fed a lard-based high fat diet (Turner *et al.* 2009), (Sunny *et al.* 2010), (Satapati *et al.* 2012), but also with a palm oil based high fat diet (de Wit *et al.* 2012). Conclusively the protocol of 9 weeks feeding a palm oil based diet induced the first hallmark of non-alcoholic fatty liver disease, which is accumulation of triglycerides. If the protection of adolescent high fat-fed mice is dependent on the fat source of the diet, remains under debate.

Prolonged feeding of lard-based high fat diets robustly induced fatty liver and further hepatic complications related to non-alcoholic fatty liver disease (Nafld) and non-alcoholic steatohepatitis (Nash) in C57BL/6J (Nakamura & Terauchi 2013). This corroborates the triglyceride accumulation observed in adolescent mice fed the palm-oil based high fat diet for 26 weeks in the presented thesis (Figure 22 B). The development of further liver injury cannot be answered from the protocol and experiments in the present study.

The liver maintains the glucose homeostasis during the fasting period. When the insulin action at the liver is blunted, hepatic glucose production is not suppressed, resulting in

elevated blood glucose (Nakamura & Terauchi 2013). The results reported here cannot describe the hepatic insulin sensitivity. Hepatic insulin resistance has been stated (Stewart *et al.* 2009), (van den Berg *et al.* 2010), (Neschen *et al.* 2005). Using a high fat diet with palmitate as predominate fatty acid, 8 weeks of feeding reduced insulin action on the hepatic glucose release in C57BL/6J mice that were 12 weeks of age when the high fat feeding was started (De Vogel-van den Bosch *et al.* 2011). In conclusion, the feeding protocol in the presented thesis potentially initiated hepatic insulin resistance. The interaction between fat accumulation and insulin action in the liver is considered complex. Lipogenic pathways may be still active in the state of depressed insulin action, which is the feature of the selective insulin sensitivity described in the liver (Nakamura & Terauchi 2013).

4.3 Mitochondria in skeletal muscle

4.3.1 *Mitochondrial density, morphology and membrane fatty acid composition*

Initially Kelley and colleagues reported a decrease in mitochondrial size and changed morphology in skeletal muscle of obese persons with and without type 2 diabetes. In this context a positive correlation between mitochondrial size and glucose uptake was established (Kelley *et al.* 2002). Insulin resistance in the skeletal muscle was associated with a reduced number of intramyofibrillar mitochondria, which are located between muscle fibres, in non-diabetic persons and patients of type 2 diabetes (Chomentowski *et al.* 2011).

The hypothesis that mitochondrial morphology and content is decreased in insulin resistant skeletal muscle was investigated in adolescent mice fed a high fat or control diet for 9 weeks. Electron microscopy illustrated intramyofibrillar mitochondria that were normal in size and morphology (Figure 12). Regarding literature reports a timeline was created. After 4 weeks of high fat feeding mitochondrial structure was normal in gastrocnemius muscle of C57BL/6J mice (Bonnard *et al.* 2008) as well as after 8 weeks of high fat feeding (Yokota *et al.* 2009), whereas after 10 weeks (Jheng *et al.* 2012) or 16 weeks (Bonnard *et al.* 2008) mitochondrial morphology had changed. Therefore alterations in mitochondrial ultrastructure due to high fat feeding only develop after feeding periods longer than 9 weeks. Noteworthy, it was not investigated in this thesis, whether this development is accelerated with aging. As final conclusion, in the adolescent mice insulin resistance in skeletal muscle occurs before possible changes in the mitochondrial morphology are obvious.

For a more comprehensive analysis how high fat diet feeding impacts mitochondrial content and the cause-effect relationship regarding skeletal muscle insulin resistance, an alternative surrogate for mitochondrial content, citrate synthase (CS) activity, was investigated. This method correlated best with mitochondrial content assessed by electron microscopy in human skeletal muscle, whereas mitochondrial DNA abundance, which is also frequently used was poorly correlated (Larsen *et al.* 2012). Therefore the further discussion focuses on CS activity measurements to describe the influence of high fat-feeding on mitochondrial content in skeletal muscle.

In literature contrary results exist about the impact of high fat feeding on mitochondrial CS activity in rodent skeletal muscle. A reduction of citrate synthase activity after 4 weeks of high fat feeding was regarded as first hint towards high fat diet induced damage in gastrocnemius muscle mitochondria, which was seen in line with human data in insulin resistant offspring of diabetic persons (Bonnard *et al.* 2008), (Petersen *et al.* 2004). Here, adolescent mice fed a high fat diet for 9 weeks displayed normal CS activity in gastrocnemius muscle compared to the adolescent control-fed mice (Table 4), which was reported before in feeding experiments with a palm-oil based diet (Hoeks *et al.* 2011). Conclusively, mitochondrial mass was not influenced in skeletal muscle of adolescent mice fed the high fat diet for 9 weeks, investigated by electron microscopy and CS activity.

In young adult and middle-aged mice mitochondrial mass was increased compared to the adolescent mice (Table 4). Here high fat feeding induced a further increase, which confirms results by others (Montgomery *et al.* 2013), (Turner *et al.* 2007), (Hancock *et al.* 2008), (van den Broek *et al.* 2010). Therefore skeletal muscle insulin resistance is unlike a consequence of a high fat diet induced reduction in mitochondrial content. Although mitochondrial mass was not assessed in skeletal muscle of mice fed the high fat diet for 26 weeks, literature reports normal CS activity in skeletal muscle after 20 weeks feeding a palm-oil based diet (Hoeks *et al.* 2011) or 6 months of feeding a high fat, high sugar diet (Franko *et al.* 2012). As final conclusion this thesis corroborates that high fat diet feeding does not reduce mitochondrial content in skeletal muscle of C57BL/6J mice.

Phospholipid composition of biological membranes has been designated to reflect dietary status, age and longevity. The quality of dietary fat intake influences the membrane composition. Obesity and metabolic syndrome were linked to a higher saturation in skeletal muscle plasma membrane (Hulbert *et al.* 2005). Mitochondrial functions related to the fatty acid composition in the phospholipids are e.g. pore formation, positioning of transport proteins, modulations of respiratory chain enzyme activity (de Wilde *et al.* 2008), (Pamplona 2008).

(de Wilde *et al.* 2008; Pamplona 2008)(de Wilde *et al.* 2008; Pamplona 2008)(de Wilde *et al.* 2008; Pamplona 2008)Feeding the palm-oil based high fat diet, which is particularly rich in saturated palmitic acid (C16) and oleic acid (C18:1), the main monounsaturated fatty acid (MUFA) (Table 15 in the Appendix) for 9 weeks, shifted the fatty acid composition of biomembranes in skeletal muscle mitochondria towards higher saturation by reducing MUFA (Table 5). This reflects exactly the results in a 4 week- feeding experiment in phospholipids of quadriceps muscle (de Wilde *et al.* 2008) and after 8 and 20 weeks of feeding in phospholipids of isolated skeletal muscle mitochondria (Hoeks *et al.* 2011) both in adolescent C57BL/6J mice.

Hoeks and colleagues addressed the question whether these changes in the phospholipid composition impair mitochondrial oxidative capacity in insulin resistant skeletal muscle. Oxidative capacity was normal in the adolescent C57BL/6J mice fed the palm-oil based high fat diet (Hoeks *et al.* 2011), which was corroborated by the results reported here for the mitochondrial respiration and extended by the normal membrane potential and ROS production rate in adolescent mice fed a high fat diet for 9 weeks (Figure 13, Figure 16). Noteworthy, the results of Hoeks and coworkers are further expanded in the present thesis by the young adult and middle-aged mice fed the high fat diet. With aging SFA were further increased whereas polyunsaturated fatty acids decreased in the middle-aged mice irrespective of the diet (Table 5). Although changes in phospholipid composition were impacted by age (Table 5) as was oxygen consumption (Figure 13), there were no correlations observed (data not shown). Especially leak respiration and the content of DHA are independent of each other, which is not in line with the assumption, that n3 fatty acids increase the proton leak (Hulbert *et al.* 2005). Conclusively a palm oil based high fat diet changes the phospholipid composition in skeletal muscle mitochondria but mitochondrial respiration is robustly performing irrespective of membrane phospholipid composition.

4.3.2 *Mitochondrial oxidative capacity in skeletal muscle*

The impaired adaptation of skeletal muscle mitochondria to excessively available fatty acids as consequence of high caloric intake was hypothesized to account for lipotoxic effects in the skeletal muscle (Serra *et al.* 2012), (Shortreed *et al.* 2009). On the contrary increased mitochondrial oxidative capacity was shown before in response to high fat feeding in skeletal muscle mitochondria (Turner *et al.* 2007) which supports the hypothesis that high fat feeding increases the capacity for fat oxidation in skeletal muscle mitochondria (Muoio & Neufer 2012). Mitochondrial oxidative capacity was tested in the present thesis with the fatty acid derivate palmitoylcarnitine to monitor mitochondrial oxygen consumption in isolated skeletal

muscle mitochondria and identify effects of high fat diet and age. The experiments were conducted in adolescent, young adult and middle-aged mice fed the high fat or control diet for 9 weeks.

In skeletal muscle mitochondria of middle-aged mice proton leak, which means the rate of oxygen consumption not contributing to membrane potential was significantly increased by high fat feeding, whereas proton leak was not affected by high fat diet in the adolescent and young adult mice (Figure 13, Figure 29). Both, high fat feeding (Catala-Niell *et al.* 2008), (Hancock *et al.* 2008), (van den Broek *et al.* 2010) and aging (Brand 2000), (Bellanti *et al.* 2013) have been suggested to induce mitochondrial uncoupling as antioxidative strategy, known as 'uncouple-to-survive' hypothesis (Brand 2000). This characteristic of aging could be accelerated by high fat diet feeding, as suggested before (Iossa *et al.* 2003). Furthermore the increased mitochondrial mass in middle-aged mice (Table 4) may assure the maintenance of oxidative capacity *in vivo*, as hypothesized in a long-term high fat feeding study in rats (van den Broek *et al.* 2010). Conclusively middle-aged mice are more susceptible to high fat diet induced changes in bioenergetics than younger age groups.

In the phosphorylating state oxygen consumption reflects the sum of proton leak respiration and ATP synthesis (Brand & Nicholls 2011). In this condition adolescent mice consume less oxygen than young adult and middle-aged mice at similar membrane potential (Figure 13 B, D). If skeletal muscle mitochondria of adolescent mice worked more coupled than mitochondria of young adult and middle-aged mice, this relation would be obvious in the leak respiration, but posthoc testing showed only a non-significant trend towards more efficient coupling in adolescent mice (Figure 13 A). When coupling efficiency does not explain the reduced oxygen consumption in adolescent mice, ATP synthesis may be reduced. Oxygen consumption in the state of excessive ADP and substrate availability is regarded proportional to the ability of mitochondria to produce ATP. Underlying causes are either reduced substrate oxidation or reduced activity of ATP synthase (Complex V) (Brand & Nicholls 2011).

In contrast, maximal enzyme activity of complexes I, II and V were decreased in middle-aged compared to adolescent mice, which confirms that aging reduces the enzyme activity of respiratory chain complexes (Navarro & Boveris 2007), but does not support that skeletal muscle mitochondria of adolescent mice are limited in the ATP synthesis. Noteworthy, isolated enzyme activity does not necessarily reflect coupled mechanisms during oxidative phosphorylation in intact mitochondria (Brand & Nicholls 2011). High fat diet did not change maximal enzyme activities in gastrocnemius muscle, confirming results by others (Feillet-Coudray *et al.* 2009).

Thus the capacity to generate ATP seems unlimited in adolescent mice and substrate oxidation rates may account for less oxygen consumption. Acylcarnitine concentration in skeletal muscle have been suggested as marker for impaired mitochondrial substrate oxidation due to high fat feeding by accumulation of intermediates deriving from β-oxidation (Koonen *et al.* 2010), (Koves *et al.* 2008). This hypothesis was tested in this thesis for the first time in isolated mitochondria. Mitochondria of high fat-fed mice did not export more acylcarnitines than controls. Conversely, high fat diet significantly reduced middle chain acylcarnitines export (C6 and C8) (Figure 14). Hydroxylated derivatives were below detection limits. This does not support the assumption that β-oxidation capacity is limited by β-hydroxyl-acyl-CoA dehydrogenase activity (Koonen *et al.* 2010) but reflects more likely fluent cycling during acyl-chain degradation.

Furthermore acylcarnitine export negatively correlates with oxygen consumption in the phosphorylating state (Figure 15 B). This observation promotes the principle that mitochondrial substrate oxidation rates depend on the demand for energy (here the rate of ATP synthesis) and not on the substrate delivery (Fisher-Wellman & Neufer 2012), (Muoio & Neufer 2012). In adolescent mice low oxygen consumption rates were observed together with high acylcarnitine release. Restricted substrate oxidation may therefore not explain the low oxygen consumption rates during ATP synthesis in these mice. Skeletal muscle mitochondria of adolescent mice also released higher rates of acylcarnitines independently of the oxygen consumption rate than middle-aged mice (Figure 15 C). Here the small, but significant reduction in gene expression of short chain specific 3-hydroxyacyl-CoA dehydrogenase (DH) and 3-keto-thiolase in middle-aged mice compared to the younger groups (Table 22) could account for less excessive acetyl-CoA production by β-oxidation. The performance of skeletal muscle mitochondria of adolescent mice is inconclusive, because potentially reduced ATP synthesis can neither be explained by reduced ATP synthase activity nor by reduced substrate oxidation. Noteworthy, these parameters need more proficient investigations, e.g. by determining substrate flux using labelled fatty acids.

In conclusion high fat feeding did neither deleteriously impair mitochondrial β-oxidation nor respiratory chain functions. In skeletal muscle of high fat-fed mice normal release of aclycarnitines excludes the potential of lipotoxic effects by acylcarnitine accumulation due to high fat diet-feeding. The small increase in uncoupling in middle-aged mice underlines the importance to include aging effects in the research for metabolic disease.

4.3.3 Mitochondrial ROS production did not induce skeletal muscle insulin resistance

Different parameters of mitochondrial performance were already tested regarding the cause-effect relationship with insulin resistance in response to diet induced obesity: reduced mitochondrial mass (Bonnard *et al.* 2008) or incomplete β-oxidation (Koves *et al.* 2008) were suggested to induce skeletal muscle insulin resistance, but in the present comprehensive analysis including effects related to aging, these parameters are unlikely to cause insulin resistance. In addition elevated reactive oxygen (ROS) production (Anderson *et al.* 2009) was suggested to impair insulin signaling. Therefore mitochondrial ROS production was monitored in the context of high fat diet induced changes in glucose tolerance to generate a timeline of events. Glucose homeostasis changed rapidly after onset of high fat feeding in mice of all three age groups (Figure 10) and skeletal muscle insulin resistance was concluded to develop at least after 5 weeks of high fat feeding (4.2.3). The production of reactive oxygen species was normal in adolescent and young adult mice fed the high fat diet for one and a half weeks (Table 3) and it was still normal in skeletal muscle mitochondria of high fat-fed mice compared to age-matched controls after 9 weeks of feeding using different substrates to induce mitochondrial respiration (Table 3, Figure 16). Even after very long high fat feeding (26 weeks), ROS production in skeletal muscle mitochondria was normal compared to control-fed mice (Table 25). In summary glucose homeostasis and skeletal muscle insulin sensitivity are affected by feeding a high fat diet within 5 weeks, but elevated mitochondrial ROS production cannot be the trigger (Figure 27). This is in contrast to the finding that excessive mitochondrial ROS production in skeletal muscle of rats after 3 weeks of high fat feeding induces skeletal muscle insulin resistance (Anderson *et al.* 2009), but provides support for the hypothesis that high-fat diet induced insulin resistance in skeletal muscle of C57BL/6J mice is not correlated to mitochondrial ROS production (Boudina *et al.* 2012). Furthermore, the general increase of mitochondrial ROS production in middle-aged mice compared to the younger mice (Figure 16), which confirms the observation that aging is correlated to increased ROS production per se (Sohal & Orr 2012), was unaffected by the high fat diet feeding.

In the state of high substrate supply it was suggested that a transient shift in the redox cycling system towards a more oxidized state, eventually leads to an inactivation of players of the insulin signaling cascade (Fisher-Wellman & Neufer 2012). This was further attributed to aging as 'redox stress hypothesis of aging' (Sohal & Orr 2012). Although ROS production was not increased by high fat diet, middle-aged mice fed a high fat diet displayed increased oxidized glutathione in skeletal muscle accompanied with increased glutathione reductase activity, suggesting a higher need for detoxification of oxidation products (Figure 17). In skeletal muscle of adolescent mice high fat feeding did not result in exceeded redox reserve

capacity. This is in contrast to reports of changes in the glutathione redox balance upon feeding C57BL/6J mice a lard based high fat diet (Yuzefovych *et al.* 2013), (Espinosa *et al.* 2013).

In conclusion insulin resistance in skeletal muscle due to high fat feeding develops in the state of normal ROS production (Figure 27). Mitochondrial function was normal after 9 weeks of high fat feeding, despite marked changes in phospholipid composition and accumulation of triglycerides in skeletal muscle of high fat-fed mice. Aging interacts with high fat feeding by means of proton leak and redox state, which underscores the higher susceptibility of older individuals to metabolic pathologies.
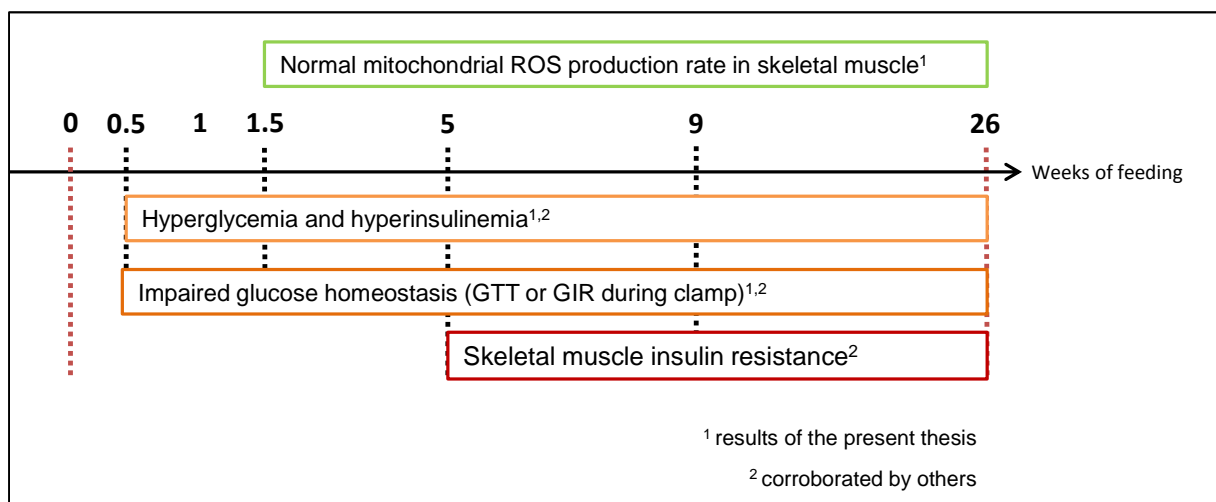
Figure 27: Timeline of high fat feeding: reported and observed changes in the glucose homeostasis and in skeletal muscle mitochondrial reactive oxygen species (ROS) production.

GTT – glucose tolerance test, GIR – glucose infusion rate during hyperinsulinemic- euglycemic clamp
Detailed literature references for the development of impaired glucose homeostasis and skeletal muscle insulin resistance are given in the paragraphs 4.2.2 and 4.2.3

4.4   Mitochondria in liver

Overnutrition especially an oversupply with fat has been associated to non-alcoholic fatty liver disease (Nafld). Underlying mechanisms are considered as complex interplay and mitochondrial involvement is widely accepted, but literature reports controversies (Begriche *et al.* 2013). In the context of fat metabolism in hepatocytes (Figure 2) the routes of fatty acids through the cell will be discussed with regard to diet induced fat accumulation in adolescent, young adult and middle-aged mice fed the high fat or control diet for 9 weeks. In general it is assumed that fat accumulates in liver cells when either the uptake and

generation of fatty acids is increased or the utilization and secretion is reduced (Serra *et al.* 2012).

4.4.1 Mitochondrial mass, bioenergetics and ROS production

Mitochondrial function was investigated during proton leak titration (Figure 19) and fatty acid oxidation (Table 7). Noteworthy, the proton leak titration was investigated in liver mitochondria of adolescent, young adult and middle-aged mice, summarized as dataset 1, whereas the mitochondrial capacity to metabolize palmitoylcarnitine was investigated in other cohorts of adolescent, young adult and middle-aged mice (dataset 2). Proton leak titration using succinate as substrate was not influenced by high fat diet in dataset 1 (Figure 19). Age related uncoupling confirms literature (Brand 2000). Oxygen consumption and membrane potential was also monitored in liver mitochondria of dataset 2 using succinate as substrate. Here, membrane potential during leak respiration was significantly reduced by high fat diet (Table 26). Noteworthy, the proton motive force consists of two components, the membrane potential and the pH difference. In the method used for dataset 1, the addition of nigericin reduces pH differences by adding this to the electrical gradient (Brand & Nicholls 2011). The method used for dataset 2 did not account for pH differences. It has therefore to be considered, if there are pH differences that are related to high fat diet feeding. Proton motive force, which finally drives ATP synthesis, remains unaffected by high fat diet.

Reduced mitochondrial capacity to oxidize fatty acids can be caused by reduced oxidative function (Vial *et al.* 2010) or simply by reduced mass. Indeed, mitochondrial mass in liver was not affected by 9 weeks of high fat-diet feeding. Noteworthy CS activity declined with age in liver tissue, resulting in an age-related decline in mitochondrial mass, here without significant posthoc testing (Table 6). Interestingly, mitochondrial mass was so far not described to decline with age. In rats hepatic mitochondrial mass is constant during aging (Navarro & Boveris 2004), (Zhao *et al.* 2014). The capacity for β-oxidation was tested by monitoring the oxygen consumption and membrane potential of liver mitochondria metabolizing fatty acid-derived palmitoylcarnitine. Here, in the phosphorylating state oxygen consumption was significantly reduced due to high fat feeding (Table 7). High fat feeding studies in rodents show controversial results regarding mitochondrial respiration using palmitoylcarnitine. Normal (Satapati *et al.* 2012), increased (Ciapaite *et al.* 2011), (Satapati *et al.* 2012) or reduced respiration (Vial *et al.* 2011) was reported. In the present thesis the mitochondrial acylcarnitine production was monitored to further characterize mitochondrial fatty acid oxidation. Interestingly, acetylcarnitine release of liver mitochondria was reduced in high fat-fed mice (Figure 21). Therefore there might be a reduction in the substrate oxidation

explaining reduced oxygen consumption in mitochondria of high fat-fed mice. Of note, in isolated mitochondria respiration was initiated with palmitoylcarnitine that is able to enter the mitochondria independently of the carnitine-palmitoyltransferase 1 (Cpt1), which is the rate limiting step of β-oxidation *in vivo* (Houten & Wanders 2010). In the proteome analysis, which was noteworthy conducted in mitochondria of different mice than the functional measurements using palmitoylcarnitine as substrate, trifunctional protein was slightly but significantly reduced. When Cpt1a activity is not limiting in the experimental assay, this reduction might account for reduced β oxidative cycles, because three enzymatic steps are catalyzed by this protein complex for several cycles, until enzymes with specific activity for middle and short chain length overtake (Wanders *et al.* 1999). This could plausibly reflect the reduced output of acetylcarnitine in liver mitochondria of high fat-fed mice (Figure 21 A). The reduction occurred in parallel with a slightly higher concentration of palmitoylcarnitine in the supernatant, which also hints towards a reduced oxidation of long chain fatty acids. On the other hand increased abundance of 3-ketoacyl-CoA thiolase (Acaa2) (Table 9), which cleaves acetyl-CoA from the acyl-chain (Wanders *et al.* 1999), indicates enhanced mitochondrial β-oxidation (Desmarchelier *et al.* 2012). Although ketogenic pathways were not indicated by the pathway analysis tools, upregulated acetyl-CoA acetyltransferase (Acat1) (Table 27), which fuses two molecules of acetyl-CoA, could also explain, why less acetylcarnitine exited the mitochondria of high fat-fed mice. Furthermore the reduction in oxygen consumption in presence of ADP could be due to inadequate electron entry at complex I or limited ATP synthase activity (Brand & Nicholls 2011). Respiration during phosphorylating ADP to ATP was not decreased, when mitochondria were fueled with succinate (Table 26 in the appendix), therefore excluding reduced ATP synthase activity. In the proteome analysis a reduction of complex I subunits in mitochondria of high fat-fed mice was found (Table 9). This could account for reduced electron entry. It has to be substantiated in further experiments, which functional detail in isolated mitochondria oxidizing fatty acids, is responsible for the reduced oxygen consumption under phosphorylating conditions.

Changes in the mitochondrial β-oxidation are one aspect of inadequate utilization of fatty acids. Besides, mitochondrial ROS production is discussed to play a role in the fat accumulation of liver (Begriche *et al.* 2013), (Serra *et al.* 2012). Interestingly, in the present study, liver mitochondria of mice fed a high fat diet for 9 weeks, which were fueled with palmitoylcarnitine, showed normal ROS production compared to mitochondria of control-fed mice (Table 7). This would be expected differently, when ROS production rates during fat oxidation serve as underlying cause for impaired fat oxidation and consequent fat accumulation. Moreover, ROS production rates with succinate as substrate during leak respiration were increased. This was concordant in dataset 1 (Figure 19 D) and dataset 2 (Table 26). From the regression analysis of membrane potential, oxygen consumption and

ROS production (Figure 20), it is conclusive, that liver mitochondria of mice fed a high fat diet indeed exhibit a higher ROS production potential. Prolonged feeding of 26 weeks was investigated to show if mitochondrial function declines in the state of fatty liver. Interestingly, proton leak was not affected by high fat diet and the rate of ROS production reflected the state after 9 weeks of high fat feeding. Noteworthy, the capacity of β-oxidation was not tested and therefore it cannot be concluded on progressive reduction in mitochondrial fatty acid oxidation. This would be of particular interest, because diet induced obese C57BL/6J mice served as model of progressive Nafld (Nakamura & Terauchi 2013). Mitochondrial function was described after comparable feeding as either increased (Guo *et al.* 2013) or impaired (Satapati *et al.* 2012)

Increased ROS production rates in liver mitochondria confirm the overall hypothesis that mitochondrial function and mitochondrial-derived oxidative stress are involved in the complex metabolic network around diet-induced disturbances leading to fat accumulation in the liver. This result confirmed former studies in rodents, which measured mitochondrial ROS production in isolated liver mitochondria (Nadal-Casellas *et al.* 2010), (Vial *et al.* 2011), (Ruiz-Ramirez *et al.* 2011) and studies, which used indirect markers of oxidative stress in liver (Raffaella *et al.* 2008), (Yuzefovych *et al.* 2013), (Satapati *et al.* 2012), (Ciapaite *et al.* 2011), (Schmid *et al.* 2004), (Midha *et al.* 2012). Only mitochondrial specific ROS production was sensitive to high fat diet feeding, because the mitochondria enriched fractions did not reveal mitochondria-independent differences in ROS production rates as deduced from the incubation of mitochondrial protein without substrate for respiration. There was no further test conducted that specifically addressed other sources of ROS, e.g. NADPH oxidase activity. In the literature, NADPH oxidase activity was normal in diet induced obese rodents (Feillet-Coudray *et al.* 2009), (Ren *et al.* 2012). Peroxisomal derived ROS production is unlikely to contribute to considerable amounts, as proteins, e.g. acyl-CoA oxidase (Acox2) or urate oxidase (Uox), which release H_2O_2 (Schrader & Fahimi 2006), were reduced on protein level (Table 9, Table 13) in mice fed a high fat diet.

4.4.2 Nrf2-mediated response in livers of diet induced obese mice

On basis of the pathway analysis tools used in the proteome study, an Nrf2-regulated antioxidative defense was induced in liver of high fat-fed mice. Mitochondrial derived hydrogen peroxide production has been described to induce Nrf2-dependent gene expression (Lo & Hannink 2008), (Vomhof-Dekrey & Picklo 2012). Some Nrf2 targets, involved in lipid-peroxide detoxification were upregulated in the proteome study (Table 13) and therefore indicate increased oxidative modifications to lipids in the liver of high fat-fed

mice. Intriguingly, the hypothesis was supported that Nrf2 is tethered in its inactivated state (fixed to Keap1) near the outer mitochondrial membrane by Pgam5 (Lo & Hannink 2008) and is therefore juxtaposed to the site of hydrogen peroxide release. This makes it a favorable sensor for changes in the oxidative status together with the observed downregulation of Pgam5, which was described to induce Nrf2 translocation (Lo & Hannink 2008). These observations were substantiated by western blot analysis (Figure 26) in the present thesis and therefore strongly indicate a mechanistic link for initiation of Nrf2 dependent gene expression in liver of high fat-fed mice.

Interestingly, Sod1 and catalase, both well-accepted targets of Nrf2 (Kobayashi & Yamamoto 2006), were in contrast downregulated. Although the progressive downregulation of Sod1 and catalase were reported before in livers of diet induced obese C57BL/6J mice (Oh *et al.* 2011), here, it leads to the hypothesis of a partly inhibited Nrf2-induced gene expression. Upregulated Hsd11b1 derived from the proteome analysis (Table 13) may explain a balanced response. Nrf2 mediated response can be negatively regulated by glucocorticoids that are produced in the adrenal glands, but activated by Hsd11b1 in hepatocytes (Kratschmar *et al.* 2012). Additionally, oxidative stress is involved in the regulation of Nrf2-mediated gene expression by enhancing competitive transcription factors for the respective DNA-binding site, too. This mechanism is considered as tool for precise adjustment (Kobayashi & Yamamoto 2006).

The idea of a balanced Nrf2 response in the here investigated diet induced obese mouse model is plausible, as a very recent review summarized that neither Nrf2 null mice nor mice that show a constitutively active Nrf2 pathway by knock-down of its inhibitor Keap1, validly reflect the situation given by the development of obesity due to a surplus of calories. Beyond, authors reinforce that therapeutic activation of Nrf2 dependent gene expression might be beneficial in an obese and/or insulin resistant state (Seo & Lee 2013). Nutritional impact on Nrf2 gene expression resulted in contrary reports. High fat diets based on lard reduce either mRNA levels of Nrf2 as well as target gene expression in liver. On the other hand, high fat feeding with milk fat or soybean oil resulted in an activation of the Nrf2 pathway (Vomhof-Dekrey & Picklo 2012). The here presented contribution states that feeding C57BL/6J mice a palm oil-enriched diet induced Nrf2-mediated antioxidative response to counteract oxidative stress.

4.4.3   Fatty acid metabolism in livers of diet induced obese mice

Besides the functional characterization, the proteome analysis elucidated that interorganelle crosstalk influenced fat metabolism in the liver (Figure 28). The regulation of 206 proteins by high fat diet was analyzed regarding the fatty acid metabolism in hepatocytes. The major regulations by high fat diet regarding the flux of fatty acids were fat oxidation, protein folding in the ER for VLDL maturation and lysosomal degradation.
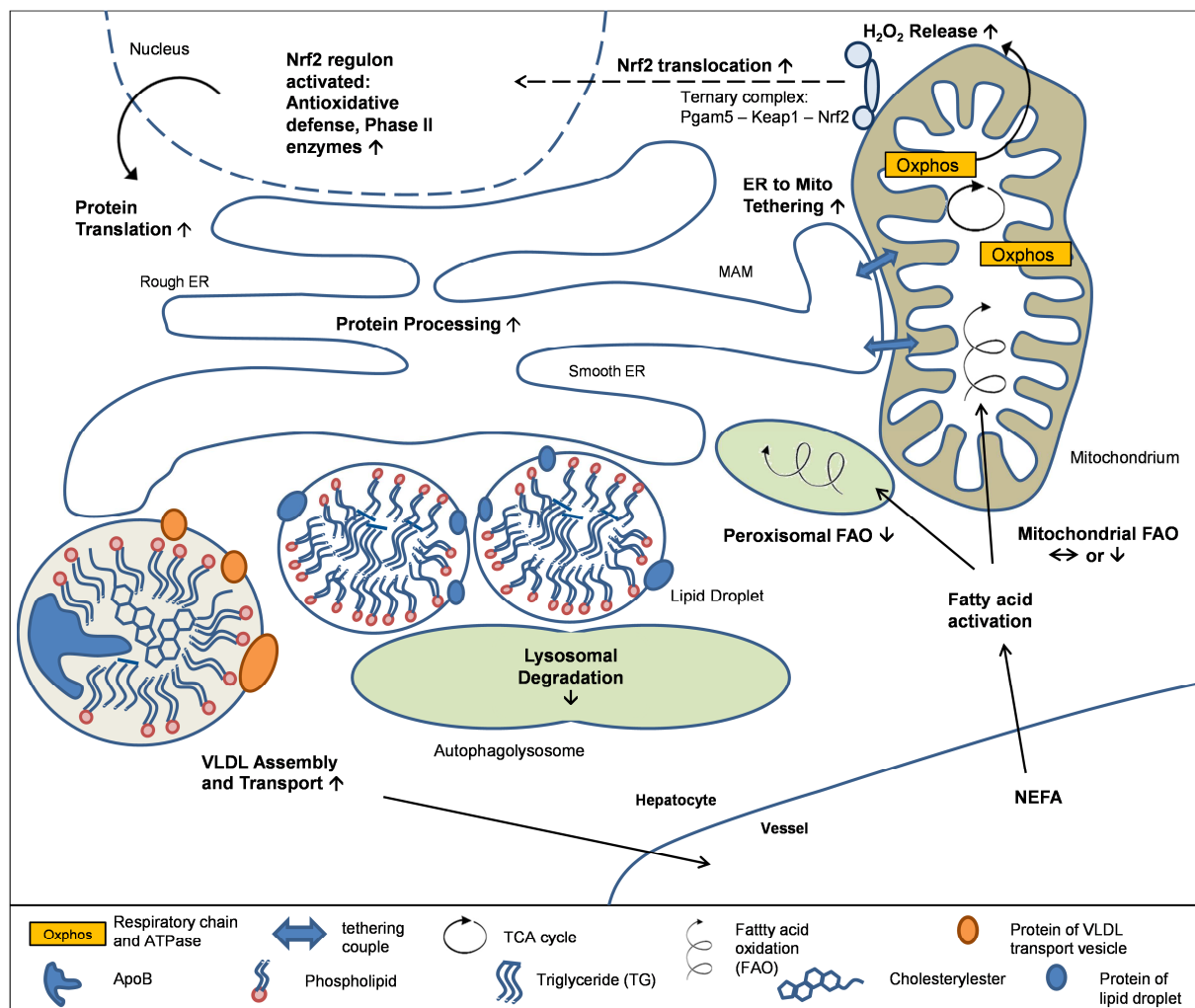
Figure 28: Mechanistic interaction of cellular compartments in the liver of high fat-fed mice
For details see text

4.4.3.1   Fatty acid oxidation

Data regarding mitochondrial fatty acid oxidation in the development of fatty liver remain inconclusive, as for example enzymes of the mitochondrial β-oxidation have been found either increased (de Fourmestraux *et al.* 2004), (Kirpich *et al.* 2011), (Midha *et al.* 2012), (Guo *et al.* 2013), (Sunny *et al.* 2010) or decreased (Oh *et al.* 2011), (Xie *et al.* 2010). In the context of the here conducted proteome study, there is neither distinct induction nor

suppression of mitochondrial fatty acid oxidation (Table 9 and 4.4.1). Cpt1a was not changed in its abundance by high fat diet (data not shown), but it has to be considered that Cpt1a activity is regulated by allosteric inhibition (Houten & Wanders 2010). Of importance, peroxisomal fatty acid oxidation was clearly suppressed in the present study. Deletion of the peroxisomal enzyme acyl-CoA oxidase induces fatty liver and related liver complications in mice (Gambino *et al.* 2011), whereas induction of peroxisomal fatty acid oxidation prevents the accumulation of fat in the liver in mice fed a high fat diet (Fiamoncini *et al.* 2013). Noteworthy, peroxisomal activity declines with aging especially with regard to FAO enzymes and catalase activity (Terlecky *et al.* 2006). Conclusively, the reduction in hepatic peroxisomal fatty acid oxidation of high fat-fed mice was not compensated by mitochondrial β-oxidation, which finally contributed to an imbalance of fatty acid availability and utilization, promoting fat accumulation upon high fat diet feeding.

4.4.3.2   Fat secretion in very low density lipoprotein

Reduced fatty acid breakdown favors fat storage. Hence, the liver is able to actively secrete triglycerides in form of very low density lipoprotein (VLDL). It is mechanistically hypothesized that the availability of triglycerides, especially in the state of excessive caloric intake, leads to consecutive secretion of VLDL (Sparks *et al.* 2012). In rodent studies, serum VLDL was increased in high fat-fed mice (Rubio-Aliaga *et al.* 2011), (de Fourmestraux *et al.* 2004), (Desmarchelier *et al.* 2012). In the proteome study, the coordinate upregulation of translation together with the ER chaperone equipment and key enzymes of VLDL maturation e.g. ApoB, strongly indicate higher VLDL production by the liver of high fat-fed mice. In the progression of Nafld the potential of the liver to secrete VLDL first increases as compensatory mechanism but finally declines due to failure of proper ApoB maturation (Jiang *et al.* 2013). Thus, the present study most likely provides insights in the state of compensatory VLDL secretion, although posttranslational degradation rates of ApoB have not been determined.

In the context of higher VLDL production, increased phospholipid synthesis is required. Although the majority of phosphatidylcholine, the main phospholipid in lipoproteins and chylomicrons, is synthesized via the CDP-choline pathway, the liver is able to alternatively build up phosphatidylcholine via the phosphatidylethanolamine-methylation pathway (PEMT) (Dahlhoff *et al.* 2013). This process involves the transfer of methyl-groups and is therefore connected to the one carbon metabolism via the demethylation of adenosyl-methionine to adenosyl-cysteine (Cole *et al.* 2012). The one carbon metabolism has been found upregulated in diet induced obese mouse models before (Dahlhoff *et al.* 2013), (Rubio-Aliaga *et al.* 2011), confirming the increased Bhmt and Mat1a expression in the present study

(Table 11). Subsequently, the induction of the one carbon metabolism connects to increased VLDL secretion from the liver into the blood (Sparks *et al.* 2006). Additionally, the Nrf2-regulon provides another connection to the one-carbon metabolism by increased Bhmt (Table 13) (Kwak *et al.* 2003).

Two particular proteins should be stressed in the context of high fat diet induced changes in hepatic lipid metabolism. The protein, that was upregulated with the highest fold change (Table 11), Ras related protein 10 (Rab10), was introduced as regulator for ER extension with accompanying recruitment of proteins necessary to provide the building elements for new ER membrane. This was concluded from cell culture experiments (English & Voeltz 2013). Therefore Rab10 seems to play an important role in the control of phospholipid biosynthesis during increased VLDL processing in livers of high fat-fed mice. Further research is needed to establish this connection on molecular level.

The other highly induced protein, sphingosine-1 phosphate lyase (Sgpl1), potentially connects phospholipid biosynthesis and sphingolipid metabolism. Sphingosine-1 phosphate lyase limits the sphingosine-1 phosphate (S1P) pool (Bektas *et al.* 2010). Degradation product of S1P is among others phosphoethanolamine, which is required for phosphatidylethanolamine synthesis (Hla & Dannenberg 2012). Noteworthy, this redirects to the PEMT pathway. Furthermore, decreasing S1P availability for ceramide synthesis may limit this bioactive molecule, which e.g. acts in pathways inhibiting insulin signaling (Samuel & Shulman 2012).

Moderate increase of different ER chaperones, like Grp78, calnexin, calreticulin, Erp44 and protein disulfide isomerases (Table 10) indicate that the machinery of unfolded protein response (UPR) was initiated to allow for correct folding during increased flux of newly synthesized proteins. One particular feature of UPR is the induction of phospholipid biosynthesis (Ron & Walter 2007), (Samuel & Shulman 2012). At the interaction site of the ER and mitochondria, the mitochondrial-associated membrane (MAM), proteins like calnexin, calreticulin and Erp44 have been identified to regulate ER to mitochondria connectivity, which is required for e.g. correct phospholipid biosynthesis (Rieusset 2011), (de Brito & Scorrano 2010). The tethering couple protein tyrosine phosphatase-interacting protein 51 (Ptpip51) and vesicle-associated membrane protein-associated protein B (Vapb) (De Vos *et al.* 2012) was increased by high fat feeding (Table 11), supporting the higher connectivity between mitochondria and ER in livers of high fat-fed mice. In the context of diet induced obesity and fatty liver, a recent study explored a structural change in liver mitochondria after 30 weeks of high fat feeding, which was suggested as adaptation for increased lipid uptake (Guo *et al.* 2013). This finding could functionally connect the observation of closer contact

between the two organelles and functional remodeling of mitochondria. In conclusion, changes in ER to mitochondria tethering demonstrate that high fat feeding intensifies the important crosstalk between these organelles.

4.4.3.3 Mobilization of lipid droplets

The intriguing phenotypic result, that hepatic triglyceride do not accumulate in adolescent mice fed a high fat diet (Figure 18 B), correlate with less degradation of lysosomal proteins in the adolescent high fat-fed mice compared to the older groups. Lysosomes are closely connected to autophagy, and the degradation of lipid droplets. First studies implicate reduced autophagy in the development of fatty liver (Christian *et al.* 2013). Liver steatosis has conversely been shown to impair autophagy by decreasing lysosomal proteases (Inami *et al.* 2011). The essential role of lysosomes in the autophagic process should be stressed, because age-related decrease in lysosomal proteins adversely affects liver function (Zhang & Cuervo 2008). Reactive oxygen species derived by mitochondria have been implicated in the regulation of autophagy in the context of various metabolic changes, such as aging, as well as the pathology of diseases as cancer, type 2 diabetes or cardiovascular disorders in humans (Wen *et al.* 2013). Conclusively high fat feeding together with the age-related decline of lysosomal proteins leads to an imbalance of fat storage and impairs the mobilization of lipid droplets.

4.4.4 Protective mechanisms

In summary, over all fatty acid breakdown was reduced by high fat feeding (Figure 28). Livers of high fat-fed mice consequently induced protein translation and processing to deal with the high availability of fatty acids. VLDL processing was increased to remove triglycerides from the liver. This regulation was not sufficient in young adult and aged mice. The reduction in mitochondrial mass with aging might further impair the rate of mitochondrial β-oxidation. Furthermore adequate expression of lysosomal proteins seems to be essential to maintain liver triglyceride homeostasis, whereas age-related decrease of lysosomal proteins together with reduced capacity for fatty acid oxidation, promotes the development of hepatic triglyceride accumulation leading to fatty liver. Another possible explanation, why adolescent mice did not accumulate fat in the liver, may arise from the fact that these mice were not fully grown up yet when the feeding experiment was started. Therefore the surplus in calories was partitioned towards growth and less energy as fatty acids entered the hepatocytes at all. Indeed, high fat feeding started in 4 week-old mice increased growth

hormones in the blood compared to mice which were fed the high fat diet at 12 weeks of age (Cordoba-Chacon *et al.* 2012). This provides evidence, that adolescent mice, which are still in their pubertal phase, channel the ingested energy towards growth metabolism.

4.5   Organ specificity

Skeletal muscle and liver are two major regulators of blood glucose. Skeletal muscle removes about 80 % of blood glucose upon a meal, whereas liver is the main hub for glucose maintenance during fasting (Serra *et al.* 2012). Therefore the question of tissue specific adaptations to high dietary fat intake was addressed in this thesis. Interestingly, some rodent studies provided first hints that skeletal muscle is more susceptible to oxidative stress during the development of diet induced obesity than liver (Iossa *et al.* 2003), (Yuzefovych *et al.* 2013). This is in contrast to the results in the present thesis. Especially in the liver mitochondrial derived ROS and a reduction in fatty acid driven ADP phosphorylation might reflect early changes in the hepatic fat metabolism. This hypothesis is corroborated by the observation, that mitochondrial bioenergetics were already changed in adolescent mice fed the high fat diet, which were protected from hepatic fat accumulation. Skeletal muscle mitochondria perform robustly in high fat-fed mice, even after 26 weeks of feeding. This confirms work of others (Franko *et al.* 2012), (Hoeks *et al.* 2011). The observed changes in the hepatic lipid metabolism involve complex interactions between organelles. Mild alterations may therefore induce complex adaptive mechanisms and a small shift in the balance of lipid uptake/generation and utilization/export might induce imbalances over time which cannot be compensated. Furthermore white adipose tissue releases free fatty acids into the blood when insulin sensitivity declines (Serra *et al.* 2012). The liver faces the increased free fatty acids in the blood by higher rates of uptake and by metabolizing fatty acids to triglycerides and lipoproteins to balance the overflow of fatty acids (Jiang *et al.* 2013). Markers of inflammation, released by white adipose tissue, may further impact the hepatic lipid metabolism (Samuel & Shulman 2012). Conclusively the comprehensive analysis of mitochondrial metabolism in skeletal muscle and liver including age-related changes in metabolism, provided in this thesis, marks liver metabolism more susceptible against high fat diet induced obesity than skeletal muscle.

4.6   Perspectives

On the basis of the proteome study, it should be investigated if hepatic mitochondrial β-oxidation or the electron transport chain is limited during the development of diet induced obesity, hyperglycemia and hyperinsulinemia. The hierarchy of events in the network of organelles is another aspect for further research with interesting players like Sgpl1 or Rab10. The connection between mitochondrial H_2O_2 release and oxidant-sensitive Nrf2 juxtaposed to mitochondria, opens interesting mechanisms how mitochondria regulate antioxidative gene expression. Moreover, the fine tuning of the Nrf2-dependent gene expression provides new aspects regarding fat metabolism in the liver.

The pivotal role of aging in the complex interactions between glucose homeostasis, insulin sensitivity and mitochondrial function requires studies that are controlled for age-related factors. In the context of the present thesis experiments should continue the timeline started with adolescent, young adult and middle-aged mice. Here, senescent mice, e.g. 24 months of age, would be expected to provide more pronounced age-related decline.

In literature the controversy about the role of mitochondrial function in the etiology of skeletal muscle insulin resistance persists (Goodpaster 2013), (Holloszy 2013). The present study underscores that mitochondrial function is not impaired by excessive fat availability alone and therefore confirms the hypothesis that skeletal muscle insulin resistance develops independently of mitochondrial performance. On the other hand the observations from human diabetic, insulin resistant and obese persons are still valid (Goodpaster 2013). Therefore it has to be refined, at which conditions mitochondrial function may play a role in the development of insulin resistance in human skeletal muscle.

5   <u>References</u>

Ackert-Bicknell C, Beamer WG, Rosen CJ , Sundberg JP (2008). Aging study: Bone mineral density and body composition of 32 inbred strains of mice. Mouse Phenome Database web site: The Jackson Laboratory, Bar Harbor, Maine USA. http://phenome.jax.org, Date of access: 17th Jan 2014

Alberti KG, Eckel RH, Grundy SM, Zimmet PZ, Cleeman JI, Donato KA, Fruchart JC, James WP, Loria CM, Smith SC, Jr., International Diabetes Federation Task Force on E, Prevention, Hational Heart L, Blood I, American Heart A, World Heart F, International Atherosclerosis S , International Association for the Study of O (2009). Harmonizing the metabolic syndrome: a joint interim statement of the International Diabetes Federation Task Force on Epidemiology and Prevention; National Heart, Lung, and Blood Institute; American Heart Association; World Heart Federation; International Atherosclerosis Society; and International Association for the Study of Obesity. *Circulation.* **120**, 1640-1645.

Alexeyev MF (2009). Is there more to aging than mitochondrial DNA and reactive oxygen species? *The FEBS journal.* **276**, 5768-5787.

Alexson SE , Nedergaard J (1988). A novel type of short- and medium-chain acyl-CoA hydrolases in brown adipose tissue mitochondria. *The Journal of biological chemistry.* **263**, 13564-13571.

American Diabetes A (2013). Standards of medical care in diabetes--2013. *Diabetes care.* **36 Suppl 1**, S11-66.

Amir M , Czaja MJ (2011). Autophagy in nonalcoholic steatohepatitis. *Expert review of gastroenterology & hepatology.* **5**, 159-166.

Anderson EJ, Lustig ME, Boyle KE, Woodlief TL, Kane DA, Lin CT, Price JW, 3rd, Kang L, Rabinovitch PS, Szeto HH, Houmard JA, Cortright RN, Wasserman DH , Neufer PD (2009). Mitochondrial H2O2 emission and cellular redox state link excess fat intake to insulin resistance in both rodents and humans. *The Journal of clinical investigation.* **119**, 573-581.

Andrikopoulos S, Blair AR, Deluca N, Fam BC , Proietto J (2008). Evaluating the glucose tolerance test in mice. *American journal of physiology. Endocrinology and metabolism.* **295**, E1323-1332.

Ayala JE, Samuel VT, Morton GJ, Obici S, Croniger CM, Shulman GI, Wasserman DH, McGuinness OP , Consortium NIHMMPC (2010). Standard operating procedures for describing and performing metabolic tests of glucose homeostasis in mice. *Disease models & mechanisms.* **3**, 525-534.

Barzilai N , Gupta G (1999). Interaction between aging and syndrome X: new insights on the pathophysiology of fat distribution. *Annals of the New York Academy of Sciences.* **892**, 58-72.

Bashan N, Kovsan J, Kachko I, Ovadia H , Rudich A (2009). Positive and negative regulation of insulin signaling by reactive oxygen and nitrogen species. *Physiological reviews.* **89**, 27-71.

Begriche K, Massart J, Robin MA, Bonnet F , Fromenty B (2013). Mitochondrial adaptations and dysfunctions in nonalcoholic fatty liver disease. *Hepatology.* **58**, 1497-1507.

Bektas M, Allende ML, Lee BG, Chen W, Amar MJ, Remaley AT, Saba JD , Proia RL (2010). Sphingosine 1-phosphate lyase deficiency disrupts lipid homeostasis in liver. *The Journal of biological chemistry.* **285**, 10880-10889.

Bellanti F, Romano AD, Giudetti AM, Rollo T, Blonda M, Tamborra R, Vendemiale G , Serviddio G (2013). Many Faces of Mitochondrial Uncoupling During Age: Damage or Defense? *The journals of gerontology. Series A, Biological sciences and medical sciences.*

Benjamini YH, Y. (1995). Controlling the false discovery rate: a practical and powerful approach to multiple testing. *Journal of the Royal Statistical Society. Series B (Methodology).* **57**, 289-300.

Beutler E (1975). *Red cell metabolism, a manual of biochemical methods.* New York: Grune and Stratton.

Beutler E (1984). *Red cell metabolism, a manual of biochemical methods.* New York: Grune and Startton.

Boden G (2011). Obesity, insulin resistance and free fatty acids. *Current opinion in endocrinology, diabetes, and obesity.* **18**, 139-143.

Bonnard C, Durand A, Peyrol S, Chanseaume E, Chauvin MA, Morio B, Vidal H , Rieusset J (2008). Mitochondrial dysfunction results from oxidative stress in the skeletal muscle of diet-induced insulin-resistant mice. *The Journal of clinical investigation.* **118**, 789-800.

Boren J, Taskinen MR, Olofsson SO , Levin M (2013). Ectopic lipid storage and insulin resistance: a harmful relationship. *Journal of internal medicine.* **274**, 25-40.

Boudina S, Sena S, Sloan C, Tebbi A, Han YH, O'Neill BT, Cooksey RC, Jones D, Holland WL, McClain DA , Abel ED (2012). Early mitochondrial adaptations in skeletal muscle to diet-induced obesity are strain dependent and determine oxidative stress and energy expenditure but not insulin sensitivity. *Endocrinology.* **153**, 2677-2688.

Bouillaud F , Blachier F (2011). Mitochondria and sulfide: a very old story of poisoning, feeding, and signaling? *Antioxidants & redox signaling.* **15**, 379-391.

Bourgeron T, Chretien D, Rotig A, Munnich A , Rustin P (1992). Isolation and characterization of mitochondria from human B lymphoblastoid cell lines. *Biochemical and biophysical research communications.* **186**, 16-23.

Bradford MM (1976). A rapid and sensitive method for the quantitation of microgram quantities of protein utilizing the principle of protein-dye binding. *Analytical biochemistry.* **72**, 248-254.

Brand MD (2000). Uncoupling to survive? The role of mitochondrial inefficiency in ageing. *Experimental gerontology.* **35**, 811-820.

Brand MD (2010). The sites and topology of mitochondrial superoxide production. *Experimental gerontology.* **45**, 466-472.

Brand MD , Nicholls DG (2011). Assessing mitochondrial dysfunction in cells. *The Biochemical journal.* **435**, 297-312.

Brewer GJ (2010). Epigenetic oxidative redox shift (EORS) theory of aging unifies the free radical and insulin signaling theories. *Experimental gerontology.* **45**, 173-179.

Cano A, Buque X, Martinez-Una M, Aurrekoetxea I, Menor A, Garcia-Rodriguez JL, Lu SC, Martinez-Chantar ML, Mato JM, Ochoa B , Aspichueta P (2011). Methionine adenosyltransferase 1A gene deletion disrupts hepatic very low-density lipoprotein assembly in mice. *Hepatology.* **54**, 1975-1986.

Capel F, Delmotte MH, Brun M, Lonchampt M, De Fanti B, Xuereb L, Baschet L, Rolland G, Galizzi JP, Lockhart B, Ktorza A , Dacquet C (2011). Aging and obesity induce

distinct gene expression adaptation in the liver of C57BL/6J mice. *Journal of nutrigenetics and nutrigenomics*. **4**, 154-164.

Catala-Niell A, Estrany ME, Proenza AM, Gianotti M , Llado I (2008). Skeletal muscle and liver oxidative metabolism in response to a voluntary isocaloric intake of a high fat diet in male and female rats. *Cellular physiology and biochemistry : international journal of experimental cellular physiology, biochemistry, and pharmacology*. **22**, 327-336.

Chandler RJ, Chandrasekaran S, Carrillo-Carrasco N, Senac JS, Hofherr SE, Barry MA , Venditti CP (2011). Adeno-associated virus serotype 8 gene transfer rescues a neonatal lethal murine model of propionic acidemia. *Human gene therapy*. **22**, 477-481.

Chapel A, Kieffer-Jaquinod S, Sagne C, Verdon Q, Ivaldi C, Mellal M, Thirion J, Jadot M, Bruley C, Garin J, Gasnier B , Journet A (2013). An extended proteome map of the lysosomal membrane reveals novel potential transporters. *Molecular & cellular proteomics : MCP*. **12**, 1572-1588.

Chomentowski P, Coen PM, Radikova Z, Goodpaster BH , Toledo FG (2011). Skeletal muscle mitochondria in insulin resistance: differences in intermyofibrillar versus subsarcolemmal subpopulations and relationship to metabolic flexibility. *The Journal of clinical endocrinology and metabolism*. **96**, 494-503.

Chow L, From A , Seaquist E (2010). Skeletal muscle insulin resistance: the interplay of local lipid excess and mitochondrial dysfunction. *Metabolism: clinical and experimental*. **59**, 70-85.

Christian P, Sacco J , Adeli K (2013). Autophagy: Emerging roles in lipid homeostasis and metabolic control. *Biochimica et biophysica acta*. **1831**, 819-824.

Ciapaite J, van den Broek NM, Te Brinke H, Nicolay K, Jeneson JA, Houten SM , Prompers JJ (2011). Differential effects of short- and long-term high-fat diet feeding on hepatic fatty acid metabolism in rats. *Biochimica et biophysica acta*. **1811**, 441-451.

Clark LC, Jr., Wolf R, Granger D , Taylor Z (1953). Continuous recording of blood oxygen tensions by polarography. *Journal of applied physiology*. **6**, 189-193.

Clee SM , Attie AD (2007). The genetic landscape of type 2 diabetes in mice. *Endocrine reviews*. **28**, 48-83.

Cole LK, Vance JE , Vance DE (2012). Phosphatidylcholine biosynthesis and lipoprotein metabolism. *Biochimica et biophysica acta*. **1821**, 754-761.

Conti M, Morand PC, Levillain P , Lemonnier A (1991). Improved fluorometric determination of malonaldehyde. *Clinical chemistry*. **37**, 1273-1275.

Cordoba-Chacon J, Gahete MD, Pozo-Salas AI, Moreno-Herrera A, Castano JP, Kineman RD , Luque RM (2012). Peripubertal-onset but not adult-onset obesity increases IGF-I and drives development of lean mass, which may lessen the metabolic impairment in adult obesity. *American journal of physiology. Endocrinology and metabolism*. **303**, E1151-1157.

Couture P , Hulbert AJ (1995). Membrane fatty acid composition of tissues is related to body mass of mammals. *The Journal of membrane biology*. **148**, 27-39.

Czech MP, Tencerova M, Pedersen DJ , Aouadi M (2013). Insulin signalling mechanisms for triacylglycerol storage. *Diabetologia*. **56**, 949-964.

Dahlhoff C, Desmarchelier C, Sailer M, Furst RW, Haag A, Ulbrich SE, Hummel B, Obeid R, Geisel J, Bader BL , Daniel H (2013). Hepatic methionine homeostasis is conserved in C57BL/6N mice on high-fat diet despite major changes in hepatic one-carbon metabolism. *PloS one*. **8**, e57387.

de Brito OM , Scorrano L (2010). An intimate liaison: spatial organization of the endoplasmic reticulum-mitochondria relationship. *The EMBO journal*. **29**, 2715-2723.

de Fourmestraux V, Neubauer H, Poussin C, Farmer P, Falquet L, Burcelin R, Delorenzi M , Thorens B (2004). Transcript profiling suggests that differential metabolic adaptation of mice to a high fat diet is associated with changes in liver to muscle lipid fluxes. *The Journal of biological chemistry*. **279**, 50743-50753.

De Vogel-van den Bosch J, van den Berg SA, Bijland S, Voshol PJ, Havekes LM, Romijn HA, Hoeks J, van Beurden D, Hesselink MK, Schrauwen P , van Dijk KW (2011). High-fat diets rich in medium- versus long-chain fatty acids induce distinct patterns of tissue specific insulin resistance. *The Journal of nutritional biochemistry*. **22**, 366-371.

De Vos KJ, Morotz GM, Stoica R, Tudor EL, Lau KF, Ackerley S, Warley A, Shaw CE , Miller CC (2012). VAPB interacts with the mitochondrial protein PTPIP51 to regulate calcium homeostasis. *Human molecular genetics*. **21**, 1299-1311.

de Wilde J, Mohren R, van den Berg S, Boekschoten M, Dijk KW, de Groot P, Muller M, Mariman E , Smit E (2008). Short-term high fat-feeding results in morphological and metabolic adaptations in the skeletal muscle of C57BL/6J mice. *Physiological genomics*. **32**, 360-369.

de Wit N, Derrien M, Bosch-Vermeulen H, Oosterink E, Keshtkar S, Duval C, de Vogel-van den Bosch J, Kleerebezem M, Muller M , van der Meer R (2012). Saturated fat stimulates obesity and hepatic steatosis and affects gut microbiota composition by an enhanced overflow of dietary fat to the distal intestine. *American journal of physiology. Gastrointestinal and liver physiology*. **303**, G589-599.

Demozay D, Mas JC, Rocchi S , Van Obberghen E (2008). FALDH reverses the deleterious action of oxidative stress induced by lipid peroxidation product 4-hydroxynonenal on insulin signaling in 3T3-L1 adipocytes. *Diabetes*. **57**, 1216-1226.

Desmarchelier C, Dahlhoff C, Keller S, Sailer M, Jahreis G , Daniel H (2012). C57Bl/6 N mice on a western diet display reduced intestinal and hepatic cholesterol levels despite a plasma hypercholesterolemia. *BMC genomics*. **13**, 84.

Dumas JF, Simard G, Flamment M, Ducluzeau PH , Ritz P (2009). Is skeletal muscle mitochondrial dysfunction a cause or an indirect consequence of insulin resistance in humans? *Diabetes & metabolism*. **35**, 159-167.

English AR , Voeltz GK (2013). Rab10 GTPase regulates ER dynamics and morphology. *Nature cell biology*. **15**, 169-178.

Espinosa A, Campos C, Diaz-Vegas A, Galgani JE, Juretic N, Osorio-Fuentealba C, Bucarey JL, Tapia G, Valenzuela R, Contreras-Ferrat A, Llanos P , Jaimovich E (2013). Insulin-dependent H2O2 production is higher in muscle fibers of mice fed with a high-fat diet. *International journal of molecular sciences*. **14**, 15740-15754.

Faust PL , Kovacs WJ (2013). Cholesterol biosynthesis and ER stress in peroxisome deficiency. *Biochimie*.

Feillet-Coudray C, Sutra T, Fouret G, Ramos J, Wrutniak-Cabello C, Cabello G, Cristol JP , Coudray C (2009). Oxidative stress in rats fed a high-fat high-sucrose diet and preventive effect of polyphenols: Involvement of mitochondrial and NAD(P)H oxidase systems. *Free radical biology & medicine*. **46**, 624-632.

Ferrick DA, Neilson A , Beeson C (2008). Advances in measuring cellular bioenergetics using extracellular flux. *Drug discovery today*. **13**, 268-274.

Fiamoncini J, Turner N, Hirabara SM, Salgado TM, Marcal AC, Leslie S, da Silva SM, Deschamps FC, Luz J, Cooney GJ , Curi R (2013). Enhanced peroxisomal beta-oxidation is associated with prevention of obesity and glucose intolerance by fish oil-enriched diets. *Obesity*. **21**, 1200-1207.

Fisher-Wellman KH , Neufer PD (2012). Linking mitochondrial bioenergetics to insulin resistance via redox biology. *Trends in endocrinology and metabolism: TEM.* **23**, 142-153.

Flegal KM, Kit BK, Orpana H , Graubard BI (2013). Association of all-cause mortality with overweight and obesity using standard body mass index categories: a systematic review and meta-analysis. *JAMA : the journal of the American Medical Association.* **309**, 71-82.

Forkink M, Smeitink JA, Brock R, Willems PH , Koopman WJ (2010). Detection and manipulation of mitochondrial reactive oxygen species in mammalian cells. *Biochimica et biophysica acta.* **1797**, 1034-1044.

Franko A, von Kleist-Retzow JC, Bose M, Sanchez-Lasheras C, Brodesser S, Krut O, Kunz WS, Wiedermann D, Hoehn M, Stohr O, Moll L, Freude S, Krone W, Schubert M , Wiesner RJ (2012). Complete failure of insulin-transmitted signaling, but not obesity-induced insulin resistance, impairs respiratory chain function in muscle. *Journal of molecular medicine.* **90**, 1145-1160.

Frenzel M, Rommelspacher H, Sugawa MD , Dencher NA (2010). Ageing alters the supramolecular architecture of OxPhos complexes in rat brain cortex. *Experimental gerontology.* **45**, 563-572.

Gambino R, Musso G , Cassader M (2011). Redox balance in the pathogenesis of nonalcoholic fatty liver disease: mechanisms and therapeutic opportunities. *Antioxidants & redox signaling.* **15**, 1325-1365.

Gentleman RC, Carey VJ, Bates DM, Bolstad B, Dettling M, Dudoit S, Ellis B, Gautier L, Ge Y, Gentry J, Hornik K, Hothorn T, Huber W, Iacus S, Irizarry R, Leisch F, Li C, Maechler M, Rossini AJ, Sawitzki G, Smith C, Smyth G, Tierney L, Yang JY , Zhang J (2004). Bioconductor: open software development for computational biology and bioinformatics. *Genome biology.* **5**, R80.

Giskes K, van Lenthe F, Avendano-Pabon M , Brug J (2011). A systematic review of environmental factors and obesogenic dietary intakes among adults: are we getting closer to understanding obesogenic environments? *Obesity reviews : an official journal of the International Association for the Study of Obesity.* **12**, e95-e106.

Goodpaster BH (2013). Mitochondrial deficiency is associated with insulin resistance. *Diabetes.* **62**, 1032-1035.

Goodpaster BH, He J, Watkins S , Kelley DE (2001). Skeletal muscle lipid content and insulin resistance: evidence for a paradox in endurance-trained athletes. *The Journal of clinical endocrinology and metabolism.* **86**, 5755-5761.

Gredilla R, Bohr VA , Stevnsner T (2010). Mitochondrial DNA repair and association with aging--an update. *Experimental gerontology.* **45**, 478-488.

Greenberg AS, Coleman RA, Kraemer FB, McManaman JL, Obin MS, Puri V, Yan QW, Miyoshi H , Mashek DG (2011). The role of lipid droplets in metabolic disease in rodents and humans. *The Journal of clinical investigation.* **121**, 2102-2110.

Grunz G, Haas K, Soukup S, Klingenspor M, Kulling SE, Daniel H , Spanier B (2012). Structural features and bioavailability of four flavonoids and their implications for lifespan-extending and antioxidant actions in C. elegans. *Mechanisms of ageing and development.* **133**, 1-10.

Guicciardi ME, Malhi H, Mott JL , Gores GJ (2013). Apoptosis and necrosis in the liver. *Comprehensive Physiology.* **3**, 977-1010.

Guo Y, Darshi M, Ma Y, Perkins GA, Shen Z, Haushalter KJ, Saito R, Chen A, Lee YS, Patel HH, Briggs SP, Ellisman MH, Olefsky JM , Taylor SS (2013). Quantitative Proteomic

and Functioanl Analysis of Liver Mitochondria from High Fat Diet Diabetic Mice. *Molecular & cellular proteomics : MCP.*

Hamza I , Dailey HA (2012). One ring to rule them all: trafficking of heme and heme synthesis intermediates in the metazoans. *Biochimica et biophysica acta.* **1823**, 1617-1632.

Hancock CR, Han DH, Chen M, Terada S, Yasuda T, Wright DC , Holloszy JO (2008). High-fat diets cause insulin resistance despite an increase in muscle mitochondria. *Proceedings of the National Academy of Sciences of the United States of America.* **105**, 7815-7820.

Hansen JM, Go YM , Jones DP (2006). Nuclear and mitochondrial compartmentation of oxidative stress and redox signaling. *Annual review of pharmacology and toxicology.* **46**, 215-234.

Haug E, Rasmussen M, Samdal O, Iannotti R, Kelly C, Borraccino A, Vereecken C, Melkevik O, Lazzeri G, Giacchi M, Ercan O, Due P, Ravens-Sieberer U, Currie C, Morgan A, Ahluwalia N , Group HOW (2009). Overweight in school-aged children and its relationship with demographic and lifestyle factors: results from the WHO-Collaborative Health Behaviour in School-aged Children (HBSC) study. *International journal of public health.* **54 Suppl 2**, 167-179.

Hildebrandt TM , Grieshaber MK (2008). Three enzymatic activities catalyze the oxidation of sulfide to thiosulfate in mammalian and invertebrate mitochondria. *The FEBS journal.* **275**, 3352-3361.

Hills AP, Byrne NM, Lindstrom R , Hill JO (2013). 'Small changes' to diet and physical activity behaviors for weight management. *Obesity facts.* **6**, 228-238.

Hirschberg V (2012). *Analysis of uncoupling protein 1 and CideA function in two mammalian cell lines.* Universitätsbibliothek der TU München: Technische Universität München.

Hla T , Dannenberg AJ (2012). Sphingolipid signaling in metabolic disorders. *Cell metabolism.* **16**, 420-434.

Hoeks J, Wilde J, Hulshof MF, Berg SA, Schaart G, Dijk KW, Smit E , Mariman EC (2011). High fat diet-induced changes in mouse muscle mitochondrial phospholipids do not impair mitochondrial respiration despite insulin resistance. *PloS one.* **6**, e27274.

Hoffler U, Hobbie K, Wilson R, Bai R, Rahman A, Malarkey D, Travlos G , Ghanayem BI (2009). Diet-induced obesity is associated with hyperleptinemia, hyperinsulinemia, hepatic steatosis, and glomerulopathy in C57Bl/6J mice. *Endocrine.* **36**, 311-325.

Hojlund K, Mogensen M, Sahlin K , Beck-Nielsen H (2008). Mitochondrial dysfunction in type 2 diabetes and obesity. *Endocrinology and metabolism clinics of North America.* **37**, 713-731, x.

Holloszy JO (2013). "Deficiency" of mitochondria in muscle does not cause insulin resistance. *Diabetes.* **62**, 1036-1040.

Houten SM , Wanders RJ (2010). A general introduction to the biochemistry of mitochondrial fatty acid beta-oxidation. *Journal of inherited metabolic disease.* **33**, 469-477.

Huang CS, Anderson ME , Meister A (1993). Amino acid sequence and function of the light subunit of rat kidney gamma-glutamylcysteine synthetase. *The Journal of biological chemistry.* **268**, 20578-20583.

Huber W, von Heydebreck A, Sultmann H, Poustka A , Vingron M (2002). Variance stabilization applied to microarray data calibration and to the quantification of differential expression. *Bioinformatics.* **18 Suppl 1**, S96-104.

Hulbert AJ, Turner N, Storlien LH , Else PL (2005). Dietary fats and membrane function: implications for metabolism and disease. *Biological reviews of the Cambridge Philosophical Society*. **80**, 155-169.

Inami Y, Yamashina S, Izumi K, Ueno T, Tanida I, Ikejima K , Watanabe S (2011). Hepatic steatosis inhibits autophagic proteolysis via impairment of autophagosomal acidification and cathepsin expression. *Biochemical and biophysical research communications*. **412**, 618-625.

Iossa S, Lionetti L, Mollica MP, Crescenzo R, Botta M, Barletta A , Liverini G (2003). Effect of high-fat feeding on metabolic efficiency and mitochondrial oxidative capacity in adult rats. *The British journal of nutrition*. **90**, 953-960.

Issop L, Rone MB , Papadopoulos V (2013). Organelle plasticity and interactions in cholesterol transport and steroid biosynthesis. *Molecular and cellular endocrinology*. **371**, 34-46.

Jacobson L (2002). Middle-aged C57BL/6 mice have impaired responses to leptin that are not improved by calorie restriction. *American journal of physiology. Endocrinology and metabolism*. **282**, E786-793.

Jastroch M, Hirschberg V , Klingenspor M (2012). Functional characterization of UCP1 in mammalian HEK293 cells excludes mitochondrial uncoupling artefacts and reveals no contribution to basal proton leak. *Biochimica et biophysica acta*. **1817**, 1660-1670.

Jelenik T , Roden M (2012). Mitochondrial Plasticity in Obesity and Diabetes Mellitus. *Antioxidants & redox signaling*.

Jheng HF, Tsai PJ, Guo SM, Kuo LH, Chang CS, Su IJ, Chang CR , Tsai YS (2012). Mitochondrial fission contributes to mitochondrial dysfunction and insulin resistance in skeletal muscle. *Molecular and cellular biology*. **32**, 309-319.

Jiang ZG, Robson SC , Yao Z (2013). Lipoprotein metabolism in nonalcoholic fatty liver disease. *Journal of biomedical research*. **27**, 1-13.

Johansson LH , Borg LA (1988). A spectrophotometric method for determination of catalase activity in small tissue samples. *Analytical biochemistry*. **174**, 331-336.

Jones DP (2008). Radical-free biology of oxidative stress. *American journal of physiology. Cell physiology*. **295**, C849-868.

Kahn R, Buse J, Ferrannini E , Stern M (2005). The metabolic syndrome: time for a critical appraisal. Joint statement from the American Diabetes Association and the European Association for the Study of Diabetes. *Diabetologia*. **48**, 1684-1699.

Kanehisa M , Goto S (2000). KEGG: kyoto encyclopedia of genes and genomes. *Nucleic acids research*. **28**, 27-30.

Kawano Y , Cohen DE (2013). Mechanisms of hepatic triglyceride accumulation in non-alcoholic fatty liver disease. *Journal of gastroenterology*. **48**, 434-441.

Kelley DE, He J, Menshikova EV , Ritov VB (2002). Dysfunction of mitochondria in human skeletal muscle in type 2 diabetes. *Diabetes*. **51**, 2944-2950.

Kelner MJ, Bagnell RD, Montoya MA, Estes LA, Forsberg L , Morgenstern R (2000). Structural organization of the microsomal glutathione S-transferase gene (MGST1) on chromosome 12p13.1-13.2. Identification of the correct promoter region and demonstration of transcriptional regulation in response to oxidative stress. *The Journal of biological chemistry*. **275**, 13000-13006.

Kim S, Sohn I, Ahn JI, Lee KH, Lee YS , Lee YS (2004). Hepatic gene expression profiles in a long-term high-fat diet-induced obesity mouse model. *Gene*. **340**, 99-109.

Kirpich IA, Gobejishvili LN, Bon Homme M, Waigel S, Cave M, Arteel G, Barve SS, McClain CJ , Deaciuc IV (2011). Integrated hepatic transcriptome and proteome analysis of

mice with high-fat diet-induced nonalcoholic fatty liver disease. *The Journal of nutritional biochemistry*. **22**, 38-45.

Kobayashi M , Yamamoto M (2006). Nrf2-Keap1 regulation of cellular defense mechanisms against electrophiles and reactive oxygen species. *Advances in enzyme regulation*. **46**, 113-140.

Koonen DP, Sung MM, Kao CK, Dolinsky VW, Koves TR, Ilkayeva O, Jacobs RL, Vance DE, Light PE, Muoio DM, Febbraio M , Dyck JR (2010). Alterations in skeletal muscle fatty acid handling predisposes middle-aged mice to diet-induced insulin resistance. *Diabetes*. **59**, 1366-1375.

Kopelman P (2007). Health risks associated with overweight and obesity. *Obesity reviews : an official journal of the International Association for the Study of Obesity*. **8 Suppl 1**, 13-17.

Kopelman PG (2000). Obesity as a medical problem. *Nature*. **404**, 635-643.

Koves TR, Ussher JR, Noland RC, Slentz D, Mosedale M, Ilkayeva O, Bain J, Stevens R, Dyck JR, Newgard CB, Lopaschuk GD , Muoio DM (2008). Mitochondrial overload and incomplete fatty acid oxidation contribute to skeletal muscle insulin resistance. *Cell metabolism*. **7**, 45-56.

Krahenbuhl S, Talos C, Wiesmann U , Hoppel CL (1994). Development and evaluation of a spectrophotometric assay for complex III in isolated mitochondria, tissues and fibroblasts from rats and humans. *Clinica chimica acta; international journal of clinical chemistry*. **230**, 177-187.

Kramer KA, Oglesbee D, Hartman SJ, Huey J, Anderson B, Magera MJ, Matern D, Rinaldo P, Robinson BH, Cameron JM , Hahn SH (2005). Automated spectrophotometric analysis of mitochondrial respiratory chain complex enzyme activities in cultured skin fibroblasts. *Clinical chemistry*. **51**, 2110-2116.

Kratschmar DV, Calabrese D, Walsh J, Lister A, Birk J, Appenzeller-Herzog C, Moulin P, Goldring CE , Odermatt A (2012). Suppression of the Nrf2-dependent antioxidant response by glucocorticoids and 11beta-HSD1-mediated glucocorticoid activation in hepatic cells. *PloS one*. **7**, e36774.

Kwak MK, Wakabayashi N, Itoh K, Motohashi H, Yamamoto M , Kensler TW (2003). Modulation of gene expression by cancer chemopreventive dithiolethiones through the Keap1-Nrf2 pathway. Identification of novel gene clusters for cell survival. *The Journal of biological chemistry*. **278**, 8135-8145.

Larsen S, Nielsen J, Hansen CN, Nielsen LB, Wibrand F, Stride N, Schroder HD, Boushel R, Helge JW, Dela F , Hey-Mogensen M (2012). Biomarkers of mitochondrial content in skeletal muscle of healthy young human subjects. *The Journal of physiology*. **590**, 3349-3360.

Lee K, Kerner J , Hoppel CL (2011a). Mitochondrial carnitine palmitoyltransferase 1a (CPT1a) is part of an outer membrane fatty acid transfer complex. *The Journal of biological chemistry*. **286**, 25655-25662.

Lee YS, Li P, Huh JY, Hwang IJ, Lu M, Kim JI, Ham M, Talukdar S, Chen A, Lu WJ, Bandyopadhyay GK, Schwendener R, Olefsky J , Kim JB (2011b). Inflammation is necessary for long-term but not short-term high-fat diet-induced insulin resistance. *Diabetes*. **60**, 2474-2483.

Li D, Hinshelwood A, Gardner R, McGarvie G , Ellis EM (2006). Mouse aldo-keto reductase AKR7A5 protects V79 cells against 4-hydroxynonenal-induced apoptosis. *Toxicology*. **226**, 172-180.

Liu K , Czaja MJ (2013). Regulation of lipid stores and metabolism by lipophagy. *Cell death and differentiation*. **20**, 3-11.

Lo SC , Hannink M (2008). PGAM5 tethers a ternary complex containing Keap1 and Nrf2 to mitochondria. *Experimental cell research*. **314**, 1789-1803.

Masuoka HC , Chalasani N (2013). Nonalcoholic fatty liver disease: an emerging threat to obese and diabetic individuals. *Annals of the New York Academy of Sciences*. **1281**, 106-122.

McCord JM , Fridovich I (1969). Superoxide dismutase. An enzymic function for erythrocuprein (hemocuprein). *The Journal of biological chemistry*. **244**, 6049-6055.

Michalakis K, Goulis DG, Vazaiou A, Mintziori G, Polymeris A , Abrahamian-Michalakis A (2013). Obesity in the ageing man. *Metabolism: clinical and experimental*. **62**, 1341-1349.

Midha MK, Tikoo K, Sinha N, Kaur S, Verma HN, Rao KV, Chatterjee S , Manivel V (2012). Extracting time-dependent obese-diabetic specific networks in hepatic proteome analysis. *Journal of proteome research*. **11**, 6030-6043.

Mikrozensus (2009). Körpermaße der Bevölkerung). Wiesbaden: Statistisches Bundesamt.

Mitchell S, Ellingson C, Coyne T, Hall L, Neill M, Christian N, Higham C, Dobrowolski SF, Tuchman M, Summar M , Urea Cycle Disorder C (2009). Genetic variation in the urea cycle: a model resource for investigating key candidate genes for common diseases. *Human mutation*. **30**, 56-60.

Modis K, Coletta C, Erdelyi K, Papapetropoulos A , Szabo C (2013). Intramitochondrial hydrogen sulfide production by 3-mercaptopyruvate sulfurtransferase maintains mitochondrial electron flow and supports cellular bioenergetics. *FASEB journal : official publication of the Federation of American Societies for Experimental Biology*. **27**, 601-611.

Montgomery MK, Hallahan NL, Brown SH, Liu M, Mitchell TW, Cooney GJ , Turner N (2013). Mouse strain-dependent variation in obesity and glucose homeostasis in response to high-fat feeding. *Diabetologia*.

Muoio DM , Neufer PD (2012). Lipid-induced mitochondrial stress and insulin action in muscle. *Cell metabolism*. **15**, 595-605.

Murphy MP (2009). How mitochondria produce reactive oxygen species. *The Biochemical journal*. **417**, 1-13.

Muscari C, Pappagallo M, Ferrari D, Giordano E, Capanni C, Caldarera CM , Guarnieri C (1998). Simultaneous detection of reduced and oxidized glutathione in tissues and mitochondria by capillary electrophoresis. *Journal of chromatography. B, Biomedical sciences and applications*. **707**, 301-307.

Nadal-Casellas A, Amengual-Cladera E, Proenza AM, Llado I , Gianotti M (2010). Long-term high-fat-diet feeding impairs mitochondrial biogenesis in liver of male and female rats. *Cellular physiology and biochemistry : international journal of experimental cellular physiology, biochemistry, and pharmacology*. **26**, 291-302.

Nakamura A , Terauchi Y (2013). Lessons from Mouse Models of High-Fat Diet-Induced NAFLD. *International journal of molecular sciences*. **14**, 21240-21257.

Navarro A , Boveris A (2004). Rat brain and liver mitochondria develop oxidative stress and lose enzymatic activities on aging. *American journal of physiology. Regulatory, integrative and comparative physiology*. **287**, R1244-1249.

Navarro A , Boveris A (2007). The mitochondrial energy transduction system and the aging process. *American journal of physiology. Cell physiology*. **292**, C670-686.

Neschen S, Morino K, Hammond LE, Zhang D, Liu ZX, Romanelli AJ, Cline GW, Pongratz RL, Zhang XM, Choi CS, Coleman RA , Shulman GI (2005). Prevention of hepatic

steatosis and hepatic insulin resistance in mitochondrial acyl-CoA:glycerol-sn-3-phosphate acyltransferase 1 knockout mice. *Cell metabolism.* **2**, 55-65.

Nishikawa S, Yasoshima A, Doi K, Nakayama H , Uetsuka K (2007). Involvement of sex, strain and age factors in high fat diet-induced obesity in C57BL/6J and BALB/cA mice. *Experimental animals / Japanese Association for Laboratory Animal Science.* **56**, 263-272.

OECD (2013). Overweight and Obesity. In *OECD Factbook 2013: Economic, Environmental and Social Statistics.* (OECD, ed): OECD Publishing.

Oh TS, Kwon EY, Choi JW, Choi MS , Yun JW (2011). Time-dependent hepatic proteome analysis in lean and diet-induced obese mice. *Journal of microbiology and biotechnology.* **21**, 1211-1227.

Okado-Matsumoto A , Fridovich I (2001). Subcellular distribution of superoxide dismutases (SOD) in rat liver: Cu,Zn-SOD in mitochondria. *The Journal of biological chemistry.* **276**, 38388-38393.

Okazaki H, Igarashi M, Nishi M, Tajima M, Sekiya M, Okazaki S, Yahagi N, Ohashi K, Tsukamoto K, Amemiya-Kudo M, Matsuzaka T, Shimano H, Yamada N, Aoki J, Morikawa R, Takanezawa Y, Arai H, Nagai R, Kadowaki T, Osuga J , Ishibashi S (2006). Identification of a novel member of the carboxylesterase family that hydrolyzes triacylglycerol: a potential role in adipocyte lipolysis. *Diabetes.* **55**, 2091-2097.

Orr AL, Quinlan CL, Perevoshchikova IV , Brand MD (2012). A refined analysis of superoxide production by mitochondrial sn-glycerol 3-phosphate dehydrogenase. *The Journal of biological chemistry.* **287**, 42921-42935.

Owen OE, Kalhan SC , Hanson RW (2002). The key role of anaplerosis and cataplerosis for citric acid cycle function. *The Journal of biological chemistry.* **277**, 30409-30412.

Pachl F, Ruprecht B, Lemeer S , Kuster B (2013). Characterization of a high field Orbitrap mass spectrometer for proteome analysis. *Proteomics.* **13**, 2552-2562.

Paglia DE , Valentine WN (1967). Studies on the quantitative and qualitative characterization of erythrocyte glutathione peroxidase. *The Journal of laboratory and clinical medicine.* **70**, 158-169.

Pagliarini DJ, Calvo SE, Chang B, Sheth SA, Vafai SB, Ong SE, Walford GA, Sugiana C, Boneh A, Chen WK, Hill DE, Vidal M, Evans JG, Thorburn DR, Carr SA , Mootha VK (2008). A mitochondrial protein compendium elucidates complex I disease biology. *Cell.* **134**, 112-123.

Pamplona R (2008). Membrane phospholipids, lipoxidative damage and molecular integrity: a causal role in aging and longevity. *Biochimica et biophysica acta.* **1777**, 1249-1262.

Perevoshchikova IV, Quinlan CL, Orr AL, Gerencser AA , Brand MD (2013). Sites of superoxide and hydrogen peroxide production during fatty acid oxidation in rat skeletal muscle mitochondria. *Free radical biology & medicine.* **61C**, 298-309.

Pertoft H, Laurent TC, Laas T , Kagedal L (1978). Density gradients prepared from colloidal silica particles coated by polyvinylpyrrolidone (Percoll). *Analytical biochemistry.* **88**, 271-282.

Petersen KF, Dufour S, Befroy D, Garcia R , Shulman GI (2004). Impaired mitochondrial activity in the insulin-resistant offspring of patients with type 2 diabetes. *The New England journal of medicine.* **350**, 664-671.

Raffaella C, Francesca B, Italia F, Marina P, Giovanna L , Susanna I (2008). Alterations in hepatic mitochondrial compartment in a model of obesity and insulin resistance. *Obesity.* **16**, 958-964.

Rahim A, Nafi-valencia E, Siddiqi S, Basha R, Runyon CC , Siddiqi SA (2012). Proteomic analysis of the very low density lipoprotein (VLDL) transport vesicles. *Journal of proteomics.* **75**, 2225-2235.

Raisanen SR, Lehenkari P, Tasanen M, Rahkila P, Harkonen PL , Vaananen HK (1999). Carbonic anhydrase III protects cells from hydrogen peroxide-induced apoptosis. *FASEB journal : official publication of the Federation of American Societies for Experimental Biology.* **13**, 513-522.

Rambold AS , Lippincott-Schwartz J (2011). Mechanisms of mitochondria and autophagy crosstalk. *Cell cycle.* **10**, 4032-4038.

Ramsay RR, Gandour RD , van der Leij FR (2001). Molecular enzymology of carnitine transfer and transport. *Biochimica et biophysica acta.* **1546**, 21-43.

Randle PJ, Garland PB, Hales CN , Newsholme EA (1963). The glucose fatty-acid cycle. Its role in insulin sensitivity and the metabolic disturbances of diabetes mellitus. *Lancet.* **1**, 785-789.

Rao JN, Warren GZ, Estolt-Povedano S, Zammit VA , Ulmer TS (2011). An environment-dependent structural switch underlies the regulation of carnitine palmitoyltransferase 1A. *The Journal of biological chemistry.* **286**, 42545-42554.

Rappsilber J, Mann M , Ishihama Y (2007). Protocol for micro-purification, enrichment, pre-fractionation and storage of peptides for proteomics using StageTips. *Nature protocols.* **2**, 1896-1906.

Raturi A , Simmen T (2013). Where the endoplasmic reticulum and the mitochondrion tie the knot: the mitochondria-associated membrane (MAM). *Biochimica et biophysica acta.* **1833**, 213-224.

Rauh K, Gabriel E, Kerschbaum E, Schuster T, von Kries R, Amann-Gassner U , Hauner H (2013). Safety and efficacy of a lifestyle intervention for pregnant women to prevent excessive maternal weight gain: a cluster-randomized controlled trial. *BMC pregnancy and childbirth.* **13**, 151.

Ren LP, Chan SM, Zeng XY, Laybutt DR, Iseli TJ, Sun RQ, Kraegen EW, Cooney GJ, Turner N , Ye JM (2012). Differing endoplasmic reticulum stress response to excess lipogenesis versus lipid oversupply in relation to hepatic steatosis and insulin resistance. *PloS one.* **7**, e30816.

Reynafarje B, Costa LE , Lehninger AL (1985). O2 solubility in aqueous media determined by a kinetic method. *Analytical biochemistry.* **145**, 406-418.

Rieusset J (2011). Mitochondria and endoplasmic reticulum: mitochondria-endoplasmic reticulum interplay in type 2 diabetes pathophysiology. *The international journal of biochemistry & cell biology.* **43**, 1257-1262.

Rinaldo P, Matern D , Bennett MJ (2002). Fatty acid oxidation disorders. *Annual review of physiology.* **64**, 477-502.

Ritov VB, Menshikova EV, He J, Ferrell RE, Goodpaster BH , Kelley DE (2005). Deficiency of subsarcolemmal mitochondria in obesity and type 2 diabetes. *Diabetes.* **54**, 8-14.

Rogers GW, Brand MD, Petrosyan S, Ashok D, Elorza AA, Ferrick DA , Murphy AN (2011). High throughput microplate respiratory measurements using minimal quantities of isolated mitochondria. *PloS one.* **6**, e21746.

Ron D , Walter P (2007). Signal integration in the endoplasmic reticulum unfolded protein response. *Nature reviews. Molecular cell biology.* **8**, 519-529.

Ronchi JA, Figueira TR, Ravagnani FG, Oliveira HC, Vercesi AE , Castilho RF (2013). A spontaneous mutation in the nicotinamide nucleotide transhydrogenase gene of

C57BL/6J mice results in mitochondrial redox abnormalities. *Free radical biology & medicine.* **63**, 446-456.

Rubio-Aliaga I, Roos B, Sailer M, McLoughlin GA, Boekschoten MV, van Erk M, Bachmair EM, van Schothorst EM, Keijer J, Coort SL, Evelo C, Gibney MJ, Daniel H, Muller M, Kleemann R , Brennan L (2011). Alterations in hepatic one-carbon metabolism and related pathways following a high-fat dietary intervention. *Physiological genomics.* **43**, 408-416.

Ruiz-Ramirez A, Chavez-Salgado M, Peneda-Flores JA, Zapata E, Masso F , El-Hafidi M (2011). High-sucrose diet increases ROS generation, FFA accumulation, UCP2 level, and proton leak in liver mitochondria. *American journal of physiology. Endocrinology and metabolism.* **301**, E1198-1207.

Saftig P , Eskelinen EL (2008). Live longer with LAMP-2. *Nature medicine.* **14**, 909-910.

Samuel VT , Shulman GI (2012). Mechanisms for insulin resistance: common threads and missing links. *Cell.* **148**, 852-871.

Satapati S, Sunny NE, Kucejova B, Fu X, He TT, Mendez-Lucas A, Shelton JM, Perales JC, Browning JD , Burgess SC (2012). Elevated TCA cycle function in the pathology of diet-induced hepatic insulin resistance and fatty liver. *Journal of lipid research.* **53**, 1080-1092.

Savage DB, Petersen KF , Shulman GI (2007). Disordered lipid metabolism and the pathogenesis of insulin resistance. *Physiological reviews.* **87**, 507-520.

Schmid GM, Converset V, Walter N, Sennitt MV, Leung KY, Byers H, Ward M, Hochstrasser DF, Cawthorne MA , Sanchez JC (2004). Effect of high-fat diet on the expression of proteins in muscle, adipose tissues, and liver of C57BL/6 mice. *Proteomics.* **4**, 2270-2282.

Schneider CA, Rasband WS , Eliceiri KW (2012). NIH Image to ImageJ: 25 years of image analysis. *Nature methods.* **9**, 671-675.

Schonfeld P , Wojtczak L (2008). Fatty acids as modulators of the cellular production of reactive oxygen species. *Free radical biology & medicine.* **45**, 231-241.

Schonfeld P , Wojtczak L (2012). Brown adipose tissue mitochondria oxidizing fatty acids generate high levels of reactive oxygen species irrespective of the uncoupling protein-1 activity state. *Biochimica et biophysica acta.* **1817**, 410-418.

Schooneman MG, Vaz FM, Houten SM , Soeters MR (2013). Acylcarnitines: reflecting or inflicting insulin resistance? *Diabetes.* **62**, 1-8.

Schrader M , Fahimi HD (2006). Peroxisomes and oxidative stress. *Biochimica et biophysica acta.* **1763**, 1755-1766.

Schrauwen P, Schrauwen-Hinderling V, Hoeks J , Hesselink MK (2010). Mitochondrial dysfunction and lipotoxicity. *Biochimica et biophysica acta.* **1801**, 266-271.

Seale P , Lazar MA (2009). Brown fat in humans: turning up the heat on obesity. *Diabetes.* **58**, 1482-1484.

Seifert EL, Estey C, Xuan JY , Harper ME (2010). Electron transport chain-dependent and -independent mechanisms of mitochondrial H2O2 emission during long-chain fatty acid oxidation. *The Journal of biological chemistry.* **285**, 5748-5758.

Seo HA , Lee IK (2013). The Role of Nrf2: Adipocyte Differentiation, Obesity, and Insulin Resistance. *Oxidative medicine and cellular longevity.* **2013**, 184598.

Serra D, Mera P, Malandrino MI, Mir JF , Herrero L (2012). Mitochondrial Fatty Acid Oxidation in Obesity. *Antioxidants & redox signaling.*

Severinghaus JW (2002). The invention and development of blood gas analysis apparatus. *Anesthesiology*. **97**, 253-256.

Shortreed KE, Krause MP, Huang JH, Dhanani D, Moradi J, Ceddia RB , Hawke TJ (2009). Muscle-specific adaptations, impaired oxidative capacity and maintenance of contractile function characterize diet-induced obese mouse skeletal muscle. *PloS one*. **4**, e7293.

Sievers F, Wilm A, Dineen D, Gibson TJ, Karplus K, Li W, Lopez R, McWilliam H, Remmert M, Soding J, Thompson JD , Higgins DG (2011). Fast, scalable generation of high-quality protein multiple sequence alignments using Clustal Omega. *Molecular systems biology*. **7**, 539.

Smith PK, Krohn RI, Hermanson GT, Mallia AK, Gartner FH, Provenzano MD, Fujimoto EK, Goeke NM, Olson BJ , Klenk DC (1985). Measurement of protein using bicinchoninic acid. *Analytical biochemistry*. **150**, 76-85.

Smyth GK (2004). Linear models and empirical bayes methods for assessing differential expression in microarray experiments. *Statistical applications in genetics and molecular biology*. **3**, Article3.

Sohal RS , Orr WC (2012). The redox stress hypothesis of aging. *Free radical biology & medicine*. **52**, 539-555.

Sparks JD, Collins HL, Chirieac DV, Cianci J, Jokinen J, Sowden MP, Galloway CA , Sparks CE (2006). Hepatic very-low-density lipoprotein and apolipoprotein B production are increased following in vivo induction of betaine-homocysteine S-methyltransferase. *The Biochemical journal*. **395**, 363-371.

Sparks JD, Sparks CE , Adeli K (2012). Selective hepatic insulin resistance, VLDL overproduction, and hypertriglyceridemia. *Arteriosclerosis, thrombosis, and vascular biology*. **32**, 2104-2112.

Stewart LK, Wang Z, Ribnicky D, Soileau JL, Cefalu WT , Gettys TW (2009). Failure of dietary quercetin to alter the temporal progression of insulin resistance among tissues of C57BL/6J mice during the development of diet-induced obesity. *Diabetologia*. **52**, 514-523.

Stowe DF , Camara AK (2009). Mitochondrial reactive oxygen species production in excitable cells: modulators of mitochondrial and cell function. *Antioxidants & redox signaling*. **11**, 1373-1414.

Sturley SL , Hussain MM (2012). Lipid droplet formation on opposing sides of the endoplasmic reticulum. *Journal of lipid research*. **53**, 1800-1810.

Styskal J, Nwagwu FA, Watkins YN, Liang H, Richardson A, Musi N , Salmon AB (2013). Methionine sulfoxide reductase A affects insulin resistance by protecting insulin receptor function. *Free radical biology & medicine*. **56**, 123-132.

Sundaram M , Yao Z (2010). Recent progress in understanding protein and lipid factors affecting hepatic VLDL assembly and secretion. *Nutrition & metabolism*. **7**, 35.

Sunny NE, Satapati S, Fu X, He T, Mehdibeigi R, Spring-Robinson C, Duarte J, Potthoff MJ, Browning JD , Burgess SC (2010). Progressive adaptation of hepatic ketogenesis in mice fed a high-fat diet. *American journal of physiology. Endocrinology and metabolism*. **298**, E1226-1235.

Surwit RS, Kuhn CM, Cochrane C, McCubbin JA , Feinglos MN (1988). Diet-induced type II diabetes in C57BL/6J mice. *Diabetes*. **37**, 1163-1167.

Tahara EB, Navarete FD , Kowaltowski AJ (2009). Tissue-, substrate-, and site-specific characteristics of mitochondrial reactive oxygen species generation. *Free radical biology & medicine*. **46**, 1283-1297.

Talbot DA , Brand MD (2005). Uncoupling protein 3 protects aconitase against inactivation in isolated skeletal muscle mitochondria. *Biochimica et biophysica acta*. **1709**, 150-156.

Tarnopolsky MA, Rennie CD, Robertshaw HA, Fedak-Tarnopolsky SN, Devries MC , Hamadeh MJ (2007). Influence of endurance exercise training and sex on intramyocellular lipid and mitochondrial ultrastructure, substrate use, and mitochondrial enzyme activity. *American journal of physiology. Regulatory, integrative and comparative physiology*. **292**, R1271-1278.

Team RDC (2011). *R: A language and environment for statistical computing.* Vienna, Austria: R Foundation for Statistical Computing.

Terlecky SR, Koepke JI , Walton PA (2006). Peroxisomes and aging. *Biochimica et biophysica acta*. **1763**, 1749-1754.

Toye AA, Lippiat JD, Proks P, Shimomura K, Bentley L, Hugill A, Mijat V, Goldsworthy M, Moir L, Haynes A, Quarterman J, Freeman HC, Ashcroft FM , Cox RD (2005). A genetic and physiological study of impaired glucose homeostasis control in C57BL/6J mice. *Diabetologia*. **48**, 675-686.

Turner N, Bruce CR, Beale SM, Hoehn KL, So T, Rolph MS , Cooney GJ (2007). Excess lipid availability increases mitochondrial fatty acid oxidative capacity in muscle: evidence against a role for reduced fatty acid oxidation in lipid-induced insulin resistance in rodents. *Diabetes*. **56**, 2085-2092.

Turner N, Hariharan K, TidAng J, Frangioudakis G, Beale SM, Wright LE, Zeng XY, Leslie SJ, Li JY, Kraegen EW, Cooney GJ , Ye JM (2009). Enhancement of muscle mitochondrial oxidative capacity and alterations in insulin action are lipid species dependent: potent tissue-specific effects of medium-chain fatty acids. *Diabetes*. **58**, 2547-2554.

Turrens JF (2003). Mitochondrial formation of reactive oxygen species. *The Journal of physiology*. **552**, 335-344.

Valencak TG, Arnold W, Tataruch F , Ruf T (2003). High content of polyunsaturated fatty acids in muscle phospholipids of a fast runner, the European brown hare (Lepus europaeus). *Journal of comparative physiology. B, Biochemical, systemic, and environmental physiology*. **173**, 695-702.

Valencak TG , Ruf T (2011). Feeding into old age: long-term effects of dietary fatty acid supplementation on tissue composition and life span in mice. *Journal of comparative physiology. B, Biochemical, systemic, and environmental physiology*. **181**, 289-298.

van den Berg SA, Guigas B, Bijland S, Ouwens M, Voshol PJ, Frants RR, Havekes LM, Romijn JA , van Dijk KW (2010). High levels of dietary stearate promote adiposity and deteriorate hepatic insulin sensitivity. *Nutrition & metabolism*. **7**, 24.

van den Broek NM, Ciapaite J, De Feyter HM, Houten SM, Wanders RJ, Jeneson JA, Nicolay K , Prompers JJ (2010). Increased mitochondrial content rescues in vivo muscle oxidative capacity in long-term high-fat-diet-fed rats. *FASEB journal : official publication of the Federation of American Societies for Experimental Biology*. **24**, 1354-1364.

Vial G, Dubouchaud H, Couturier K, Cottet-Rousselle C, Taleux N, Athias A, Galinier A, Casteilla L , Leverve XM (2011). Effects of a high-fat diet on energy metabolism and ROS production in rat liver. *Journal of hepatology*. **54**, 348-356.

Vial G, Dubouchaud H , Leverve XM (2010). Liver mitochondria and insulin resistance. *Acta biochimica Polonica*. **57**, 389-392.

Vomhof-Dekrey EE , Picklo MJ, Sr. (2012). The Nrf2-antioxidant response element pathway: a target for regulating energy metabolism. *The Journal of nutritional biochemistry*. **23**, 1201-1206.

Wanders RJ, Vreken P, den Boer ME, Wijburg FA, van Gennip AH , L IJ (1999). Disorders of mitochondrial fatty acyl-CoA beta-oxidation. *Journal of inherited metabolic disease*. **22**, 442-487.

Wang S, Chen Z, Lam V, Han J, Hassler J, Finck BN, Davidson NO , Kaufman RJ (2012a). IRE1alpha-XBP1s induces PDI expression to increase MTP activity for hepatic VLDL assembly and lipid homeostasis. *Cell metabolism*. **16**, 473-486.

Wang WA, Groenendyk J , Michalak M (2012b). Calreticulin signaling in health and disease. *The international journal of biochemistry & cell biology*. **44**, 842-846.

Wen X, Wu J, Wang F, Liu B, Huang C , Wei Y (2013). Deconvoluting the role of reactive oxygen species and autophagy in human diseases. *Free radical biology & medicine*. **65C**, 402-410.

WHO (2013). *World Health Statistics*: World Health Organization.

Williams KJ (2008). Molecular processes that handle -- and mishandle -- dietary lipids. *The Journal of clinical investigation*. **118**, 3247-3259.

Wisniewski JR, Zougman A , Mann M (2009a). Combination of FASP and StageTip-based fractionation allows in-depth analysis of the hippocampal membrane proteome. *Journal of proteome research*. **8**, 5674-5678.

Wisniewski JR, Zougman A, Nagaraj N , Mann M (2009b). Universal sample preparation method for proteome analysis. *Nature methods*. **6**, 359-362.

Wu X , Williams KJ (2012). NOX4 pathway as a source of selective insulin resistance and responsiveness. *Arteriosclerosis, thrombosis, and vascular biology*. **32**, 1236-1245.

Xie Z, Li H, Wang K, Lin J, Wang Q, Zhao G, Jia W , Zhang Q (2010). Analysis of transcriptome and metabolome profiles alterations in fatty liver induced by high-fat diet in rat. *Metabolism: clinical and experimental*. **59**, 554-560.

Yokota T, Kinugawa S, Hirabayashi K, Matsushima S, Inoue N, Ohta Y, Hamaguchi S, Sobirin MA, Ono T, Suga T, Kuroda S, Tanaka S, Terasaki F, Okita K , Tsutsui H (2009). Oxidative stress in skeletal muscle impairs mitochondrial respiration and limits exercise capacity in type 2 diabetic mice. *American journal of physiology. Heart and circulatory physiology*. **297**, H1069-1077.

Yuzefovych LV, Musiyenko SI, Wilson GL , Rachek LI (2013). Mitochondrial DNA damage and dysfunction, and oxidative stress are associated with endoplasmic reticulum stress, protein degradation and apoptosis in high fat diet-induced insulin resistance mice. *PloS one*. **8**, e54059.

Zhang C , Cuervo AM (2008). Restoration of chaperone-mediated autophagy in aging liver improves cellular maintenance and hepatic function. *Nature medicine*. **14**, 959-965.

Zhao L, Zou X, Feng Z, Luo C, Liu J, Li H, Chang L, Wang H, Li Y, Long J, Gao F , Liu J (2014). Evidence for association of mitochondrial metabolism alteration with lipid accumulation in aging rats. *Experimental gerontology*.

Appendix

Ad: Material and Methods

Table 14: List of chemicals, kits, enzymes and antibodies, experimental diets, instruments

Chemicals	Article No.	Supplier, Country
2 - Mercaptoethanol	4227.3	Carl Roth, Germany
Acetyl-CoA	A2056	Sigma-Aldrich, USA
ADP (Adenosine 5′-diphosphate sodium salt bacterial)	A2754	Sigma-Aldrich, USA
Amplex Red	A12222	Invitrogen, UK
AMPS (Ammoniumperoxide disulfate)	9593.2	Carl Roth, Germany
Antimycin A	A8674	Sigma-Aldrich, USA
ATP (Adenosine 5′-triphosphate disodium salt hydrate 99%)	A26209	Sigma-Aldrich, USA
Bromphenol blue	A512.1	Carl Roth, Germany
BSA (Albumin Fraction V)	8076.2	Carl Roth, Germany
BSA (Albumin from bovine serum)	A3803	Sigma-Aldrich, USA
Chloroform	Y015.1	Carl Roth, Germany
DEPC (Diethylpyrocarbonate)	D5758	Sigma-Aldrich, USA
DMSO	2189.2	Carl Roth, Germany
DTNB (5,5'dithiobis(2-nitrobenzoic acid)	D21800	Sigma-Aldrich, USA
DTT (Dithiotreitol)	6908.2	Carl Roth, Germany
EDTA	8043.2	Carl Roth, Germany
EGTA	3054.2	Carl Roth, Germany
EtOH 99,8%	9065.4	Carl Roth, Germany
FCCP (Carbonyl cyanide 4-(trifluoromethoxy)phenylhydrazone)	C2920	Sigma-Aldrich, USA
Glucose 20 % Solution	PZN436080	B.Braun, Germany
Glycerol	3783.1	Carl Roth, Germany
Glycerol standard solution	G7793	Sigma-Aldrich, USA
Glycine	3908.2	Carl Roth, Germany
H_2DCFDA (2′,7′-Dichlorofluorescein diacetate)	D6883	Sigma-Aldrich, USA
H_2O_2 (Hydrogen Peroxide)	8070.2	Carl Roth, Germany
HCl	0281.1	Carl Roth, Germany
HEPES	9105.4	Carl Roth, Germany
KCl	6781	Carl Roth, Germany
KH_2PO_4	3904.1	Carl Roth, Germany
KOH	7986.1	Carl Roth, Germany
Malate	M9138	Sigma-Aldrich, USA
Malonate	M129-6	Sigma-Aldrich, USA
Methanol	4627.5	Carl Roth, Germany
$MgCl_2$x 6 H_2O	2189.2	Carl Roth, Germany
NaCl	3957.1	Carl Roth, Germany
NaH_2PO_4 x 2H_2O	T8792.2	Carl Roth, Germany

Nigericin	N7143	Sigma-Aldrich, USA
Oligomycin	O4876	Sigma-Aldrich, USA
Orange G	0318.2	Carl Roth, Germany
Oxaloacetate	O4126	Sigma-Aldrich, USA
Palmitoyl-L-carnitine chloride	P1645	Sigma-Aldrich, USA
PBS (phosphate buffered saline)	P4417	Sigma-Aldrich, USA
Polyoxyetylen-10-tridecylether	P2393	Sigma-Aldrich, USA
Rotenone	477737	Sigma-Aldrich, USA
Roti Quant	K015.3	Carl Roth, Germany
Rotiphorese Gel 30 Acrylamid solution	3025.1	Carl Roth, Germany
RotiSafe	3865.1	Carl Roth, Germany
Safranin O	S8884	Sigma-Aldrich, USA
SDS (sodium dodecyl sulfate)	4360.2	Carl Roth, Germany
Succinate	S3674	Sigma-Aldrich, USA
Sucrose	4621.1	Carl Roth, Germany
TEMED	2367.1	Carl Roth, Germany
TES	9137.2	Carl Roth, Germany
TPMP (Methyltriphenylphosphonium bromide)	130079	Sigma-Aldrich, USA
Tris	4855.2	Carl Roth, Germany
Tris-HCl	9090.2	Carl Roth, Germany
TRIsure	BIO-38033	Bioline, UK
Triton X-100	3051.3	Carl Roth, Germany
Tween 20	9127.2	Carl Roth, Germany

Kits	Article No	Supplier, Country
BCA Protein Assay Kit	23227	Thermo Scientific, USA
LightCycler® 480 ProbesMaster	4887301001	Roche, Switzerland
QuantiTect Reverse Transcription Kit	205313	Quiagen, USA
SensiMix No-Rox	QT650-20	Bioline, UK
Serum TG Determination Kit	Tr0100	Sigma-Aldrich, USA
SV Total RNA Isolation System	Z3100	Promega, USA
Ultrasensitive Mouse Insulin Elisa	10-1249-01	Mercodia, Sweden
Wizard® SV Genomic DNA Purification System	A2360	Promega, USA

Enzymes	Article No	Supplier, Country
Bacillus licheniformis Type VIII (subtilisin A)	A5380	Sigma-Aldrich, USA
HRP (Horseradish peroxidase)	P8375	Sigma-Aldrich, USA
Proteinase K	EO0491	Thermo Scientific, USA
SOD (Superoxide Dismutase)	S5639	Sigma-Aldrich, USA

Antibodies	Article No	Supplier, Country
Monoclonal mouse anti Sod2 (Superoxide Dismutase 2)	ab16956	Abcam, UK
Polyclonal rabbit anti CS (Citrate Synthase)	ab96600	Abcam, UK
Polyclonal rabbit anti Nrf2 (nuclear factor erythroid 2-related factor 2)	sc-13032	Santa Cruz, USA
Polyclonal rabbit anti Pgam5 (Phosphoglycerate Mutase 5)	ab126534	Abcam, UK
Goat Anti-rabbit IR dye 680 CW	926-32221	LICOR, USA
Goat Anti-rabbit IR dye 800 CW	926-32211	LICOR, USA
Donkey Anti-mouse IR dye 800 CW	926-32210	LICOR, USA

Experimental Diets	Article No	Supplier, Country
Control Diet	S5745-E702	ssniffSpezialdiäten GmbH, Germany
High Fat Diet	S5745-E712	ssniffSpezialdiäten GmbH, Germany

Instruments	Article No	Supplier, Country
7 ml Perspex Electrode	OXY040A	Rank Brothers, UK
96 well black, chimney, F-bottom, clear bottom	655096	Greiner Bio One, Germany
Blotting paper	GB003	Whatman (part of GE Healthcare, Sweden)
Combined Polarising Circuit and Readout Meter	OXY030A	Rank Brothers, UK
Controller Digital Model 10	OXY020A	Rank Brothers, UK
Electronic stirring head Type 1 (for oxygen chambers)	MAG101A	Rank Brothers, UK
Eppendorf Centrifuge 5804 R	5805 000.327	Eppendorf, Germany
Eppendorf Microfuge 5417 R		Eppendorf, Germany
Fixed Angle rotor FA-45-24-11	5427 710.000	Eppendorf, Germany
FreeStyle Lite Test Strips	PZN158931	Abbott Diabetes Care Inc., USA
FreeStyleLite Glucometer		Abbott Diabetes Care Inc., USA
Infinite M200	SN803004472	Tecan, Austria
Light Cycler® LC 480 (96 well)	SN20721	Roche, Switzerland
LightCycler® 480 MultiWell Plate 96	4729692001	Roche, Switzerland
Microvette CB300LH	16,443	Sarstedt, Germany
Mini Protean Tetra Cell	SN 552BR	BioRad, USA
MiniSpec md series		Bruker Corporation, USA
NanoQuant Plate		Tecan, Austria
Nitrocellulose Membrane	P/N 926-31092	Li-Cor Bioscience, USA
NUNC F96 transparent	1019-4761	Fisher Scientific, USA
Polytron PT 3100		Kinematica, Switzerland
POLYTRON PT-DA 3020/2		Kinematica, Switzerland
Power Lab 26T (LTS) and LabChart 6 software	ML4856	ADInstruments, Australia
Power Pac Basic		BioRad, USA
Sorvall Evolution RC	728211	Thermo Scientific, USA
SS34 fixed angle rotor		Thermo Scientific, USA
Stainless Steel Beads, 5 mm	69989	Quiagen, Germany
Stirrer Model 300 Control Box only	MAG007B	Rank Brothers, UK
Swinging buck rotor A-2-DWP	5804 740.009	Eppendorf, Germany
Swinging buck rotor A-4-44	5804 719.000	Eppendorf, Germany
Syringe 10 µl	701	Hamilton, Switzerland
Thermomixer compact		Eppendorf, Germany
Tissue Lyser II	85300	Quiagen, Germany
Trans-Blot SD Semi-Dry Transfer Cell		BioRad, USA
Waterbath Julabo F12-ED	9116612	Julabo, Germany
XF96 Flux Analyzer		Seahorse Bioscience, USA
XF96 FluxPak	102310-001	Seahorse Bioscience, USA
YSI Model 5794 high sensitivity membrane kit	5794	YSI incorporated (Vertrieb Kreienbaum)

2.1.1: Fatty acid composition in the experimental diets

Table 15: Fatty acid composition of the experimental control and high fat diet

	Control S5745-E702	High Fat S5745-E712
Source	Soy Oil	Soy Oil + Palm Oil
Total Fat wt %	5	5+20
Fatty Acid Composition [% of Total Fat]		
C14:0	0.6	0.9
C16:0	10.6	36.4
C16:1	0.6	0.5
C18:0	4.6	4.9
C18:1	25.8	35.9
C18:2	51.0	19.1
C18:3	6.3	1.8
C20:0	0.6	0.5
SFA	16.3	42.7
MUFA	26.3	36.4
PUFA	57.3	20.9
n6	51.0	19.1
n3	6.3	1.8
n3/n6	0.12	0.09
UI	147.3	80.0

*C-number-colon-number – chain length of fatty acid carbon
chain –colon – number of double bounds;
SFA – saturated fatty acids; MUFA – monounsaturated fatty
acids; PUFA – polyunsaturated fatty acids;
n6 – omega-6 fatty acids; n3 – omega-3 fatty acids;
UI – unsaturation index*

2.9.1: Protocol for measurement in the XF 96 flux analyzer:

Table 16: Protocol for two port measurement in XF 96 flux analyzer

Course	Action	Time [min]	Course	Action	Time [min]
1	Calibrate Probes	20	10	Mix	1
2	Mix	1.5	11	Inject Port A	
3	Wait	3	12	Mix	2
4	Mix	1.5	13	Measure	3
5	Wait	3	14	Mix	2
6	Mix	1.5	15	Inject Port D	
7	Measure	3	16	Mix	2
8	Mix	2	17	Measure	3
9	Measure	3			

2.14.3 Primer sequences

Table 17: Primer sequences for quantitative polymerase chain reaction (qPCR)

Gene	Gene Symbol	Primer forward	Primer reverse
3-hydroxyacyl-CoA DH	Hcdh	CGGTTCACGATAAATCCAGG	CCACCAGACAAGACCGATTT
3-ketoacyl-CoA thiolase	Acaa1	AGACCATTTCTGATGCCAC	GCTTCAAGGACACCACCC
Acyl-CoA DH medium chain	Acadm	GTTGAATCCATAGCCTCCGA	GCTAGTGGAGCACCAAGGAG
Acyl-CoA hydrolase	Acot13	TAATAAACTGGGCACGCTCC	TCCTGTGGTCTTGTTGGTCA
CPT1b	Cpt1b	GGCAACAGTTGCTTGCAACTACT	CAGGAAGCTTAGGCATGTACGTT
Trifunctional protein	Hadha	GATCCCTTCCTGTAGGCACA	ATGGTCTCCAAGGGCTTCTT

Ad: Results

3.1.1 Fat mass gain and lean mass gain during 9 week feeding

Table 18: Change in body composition upon 9 weeks of feeding

	Adolescent		Young Adult		Middle-Aged		Two-Way ANOVA
	Control	High Fat	Control	High Fat	Control	High Fat	
Lean Mass Gain [g]	2.2 ± 0.3	3.8 ± 0.6	0.6 ± 0.6	0.4 ± 0.3	-1.0 ± 1.1	-1.1 ± 1.4	*A, A x D*
Fat Mass Gain [g]	0.4 ± 0.2	4.9 ± 0.8	0.2 ± 0.3	9.1 ± 1.8	0.4 ± 0.8	13.9 ± 1.2	*A, D, A x D*

A - age effect, D - diet effect, A x D statistical interaction, n = 6 per experimental group

3.1.2 Area and incremental area under the curve

Table 19: Area under the curve (AUC) and incremental AUC (iAUC) for intraperitoneal glucose tolerance tests curves in Figure 10

		Adolescent		Young Adult		Middle-Aged		Two-Way ANOVA
		Control	High Fat	Control	High Fat	Control	High Fat	
AUC[1]	Baseline			1.0 ± 0.1	1.0 ± 0.1	0.9 ± 0.1	1.0 ± 0.1	*n.s.*
	1 week	1.1 ± 0.2	1.3 ± 0.2	1.0 ± 0.1	1.5 ± 0.2[#]	0.9 ± 0.1	1.4 ± 0.2[#]	*D*
	9 weeks	0.9 ± 0.2	1.3 ± 0.2[#]	1.1 ± 0.2	1.6 ± 0.3[#]	1.0 ± 0.2	1.6 ± 0.2[#]	*A, D*
iAUC[2]	Baseline			1.0 ± 0.5	0.8 ± 0.1	1.2 ± 0.4	1.9 ± 0.5	*A*
	1 week	1.4 ± 0.6	2.0 ± 1.2	0.8 ± 0.6	1.9 ± 0.8[#]	1.4 ± 1.1	3.2 ± 0.6[#]	*A, D*
	9 weeks	0.6 ± 0.2	1.4 ± 0.9	0.9 ± 0.5	2.6 ± 1.2[#]	1.6 ± 0.6	3.8 ± 1.0[#]	*A, D*
Two-Way ANOVA[3]	**AUC**	*D*		*D, T, D x T*		*D, T, D x T*		
	iAUC	*T*		*D, T, D x T*		*D, T, D x T*		

[1] relative to Young Adult Control at Baseline
[2] relative to Young Adult Control at Baseline
[3] repeated measurements
[#]significant difference in posthoc testing (Holm-Sidak) between control and high fat group in the respective age and time point

D – Diet effect
T – Time effect
A – Age effect
n.s. – not significant
x – significant interaction

3.2.1 Oxygen consumption data after 1.5 weeks and 9 weeks of high fat feeding

Table 20: Oxygen consumption in skeletal muscle mitochondria fueled with succinate in presence of rotenone

Oxygen Consumption [nmol O$_2$ x mg^{-1} x min^{-1}]		Adolescent		Young Adult		Two-Way ANOVA
		Control	High Fat	Control	High Fat	
1.5 weeks	- ADP	132 ± 49	137 ± 51	67 ± 10	58 ± 23	*A*
	+ ADP	322 ± 150	369 ± 132	241 ± 24	227 ± 68	*A*
9 weeks	- ADP	48 ± 13	50 ± 11	60 ± 10	70 ± 6	*A*
	+ ADP	176 ± 45	178 ± 38	214 ± 52	247 ± 31	*A*

A – age effect, n = 5 – 6 per group

3.2.2.3 Oxygen capacity in skeletal muscle mitochondria after high fat feeding for 9 weeks
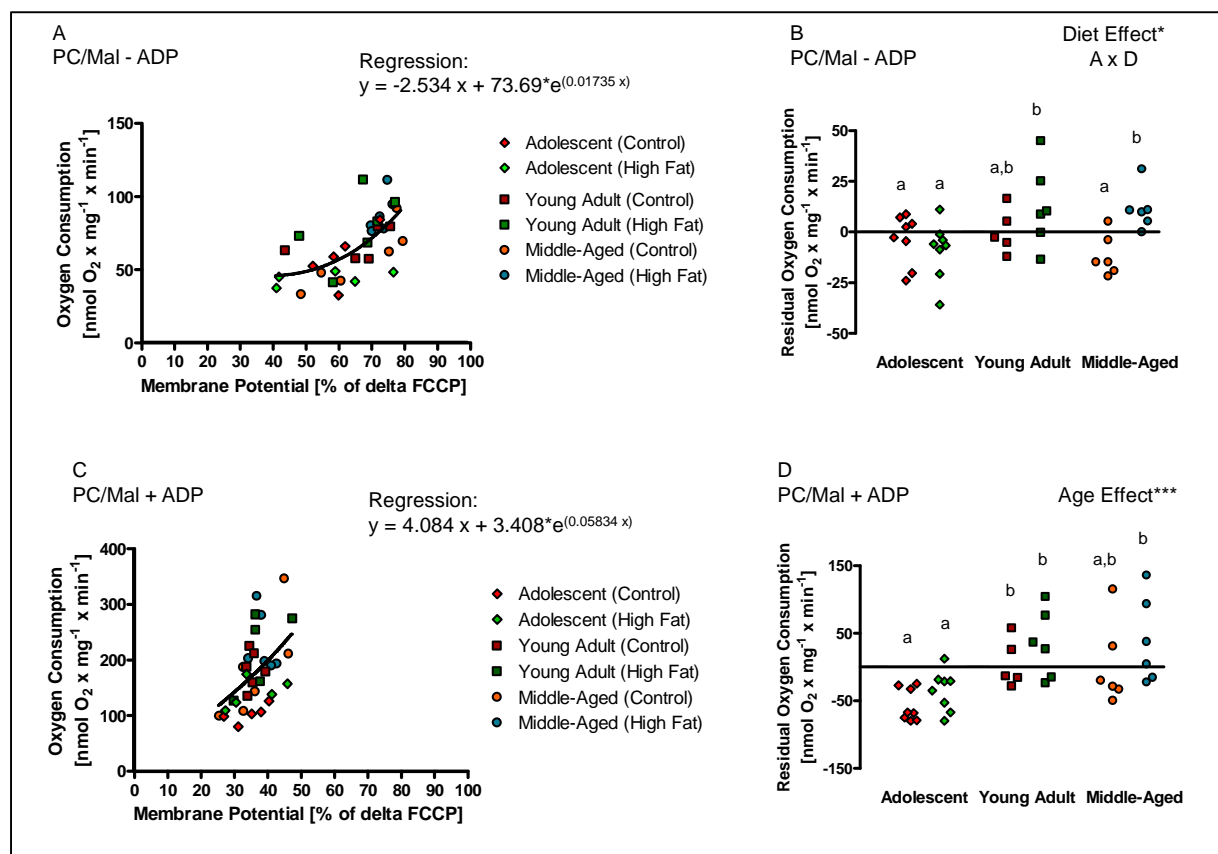
Figure 29: Correlation between fatty acid driven respiration and proton leak in skeletal muscle mitochondria isolated from adolescent, young adult and middle-aged mice fed a high fat or control diet for 9 weeks.

A) Leak respiration (- ADP) and C) phosphorylating respiration (+ ADP) plotted against the respective membrane potential with palmitoylcarnitine/malate (PC/Mal) as substrate including nonlinear regression analysis (Jastroch *et al.* 2012). B) and D) Residual oxygen consumption of skeletal muscle mitochondria of the respective age and diet groups. Two-Way ANOVA statistics are given with * p < 0.05, *** p < 0.001, A x D designates significant interaction of age and diet. Different letters indicate significant differences upon posthoc testing (Holm-Sidak)

Table 21: Respiratory chain complex activity in gastrocnemius muscle after 9 weeks of feeding

		Adolescent		Middle-Aged		Two-Way ANOVA
		Control	High Fat	Control	High Fat	
relative Enzyme Activity	C I	1.0 ± 0.0	0.9 ± 0.1	0.8 ± 0.1	0.7 ± 0.2	*A*
	C II	1.0 ± 0.1	0.9 ± 0.1	0.9 ± 0.1	0.8 ± 0.1	*A*
	C III	1.0 ± 0.1	0.9 ± 0.1	0.9 ± 0.1	1.0 ± 0.5	*n.s.*
	C IV	1.0 ± 0.2	1.0 ± 0.2	0.9 ± 0.3	0.8 ± 0.2	*n.s.*
	C V	1.0 ± 0.2	1.1 ± 0.3	0.9 ± 0.1	0.7 ± 0.2	*A*

C I – V – respiratory chain complex I - V
Data were normalized to CS activity and standardized to adolescent controls

3.2.2.4 Gene expression of enzymes involved in mitochondrial fatty acid breakdown

Table 22: Normalized mRNA abundance of genes involved in mitochondrial fat metabolism in skeletal muscle

	Adolescent		Young Adult		Middle-Aged		Two-Way ANOVA
	Control	High Fat	Control	High Fat	Control	High Fat	
CPT 1 β	1.0 ± 0.5	1.5 ± 0.7	1.9 ± 0.6	1.9 ± 1.0	1.0 ± 0.8	1.4 ± 1.4	*n.s.*
Acyl-CoA DH medium chain	1.0 ± 0.1	1.3 ± 0.4	1.0 ± 0.3	1.3 ± 0.6	1.1 ± 0.3	1.2 ± 0.4	*n.s.*
Trifunctional Protein	1.0 ± 0.1	1.5 ± 0.4	1.5 ± 0.3	1.7 ± 0.6	1.0 ± 0.2	1.2 ± 0.4	*A, D*
3-hydroxyacyl-CoA DH	1.0 ± 0.3	1.0 ± 0.3	0.9 ± 0.1	1.3 ± 0.6	0.6 ± 0.2	0.8 ± 0.2	*A*
3-ketoacyl-CoA thiolase	1.0 ± 0.3	1.2 ± 0.2	1.5 ± 0.4	1.2 ± 0.4	0.8 ± 0.1	0.8 ± 0.3	*A*
Acyl-CoA-Hydrolase	1.0 ± 0.2	1.0 ± 0.1	1.0 ± 0.3	0.9 ± 0.3	1.2 ± 0.4	1.0 ± 0.2	*n.s.*

Data were standardized to the Adolescent control group. A – age effect
D – diet effect, n.s. – not significant, n = 5 – 6 per group

3.2.2.5 Oxidative stress markers, antioxidative enzymes and glutathione biosynthesis in gastrocnemius muscle of adolescent and middle-aged mice after 9 weeks of high fat feeding

Table 23: Malondialdehyde (MDH) concentration and antioxidative enzymes activities in gastrocnemius muscle of adolescent and middle-aged mice after 9 weeks of feeding

		Adolescent		Middle-Aged		Two-Way ANOVA
		Control	High Fat	Control	High Fat	
MDA [nmol x mg^{-1}]		0.16 ± 0.09	0.21 ± 0.11	0.12 ± 0.11	0.17 ± 0.14	*n.s.*
Enzyme Activity [U x (g protein)$^{-1}$]	G6PDH	3.1 ± 1.1	2.6 ± 0.5	2.8 ± 1.1	2.1 ± 0.7	*A*
	SOD-Cu/Zn	4430 ± 307	5446 ± 1030	5271 ± 826	4974 ± 344	*A*
	SOD-Mn	5179 ± 633	6364 ± 1251	6158 ± 2671	5145 ± 572	*n.s.*
	Catalase	11 ± 2	10 ± 2	9 ± 3	11 ± 2	*n.s.*
	GS	174 ± 43	171 ± 38	147 ± 16	125 ± 30	*A*
	GCS	105 ± 15	91 ± 13	77 ± 13	80 ± 14	*A, D*

3.2.3: Characterization of skeletal muscle mitochondria after 26 weeks of high fat feeding

Table 24: Muscle mass and mitochondrial content after 26 weeks of high fat feeding

	Adolescent		Young Adult		Two-Way ANOVA
	Control	High Fat	Control	High Fat	
TA mass [mg]	48.9 ± 3.3	56.5 ± 9.0	51.9 ± 3.3	52.2 ± 4.8	*n.s.*
mtDNA TA[1]	1.0 ± 0.4	1.6 ± 0.6	1.0 ± 0.2	2.1 ± 2.5	*n.s.*
mt CS	1.4 ± 0.3	1.4 ± 0.2	1.7 ± 0.2	1.9 ± 0.1	*n.a.[2]*
rel mt CS[1]	1.0 ± 0.2	1.0 ± 0.1	1.0 ± 0.1	1.1 ± 0.1	*n.s.*

[1] *relative to mean of controls of the respective cohort*
[2] *due to different storage periods of mitochondrial protein, statistics were not attributable*
TA - tibialis anterior muscle, mt – mitochondrial,
CS – Citrate Synthase activity in [U x mg^{-1}], n.s. – not significant, n.a. – not analyzed

Table 25: Characteristics of bioenergetics with palmitoylcarnitine/malate as substrate in skeletal muscle mitochondria of adolescent and young adult mice fed a high fat or control diet for 26 weeks

		Juvenile		Young Adult		Two-Way ANOVA
		Control	High Fat	Control	High Fat	
Oxygen Consumption	- ADP	13.7 ± 9.1	14.5 ± 4.6	27 ± 15.5	61.3 ± 41.3	*n.a.[1]*
	+ ADP	37.5 ± 18.5	41.2 ± 7.7	86.9 ± 19.8	167.8 ± 51.3	*n.a.[1]*
relative Oxygen Consumption[2]	- ADP	1.0 ± 0.7	1.2 ± 0.5	1.0 ± 0.2	2.0 ± 0.6	*A, D, A x D*
	+ ADP	1.0 ± 0.5	1.1 ± 0.2	1.0 ± 0.2	2.0 ± 0.7	*A, D, A x D*
relative Membrane Potential	- ADP	1.0 ± 0.1	1.0 ± 0.1	1.0 ± 0.2	1.2 ± 0.04	*n.s.*
	+ ADP	1.0 ± 0.05	1.0 ± 0.1	1.0 ± 0.2	1.1 ± 0.2	*n.s.*
ROS Production Rate	- ADP	0.06 ± 0.02	0.06 ± 0.01	0.05 ± 0.02	0.05 ± 0.01	*n.s.*
	+ ADP	0.05 ± 0.03	0.06 ± 0.03	0.04 ± 0.01	0.06 ± 0.01	*n.s.*

[1]*different instruments for recording oxygen consumption were used,*
[2] *relative to mean value of age-matched control-fed mice*
Oxygen Consumption – [nmol O$_2$ x mg^{-1} x min^{-1}],
ROS production rate - [nmol H$_2$O$_2$ x mg^{-1} x min^{-1}]

3.3.2: Respiratory profile of liver mitochondria of three age groups after 9 weeks of high fat feeding using the complex II substrate succinate

Table 26: Mitochondrial performance for liver of dataset 2 measured with the Seahorse device for oxygen consumption (VO$_2$), Safranin O for membrane potential (Δψ) and ROS production rate (H$_2$O$_2$) in the presence of BSA, n = 5 -6

Succinate		Adolescent		Young Adult		Middle-Aged		Two-Way ANOVA
		Control	High Fat	Control	High Fat	Control	High Fat	
VO$_2$	- ADP	13.1 ± 5.1	14.6 ± 8.0	25.6 ± 8.3	21.4 ± 5.1	50.4 ± 16.4	57.8 ± 19.1	*A*
	+ ADP	45.2 ± 17.3	44.1 ± 16.8	64.1 ± 35.9	57.0 ± 10.4	127.5 ± 23.2	155.3 ± 46.0	*A*
Δψ	- ADP	46.2 ± 9.6	46.0 ± 1.4	58.5 ± 6.7	51.0 ± 6.2	68.9 ± 2.9	65.9 ± 4.2	*D*
	+ ADP	62.0 ± 6.3	56.7 ± 3.9	59.4 ± 12.5	56.9 ± 5.8	69 ± 7.6	67.8 ± 4.4	*A*
H$_2$O$_2$	- ADP	0.27 ± 0.03	0.29 ± 0.02	0.25 ± 0.04	0.27 ± 0.04	0.20 ± 0.04	0.28 ± 0.05	*A, D*
	+ ADP	0.25 ± 0.04	0.24 ± 0.05	0.23 ± 0.03	0.23 ± 0.04	0.19 ± 0.04	0.21 ± 0.03	*A*

VO$_2$ in [nmol O$_2$ x mg^{-1} x min^{-1}], Δψ in [% of Δ FCCP], H$_2$O$_2$ in [nmol H$_2$O$_2$ x mg^{-1} x min^{-1}]
A – age effect, D – diet effect

3.3.3 Regression analysis of acylcarnitine output of hepatic mitochondria and oxygen consumption
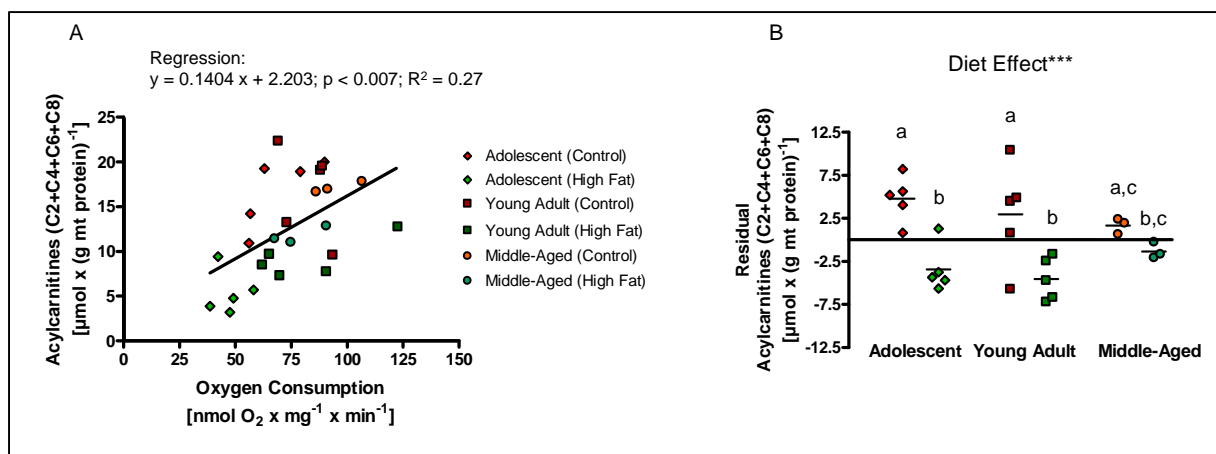
Figure 30: Correlation of acylcarnitine release to oxygen consumption in hepatic mitochondria of mice fed high fat and control diet for 9 weeks

A) The sum of acylcarnitines with chain lengths of 2, 4, 6 and 8 carbon atoms was plotted against oxygen consumption including regression analysis. B) Residual acylcarnitine release was statistically tested by Two Way ANOVA with *** p < 0.001. Significant posthoc testing (Holm-Sidak) is indicated by different letters. n = 3 – 5 per group

3.4 Proteome analysis in hepatic mitochondria-enriched protein suspensions

Table 27: Complete list of proteins significantly changed by high fat diet

Uniprot Accession	Gene Symbol	Gene Name	FC HF/C	-log$_{10}$ (p)	Localization	Cluster
Q3U621	RAB10	RAB10, member RAS oncogene family	9.8	1.9	other	12
Q3UDJ2	SGPL1	sphingosine-1-phosphate lyase 1	4.9	1.3	ER	9
Q3TK73	RPL7	ribosomal protein L7	4.9	1.3	R, Ct	3
P15105	GLUL	glutamate-ammonia ligase	4.1	3.7	M, ER, V	12
Q9CWE0	MTFR1L	mitochondrial fission regulator 1-like	3.9	1.4	M	9
Q3TX45	APOE	apolipoprotein E	3.7	1.3	other	9
A2AWN8	YTHDF1	YTH domain family, member 1	3.3	2.1	unknown	3
D3YTQ9	RPS15	ribosomal protein S15	3.3	2.5	R, Ct	12
Q3TI98	FARSB	phenylalanyl-tRNA synthetase, beta subunit	2.9	1.6	other	12
Q3TA21	CYP7B1	cytochrome P450, family 7, subfamily B, polypeptide 1	2.7	1.8	ER, V	10
B9EHY2	ZMPSTE24	zinc metallopeptidase STE24	2.6	1.5	ER	1
Q64435	UGT1A6	UDP glucuronosyltransferase 1 family, polypeptide A6	2.6	1.7	ER	9
Q3TMR2	Ces2a	carboxylesterase 2A	2.4	1.4	V	12
Q9D0L4	ADCK1	aarF domain containing kinase 1	2.3	2.6	M	10
Q3UKH3	ACAA2	acetyl-CoA acyltransferase 2	2.3	1.7	M	10
P16015	CA3	carbonic anhydrase III, muscle specific	2.2	1.4	other	8
A2ALP9	BHMT-ps1	betaine--homocysteine S-methyltransferase, pseudogene	2.2	1.7	other	3
D3Z5R8	RPS19	ribosomal protein S19	2.2	1.7	R, Ct	12
Q3UBI6	RPL7	ribosomal protein L7	2.2	1.9	R, Ct	2
Q9DCX8	IYD	iodotyrosine deiodinase	2.1	3.1	V	9
Q3UZ06	Sec22b	SEC22 vesicle trafficking protein homolog B (S. cerevisiae)	2.1	1.4	ER	8
B1ATI0	ALDH3A2	aldehyde dehydrogenase 3 family, member A2	2.1	1.4	M, ER, V, Ct	11
Q3TJI8	HSD11B1	hydroxysteroid (11-beta) dehydrogenase 1	2.0	2.1	ER, V	3
Q8C3X8	LMF2	lipase maturation factor 2	2.0	2.1	ER	1
A2RS53	TMED2	transmembrane emp24 protein transport domain containing	2.0	2.6	V	12
A2RS96	TMED5	transmembrane emp24 protein transport domain containing 5	2.0	1.6	ER	1
Q8CGG8	APOB	apolipoprotein B (including Ag(x) antigen)	1.9	2.2	ER, V	11
O35490	BHMT	betaine--homocysteine S-methyltransferase	1.9	2.7	other	10
Q922Q8	LRRC59	leucine rich repeat containing 59	1.9	2.5	M, ER	10
Q3TXE5	CANX	calnexin	1.9	2.3	ER, R	11
A2AQ17	NDUFAF1	NADH dehydrogenase (ubiquinone) complex I, assembly factor 1	1.9	1.7	M	9
Q3U026	MOGS	mannosyl-oligosaccharide glucosidase	1.9	2.0	ER	3
Q3TY87	FAH	fumarylacetoacetate hydrolase (fumarylacetoacetase)	1.9	2.1	unknown	1
Q8R0N6-2	ADHFE1	alcohol dehydrogenase, iron containing, 1	1.9	1.9	M	10
D3Z7B4	RPL15-ps2	ribosomal protein L15, pseudogene	1.8	1.9	other	12
D3Z0E6	BPNT1	3'(2'), 5'-bisphosphate nucleotidase 1	1.8	1.4	Ct	10
Q8VCW9	Cyp2a12	cytochrome P450, family 2, subfamily a, polypeptide 12	1.8	2.0	ER, V	7

Table 27 continued

Uniprot Accession	Gene Symbol	Gene Name	FC HF/C	-log$_{10}$ (p)	Localization	Cluster
Q5M9K7	RPS10	RPS10-NUDT3 readthrough	1.8	1.8	R, Ct	12
D3YZH3	RPL9-ps7	ribosomal protein L9, pseudogene	1.8	2.3	other	1
Q921I1	TF	transferrin	1.8	2.2	other	8
Q8R0Y9	SOAT2	sterol O-acyltransferase 2	1.8	1.4	ER, V	5
Q14DH7	ACSS3	acyl-CoA synthetase short-chain family member 3	1.7	2.3	M	9
Q8C1Q6	UPF0640	small integral membrane protein 4 (Homo sapiens, rattus norwegicus)	1.7	1.5	M	11
Q3TK12	Rps17	ribosomal protein S17	1.7	1.4	R, Ct	3
Q8BN32	PABPC1	poly(A) binding protein, cytoplasmic 1	1.7	2.2	other	3
Q05BJ1	HGD	homogentisate 1,2-dioxygenase	1.7	1.7	unknown	10
Q9D8V0-3	HM13	histocompatibility (minor) 13	1.7	1.6	ER	9
D3YX47	RPL21-ps6	ribosomal protein L21, pseudogene	1.7	1.7	R	7
Q5FW60	Mup20	major urinary protein 1	1.7	1.5	other	1
Q8BSE0	RMDN2	regulator of microtubule dynamics 2	1.7	3.0	M	8
Q91X34	BAAT	bile acid CoA: amino acid N-acyltransferase (glycine N-choloyltransferase)	1.7	2.8	P, Ct	11
D3YZ47	Gm5879	predicted gene 5879	1.7	1.4	other	10
Q3UNR3	SLC27A2	solute carrier family 27 (fatty acid transporter), member 2	1.7	2.5	M, ER, P, V	12
D3Z7R0	BCKDK	branched chain ketoacid dehydrogenase kinase	1.7	2.1	M	11
B6VGH4	CYP1A2	cytochrome P450, family 1, subfamily A, polypeptide 2	1.6	2.5	ER, V	7
Q8BJL4	LMAN2	lectin, mannose-binding 2	1.6	1.5	other	1
D3YVH7	PA2G4	proliferation-associated 2G4, 38kDa	1.6	1.5	other	3
Q8JZZ1	Gulo	gulonolactone (L-) oxidase	1.6	1.5	ER	10
Q63880-2	CES3	carboxylesterase 3	1.6	2.5	ER	1
Q3U4Z7	HDLBP	high density lipoprotein binding protein	1.6	2.7	other	10
Q9JKY7	Cyp2d22	cytochrome P450, family 2, subfamily d, polypeptide 22	1.6	1.8	M, V	7
A2A9W4	MRPS7	mitochondrial ribosomal protein S7	1.6	1.7	M, R	9
Q5RKP4	RPN1	ribophorin I	1.6	1.7	ER, V	3
Q5BLJ7	RPS13	ribosomal protein S13	1.6	2.2	R	5
Q9DBL7	COASY	CoA synthase	1.6	1.4	other	8
B2MWM9	CALR	calreticulin	1.6	1.8	ER, V, Ct	12
P51658	HSD17B2	hydroxysteroid (17-beta) dehydrogenase 2	1.5	1.9	V	3
Q497N1	RPS26	ribosomal protein S26	1.5	3.2	R, Ct	7
B1AY76	ERP44	endoplasmic reticulum protein 44	1.5	1.4	ER	1
Q0PD65	RAB2A	RAB2A, member RAS oncogene family	1.5	1.5	ER	1
Q62087	PON3	paraoxonase 3	1.5	1.5	V	8
Q91X83	MAT1A	methionine adenosyltransferase I, alpha	1.5	1.7	unknown	11
D3YXG3	Gm4963	predicted gene 4963	1.5	2.9	unknown	7
A2AC46	ABCB7	ATP-binding cassette, sub-family B (MDR/TAP), member 7	1.5	1.7	M	11
Q8R086	SUOX	sulfite oxidase	1.5	2.2	M, Ct	8
Q58EW0	RPL18	ribosomal protein L18	1.5	2.4	R, Ct	3
Q3TG75	OAT	ornithine aminotransferase	1.5	1.5	M	9

Table 27 continued

Uniprot Accession	Gene Symbol	Gene Name	FC HF/C	-log$_{10}$ (p)	Localization	Cluster
A2AIW8	PMPCA	peptidase (mitochondrial processing) alpha	1.5	1.7	M	11
Q6P3A8	BCKDHB	branched chain keto acid dehydrogenase E1, beta polypeptide	1.5	2.7	M	7
Q6GQT9	NOMO1	NODAL modulator 1	1.5	1.9	other	5
Q3UEG6	AGXT2	alanine--glyoxylate aminotransferase 2	1.5	1.8	M	8
Q8CEY5	MTCH1	mitochondrial carrier 1	1.5	1.6	M	10
Q3UC51	DDOST	dolichyl-diphosphooligosaccharide--protein glycosyltransferase subunit (non-catalytic)	1.4	2.4	ER, V	1
D3Z722	RPS19	ribosomal protein S19	1.4	2.3	R, Ct	3
Q9CYN2	SPCS2	signal peptidase complex subunit 2 homolog (S. cerevisiae)	1.4	1.5	ER	11
Q0PD50	RAB8A	RAB8A, member RAS oncogene family	1.4	1.8	other	5
B2CY77	RPSA	ribosomal protein SA	1.4	1.8	R, Ct	12
D3Z1D6	Gm10335= Rpl23a-ps	Ribosomal protein L23a, pseudogene	1.4	1.5	unknown	3
Q99MR8	MCCC1	methylcrotonoyl-CoA carboxylase 1 (alpha)	1.4	3.4	M	11
Q8BH86	C14orf159	chromosome 14 open reading frame 159	1.4	2.2	M	8
A2AMV3	AKR7A2	aldo-keto reductase family 7, member A2 (aflatoxin aldehyde reductase)	1.4	2.0	M	8
Q3TRW3	SND1	staphylococcal nuclease and tudor domain containing 1	1.4	2.9	M	7
Q544Z9	CYB5A	cytochrome b5 type A (microsomal)	1.4	1.4	M	5
B2RY90	ISOC2	isochorismatase domain containing 2	1.4	2.1	M	11
Q3UDS4	SQRDL	sulfide quinone reductase-like (yeast)	1.4	2.4	M	1
Q5EBQ7	MSRA	methionine sulfoxide reductase A	1.4	1.6	M	12
Q3U900	RPN1	ribophorin I	1.4	1.4	ER, V	1
A2A547	RPL19	ribosomal protein L19	1.4	2.0	R, Ct	12
P27773	PDIA3	protein disulfide isomerase family A, member 3	1.4	2.7	ER	1
Q3UJU9	RMDN3	regulator of microtubule dynamics 3	1.4	3.3	M	11
Q9JJI8	RPL38	ribosomal protein L38	1.4	2.1	R, Ct	9
Q8CIM7	Cyp2d26	cytochrome P450, family 2, subfamily d, polypeptide 26	1.4	2.4	ER, V	5
A2ACG7	RPN2	ribophorin II	1.4	1.5	ER, V	7
Q8CFJ7	SLC25A45	solute carrier family 25, member 45	1.4	1.5	M	11
P26443	GLUD1	glutamate dehydrogenase 1	1.4	3.0	M	11
A2A8C9	DNAJC11	DnaJ (Hsp40) homolog, subfamily C, member 11	1.4	1.5	M	8
Q8C7H1	MMAA	methylmalonic aciduria (cobalamin deficiency) cblA type	1.4	2.8	M	7
Q3TF72	P4HB	prolyl 4-hydroxylase, beta polypeptide	1.3	4.3	ER, V	1
D3Z2T7	Gm10247= Rpl35a-ps	ribobosomal protein L35a, pseudogene	1.3	1.8	other	12
Q3UCC6	SUCLA2	succinate-CoA ligase, ADP-forming, beta subunit	1.3	1.5	M	2
Q9CWI9	RPS23	ribosomal protein S23	1.3	1.6	R, Ct	5
Q6P8N6	GCDH	glutaryl-CoA dehydrogenase	1.3	1.5	M	11
Q8BH80	VAPB	VAMP (vesicle-associated membrane protein)-associated protein B and C	1.3	2.1	ER	10
Q80TX7	OPA1	optic atrophy 1 (autosomal dominant)	1.3	1.3	M	11
Q9Z2I0	LETM1	leucine zipper-EF-hand containing transmembrane protein 1	1.3	1.7	M	8

Table 27 continued

Uniprot Accession	Gene Symbol	Gene Name	FC HF/C	-log$_{10}$ (p)	Localization	Cluster
Q5EBH4	DMGDH	dimethylglycine dehydrogenase	1.3	2.7	M	8
Q3TT79	PDIA4	protein disulfide isomerase family A, member 4	1.3	1.6	ER	7
Q3UCL7	RPS3	ribosomal protein S3	1.3	2.3	R, Ct	7
Q3TVJ8	SSR4	signal sequence receptor, delta	1.3	1.6	ER	1
A2AUF6	HSPA5	heat shock 70kDa protein 5 (glucose-regulated protein, 78kDa)	1.3	2.2	ER	1
Q8K370	ACAD10	acyl-CoA dehydrogenase family, member 10	1.3	2.1	M	8
Q91VS7	MGST1	microsomal glutathione S-transferase 1	1.3	2.2	M, ER, P, V	3
Q8JZU2	SLC25A1	solute carrier family 25 (mitochondrial carrier; citrate transporter), member 1	1.3	1.6	M	5
Q3U832	CCNT2	cyclin T2	1.3	1.4	other	9
Q3TG02	STT3A	STT3A, subunit of the oligosaccharyltransferase complex (catalytic)	1.3	1.4	ER	12
Q3UWB1	Ces1f	carboxylesterase 1F	1.3	2.2	Ct	2
C6EQH3	SUCLG2	succinate-CoA ligase, GDP-forming, beta subunit	1.3	1.7	M	3
B1ATZ4	SLC25A10	solute carrier family 25 (mitochondrial carrier; dicarboxylate transporter), member 10	1.2	1.4	M	2
Q8VCW8	ACSF2	acyl-CoA synthetase family member 2	1.2	2.0	M	5
Q9D172	C21orf33	chromosome 21 open reading frame 33	1.2	1.7	M	1
Q3U3J1	BCKDHA	branched chain keto acid dehydrogenase E1, alpha polypeptide	1.2	1.6	M	5
A2A6S3	FDXR	ferredoxin reductase	1.2	1.4	M	1
Q8R1A8	OTC	ornithine carbamoyltransferase	1.2	3.8	M	11
P14115	RPL27A	ribosomal protein L27a	1.2	1.3	R, Ct	7
Q91W85	ACADS	acyl-CoA dehydrogenase, C-2 to C-3 short chain	1.2	1.7	M	1
Q8QZT1	ACAT1	acetyl-CoA acetyltransferase 1	1.2	1.5	M	8
Q3TDN8	BPHL	biphenyl hydrolase-like (serine hydrolase)	1.2	2.7	M	11
Q5M9J2	HINT2	histidine triad nucleotide binding protein 2	1.2	1.3	M	8
Q3UNX5-2	ACSM3	acyl-CoA synthetase medium-chain family member 3	1.2	2.0	M	11
P05202	GOT2	glutamic-oxaloacetic transaminase 2, mitochondrial (aspartate aminotransferase 2)	1.1	1.5	M	8
Q8C140	SLC25A13	solute carrier family 25 (aspartate/glutamate carrier), member 13	1.1	2.3	M	8
Q3UGC8	PCCA	propionyl CoA carboxylase, alpha polypeptide	1.1	1.9	M	1
Q8BMS1	HADHA	hydroxyacyl-CoA dehydrogenase/3-ketoacyl-CoA thiolase/enoyl-CoA hydratase (trifunctional protein), alpha subunit	0.9	1.4	M	6
Q56A15	Cytcs	cytochrome c, somatic	0.9	1.9	M	4
Q8C196	CPS1	carbamoyl-phosphate synthase 1, mitochondrial	0.9	2.4	M	4
Q3UEQ9	AASS	aminoadipate-semialdehyde synthase	0.8	1.6	M	4
A2A430	LAMP2	lysosomal-associated membrane protein 2	0.8	2.0	L	4
Q8VCI0	PLBD1	phospholipase B domain containing 1	0.8	1.4	L	4
Q3UEN9	AGXT	alanine-glyoxylate aminotransferase	0.8	2.3	M, P	4
Q3UBR4	CTSS	cathepsin S	0.8	1.3	L	4

Table 27 continued

Uniprot Accession	Gene Symbol	Gene Name	FC HF/C	-log$_{10}$ (p)	Localization	Cluster
P52503	NDUFS6	NADH dehydrogenase (ubiquinone) Fe-S protein 6, 13kDa (NADH-coenzyme Q reductase)	0.8	1.9	M	4
A2AJX2	NDUFAF4	NADH dehydrogenase (ubiquinone) complex I, assembly factor 4	0.7	1.7	M	6
A2AKK5-2	Acnat1	acyl-coenzyme A amino acid N-acyltransferase 1	0.7	1.5	P	6
Q543J0	Uox	urate oxidase	0.7	2.2	M, P	4
Q9DBN5	LONP2	lon peptidase 2, peroxisomal	0.7	1.6	P	6
A2AHS8	MRPS5	mitochondrial ribosomal protein S5	0.7	1.6	M, R	4
Q3U6T2	NAGA	N-acetylgalactosaminidase, alpha-	0.7	1.7	L	4
Q3UEE8	HAO1	hydroxyacid oxidase (glycolate oxidase) 1	0.7	1.4	P	4
Q3UC49	FECH	ferrochelatase	0.7	1.3	M	4
Q9CZ08	GCAT	glycine C-acetyltransferase	0.7	3.8	M	4
Q3U0K4	PAFAH2	platelet-activating factor acetylhydrolase 2, 40kDa	0.7	1.4	other	6
Q8CC47	GALNS	galactosamine (N-acetyl)-6-sulfate sulfatase	0.7	1.4	L	4
Q3TXQ6	CAT	catalase	0.7	3.4	M, ER, P, L, Ct	6
B2RUD7	PSAP	prosaposin	0.7	2.4	M, L	4
Q3UCD6	CTSH	cathepsin H	0.7	3.6	L, Ct	4
Q9D2D1	CTSA	cathepsin A	0.7	3.8	M, L	4
Q9DCM0	ETHE1	ethylmalonic encephalopathy 1	0.7	4.2	M	4
Q8VCB0	ACOX2	acyl-CoA oxidase 2, branched chain	0.7	4.4	P	4
Q9CRB3	1190003J15 Rik	RIKEN cDNA 1190003J15 gene	0.7	1.5	M, P	4
Q9WVJ3-2	CPQ	carboxypeptidase Q	0.7	1.7	unknown	4
P08228	SOD1	superoxide dismutase 1, soluble	0.6	2.0	M, P, Ct	4
D3Z220	CTSC	cathepsin C	0.6	1.3	ER, L	4
Q3TC17	CTSB	cathepsin B	0.6	4.7	M, L	4
A2RSC2	ACOT12	acyl-CoA thioesterase 12	0.6	1.6	Ct	6
Q921H9	SELRC1	Sel1 repeat containing 1	0.6	1.3	unknown	6
P51175	PPOX	protoporphyrinogen oxidase	0.6	1.4	M	4
A2AEG2	OFD1	oral-facial-digital syndrome 1	0.6	2.0	other	6
Q62452	UGT1A9	UDP glucuronosyltransferase 1 family, polypeptide A8	0.6	1.6	ER, V	4
Q9CQ06	MRPL24	mitochondrial ribosomal protein L24	0.6	1.5	M, R	4
Q8R082	DPP7	dipeptidyl-peptidase 7	0.6	1.5	L, Ct	4
Q8K2I4	MANBA	mannosidase, beta A, lysosomal	0.6	1.9	L	4
Q9DC50	CROT	carnitine O-octanoyltransferase	0.5	3.3	M, P	6
P97930	DTYMK	deoxythymidylate kinase (thymidylate kinase)	0.5	1.6	M	4
Q9D625	SCPEP1	serine carboxypeptidase 1	0.5	3.8	Ct	4
Q4FK74	ATP5D	ATP synthase, H+ transporting, mitochondrial F1 complex, delta subunit	0.5	1.5	M	4
Q8R0N6	ADHFE1	alcohol dehydrogenase, iron containing, 1	0.5	1.4	M	4
A2APM1	CD44	CD44 molecule (Indian blood group)	0.5	1.8	other	4
Q8BGH2	SAMM50	sorting and assembly machinery component 50 homolog (S. cerevisiae)	0.5	3.0	M	6

Table 27 continued

Uniprot Accession	Gene Symbol	Gene Name	FC HF/C	-$\log_{10}$ (p)	Localization	Cluster
Q8R1G2	CMBL	carboxymethylenebutenolidase homolog (Pseudomonas)	0.5	2.2	other	6
Q3UGL8	NUDT12	nudix (nucleoside diphosphate linked moiety X)-type motif 12	0.5	1.3	P	6
Q9QYF1	RDH11	retinol dehydrogenase 11 (all-trans/9-cis/11-cis)	0.5	1.3	ER	6
A1A4A7	PGAM5	phosphoglycerate mutase family member 5	0.5	1.6	M	6
O88668	CREG1	cellular repressor of E1A-stimulated genes 1	0.5	3.7	other	6
O88833	CYP4A10	cytochrome P450, family 4, subfamily A, polypeptide 11	0.5	2.0	ER	6
Q547C4	SCD	stearoyl-CoA desaturase (delta-9-desaturase)	0.4	1.4	ER	6
Q3TXQ4	NPC2	Niemann-Pick disease, type C2	0.4	7.8	L	4
O35728	Cyp4a14	cytochrome P450, family 4, subfamily a, polypeptide 14	0.4	2.2	ER, V	6
Q7TNZ4	GPLD1	glycosylphosphatidylinositol specific phospholipase D1	0.4	1.4	V	6
Q9DBM2	EHHADH	enoyl-CoA, hydratase/3-hydroxyacyl CoA dehydrogenase	0.4	3.7	M, P	6
Q3TND6	MAN2B2	mannosidase, alpha, class 2B, member 2	0.3	2.1	L	6
A2ALL2	MINOS1	mitochondrial inner membrane organizing system 1	0.3	1.8	M	4
Q3T9E5	NCSTN	nicastrin	0.3	1.4	ER, L	4
Q3TLH6	FABP5	fatty acid binding protein 5 (psoriasis-associated)	0.2	5.3	other	4
D3YU64	Fabp5l2	fatty acid binding protein 5 like2, pseudogene	0.1	1.6	unknown	4
A2AS95	CELA2A	chymotrypsin-like elastase family, member 2A	0.1	1.6	other	4
Q4VBW6	AMY2A	amylase, alpha 2A (pancreatic)	0.04	3.9	other	4

FC – fold change; HF – high fat; C – control; Localization: M - mitochondria, ER - endoplasmic reticulum, P - peroxisome, R - ribosome, L - lysosome, V - vesicle, Ct – cytosol
"Cluster" refers to the age-related expression pattern graphed in Figure 25 B

Table 28: Alignment of "putative uncharacterized" entries with respective validated entry

Gene Symbol	Identified "putative uncharacterized" Protein [Uniprot Accession]	Reference Protein [Uniprot Accession]	Clustal Omega[1] alignment sequence identity [%]
RPL7	Q3TK73	P14148	99.6
RPS15	D3YTQ9	P62843	81.4
RPS19	D3Z5R8	Q9CZX8	76.8
PABPC1	Q8BN32	P29341	99.8
PA2G4	D3YVH7	P50580	70
STT3A	Q3TG02	P46978	99.9
SSR4	Q3TVJ8	Q62186	100
VAPB	Q8BH80	Q9QY76	99.6
P4HB	Q3TF72	P09103	99.8
CANX	Q3TXE5	P35564	99.8
CES1f	Q3UWB1	Q91WU0	99.7
NPC2	Q3TXQ4	Q9Z0J0	99.3
SEC22B	Q3UZ06	O08547	75.8
SCD	Q547C4	P13516	100
RAB10	Q3U621	P61027	99.5
SGPL1	Q3UDJ2	Q8R0X7	99.8
NAGA	Q3U6T2	Q9QWR8	99.8
GALNS	Q8CC47	Q571E4	84.6
CTSC	D3Z220	P97821	54.7
NCSTN	Q3T9E5	P57716	99.7
CTSB	Q3TC17	P10605	99.4
CTSS	Q3UBR4	O70370	95.9
CTSA	Q9D2D1	P16675	99.8
ACAA2	Q3UKH3	Q8BWT1	99.7
SLC27A2	Q3UNR3	O35488	98.7
NDUFAF4	A2AJX2	Q9D1H6	100
CES2A	Q3TMR2	Q8QZR3	100
MOGS	Q3U026	Q80UM7	99.9
DDOST	Q3UC51	O54734	99.8
APOB	Q8CGG8	E9Q414	100
APOE	Q3TX45	P08226	99.7

[1](Sievers *et al.* 2011)

Table 29: Pathways indicated by Genomatix (GePS) or Ingenuity (IPA) with respect of mitochondrial proteins

Uniprot ID	Gene Symbol	FC	Pathway (IPA and GePS)
Q8R1A8	Otc	1.2	urea cycle
Q8C196	Cps1	0.9	urea cycle
D3Z7R0	Bckdk	1.7	catabolism of brached chain amino acids
Q6P3A8	Bckdhb	1.5	catabolism of brached chain amino acids
Q3U3J1	Bckdha	1.2	catabolism of brached chain amino acids
Q3UC49	Fech	0.7	heme biosynthetic process
P51175	Ppox	0.6	heme biosynthetic process
Q3TXQ6	Cat	0.7	Superoxide detoxification
P08228	Sod1	0.6	Superoxide detoxification

Acknowledgements

There are a considerable number of persons, without the support and consideration of which this work would have been impossible. Beyond all, my thanks go to Prof. Dr. Martin Klingenspor for the opportunity to do my Dissertation in his lab. During the development of the project, Prof. Klingenspor was always well aware of the progress and considered all possible directions for supporting the thesis. I always appreciated his advice and supervision.

Further I thank Prof. Dr. Hannelore Daniel for the examination of my thesis. She also contributed during the project meetings and provided resources for cooperation. Here, I would like to say thank you to Alexander Haag for sample processing and to Dr. Kerstin Geillinger for providing advice and antibodies.

I am obliged to my cooperation partners, especially at the Chair of Proteomics and Bioanalytics. Many thanks go to Fiona Pachl for introducing me to the proteomic analysis, to Amin Gholami for explaining the statistics and last but not least Prof. Dr. Bernhard Küster, who agreed to supervise the examination committee for the approval of this thesis.

The cooperation with the Mitoxis® platform provided me a valuable contribution. Furthermore, my thanks go to Dr. Teresa Valencak at the VetMed Vienna and Dr. Michaela Aichler at the Pathology Unit at the Helmholtz Center Munich for the comfortable cooperation.

I send many thanks to all my colleagues for the great time in the lab. Special thanks are attributed to Drs. Tobias Fromme and Florian Bolze for proof reading my thesis, and to Anika Zimmermann and Sabine Mocek, because they always helped me out, when time and advice was short. My office mates Theresa Schöttl and Christoph Hoffmann made my days by extensively discussing work and virtually all subjects that mattered. Thank you!

Finally I am grateful to my parents for their never-ending support and to Stefan, who never complained about my working hours, especially during the last months. I deeply appreciated that!

Eidesstattliche Erklärung

Ich erkläre an Eides statt, dass ich die bei der Fakultät Wissenschaftszentrum Weihenstephan für Ernährung, Landnutzung und Umwelt (promotionsführenden Einrichtung)

der TUM zur Promotionsprüfung vorgelegte Arbeit mit dem Titel:

Diet induced obesity differentially affects mitochondrial function in skeletal muscle and liver of C57BL/6J mice

am Lehrstuhl für Molekulare Ernährungsmedizin unter der Anleitung und Betreuung durch Prof. Dr. Martin Klingenspor ohne sonstige Hilfe erstellt und bei der Abfassung nur die gemäß § 6 Abs. 6 und 7 Satz 2 angegebenen Hilfsmittel benutzt habe.

Ich habe keine Organisation eingeschaltet, die gegen Entgelt Betreuerinnen und Betreuer für die Anfertigung von Dissertationen sucht, oder die mir obliegenden Pflichten hinsichtlich der Prüfungsleistungen für mich ganz oder teilweise erledigt.

Ich habe die Dissertation in dieser oder ähnlicher Form in keinem anderen Prüfungsverfahren als Prüfungsleistung vorgelegt.

Ich habe den angestrebten Doktorgrad noch nicht erworben und bin nicht in einem früheren Promotionsverfahren für den angestrebten Doktorgrad endgültig gescheitert.

Die öffentlich zugängliche Promotionsordnung der TUM ist mir bekannt, insbesondere habe ich die Bedeutung von § 28 (Nichtigkeit der Promotion) und § 29 (Entzug des Doktorgrades) zur Kenntnis genommen. Ich bin mir der Konsequenzen einer falschen Eidesstattlichen Erklärung bewusst.

Mit der Aufnahme meiner personenbezogenen Daten in die Alumni-Datei bei der TUM bin ich einverstanden

München, den ....

Unterschrift

Curriculum Vitae

Promotion und Studium

Seit 11/2009	**Promotion** an der Technischen Universität München Lehrstuhl für Molekulare Ernährungsmedizin *von 11/2009 – 05/2013:* Förderung durch das Bundesministerium für Bildung und Forschung über Mittel, die dem Deutschen Zentrum für Diabetesforschung e.V. zur Verfügung gestellt wurden.
10/2007 – 11/2009	**Studium der Ernährungswissenschaft** an der Technischen Universität München *Master of Science*, Abschluss gut (1,7)
10/2004 – 07/2007	**Studium der Ernährungswissenschaft** an der Technischen Universität München *Bachelor of Science*, Abschluss sehr gut (1,4)

Schulbildung

09/1995 – 07/2004	König-Karlmann-Gymnasium, Altötting *Abitur* (Note 1,2)

Praktika

09/2008 – 10/2008	Deutsches Krebsforschungs-Zentrum (DKFZ), Heidelberg, Epigenomik und Krebsrisikofaktoren, Abt Chemoprävention • Projekt: Hemmung der Proteasom-Aktivität durch Pflanzenstoffe • Methoden: Sterilarbeiten in der Zellkultur, Fluorometrie
11/2007 – 04/2008	Medical Research Council-Human Nutrition Research (MRC-HNR), Cambridge, England Section Micronutrient Status Research • Projekt: Löslichkeit von Mikronährstoffen *in vitro* • Methoden: ICP-OES, Teilchengrößenbestimmung • Arbeiten nach GLP Standards • Stipendium: Erasmus Studierendenmobilität Praktikum
09/2006 – 10/2006	Else-Kröner-Fresenius Zentrum für Ernährungsmedizin des Krankenhauses Rechts der Isar (EKFZ), München
08/2006 – 09/2006	Landesamt für Gesundheit und Lebensmittelsicherheit (LGL), Oberschleißheim: Mykotoxinlabor

Posterbeiträge zu Konferenzen

K. Haas, F. Pachl, B. Küster, M. Klingenspor (2013): A proteomic approach to detect regulatory networks in high fat induced fatty liver, *Book of Abstracts 10th NuGOweek*, Wageningen Academic Publishers, The Netherlands, 45

K. Haas, M. Aichler, M. Conti, S. Loric, A. Walch, H. Daniel, M. Klingenspor (2012): High fat diet impairs glucose tolerance but not mitochondrial function in skeletal muscle of C57BL/6J mice, *Diabetologia* **55 Suppl 1**, S273

K. Haas, M. Klingenspor (2012): Age and high fat diet associated changes in mitochondrial ROS production in the liver, *BBA Bioenergetics* **1817**, S99

K. Haas, H. Daniel, M. Klingenspor (2011): Glucose tolerance and mitochondrial ROS production after short-term high fat feeding in mice, *Proceedings of the German Nutrition Society* **15**, 98

Beitrag zu einer wissenschaftlichen Veröffentlichung

G. Grünz, K. Haas, S. Soukup, M. Klingenspor, S. Kulling, H. Daniel, B. Spanier: Structural features and bioavailability of four flavonoids and their implications for lifespan-extending and antioxidant actions in C. elegans, *Mechanisms of Ageing and Development* **133**, 1-10

Persönliche Daten

Name: Kerstin Elisabeth Haas
Geburtstag: 13.10.1984
Geburtsort: Ulm/Donau

Kontakt

Adresse: Hermann-Winter-Weg 13, 84405 Dorfen
Telefon: 08081-5528263
Mobil: 0151-54863439
Email: haask751@gmail.com